UNIVERSITY OF SOUTHAMPTON

FACULTY OF NATURAL AND ENVIRONMENTAL SCIENCES

School of Chemistry

Amperometric Enzyme Electrodes

by

Firas Ahmed Thanon Al-Lolage

Thesis for the degree of Doctor of Philosophy

February 2018

UNIVERSITY OF SOUTHAMPTON

ABSTRACT

FACULTY OF NATURAL AND ENVIRONMENTAL SCIENCES

School of Chemistry

Thesis for the degree of Doctor of Philosophy

AMPEROMETRIC ENZYME ELECTRODES

Firas Ahmed Thanon Al-Lolage

This thesis studies the conditions required to achieve direct electron transfer and the experimental tests needed to unequivocally demonstrate that it occurs. Many publications claim to observe direct electron transfer to redox enzymes (for example in the case of glucose oxidase) but the evidence presented is often incomplete and unconvincing. The first part of this thesis argues that the vast majority, if not all, of these claims of DET for GOx are incorrect. It presents results for glucose oxidase (GOx) adsorbed on multi-walled carbon nanotubes (MWCNTs), a typical nanostructured GOx electrode, that clearly show that the surface redox peaks usually observed in these cases are due to free, adsorbed flavin and not due, as claimed, to DET to flavin within the enzyme. Also, the results can be explained by adsorption of enzymatically active GOx at the electrode surface and the detection of the decrease in the oxygen concentration at the electrode surface due to the enzyme catalysed oxidation of D-glucose.

The second part of this thesis establishes a flexible and structured method based on the use of site-directed mutagenesis to introduce cysteine residues at specific locations on the enzyme surface followed by the reaction between the free thiol group and maleimide groups formed on the electrode surface to immobilise the mutated enzymes. It is preferable to immobilise redox proteins and enzymes in a specific orientation, but still with some flexibility to optimise reaction kinetics. Using cellobiose dehydrogenase (CDH) as a model system, multiwall carbon nanotube electrodes were first covalently modified with maleimide groups following a modular approach combining electrochemical surface attachment and solid phase synthesis methodology. Five CDH variants were used in this study, the CDH-modified electrodes were tested for direct electron transfer (DET), showing high catalytic currents and excellent long-term storage stability. A potential-dependent Michaelis-Menten model for the CDH modified GC/MWCNT has been constructed and a master equation employed to simulate the DET and MET experimental results. Several mechanisms were suggested to explain the DET and MET for CDH. The internal electron transfer (IET) has been shown to be the rate determining step in the proposed mechanism. This was confirmed by the simulated data along with the experimental results. The simulated data suggests the presence of two populations of immobilised enzymes, MET and DET enzyme.

The validity of the aforementioned immobilisation method, was further examined. Three bilirubin oxidase (BOD) variants were used in this study, which were modified to bear a free cysteine residue in different positions at the surface of the enzyme, allowing fast and selective attachment to maleimide-modified GC/MWCNT electrodes. The catalytic mechanism of O_2 reduction by the *Magnaporthe oryzae* BOD covalently immobilized on multiwall carbon nanotube (MWCNT) electrodes, in the presence of Cl^- and at different pH, was electrochemically investigated. The results highlight for the first time the influence of chloride ions on the direct oxygen reduction by *Mo*BOD as a function of pH.

Table of Contents

Declaration of Authorship

I, Firas Ahmed Thanon Al-Lolage declare that this thesis and the work presented in it are my own and has been generated by me as the result of my own original research.

AMPEROMETRIC ENZYME ELECTRODES

I confirm that:

1. This work was done wholly or mainly while in candidature for a research degree at this University;
2. Where any part of this thesis has previously been submitted for a degree or any other qualification at this University or any other institution, this has been clearly stated;
3. Where I have consulted the published work of others, this is always clearly attributed;
4. Where I have quoted from the work of others, the source is always given. With the exception of such quotations, this thesis is entirely my own work;
5. I have acknowledged all main sources of help;
6. Where the thesis is based on work done by myself jointly with others, I have made clear exactly what was done by others and what I have contributed myself;
7. Parts of this work have been published as:

Al-Lolage, F. A.; Meneghello, M.; Ma, S.; Ludwig, R.; Bartlett, P. N., A flexible method for the stable, covalent immobilization of enzymes at electrode surfaces. *ChemElectroChem* **2017**, 1528-1534.

Bartlett, P. N.; Al-Lolage, F. A., There is no evidence to support literature claims of direct electron transfer (DET) for native glucose oxidase (GOx) at carbon nanotubes or graphene. *J. Electroanal. Chem.* **2017**, in press.

Signed: .....

Date: .....

Acknowledgements

I would like to express my deep and sincere gratitude to my supervisor, Professor Philip N Bartlett, for his enthusiasm, his inspiration, and his great efforts to explain things clearly. Throughout my thesis-writing interval, he provided encouragement, sound advice and comments, good teaching, and lots of good ideas. It is a huge transition for me, from radiation chemistry background to working on bioelectrochemistry. I would have been lost without his guidance. I would also like to thank my advisor, Dr Peter R Birkin for his comments for my quarterly reports.

My sincere thanks to my collaborators, Marta Meneghell, Dr. Roland Ludwig, Dr. Su Ma and Dr Nicolas Mano. Special thanks go to the former and current members of Bartlett research group: Dr. David Cook, Dr. Gabriela Kissling, Dr. Charlie Cummings, Dr Peter Richardson, Dr. Hisham Hamzah and Dr. Eva Papadopoulou. My high gratitude goes to Saiful Arifin for sharing his knowledge and without him this journey would be dull. I would like to thank my office mates; Turgut, Ana, David, Howard, and Alex for the wonderful friendship.

I would also like to thank the Ministry of Higher Education and Scientific Research of Iraq for the financial support for my language and PhD study.

I would like to dedicate this thesis to my two sons, my inspiration and to my loving wife Ibaa for her love, endless patience, understanding and absolute confidence in me.

Finally, I would like to thank my father, mother, brother and sisters for their support, love and caring.

Definitions and Abbreviations

A	Electrode area
AgNWs	Silver nanowires
ATPES	3-aminopropyltriethoxysilane
AuNPs	Gold nanoparticles
BDD	Boron doped diamond
BOD	Bilirubin oxidase
CDH	Cellobiose dehydrogenase
C_{dl}	Double layer capacitance
CMEs	Chemically modified electrodes
CNT	Carbon nanotube
CS	Chitosan
CV	Cyclic voltammetry
CYT	Cytochrome domain
cyt *c*	Cytochrome *c*
Da	Dalton
DET	Direct electron transfer
DH	Dehydrogenase domain
DMF	Dimethylformamide
DPV	Differential pulse voltammetry
D_{S}	Diffusion coefficient
E	Experimental potential *vs.* reference electrode
E^0	Formal potential
$E_{1/2}$	half-wave potential
EDC	*N*-(3-Dimethylaminopropyl)-*N*′-ethylcarbodiimide

EGr	Electroactivated graphite
EIS	Electrochemical impedance spectroscopy
E_p	Potential of the peak
ERCGr	Electrochemically reduced carboxy-graphene
ERGO	Electrochemically reduced grapheme oxide
ES	Enzyme-substrate complex
e-SnS_2	Exfoliated tin disulphide
F	Faraday constant
FAD	Flavin adenine dinucleotide
Fc	Ferrocene
FCF	Flexible carbon fibre
FcMA	Ferrocene monocarboxylic acid
FcMeOH	Ferrocene methanol
FESEM	Field emission scanning electron microscopy
GA	Glutaraldehyde
GC	Glassy carbon
GE	Graphite electrode
GO	Exfoliated graphene oxide
GOx	Glucose oxidase
GR-MWCNTs	graphene-multiwalled carbon nanotubes
HAD	*N*-Boc-1,6 hexanediamine
Hb	Hemoglobin
I	Current
IET	Internal electron transfer
I_p	Peak current

k_{cat}	Turnover number
k_{int}	Rate constants for the re-oxidation of FAD via haem group
K_m	Michaelis-Menten constant
K_m^{app}	Apparent Michaelis-Menten constant
k_{med}	Rate constants for the re-oxidation of FAD via the ferrocene
k_s	Standard rate constant
MET	Mediated electron transfer
MHA	Mercaptohexadecyl acid
*Mo*BOD	Bilirubin oxidase from *Magnaporthae oryzae*
*Mt*CDH	Cellobiose dehydrogenase from *Myriococcum thermophilum*
MUA	Mercaptoundecanoic acid
MWCNTs	Multiwall carbon nanotubes
n	Number of electrons
NCNs@CNFs	Nitrogen-doped carbon nanospheres@carbon nanofibres
NCNT	Nitrogen-doped carbon nanotube
NHS	*N*-Hydroxysuccinimide ester
NS-G	Nitrogen, sulfur dual-doped graphene
PANi	Poly(aniline)
PBS	Phosphate buffer solution
PDA	Polydopamine
PEI	Poly(ethylenimine)
PGE	Pencil graphite electrode
PVA	Polyvinyl alcohol
Q	Charge
R	Universal gas constant

rGO	Reduced graphene oxide
SPCE	Screen printed carbon electrode
SWCNT	Single walled carbon nanotube
SWV	square wave voltammetry
T	Temperature
TNT-GNP	Titanate nanotube-gold nanoparticle
v	Potential sweep rate
V_0	Reaction velocity
V_{max}	Maximum reaction velocity
WE	Working electrode
α	Transfer coefficient
Γ	Surface coverage
ΔE	Peak separation

Chapter 1 Introduction

1.1 Electron transfer mechanisms

Electron transfer (ET) is a ubiquitous process in chemistry and biology.[1-2] Therefore, comprehending this process is one of the most active research areas of science at the moment. The field of electron transfer processes has developed enormously, namely, in the field of bioelectrochemistry.[3] The early studies in the ET field were on "isotopic exchange reactions". These self-exchange reactions are the simplest class of reactions in chemistry because the reaction products are identical with the reactants, and no chemical bonds are broken or formed.[4] The electron transfer reactions are omnipresent because they are the fundamental event in inorganic and organic redox chemistry, and in electrochemical processes and they are important to the processes by which living cells obtain and use energy.[1]

In homogeneous solution, there are two mechanisms of ET: i) inner sphere ET where the donor and acceptor are covalently bonded and the charge transfer proceeds through a binuclear ligand-bridged complex between the two groups involved; ii) outer sphere ET**,** where the charge transfer is completed with the primary coordination sphere (central atom or ion) remaining intact, meaning that the two species involved (donor and acceptor) remain separate species before, during, and after the ET reaction. In the case of the homogeneous redox reactions, both the donor and acceptor are in solution. Thus, the ET mechanism only involves species in solution. In contrast for homogeneous redox reactions, at electrodes, charge transfer is accomplished heterogeneously between an electrode and an ionic conducting solution (containing the electroactive species), meaning that the electrons move across the boundary between two phases.

ET is a quantum process.[1] The simple model for ET reactions was formulated by Marcus, Hush, Levich and Dogonadze in a series of articles starting in the 1950s.[1, 6-7] Marcus introduced a theory of electron transfer, now referred to as Marcus theory. He received the Noble Prize in Chemistry for this achievement in 1992.[6] ET according to Marcus theory is mainly dependent on the distance between the electron donor and acceptor, it expects that the rate of ET between a donor and an acceptor is dependent on the thermodynamic driving force for the reaction (ΔG^0), nuclear reorganization energy (E_R), temperature (T) and the electronic coupling between an electron donor and acceptor (H_{DA}).[8] The basic versions of the theory are based on the segregation of fast electronic motion and slow nuclear motion as suggested by Franck-Condon approximation. Accordingly, the ET happens by tunnelling between reactant and product nuclear vibrational surfaces. The activation energy for the ET reaction ($\Delta G^{\ddagger}$)

derives from the rearrangement of the nuclear and solvent coordinates needed to transport the reactant to an arrangement in which the electron can transfer adiabatically to the product surface.[1] Figure. 1.1 shows the Gibbs free energy surface $G(q)$ for an electron transfer reaction illustrating the reactant and product curves, where q is the reaction coordinate that includes both the inner and outer contributions; the inner contributions refer to the nuclear reorganization of the nuclei of the redox centres and the outer contributions are related to the solvent environment around the reactant centres.

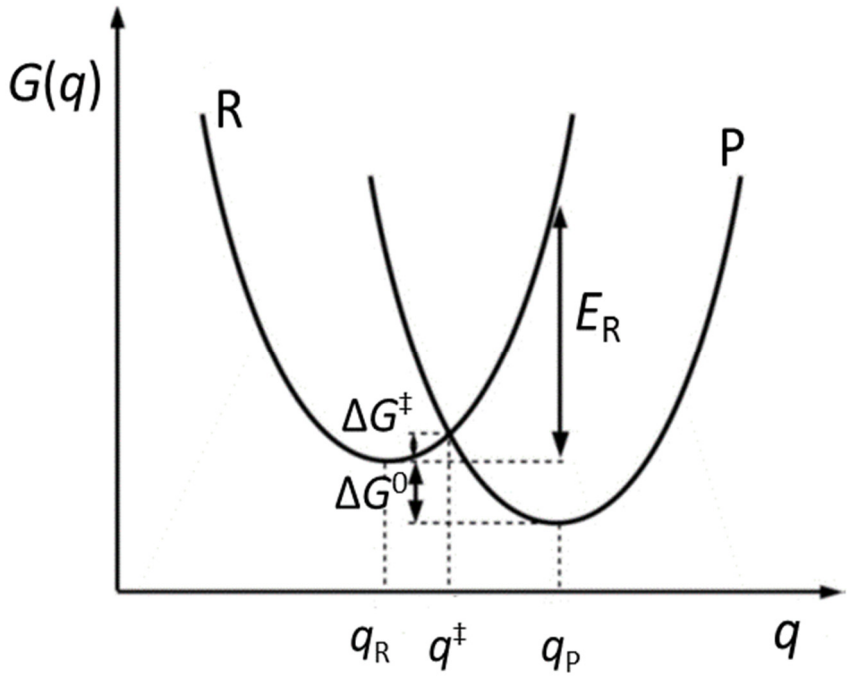

Figure 1.1. *Gibbs free energy surface G(q), q is the reaction coordinate, for an electron transport reaction illustrating the reactant and product curves. ΔG^0 is the thermodynamic driving force for the reaction, E_R the reorganisation energy, $\Delta G^{\ddagger}$ is the activation free energy, q_R, $q^{\ddagger}$ and q_P are the reactant, transition state and product configurations, respectively.[1]*

In the simple analysis of ET kinetics, the reactant and product energy surfaces are given as parabolic (Figure 1.1). ΔG^0 is the thermodynamic driving force and $\Delta G^{\ddagger}$ is the activation energy for the ET reaction. The rate constant for ET between the donor and acceptor

$$\mathrm{D} + \mathrm{A} \rightarrow \mathrm{D}^{+} + \mathrm{A}^{-} \qquad Eq.(1.1)$$

is given by:

$$k_{\mathrm{DA}} = \kappa_{\mathrm{el}} \frac{\omega_{\mathrm{eff}}}{2\pi} e^{\frac{-\Delta G^{\ddagger}}{RT}} \qquad Eq.(1.2)$$

where k_{DA} is the electron transfer rate, ω_{eff} is the effective frequency of the nuclear motions that transports the system to the transition state arrangement $q^{\ddagger}$, κ_{el} is the electron transfer

probability at the nuclear arrangement of the transition state, R is the universal gas constant and T is the absolute temperature. Adopting that the energy surfaces of the reactant and product are parabolic and have the same form, the activation free energy can be given by:

$$\Delta G^{\ddagger} = \frac{(E_R - \Delta G^0)^2}{4E_R} \qquad (Eq.\ 1.3)$$

To better understand the parameters included in *Eq.* 1.3, a simple model is shown in Figure 1.1. The reorganisation energy (E_R) depends on the free energy necessary to rearrange the nuclear coordinates for the reactant at the equilibrium state from those related to equilibrium state for the reactants q_R, to those related to the equilibrium state for the products, q_P, without transfer of the electron (see Figure 1.1). E_R, consists of two parts: inner sphere contribution (energy needed to change bond distances) and outer sphere contributions (energy required to reorient the solvent).[1, 8] Thus, small values of E_R, relating to similar structures for reactants and products, and/or wide parabolic free energy surface correspond to larger values of the k_{DA} because of the easy rearrangement process.[9-10] The rearrangement process is essential in defining the kinetics of ET between donor and acceptor. However, to unearth the nature of the selectivity in the kinetics of ET between biological partners, it is crucial to consider the pre-exponential term k_{el} in *Eq.* 1.2. In accordance with the semiclassical model k_{el} is given by:

$$\kappa_{el} = \sqrt{\frac{\pi}{\hbar^2 E_R RT}} H_{DA}^2 \qquad (Eq.\ 1.4)$$

where H_{DA}^2 defines the strength of coupling between the reactant and product states at the transition state arrangement $q^{\ddagger}$, and $\hbar$ is the reduced Planck constant.

Many studies have been carried out to calculate H_{DA} in proteins. Nonetheless, the square-barrier model assumes the protein as a "frozen organic glass".[1] According to this model the H_{DA} decays exponentially with the distance between donor and acceptor:

$$H_{DA}(r) = H_{DA}(r_0)\exp\left(\frac{-\beta(r-r_0)}{2}\right) \qquad (Eq.\ 1.5)$$

where r_0 is the van der Waals contact distance, r is the distance between the donor and the acceptor and β represents the exponential reduction of the overlap with distance (decay constant) between the donor and acceptor.[10-11] Therefore, *Eq.*1.2 can be divided into electronic (pre-exponential) and nuclear (exponential) terms; ET reaches its maximum value when the nuclear factor is optimised, namely, when $-\Delta G^0 = E_R$, and under this circumstances, it only depends on the electronic factor (H_{DA}). The exponential dependence of the rate of ET with distance calculated by *Eq.*1.2 to 1.5 can be comprehended in terms of the decrease in the electronic wave-functions of the donor HOMO and acceptor LUMO orbitals with distance.

Basically, these will decrease exponentially at larger distances from the redox center.[1] Indeed, Marcus theory was initially formulated to take into account outer sphere ET reactions. Later, it was extended to consider the inner sphere ET reactions and heterogeneous ET.[7]

In biological systems, bioenergetic processes such as respiration and photosynthesis are accomplished via proteins and enzymes that form the electron transfer chains.[12] This means, events like multi-step ET occur in addition to single-step ET, the multi-range ET is controlled by proteins that contain metal ion complex cofactors, namely, metalloproteins.[13-14] Generally, a protein controls the electron transfer by modulating the formal potentials of its redox centres, defining the local conditions to control the E_R, and forming proper electron tunnelling pathways between redox active sites.[15] In spite of the complexity of the different ET chains, nature employs a reasonably limited palette of redox active centres; the redox-active cofactors can be grouped into organic and inorganic cofactors. The organic cofactors that can be either tightly or loosely bound to the protein include quinones, haem (*a*, *b*, and *c*), and flavins (FAD and FMN), the inorganic cofactors involve iron-sulphur clusters , Cu, Fe, Ni, Se, Mg, etc.[1]

During the past few decades, the understanding of biological electron transport has developed remarkably.[7, 10, 16] In biological systems, ET happens at protein-protein interfaces and many enzymes can only maintain their activity in biological membranes. Therefore, ET to redox proteins and enzymes that are immobilized at the surface-modified electrodes (heterogeneous ET reactions) provides a suitable model system for addressing some essential aspects of enzyme ET.[15, 17] The other inspiration for investigating protein ET at an electrode are the demands for biosensors and biofuel cells.[18-20]

There are generally two mechanisms of ET between the electrode and an enzyme, direct electron transfer (DET) and mediated electron transfer (MET). The mediated systems have been extensively investigated and usually exhibit high activity, however the long term stability can be limited by loss of mediator. It is widely believed that DET would not have the same drawbacks with stability. Efficient DET requires a good connection between the electrode and enzyme with the correct orientation and favourable distance as suggested by Marcus theory.[21] To achieve this it is essential to employ a highly controlled technique of electrode modification, in Chapter 4 we adopt a selective and flexible immobilization approach that utilises the coupling of an amino acid residue, namely cysteine, with maleimide group, to form stable thioether bonds.[22]

Apart from mechanistic studies, the major driving forces for electrochemical studies of redox enzymes at electrode surfaces are focused towards “third generation” biosensors and biofuel cells. DET between enzymes and electrodes is an essential system for studying the mechanisms of biochemical reactions. Nevertheless, DET between enzyme and electrode remains a great

challenge as a result of enzyme denaturation, affected by biocompatibility, and the distance between the active redox centre and the electrode.[23] One of the possible ways that has been suggested in the literature to circumvent this problem is by controlling the enzyme orientation on the electrode surface.[24-26] The work presented in Chapters 3, 4 and 6 attempts to meet this challenge.[22, 27]

1.1.1 Direct electron transfer (DET)

Direct electrochemistry between a redox-active centre of protein and the electrode surface has been investigated for a number of proteins such as cytochrome *c*, horseradish peroxidase and glucose oxidase, etc.[28] Investigation in this research area increased in the late 1960s, and was motivated mainly by the promise of feasible biosensors for medical applications.[29] The notion of direct electron transfer (DET) is simple; combine a conductive electrode and an enzyme, then apply an electrochemical potential to regulate the flow of electrons between the two. Redox centres are investigated by observing the resulting electrical current.[30] Figure 1.2 shows the DET mechanism of bio-electrochemical oxidation or reduction of a substrate by an oxidoreductase with its redox cofactor.

Reversible DET between a protein and an electrode was reported for the first time for cytochrome *c* in the late 1970s at a tin doped indium oxide electrode[31] and at gold electrodes in the presence of 4,4-bipyridyl (bipy) in solution.[30] However, DET is not a common feature of protein-modified electrodes; for many enzymes the redox-active centre is shielded by the apoprotein, therefore, ET is slow or not feasible at all.[32] Hence, mediators that shuttle electrons between electrodes and enzymes are utilized. Despite the fact that many attempts have been done in developing the concept of mediated electrochemistry of redox enzymes, but the mediation may not be the best approach to investigate fundamentals of catalytic enzyme reactions. Nonetheless, mediation remains essential for redox enzymes for which direct, fast electron exchange between the active site of the redox enzyme and the electrode surface is difficult.[1] The electrochemical investigation of redox-active proteins at electrodes established an electrochemical basis for the study of enzyme structure, obtaining valuable information about the kinetic and thermodynamic properties of the redox protein, and the mechanisms of redox changes of protein molecules.[33]

To date, DET has been observed for less than 10% of known redox proteins. This is because of the fact that the electrochemically active centre of the enzyme is often buried deep in the protein structure.[32] The process of ET is, at its core, an electron tunnelling process. Therefore, Marcus' theory predicts, and experiments show that, the rate of electron transfer decays exponentially with distance, namely, when the distance goes significantly beyond atomic

dimensions (>3 Å).[34] According to Marcus' theory ET rates are expected to drop by 10^4 when the distance between an electron donor and acceptor is increased from 8 to 17 Å.[21, 35]

Redox enzymes can be classified into extrinsic and intrinsic enzymes according to the mechanism of the ET reaction. Intrinsic enzymes, such as glucose oxidase (GOx), have one region, namely, the vicinity of the prosthetic group, where the ET reaction between the substrate and redox active sites of the redox enzyme happens. Since there is no natural requirement for long range ET pathways to the surface of the protein, DET is very difficult to achieve[32, 36] (see Chapter 3). On the other hand, for extrinsic redox enzymes such as cellobiose dehydrogenase (CDH), an electron-accepting or donating center is essential which binds to the enzyme in some protein fragment or at a site not extremely close to the active site and hence there are an electron pathway to the surface and/or additional active site on the surface for another protein to connect to, making them an excellent choice for DET.[36] For CDH the electrons are transported via internal electron transfer (IET) from the catalytically active flavin domain to the haem domain which is able to communicate with electrodes in a DET reaction.[32] Therefore, it would be crucial to immobilise enzymes in a particular orientation, but still with some flexibility to adjust reaction kinetics. In Chapter 4, we suggest such a method using site-directed mutagenesis to introduce free cysteine residues at specific locations on the CDH surface and utilize the reaction between the thiol group and maleimide groups formed at the electrode surface to attach the mutated enzymes.[22]

In this thesis, ET reaction is believed to be DET in the sense of direct bioelectrocatalysis if the reaction meets the following conditions: i) the redox group of the enzyme remains bound with the enzyme during ET, ii) ET is not mediated by a diffusive or a non-diffusive artificial electroactive species, and iii) the oxidized/reduced forms of the substrate can be monitored upon its addition to the reaction system.[22, 27, 37]

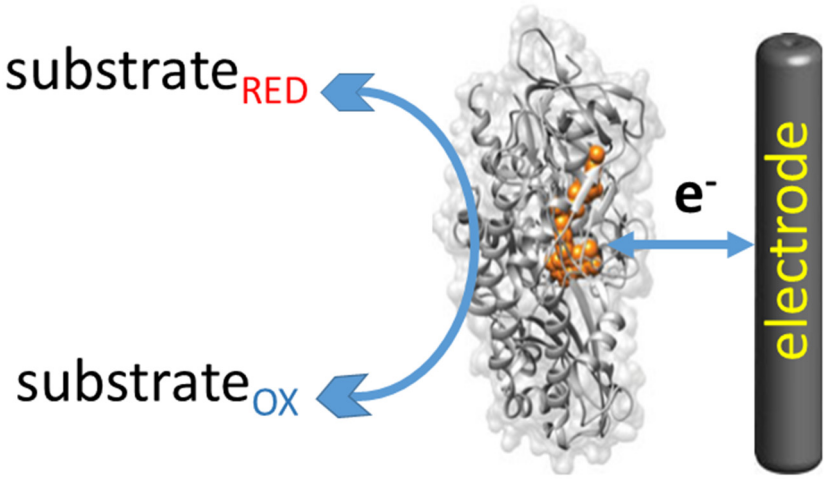

Figure 1.2. *DET for bio-electrochemical reduction or oxidation of a substrate by an oxidoreductase with its redox active cofactor indicated in orange.[37] Adapted from reference 37.*

1.1.2 Mediated electron transfer (MET)

Apart from a few exceptions, such as horseradish peroxidase,[38] in practice, however, DET for intrinsic enzymes has not been very effective. Indeed, when an electrochemical signal could be detected, it often exhibited characteristics of slow electron transfer.[30] Alternatively, redox proteins are able to use small electroactive molecules (soluble mediators) to undergo mediated electron transfer (MET) with an electrode. However, some requirements are necessary to create electronic communication.[37] From a practical point of view, the following features are considered essential for ideal redox mediators: i) well defined reversible voltammetry with a fast heterogeneous rate constant, ii) fast reaction with the oxidoreductase enzymes to avoid blocking of the active site, iii) good solubility and stability in both oxidized and reduced forms to allow fast diffusion between the enzyme and electrode, and iv) easy re-oxidation/reduction of the mediator at the electrode surface at a low overpotential that is unaffected by pH.[1] Widely used soluble mediators include quinone and ferrocene derivatives[1, 39-41] as well as metal complexes based on Os, Ru and Fe. Commercial biosensors based on diffusional mediators have been commonly utilized in glucose biosensors. Theory to quantitatively describe MET for a variety of electrode designs was formulated by Bartlett and others.[1] Figure 1.3 shows the MET mechanism of bio-electrochemical oxidation or reduction of a substrate by an oxidoreductase with its redox cofactor.

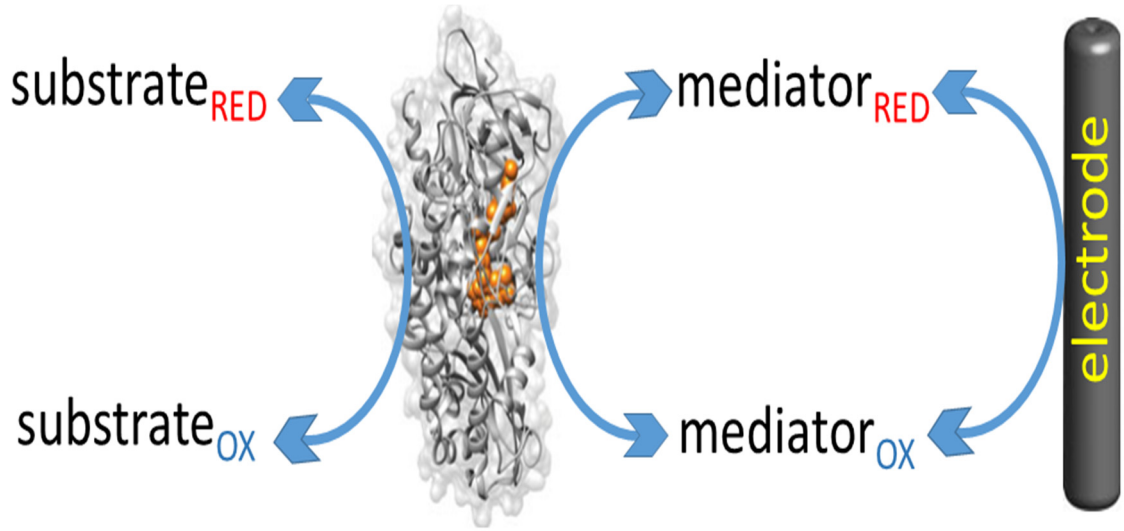

Figure 1.3. *MET for bio-electrochemical reduction or oxidation of a substrate by an oxidoreductase with its redox active cofactor indicated in orange.[37] Adapted from reference 37.*

Mediators can be combined with the structure of the matrix used to immobilise the enzyme onto the electrode surface. Moreover, enzymes and redox proteins can be modified to have mediators integrated with their structure.[42] The efficacy of ET depends on the transport

characteristics of the mediator and the ET steps in the system under investigation. Ideally, the mediator would be integrated close to the prosthetic group of the enzyme, allowing fast electron exchange between the redox group and the mediator.[43]

In this work, we have used ferrocenecarboxylic acid and 2, 2'-azino-bis (3-ethylbenzothiazoline-6-sulphonic acid) (ABTS) to compare DET and MET behaviour of the cellobiose dehydrogenase (CDH) (Chapter 4) and bilirubin oxidase (BOD) (Chapter 6) respectively.

1.2 Enzymes

Enzymes were first discovered in 1833 by Anselme Payen and Jean Persoz.[44] They are extraordinary biological catalysts with high efficiency and specificity.[45] An enzyme active site can be defined as the district that binds the substrate, mediates catalysis, and releases the product.[46] Comprehending the mechanisms of enzyme-catalysed reactions is important to the study of bio-electrochemical reactions.[47] Theoretically, better understanding can contribute to the development of new implantable medical devices or environmental, self-powered biosensors.[18-19] It is necessary to discuss some basic terms used in enzymology. A complex enzyme consists of one or more polypeptide chains and a metal ion or a low molecular mass organic molecule at its active site. The term holoenzyme represents the complete catalytically active enzyme, while the term apoenzyme means only the protein constituent. A metal ion cofactor is the metal ion that binds directly to the protein. A prosthetic group is a small organic molecule that can be either tightly or covalently bound to the enzyme.[45] In the 1960s, the functional information about enzymes was systematically encapsulated into EC numbers. The EC is a way to classify enzymes, by categorizing the reaction they accelerate. The classification is based on several features of the overall chemistry such as the nature of the chemical bonds that are broken or formed, cofactors involved and the nature of the substrates experiencing transformation.[48]

Enzymes are challenging, and it has been complicated in many cases to prove the mechanisms of their catalysed reactions, from experiments alone. Therefore, simulations and modelling are increasingly significant, supplementing experimental approaches.[47]

1.3 Modification of electrode surfaces

The notion of chemically modified electrodes (CMEs) was born as a consequence of the electrochemists' ambition to obtain complete control of the chemical nature of the electrode surface. Basically, by attaching chemical groups to the surface, the electrochemists believed that the electrode surface would take on the chemical features of the attached groups.[49] The

modification of electrode surfaces can provide insight into mechanisms of electron transfer,[22, 24] and surfaces of interest for a range of applications in analytical electrochemistry and in energy conversion.[50] Therefore, it has been an active area of research for over 40 years dating back to the pioneering work by Lane and Hubbard (1973),[51] who described the strong chemisorption of electroactive allyl compounds on platinum (Pt) electrodes. Two years later, Murray[52] attached organosilanes to the hydroxyl groups present on metal oxide surfaces in order to functionalise electrodes with amino groups. This was a significant step because one can rationally plan coupling reactions with the amino-modified surface to attach other interesting molecules to it via conventional solid phase synthesis.[53] Therefore, if a suitable reagent were chosen for the electrode modification, required features such as reagent-based control of the rates, sensitivity, selectivity, specificity and stability compared to the bare electrode surface might be obtained.[49]

There have been numerous types of electrode used for constructing CMEs in the literature, including platinum,[54] gold,[55] diamond,[56] indium tin oxide,[57] graphene,[58] glassy carbon (GC),[59] carbon nanotube,[60] boron doped diamond (BDD)[61] and many other electrode materials. Three different carbon-based electrodes (GC, BDD and GC/MWCNT) were employed in this study. GC was chosen due to its high electrical conductivity, good mechanical and dimensional stability, impermeability to gases, and high chemical resistance. Furthermore, it has a wide potential range and is suitable for operating in acidic and alkaline condition.[62] On the other hand, BDD was used because of its excellent material properties, namely, the small background currents and the low adsorption tendency (reduced fouling) compared to other electrodes. However, BDD is not a characteristic electrode material, it is indeed a semi-conductor doped with boron to exhibit semi-metallic features.[63] Indeed, glassy carbon electrodes modified with multiwall carbon nanotubes (GC/MWCNT) were the main electrode type used in this research, they were chosen as a model for carbon-based electrodes because of their high surface area combined with relatively low capacitance.[22, 64] These were covalently modified with maleimide groups following a method based on electrochemical surface attachment and solid phase synthesis methodology,[24] detailed discussion will be provided in subsequent sections.

1.4 Immobilisation of enzymes

The term “immobilised enzymes” was approved, in agreement with Katchalski-Katzir's suggestion, at the first Enzyme Engineering Conference in 1971 to denote “enzymes physically confined or localised in a certain defined region of space, with retention of their catalytic activities, and which can be used repeatedly and continuously”.[65] The enzymes can be immobilised onto an electrode by interactions ranging from physical adsorption and ionic binding to covalent bonds.[66-69]

1.4.1 Reversible physical adsorption

One of the simplest immobilization technique is non-specific adsorption, which is predominantly based on physical adsorption or ionic binding.[66] Physical methods are characterised by weak interactions such as hydrogen bonds, Van der Waals forces, affinity binding, hydrophobic interactions, ionic binding or mechanical containment of the enzyme within the support.[66, 69-70] Therefore, enzymes can be removed from the electrode (support) under gentle conditions.[66] Enzymes can be adsorbed onto electrodes of all types, but may denature and block electron transfer. Other non-covalent interactions are hydrophobic adsorption,[70-71] affinity binding[72] and chelation or metal binding.[73] The use of physical adsorption or ionic binding for enzyme immobilization is highly desirable because once the enzymatic activity decays, the electrode can be renewed and re-loaded with active enzyme.[66] Therefore, such techniques are economically attractive. However, it suffers from technical problems such as enzyme leakage from the matrix due to a weak interaction to the electrode surface.

1.4.2 Irreversible enzyme immobilization

The most commonly used methods for enzyme immobilization are irreversible procedures such as entrapment in polymers[74-75] and formation of covalent bonds. For the latter method, various reactions have been established depending on the functional groups presented on the surface.[76] Such functional groups can also be introduced on the electrode by covalent modification. Cross-linking is another irreversible method of enzyme immobilization, accomplished by formation of intermolecular cross-linkages between the enzyme molecules using bi- or multifunctional reagents such as glutaraldehyde.[77] However, for a more stable and controlled immobilization, obtaining covalent bonds between the enzyme and the electrode is of interest.

1.4.2.1 Formation of covalent bonds

The reaction with functional groups present on the protein surface often results in covalent bonding. For example, the free amino groups of lysine residues easily react with electrodes bearing active esters, such as the commonly used N-hydroxysuccinimide (NHS) esters, to create stable amide bonds. Unfortunately, the immobilisation of proteins in aqueous buffers will compete with ester hydrolysis for the modification sites considering that NHS esters are unstable under aqueous conditions.[68] In addition, the nucleophilicity of the amino groups enables interactions to occur with epoxide functionalised materials, which is more preferable considering that they are relatively stable to hydrolysis at neutral pH. Nonetheless, random

orientations of enzymes immobilized through their amino groups are caused by the large number of lysine residues in proteins.

Other functional groups used for protein immobilization are the carboxylic groups of aspartic and glutamic acid residues, which are usually converted to their corresponding active esters *in situ* using a carbodiimide coupling reagent and an auxiliary nucleophile such as *N*-(3-dimethylaminopropyl)-*N*′-ethylcarbodiimide (EDC) and NHS. The active esters can then react with amine-bearing supports. However, this method presents the same disadvantages as the previous one, since aspartic and glutamic acid residues are rather plentiful in proteins. Furthermore, carbodiimides and the generated esters are quite unstable in aqueous media, leading to relatively low reaction yields. Also, there is the risk that NHS esters formed on the protein molecule may couple to the lysine residues of other protein molecules.

A few selective immobilization methods that can proceed under mild physiological conditions have gained popularity in order to address the problem of random enzyme orientation at the electrode surfaces.[78] Some of these methods depend on the labelling of proteins with an azide moiety, which can then react with alkynes[79-80] or be activated with a phosphine to react with a variety of electrophiles.[81-83] Nevertheless, the site-selective attachment technique also needs an enzymatic site-selective labelling procedure for the azide moiety. In addition, quantitative reaction yields require activation reagents or catalysts.

Another site-specific immobilization approach is performed by the introduction of genetically encoded affinity tags in the protein structure. Undoubtedly, the most well-known tag is the polyhistidine tag (His-tag), usually consisting of six sequential histidine residues that can chelate metals such as Cu(II), Co(II), Zn(II) or Ni(II).[84-85] Nevertheless, the strength of the binding interaction is relatively weak ($K_d \approx$ 1-10 μM), and the selectivity of this method is slightly low as numerous proteins have been identified that are able to bind to metal ions, and consequently, competing with the desired histidine tag. Furthermore, this technique is generally used to attach the tag at either the C- or N-terminus of the polypeptide chain and the His-tag is a bulky group, hence, the choice of orientation is limited.

1.4.2.2 A generic, modular approach to the modification of carbon electrodes with maleimide groups

In Chapter 4, we examine a selective immobilization method, recently suggested by Bartlett and co-workers,[22, 24] which employs the coupling of an amino acid residue, namely cysteine, with unsaturated carbonyls, such as maleimide, to form stable thioether bonds. The key advantage of this method is its modular approach that allows the single elements of the modification to be varied independently. In this case these elements are a “linker”, a “spacer”, and a “reactive group” (Scheme 1.1). This methodology is highly site-selective, particularly for

engineered proteins to have a single cysteine on the surface; proteins are known to have a small amount of surface-exposed cysteine residues.[86] This means, the protein of interest can be engineered to introduce a single cysteine on the surface or to remove all but one cysteine on the surface.

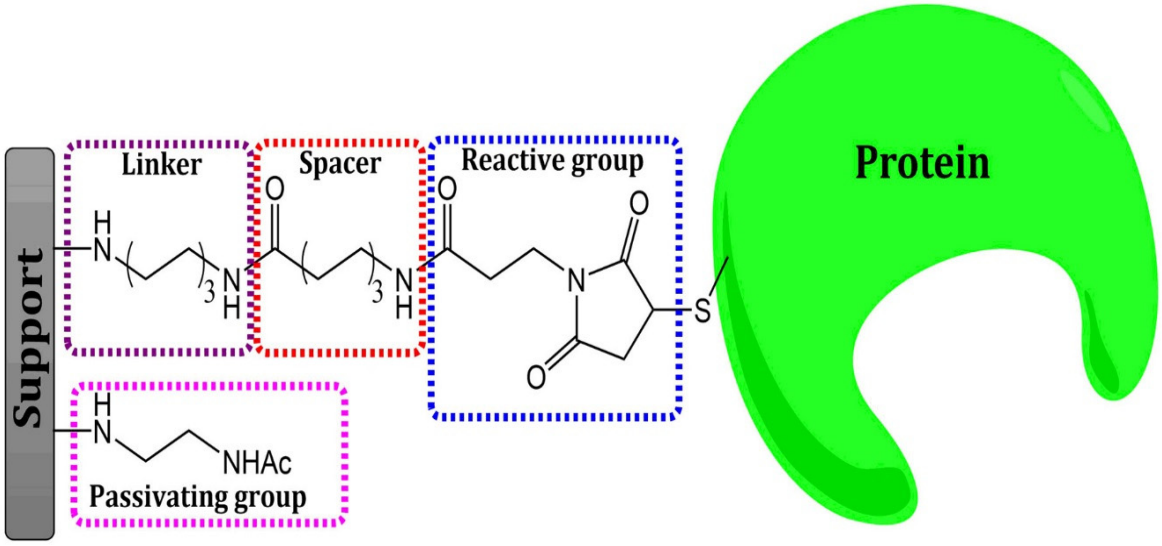

Scheme 1.1. *Reaction of a maleimide group immobilised onto a support with the thiol of a cysteine residue.*

Dilution of the maleimide groups on the surface, a condition suitable for accommodating big biomolecules such as enzymes, was achieved by introducing a "passivating group" (see Scheme 1.1) . The latter is a small molecule co-grafted at the electrode surface with the linker to form a two-component monolayer on the electrode. The partial coverage of the linker and, consequently, of the maleimide on the electrode surface is suitable to access the target functional group of the protein (cysteine in this case) and accommodate the bulky macromolecule. Moreover, the polarity/charge of the modified surface around the reactive group (attachment point) should be compatible with the protein surface around the target functional group, to reduce repulsion or denaturation of the enzyme. Detailed discussion will be provided in Chapter 4, Section 4.4.

1.5 Biosensors

According to the International Union of Pure and Applied Chemistry (IUPAC), biosensor can be defined as "an integrated receptor-transducer device, which is capable of providing selective quantitative or semi-quantitative analytical information using a biological recognition element".[87]

Diabetes mellitus is an international health problem. It is a metabolic health disorder caused by insulin deficiency and hyperglycemia, which results in blood glucose levels being either higher or lower than the average 80-120 mg/dL (4.4-6.6 mM).[88] People with diabetes are statistically more likely to develop heart disease, blindness and kidney failure and as a consequence it is one of the highest causes of disability and death in the world.[89] The complications of diabetes can be reduced through personal control of blood glucose by both management and diagnosis of diabetes mellitus which require regular monitoring of blood glucose levels. As a consequence glucose is the most tested biological analyte with glucose biosensors making up 85% of the whole biosensor market. Most diabetics must test their blood glucose levels every day.[90] Due to the demand, measurement of blood glucose has been widely used as a model for researching new biosensor techniques. The need for glucose diagnostics to be reliable and controlled has led to a great deal of research with many new detection mechanisms being proposed.[88-89]

Electrochemical glucose biosensors are very prominent due to the high sensitivity, ease of maintenance, low cost and reproducibility they provide. Glucose oxidase enzyme based amperometric glucose biosensors are the most common testing devices available and have been consistently tested. These sensors measure currents produced when electrons transfer occurs between the glucose oxidase enzyme (GOx) and an electrode surface.[91]

Consequently, an enormous number of publications on electrochemical glucose biosensors have appeared since Clark's initial publication.[92] Electron shuttles, i.e. redox mediators, have been used to achieve fast electron transfer (ET) between the redox centre flavin adenine dinucleotide (FAD) (which is deeply buried in GOx) and the electrode.[90] These electrochemical glucose biosensors can be classified into three groups. So called "first generation"[92] glucose biosensors, like the work of Clark; "second generation" glucose biosensors where an artificial, freely diffusing redox mediator is used; and "third generation" glucose biosensors in which direct electrochemical oxidation of the flavin active site of glucose oxidase occurs.

1.5.1 First-generation glucose biosensors

Early biosensors were based on monitoring dissolved oxygen consumption or detecting the production of hydrogen peroxide (Figure 1.4A). According to Clark,[93] O_2 may be reduced at a platinum (Pt) electrode at a potential of -0.6 V *vs.* Ag/AgCl and the reduction current should correspond to the concentration of glucose in the solution. However, in the case of low concentrations of glucose, the sensitivity of the suggested electrode was not sufficient to record the small change in O_2 concentration. Also, changes in temperature and the ionic strength of the solution can lead to fluctuation in the background oxygen concentration. This technique is good in that it is simple to monitor, especially when the devices are small.[90] On the other hand,

hydrogen peroxide (H_2O_2) can be oxidised at Pt electrode at *ca.* +0.6 V Ag/AgCl, this system has been used in several commercial glucose biosensor. However, the key problem with the early glucose biosensors is that the measurement of hydrogen peroxide needed to be highly sensitive. As this was influenced by interference of endogenous electroactive species (such as ascorbic acid, uric acid and drugs) a considerable body of research was done in the 1980s to lessen the interference of other species present. Another problem was oxygen deficit where the oxygen in biological fluids caused differences in oxygen tension due to low solubility.[94]

1.5.2 Second-generation glucose biosensors

Second-generation glucose sensors were produced to counter first-generation limitations by using mediators (Figure 1.4B). This was done by replacing oxygen with redox mediators (non-physiological electron acceptors) which were able to transport electrons from the reduced $FADH_2$ of the enzyme itself to the working electrode. Instead of hydrogen peroxide a reduced mediator is produced, resulting in an amperometric signal and regeneration of the oxidized mediator.[94] A large number of electron mediators were employed to enhance the efficacy of the sensor including ferrocene, tetracyanoquinodimethane (TCNQ), ferricyanide, thionine, methylene blue, tetrathialfulvalene (TTF), quinones, and methyl viologen.[95]

The main drawbacks of this method were the contamination of the samples due to mediator leakage as well as the low selectivity of the mediators. To address this problem, a polymeric backbone was introduced, on which the mediator is incorporated to produce a redox hydrogel as a matrix for enzyme immobilisation. This suggestion was the first step toward "reagentless" amperometric biosensors.[96] Os-complex polymers were applied in this field for wiring GOx with the purpose of measuring glucose concentration in biological samples.[97]

1.5.3 Third-generation of glucose biosensors

The third generation of glucose biosensors are established based upon direct electron transfer between the electrode and the enzyme and thus do not require redox mediators. (Figure 1.4C). Greater selectivity is expected when mediators are not used. Nonetheless, only a small number of enzymes, including peroxidases, have been shown to be able to demonstrate direct electron transfer at normal electrode surfaces.[98-99]

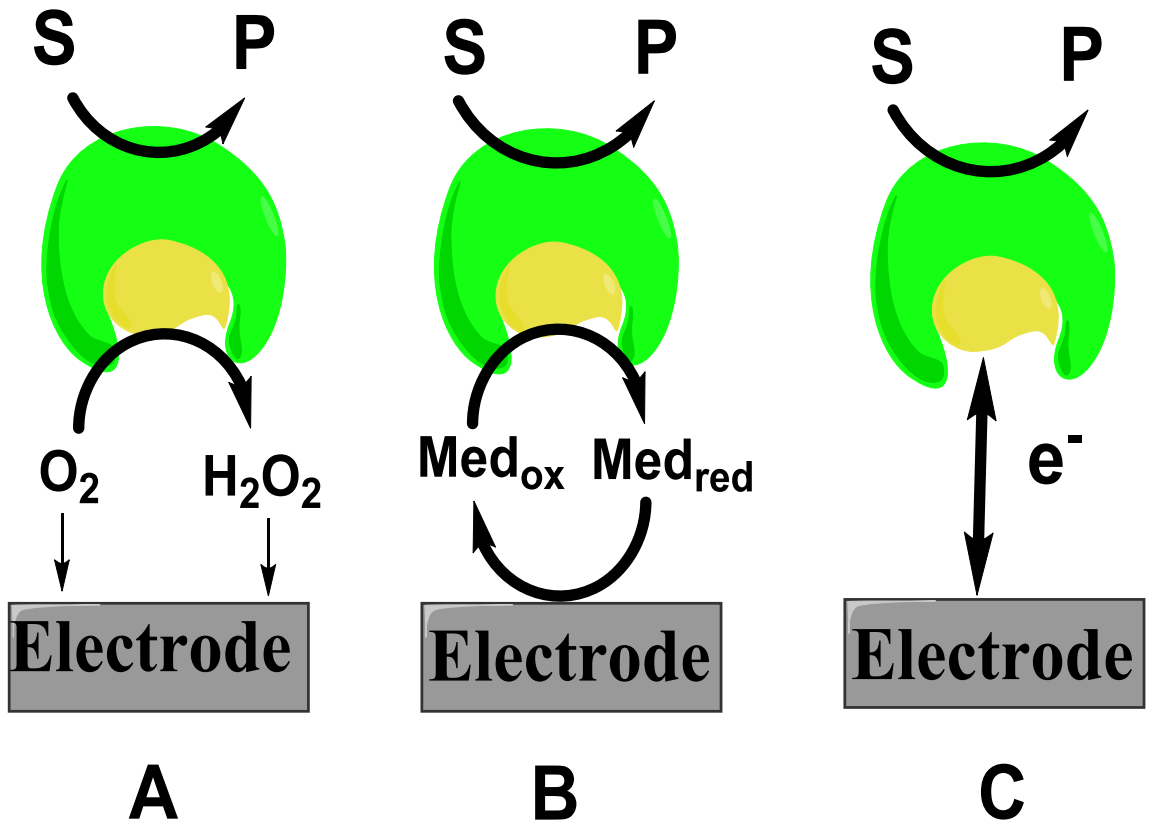

Figure 1.4. *Three generations of electrochemical glucose biosensors based on (A) the use of natural oxygen cofactor, (B) artificial redox mediators, and (C) direct electron transfer between GOx and the electrode surface. S: substrate; P: product.*[90]

Direct electron transfer between redox enzymes which are close to the electrode surface is usually very slow. It may even prove impossible because of the screenings of the redox-active cofactors of the enzyme by the insulating protein shell. In spite of the issue of the large electron transfer distance, there are continuing attempts to demonstrate direct electron transfer between GOx and specifically prepared electrode surfaces.

There are mixed reports in the literature concerning the DET catalysed by GOx and they claim to obtain DET to GOx. However, the evidence presented is often poorly supported and unconvincing.

Organic-conducting materials has been suggested to achieve direct electron transfer from the surface based upon charge-transfer complexes.[100] However the evidence suggest that this is not direct electron transfer but rather mediated by soluble component of the salt.[101] Organic salts, such as tetrathiafulvalene-tetracyanoquinodimethane (TTF-TCNQ), are found to mediate the electrochemistry of pyrrole-quinolinequinone enzymes (GDH-PQQ) along with flavoproteins (GOx). Indeed, many groups have tried to demonstrate direct electron transfer on third generation glucose biosensors, including TTF-TFNQ crystals,[102] a material consisting of a water dispersed complex of polypyrrole-polystyrensulfonate (PPy) embedded in

polyacrylamide (PA) which has been prepared and tested as enzyme immobilising system for its applications in amperometric biosensors.[103]

One route for creating third-generation glucose biosensors is to use conducting polymers such as polypyrrole. Aizawa *et al*.[104] reported direct electron transfer from PPy-entrapped GOx on a platinum electrode. Mediatorless glucose biosensors based on the GOx/polypyrrole system were also suggested by Koopal *et al.*[105] Nevertheless, the high anodic potential of this system *vs.* the redox potential of $FAD/FADH_2$ implies the possibility of electron transfer mediated by a surface-oligomeric pyrroles.[90] A study conducted on *in situ* potentiostatic electropolymerization of pyrrole on a Pt electrode in a thin layer amperometric cell and the entrapment of the enzyme glucose oxidase and boron-doped diamond electrode has also been reported.[106]

There have been a lot of studies into biosensors based on direct electron transfer, many of which produced detailed reviews.[107-108] On many electrode materials, proteins can unexpectedly adsorb.[109] The interaction of the electrodes with proteins is mainly controlled by hydrogen bonding as well as dipole-dipole, electrostatic, and hydrophobic interactions. It is essential to take into account this adsorption at the electrode surface because it may contribute to the overall current signal of biosensors based on more complex architectures. The suitability of this can be tested in control experiments. Enzyme can be denatured at the electrode surface during this kind of adsorption process on noble metal or carbon electrodes so it is important that this is considered. Also the stability of the adsorbed enzyme layer is dependent on a number of factors such as the ionic strength of the solution, the pH, the temperature and the material of the electrode.[110]

A number of existing papers suggesting direct electron transfer of GOx will be discussed. Direct electrochemistry was investigated for GOx adsorbed on boron-doped carbon nanotubes/glassy carbon (BCNTs/GC) electrode with cyclic voltammetry.[111] Similarly, glucose oxidase was effectively immobilized on the surface of an indium tin oxide electrode which was modified using inverse TiO_2 opal structure.[112] GOx was assembled on single wall carbon nanotubes in combination with a new amine-terminated ionic liquid and gold nanoparticle which were electrodeposited onto this composite.[113] GOx was also immobilized on a nitrogen-doped carbon nanotube modified electrode.[114] Based on GOx incorporated polyaniline nanowires on carbon cloth (CC) electrode, an amperometric enzyme biosensor was demonstrated,[115] and the direct electrochemistry of GOx immobilized in a film of graphite nanosheets and Nafion was examined.[116] In all the contributions mentioned above cyclic voltammetry showed stable and well-defined redox peaks attributed to direct electrochemistry of GOx in the absence of glucose. Those redox peaks were apparently enhanced in the presence of glucose.

To explain the apparent direct electrochemistry of the GOx enzyme, other reports stated that glucose could be detected based on a decrease of the electro-catalytic response of the reduced form of GOx to dissolved oxygen.[33, 117] For example a composite was constructed by dispersing multi walled carbon nanotubes with a gold nanoparticle colloid stabilized by ionic liquid and chitosan,[118] or by means of complex multicomponent immobilization layers such as GOx-graphene-chitosan.[119] In addition, a conductive cellulose-multiwall carbon nanotube matrix with a porous structure and good biocompatibility was prepared using a room temperature ionic liquid as solvent and encapsulating GOx within this matrix.[120] Finally CdTe QDs of about 3 nm diameter were prepared and an electrochemical biosensing platform for glucose based on CdTe/CNTs electrode was explored.[121] The claimed DET of GOx at these carbon and other nanomaterials is often ascribed to some "special", but not evidently specified, properties of the nanocarbon material or feasibly some specific interaction of the enzyme and the carbon nanotubes.[122-126]

So far, we have focussed on the papers that claim DET for GOx (third-generation glucose biosensor) based on the appearance of a pair of surface bound redox peaks at around -0.46 V *vs.* SCE at pH 7, assumed to be the flavin in the active enzyme, and the change in cathodic current on addition of glucose at -0.25 V vs SCE. It is this claimed third generation of glucose biosensors that we consider and show in Chapter 3. Our argument is that for the great majority of papers that claim such DET to native GOx there is no evidence to support the claim and that the results support a completely different conclusion.[27]

Nevertheless, there are a few examples in which the catalytic oxidation of glucose appears to happen giving some evidence for DET. For instance, a study conducted by Jiang and co-workers[127] attached GOx to a gold electrode using 3,3'-bithiobis-sulfosuccinimidylpropionate (DTSSP). The enzyme was first allowed to react with DTSSP overnight to build an amide bond between its lysine residues and the DTSSP ester group and then the disulfide of the DTSSP was reductively attached to the electrode surface to produce a monolayer of the immobilized enzyme. The authors noticed surface redox peaks for the modified electrode at about -282 mV *vs.* Ag/AgCl in solution at pH 6.3. Remarkably, this is ~80 mV more positive than the potential for adsorbed flavin. The evidence for DET for that modified electrode was also supported by the observed catalytic currents for glucose oxidation at -200 mV *vs.* Ag/AgCl, suggesting that the immobilisation may have distorted the enzyme structure to make the flavin more accessible. Demin and Hall [128] investigated deglycosylated GOx (dGOx). They used a His tag at the C-terminus to immobilize the non-glycosylated GOx at a Cu-NTA modified glassy carbon electrode. Compared to flavin adsorbed at the same electrode, the authors obtained a 104 mV positive shift in the redox potential for the dGOx. Although they only show very preliminary data for the response to glucose, they do report what seems to be catalytic activity for the reduction of oxygen.

There are also examples in which the apoenzyme has been reconstituted around a flavin covalently attached to the electrode surface. For instance Liu and his co-workers[129] reconstituted apoGOx around flavin covalently attached to the ends of SWCNTs aligned normal to a thiol on top of a gold electrode by self-assembly. They demonstrated that for the free flavin the surface redox potential was -423 mV *vs.* Ag/AgCl in pH 7.0 solution and that this moved to -380 mV upon reconstitution into the GOx. No results for glucose response were provided in this paper to show that the reconstituted enzyme was active.

Thus, the existing publications about direct electron transfer of GOx can be split in to three groups: for the first group the presence of cyclic or differential pulse voltammetric peaks (seen around -0.46 V vs SCE) attributable to oxidation or reduction of the flavin cofactor portion of glucose oxidase is claimed as positive evidence for direct electron transfer between the immobilized enzyme and the electrode surface. The second group relates to the first but there are some attempts to prove that the direct electron transfer is due to the FAD in the active site and not from the free FAD or some other effect. Groups have tried to show this using guanidine hydrochloride which can easily strip the FAD active centre from the GOx molecule and/or remove the adsorbed GOx from the electrode surface, however, it has been shown to be quite efficient in eliminating adsorbed free FAD from the electrode surface. The third group investigated the electron transfer for a non-glycosylated redox variant of GOx. This modified GOx enables its active site to be closer to the electrode, and within charge transfer distances suggested by Marcus theory.

1.6 Carbon nanotubes

Carbon nanotubes (CNTs) were first discovered in the early 1990s by Iijima.[130] Extensive research on CNTs was initiated in the 1990s. Indeed, this was preceded in 1980 by the first industrial creation of some products now known as CNTs and also the recorded observations of hollow carbon nanofibers in the early 1950s.[131] CNTs have a tubular structure and composed of hexagonal honeycomb lattices built from sp^2 carbon units.[132] The diameters of CNTs are usually several nanometres and the length is several micrometres.[110] Basically, there are two forms of CNT, single-walled carbon nanotubes (SWCNTs) and multi-walled carbon nanotubes (MWCNTs).[133-134] SWNTs (Figure 1.5A) consist of one layer of a seamless 1D structure of rolled-up graphene[131] and MWCNTs (Figure 1.5B) which, as the name implies, include numerous sheets of graphite rolled into concentric tubes. On one hand, if these nanotubes are located one within the other, the subsequent structure is that of a hollow multi-walled carbon nanotubes (h-MWCNT).[135] On the other hand, if the tubes are situated at a specific angle to the axis of the tube, the resulting structure is that of bamboo-like multi-walled carbon nanotubes

(b-MWCNT). This latter arrangement leads to a high quantity of edge sites on these CNTs.[136] Figure 1.5C shows the various different MWCNT morphologies.

CNTs represent a significant group of nanostructured materials with features very different from those of conventional materials, they have a higher tensile strength than steel and their thermal conductivity is better than all but purest diamond, both properties can be attributed to the strong sp^2 bonds between the individual carbon atoms. Furthermore, the electrical conductivity of CNTs are comparable to copper with the capability to carry bigger currents.[131]

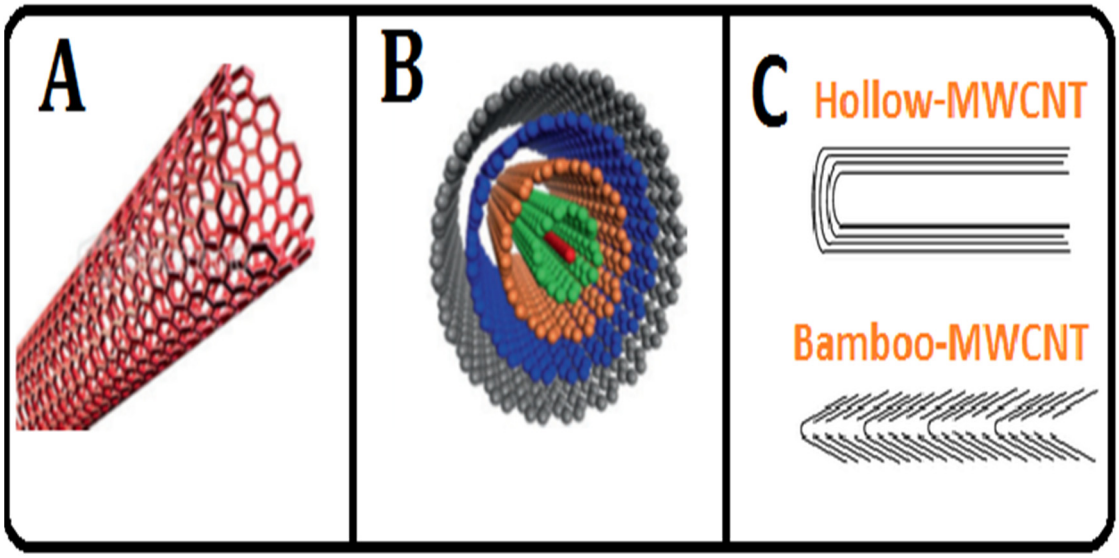

Figure 1.5. *Basic structures of (A) single-walled, (B) multi-walled CNTs,[134,135] and (C) the various different MWCNT morphologies.[136] Adapted from references. 134, 135 and 136.*

CNTs are interesting for use in electrochemical biosensors because of their electron transfer properties.[137] It has been suggested that the ET features of CNTs can be enhanced by producing surface groups such as amino groups, NO_2, carboxyl groups or oxygen.[110, 138] The suitability of CNTs as immobilization templates for enhancing the activity of some enzymes has been actively studied.[139] Moreover, the large surface area of CNTs increases the surface area for enzyme immobilization and CNTs can inhibit electrode fouling which can happen in NADH oxidation.[110, 140]

The construction of electrodes modified with CNTs is difficult because of the low solubility of CNTs in most common solvents. Also, CNTs are usually hydrophobic, so they are not readily dispersed in water. Therefore, CNTs are often dispersed in organic solvents and then drop-coated on to an electrode in order to modify it. CNTs are also combined with Teflon binder (CNT/Teflon composite electrode).[110, 141] Among various functionalities on the CNT surface, in this work, we used a simple carboxyl-modified MWCNT to obtain homogeneous CNT dispersions.

1.7 Research aims and thesis overview

It has been widely claimed that native GOx undergoes direct electron transfer (DET) at nanostructured electrodes. This thesis demonstrates that the vast majority of these claims are incorrect.

Hence, the research described in this thesis mainly focuses on the development and examination of a new strategy for the stable immobilization of redox protein onto carbon-based electrode surfaces for efficient direct electron transfer. The attachment of enzymes at electrodes is of use in many areas including biosensors and biofuel cells. For the direct electron transfer, the orientation of the enzyme active centre, which is often hidden inside the protein shell, has to be controlled in order to minimise the electron transfer distance and, consequently, avoid the use of the redox mediators. Therefore, the electrode surface should be functionalised with monolayers of organic molecules appropriate to accommodate the enzyme of choice, taking into account steric considerations. Also, the polarity of the modified electrode surface around the binding group should be compatible with the protein surface nearby the target functional group, to prevent the denaturation of the immobilised enzyme.

In this study, we will show a pioneering method for the covalent immobilisation of redox proteins at carbon-based electrodes modified with maleimide groups, which only react with cysteine residues introduced at the surface of the protein by genetic engineering. In this way, protein molecules should be immobilised at the electrode surface in a fixed orientation.

Chapter 2 gives details of the equipment, chemicals, the fabrication and characterisation of the working electrodes (GC/MWCNT), the construction of the reference electrodes (SCE and SMSE) as well as the counter electrode, methods for the electrografting and chemical modification of carbon based electrodes, and the immobilisation of the enzymes GOx, CDH and BOD.

Chapter 3 investigates critically the experimental evidence and points out the misconceptions that are common in the literature when DET of GOx is claimed. To that aim, we present experimental results for the study of GOx adsorbed on MWCNTs. The results are essentially identical to those in many papers that claim DET to GOx for CNTs. We will show how these results can be critically analysed to support an entirely different conclusion.

Chapter 4 adopts a flexible and structured method based on the use of site-directed mutagenesis to introduce cysteine residues at specific locations on the protein surface followed by the reaction between the free thiol group and maleimide groups formed at the electrode surface to attach the mutated enzyme. As a model system, we use genetically engineered

cellobiose dehydrogenase (CDH) variants with cysteine at different locations on the enzyme surface.

Moreover, this Chapter aims to study the kinetics and electro-catalytic features of cellobiose dehydrogenase from *Myriococcum thermophilum* (*Mt*CDH). The electro-catalytic properties of the immobilised *Mt*CDH were investigated using cyclic voltammetry, taking into account the effect of solution pH, presence of calcium ion and different substrates. To study the effect of the position of the free cysteine on the enzyme surface, five *Mt*CDH variants were used in this work, which were engineered to have a single free cysteine residue in different positions at the surface of the enzyme.

Chapter 5 provides a kinetic analysis for the results obtained in Chapter 4, based on the steady-state kinetics. A potential-dependent Michaelis-Menten model for the CDH modified GC/MWCNT was constructed and a master equation was employed to simulate the DET and MET experimental results.

Chapter 6 broadens the validity of the same immobilisation method (based on the covalent attachment of cysteine-modified genetically engineered enzymes at maleimide modified electrodes). Bilirubin oxidase (BOD) is a promising redox enzyme in the field of biofuel cells, namely in the construction of efficient bio-cathodes. In this study, BOD variants genetically engineered to bear a free cysteine residue in different positions at their surface were covalently attached to maleimide-modified GC/MWCNT electrodes. BOD is considered to be Cl^- resistant. Thus, the effect of chloride and pH on the redox state of the immobilized BOD were investigated.

Chapter 7 presents an answer for the question that arises from this work: What evidence is required to demonstrate DET? As well as recommendations and suggestions for future work.

Chapter 2 Materials and methods

2.1 Reagents

Glucose oxidase type II (EC 1.1.3.4, from *Aspergillus niger,* 17 U/mg solid), glucose oxidase type X-S (EC 1.1.3.4, from *Aspergillus niger,* 228 U/mg solid), glucose oxidase type VII (EC 1.1.3.4, from *Aspergillus niger,* 100 U/mg solid) were purchased from Sigma, and stored at - 20°C when not in use. Glucose oxidase type GO3A, batch 614Z, (EC 1.1.3.4, from *Aspergillus niger,* 335 U/mg protein), GOx / CAT ratio ≥ 27500 was purchased from BBI Solutions, UK. Catalase enzyme (CAT) from bovine liver 2000-5000 U/mg was purchased from Sigma. The cellobiose dehydrogenase variants were a kind gift from Dr Roland Ludwig from the Department of Food Science and Technology Food Biotechnology Laboratory, BOKU-University of Natural Resources and Life Sciences, Muthgasse 18, 1190 Vienna, Austria. The bilirubin oxidase variants were kindly supplied by Dr Nicolas Mano from the Centre de Recherche Paul Pascal (CRPP-UPR 8641), 115 Avenue Albert Schweitzer 33600 Pessac, France. Multi-walled carbon nanotubes (30 ± 10 nm in diameter and 1 – 5 μm in length) were purchased from NanoLab, Inc. Multi-walled carbon nanotubes carboxylic acid functionalized (> 8% carboxylic acid functionalized, 9.5 nm avg. diameter and 1.5 μm in length) were purchased from Aldrich. All other chemicals were of analytical grade and used without further purification. All aqueous solutions were prepared using deionized Millipore-Q water (18.2 MΩ cm) from a Purite purification system. All glassware was immersed in 5% Decon 90 (BDH) with distilled water overnight. They were then washed and rinsed with deionised water thoroughly before drying in an oven (LEEC Limited) at 40 °C prior to usage. Argon (Pureshield, 99.998%) and oxygen were supplied by BOC gasses. The other chemicals used in this study are listed in Table 2.1.

Table 2.1. *List of Chemical used in this study.*

Chemical	**CAS Number**	**Purity / Grade**	**Supplier**
1, 4 Dioxane	123-91-1	Certified ACS	Fisher Scientific
3-Succinimidopropionic acid	5724-76-5	≥97.0 %	Sigma Aldrich
Acetone	Lab reagent grade	N-Grade	Fisher Scientific

Acetonitrile	75-05-8	HPLC	Fisher Scientific
Alumina	40-6321-016/080		Buehler
Calcium chloride	10035-04-8	≥99.0%	Fisher Scientific
Cellobiose	528-50-7	≥98.0%	Sigma Aldrich
Citric acid	77-92-9	≥99.5%	Sigma Aldrich
D (+) glucose	50-99-7	≥99.5%	Sigma Aldrich
Dimethylformamide (DMF)	68-12-2	HPLC	Fisher Scientific
Ethanol	64-17-5	HPLC	Fisher Scientific
Ferrocenecarboxylic acid	1271-42-7	≥97.0%	Sigma Aldrich
Flavin adenine dinucleotide disodium salt hydrate	84366-81-4 (anhydrous)	≥ 95.0%	Sigma Aldrich
Hydrochloric acid	7647-01-0	37%	BDH
L (+) glucose	921-60-8	≥99.0%	Sigma Aldrich
Liquid mercury		99.9998	Alfa Aesar
Mercury chloride		≥95.0%	Alfa Aesar
Mercury sulphate		≥95.5%	BDH
N-(2-aminoethyl) acetamide	1001-53-2	≥90.0%	Sigma Aldrich
N-(3-dimethylaminopropyl)-*N*′-ethylcarbodiimide (EDC)	25952-53-8	≥98.0%	Sigma Aldrich
N-Boc-1,6-hexanediamine	51857-17-1	≥98.0%	Sigma Aldrich
N-Boc-6-aminohexanoic acid	6404-29-1	≥99.0 %	Sigma Aldrich
N-hydroxysuccinimide (NHS)	6066-82-6	≥98.0%	Sigma Aldrich

N-Maleoyl-β-alanine	7423-55-4	≥97.0 %	Sigma Aldrich
Platinum (mesh)	7440-06-4	99.9%	Goodfellow
Potassium chloride	7447-40-7	≥ 99%	Fisher Scientific
Sodium dihydrogen orthophosphate (Sodium phosphate monobasic)	7558-80-7	≥ 99%	Sigma Aldrich
Sodium hydroxide	1310-73-2	≥97.0%	Sigma Aldrich
Tetrabutylammonium tetrafluoroborate (TBATFB)	429-42-5	≥99.0%	Sigma Aldrich
Tris(hydroxymethyl)aminomethane	77-86-1	≥99.9%	Sigma Aldrich

2.2 Electrodes

2.2.1 Working electrodes

Working carbon electrodes used in this study are glassy carbon (GC), boron doped diamond (BDD) and multi-walled carbon nanotubes (MWCNT). 3 mm diameter (0.071 cm^2) GC disc electrodes (SIGRADUR HTW Hochtemperatur – Werkstoffe GmbH, Germany), sealed in glass tubes and contacted using copper wire and melted indium (Aldrich), BDD electrodes in inert Teflon body were purchased from Windsor Scientific (Figure 2.1 A) . To prepare the GC/ CNT electrodes a 5 µL of the MWCNT dispersion were placed onto the clean surface of each GC electrode, using a plastic mask (Figure 2.1 B) of the same dimension as the GC disc to control the spread of the CNT dispersion, and allowed to dry at room temperature for 2 days. 5 µL of the dispersion was used as this gives a reasonably uniform MWCNT coverage. Figure 2.2 shows the optical micrographs of glassy carbon (GC) electrodes modified with different volumes of the 1 mg/mL DMF dispersion of multi-walled carbon nanotubes (MWCNT, > 8 % carboxylic acid functionalised, 9.5 nm avg. diameter, 1.5 µm length, Sigma-Aldrich). 5 µL was chosen for the enzyme immobilisation experiments as it gives a reasonably uniform surface coverage.

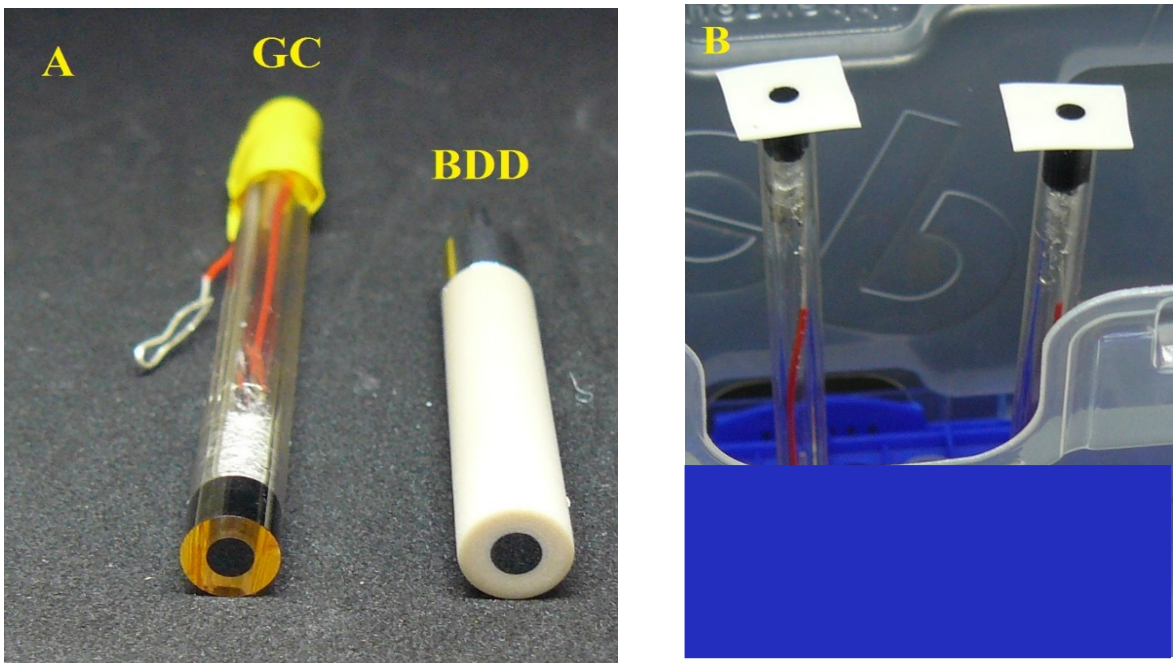

Figure 2.1. *(A) Examples of the GC and BDD electrodes employed during of this study. (B) The plastic mask of the same dimension as the GC disc which was used to control the spread of the CNT dispersion.*

CNTs are regarded as a toxic material. Indeed, depending on the method of creation, CNT may contain a number of toxic residual metallic impurities such as Co, Fe, Ni, and Mo, all of which have reported toxic effects. Other reports have highlighted the potential role of CNT synthesis size, composition, surface area, and organics in the toxicity of nanotubes.[142] Because of the associated hazards of handling and disposing of CNT, we treated this material carefully, for instance, lab coat, mask, safety glasses, and double gloves were worn at all time when preparing the CNT dispersion. All used CNT dispersions, samples, and modified electrodes were kept in a plastic box before disposal.

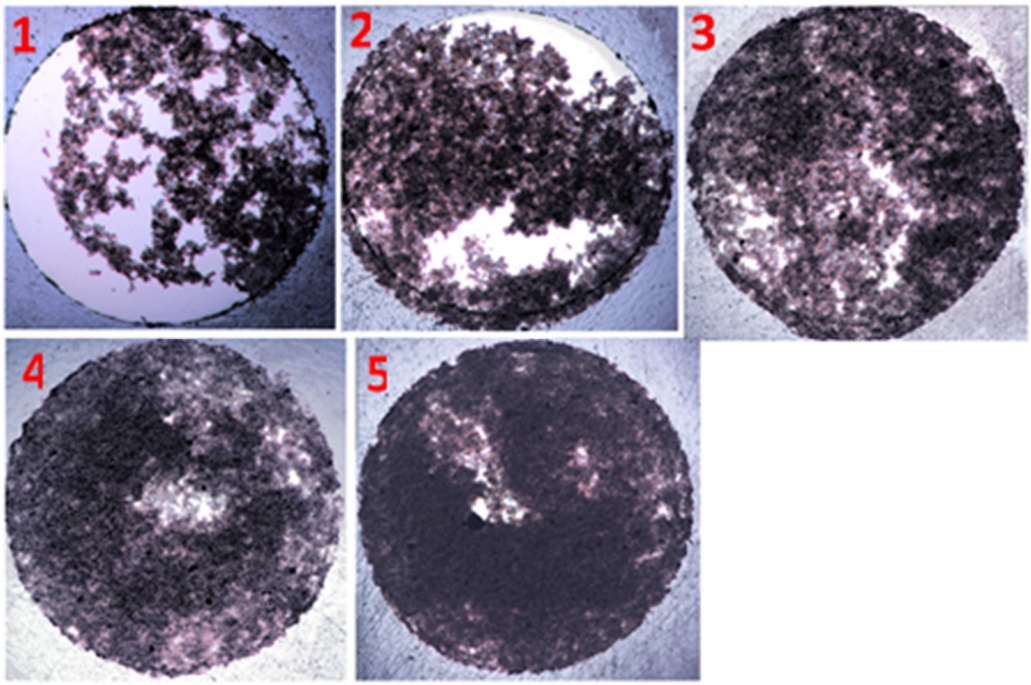

Figure 2.2. *Optical microscope images of GC electrodes (3 mm in diameter) modified with MWCNT by drop casting 1, 2, 3, 4 and 5 µL of 1 mg mL^{-1} MWCNT solution in DMF.*

In order to characterize the immobilised MWCNT onto the GC, images were taken with a Jeol 6500F field emission gun scanning electron microscope (FESEM). The FESEM was utilized to characterize the morphology of the MWCNT and the carboxylic acid functionalized MWCNT with the electron beam energized at 20 kV.

Figure 2.3 shows the FESEM images of the carboxylic acid functionalized MWCNT on the surface of the GC electrode at different magnification using imaging mode of secondary electron image (SEI). At lower magnification, the MWCNT has a rough electrode surface with flake-like structure as seen in Figure 2.4. As higher magnification was employed, a web-like structure which is attributed to the MWCNT can be seen as shown in Figure 2.3. Both functionalised and bare MWCNTs are formed as bundles with some bundles twisted together.

Figure 2.4 shows the FESEM images of the bare MWCNTs on a GC electrode prepared using the drop-casting technique. Unlike MWCNTs functionalised with carboxylic acid, the bare MWCNTs have a much rougher surface with a granular structure at low magnifications as seen in Figure 2.4. However, the bare MWCNTs have the same morphologies as the functionalised MWCNTs at higher magnification as shown in Figure 2.3. The FESEM images also reveal that both functionalised and bare MWCNTs are well distributed on the surface of the GC electrode. This implies that the surface area of the bare MWCNTs may be larger than the surface area of the MWCNTs functionalised with carboxylic acid.

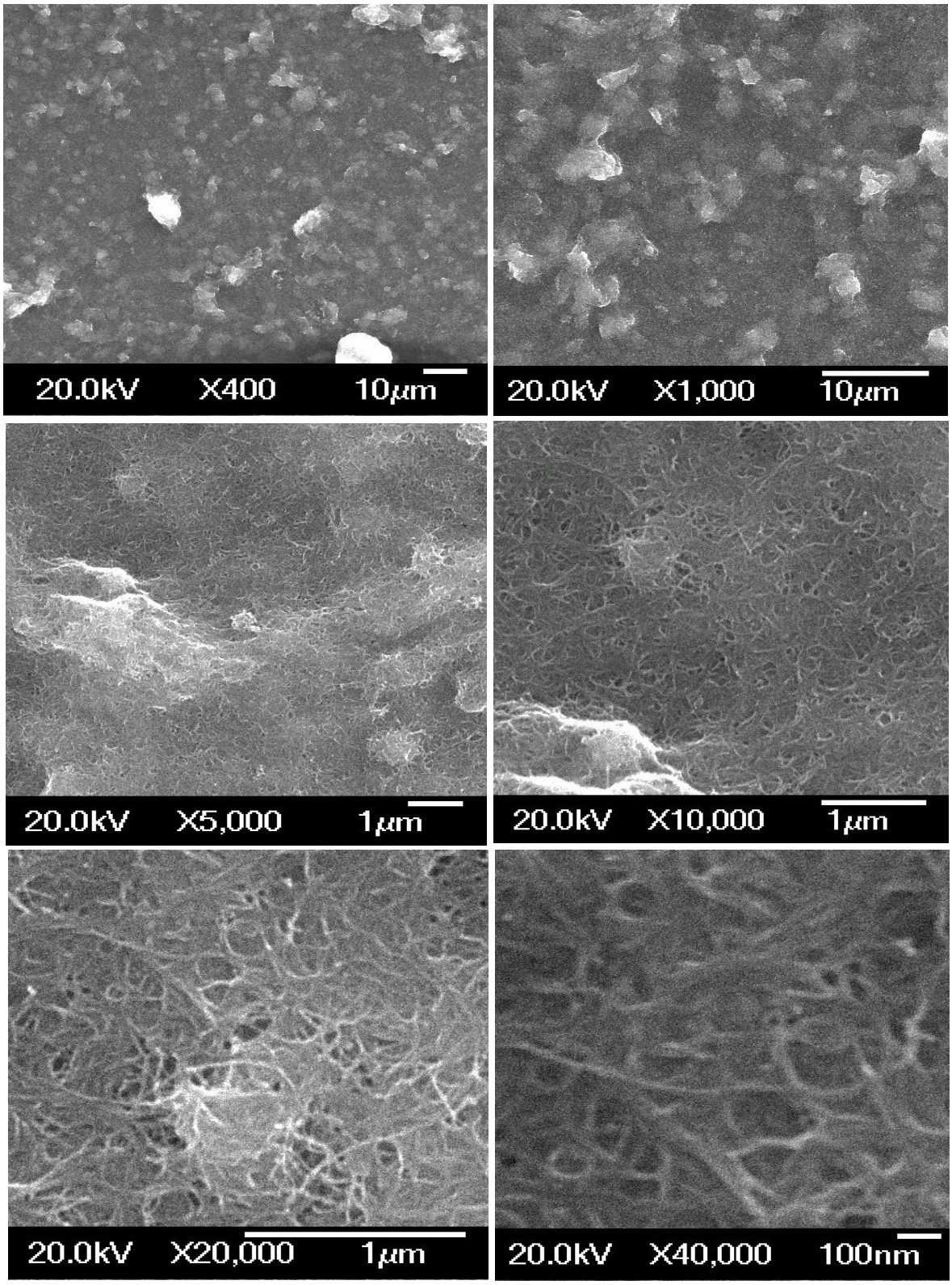

Figure 2.3. *FESEM images of the carboxylic acid functionalized MWCNTs on the surface of GC electrode with different magnifications. The GC/MWCNT electrode was prepared by drop casting of a 5 μL aliquot of 1 mg mL^{-1} MWCNT dispersion onto the cleaned surface of GC.*

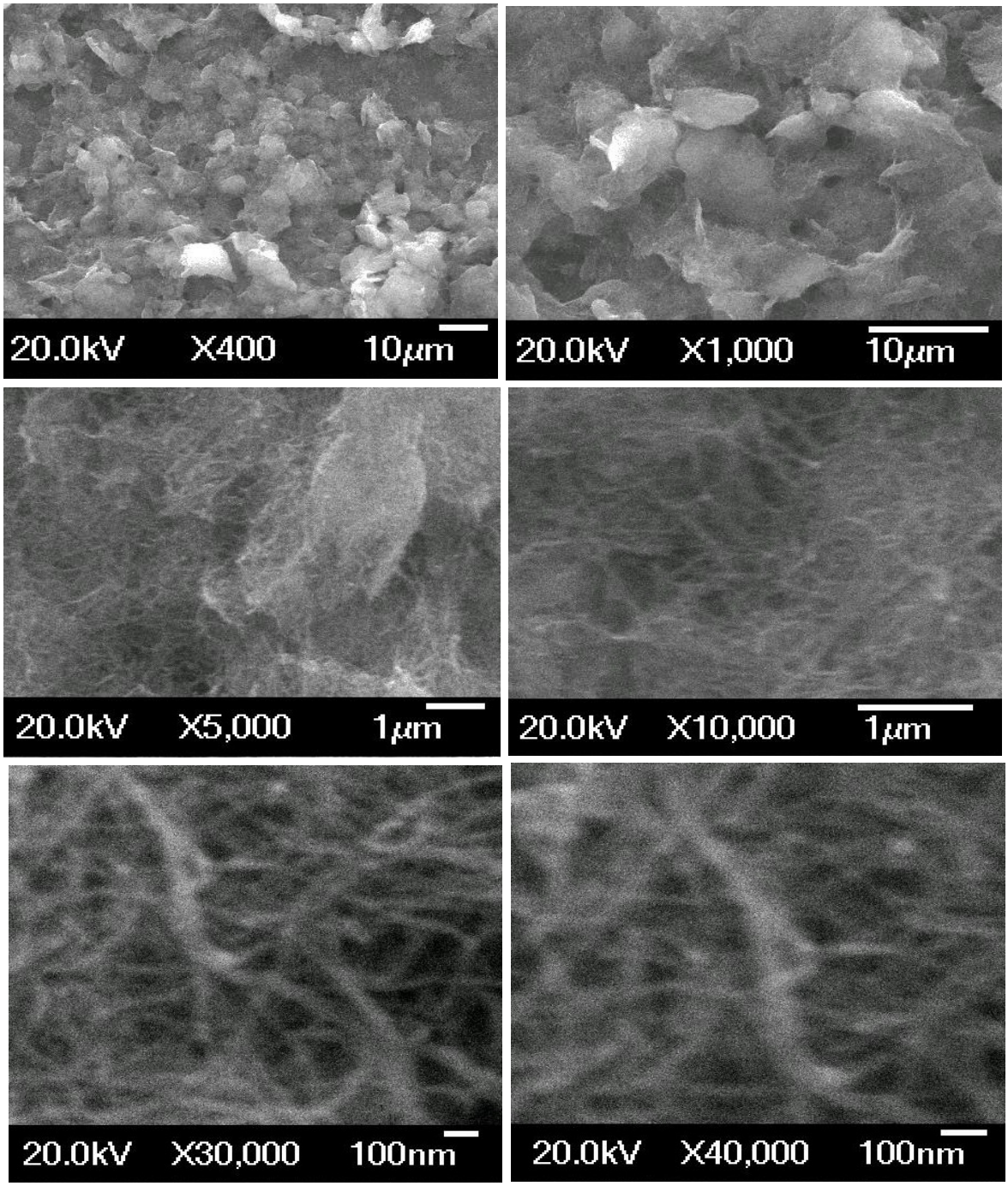

Figure 2.4. *FESEM images of MWCNTs on the surface of GC electrode with different magnifications. The GC/MWCNT electrode was prepared by drop casting of a 5 μL aliquot of 1 mg* mL^{-1} *MWCNT dispersion onto the cleaned surface of GC.*

2.2.2 Reference electrodes and counter electrodes

For all electrochemical measurements described in this study, a homemade saturated calomel electrode (SCE) was used as the reference electrode. However, when the chloride ion is not desired in the electrolyte, a homemade saturated mercurous sulfate electrode (SMSE) was

employed as the reference electrode. The reference electrodes were fabricated as reported by Bartlett[143] and inherited from the previous student. The reference electrodes consist of two body parts; one piece was a glass tube with a platinum wire sealed in the middle of the tube in which both ends of the wire were left exposed to the air and another piece was like a Pasteur pipette with a fine sintered glass frit at the tip as shown in Figure 2.5.

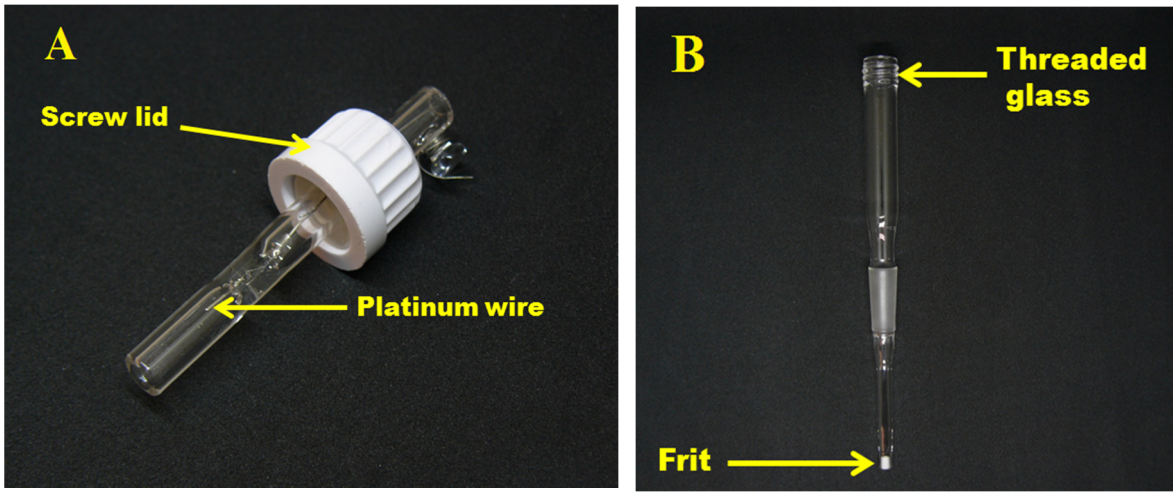

Figure 2.5. *(A) A platinum wire sealed inside a glass tube with both ends of the wire are exposed. The screw lid was used to connect the two body parts together. (B) pipette-like glass body with thread at one end and frit at the other end.*

Liquid mercury was placed on one side of the glass tube until the platinum wire was entirely covered. In making an SCE, a paste made out of Hg_2Cl_2, KCl, and liquid mercury was put in the glass tube and a glass wool plug was used to hold the paste in the tube. The filled glass tube is shown in Figure 2.6.

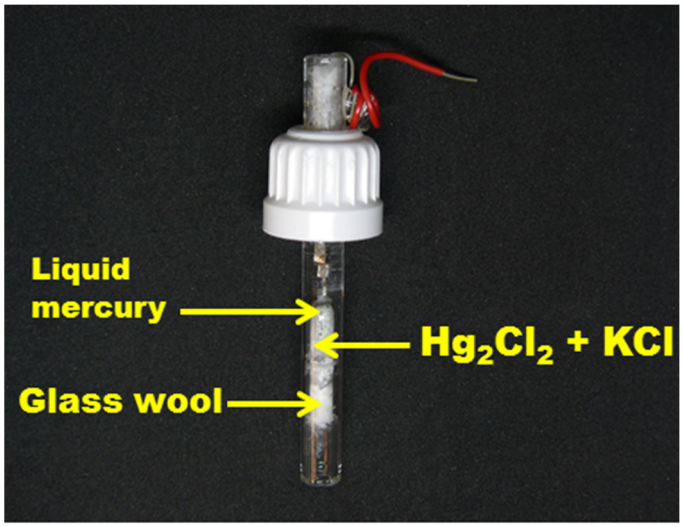

Figure 2.6. *The glass tube filled with liquid mercury and a paste made out of Hg_2Cl_2 and KCl. A glass wool plug was used to hold the paste in the tube.*

The glass tube was then put inside the pipette-like glass body which was filled with saturated KCl. The same procedure was followed to make an SMSE but a paste made out of K_2SO_4 and Hg_2SO_4 was used instead of the paste made out of the Hg_2Cl_2 and KCl while the pipette-like glass body was filled with saturated K_2SO_4 instead of the saturated KCl respectively. The tip of the SMSE and SCE were immersed in saturated K_2SO_4 and saturated KCl respectively when not in use. The reference electrodes were always rinsed with the purified deionised water and dried in a stream of argon gas before use. The reference electrodes were checked regularly for bubbles, and the respective solution was added when necessary. The SMSE was normally employed in order to avoid chloride ion contamination. In most cases, the SCE was used for easier comparison.

A platinum gauze (1.0 cm^2) was employed as the counter electrode. A platinum wire was sealed inside a glass body with both ends of the platinum wire exposed to the air. A platinum gauze was connected to the platinum wire using a spot welder. The counter electrodes were cleaned with flame prior to usage to remove any contaminants. Figure 2.7 shows the platinum gauze used during the electrochemical experiments.

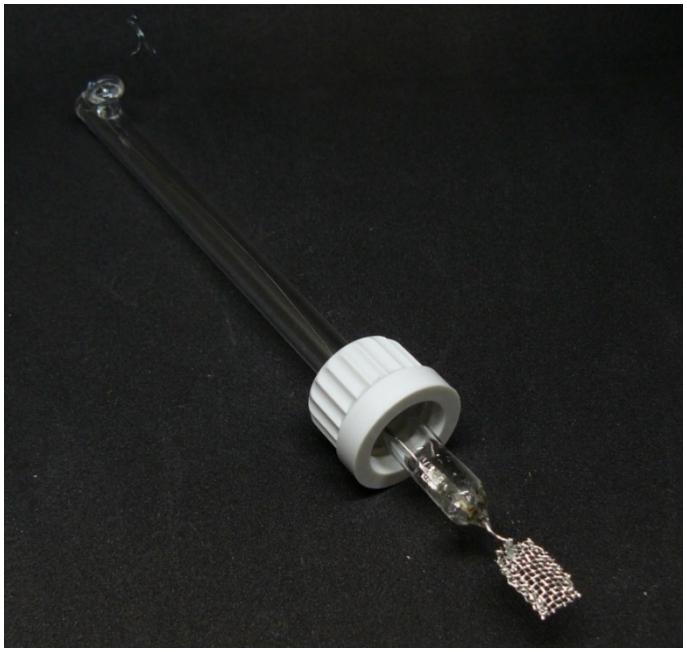

Figure 2.7. *Platinum gauze used in this work.*

2.3 Electrochemical cell

Electrochemical glass cells (10 mL) with five necks were employed when the solutions need to be either deoxygenated with Ar (Pureshield, BOC) or oxygenated with the pure oxygen (Pureshield, BOC). Figure 2.8 shows electrochemical cell used in this work.

Figure 2.8. *The jacketed glass cell used for the electrochemical experiments in this work; five-neck cell. The glass cells can be connected to a thermostatically controlled water bath using rubber tubes.*

Electrochemical measurements were performed in the glass cell with a standard three-electrode arrangement, using either a μAutolab type III or an Autolab PGSTAT 302 (Ecochemie, Netherlands). The three-electrode system consists of a working electrode, a reference electrode and a counter electrode Figure 2.9 shows a schematic diagram of the experimental setup used in this project.

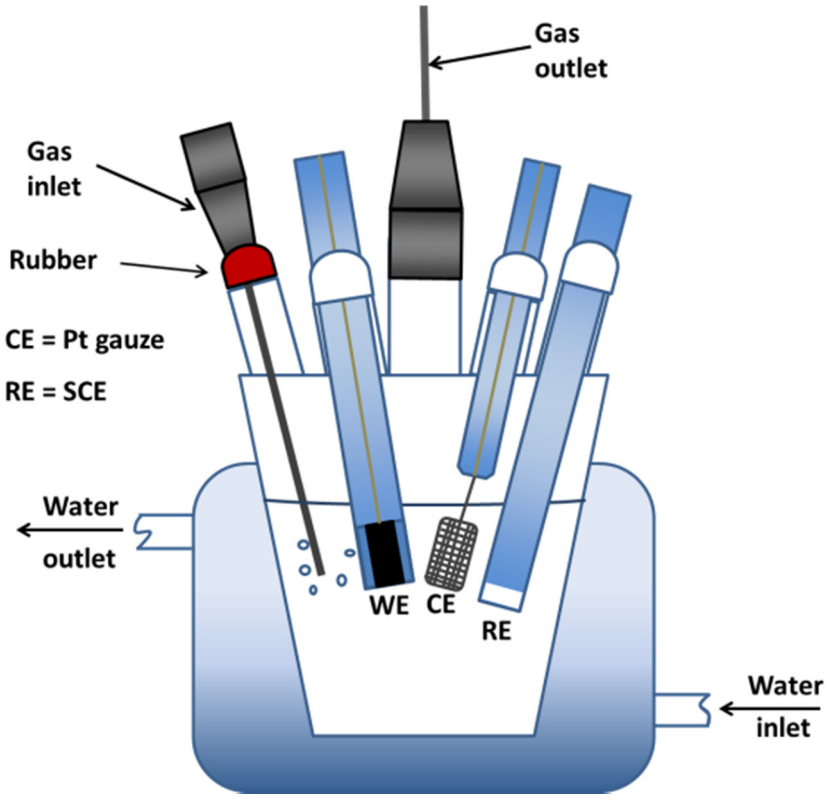

Figure 2.9. *Schematic diagram of the experimental setup used in this project.*

2.4 Glassy carbon (GC) electrode polishing

Before the experiments, the GC electrodes were polished by using silicon carbide polishing paper (grade 1200), then alumina slurries (1.0 and 0.3 μm, Buehler) on polishing cloths (Buehler). The polished GCE was sonicated in deionized water (DI) for 7 min and it was dried in a stream of argon (Ar) gas. Then, it was sonicated again in ethanol for 13 min. Furthermore, the cleaned surface of glassy carbon electrodes were dried in a stream of argon (Ar) gas and the cleaned electrodes were covered with pipette tips.

2.5 Fabrication of GC/MWCNT electrodes and immobilization of GOx

10 mg of MWCNTs was dispersed in 10 mL dimethylformamide (DMF) with the aid of ultra-sonication to give a 1 mg mL^{-1} black suspension. The MWCNT modified glassy carbon (GC/MWCNTs) electrode was prepared by drop casting of 5 μL of the MWCNT dispersion onto the cleaned surface of GC. Then, the modified GC electrode was allowed to dry at ambient temperature before use. To immobilize GOx, the GC/MWCNT electrode was incubated in a solution of 1 kU GOx (corresponding to a 1 mM solution of enzyme) dissolved in 0.1 M phosphate buffer solution (pH 6.8) for 12 hours. 1 U of GOx will oxidize 1.0 μmole of β-D-glucose to D-gluconolactone and H_2O_2 per minute at pH 5.1 at 35 ˚C.

2.5.1 Electrochemical analysis of GOx-modified GC/MWCNT electrodes

Cyclic voltammetry measurements of GOx-modified GC/MWCNT electrodes were carried out in 0.1 M deoxygenated phosphate buffer solution (pH 6.8) from -0.8 to -0.2 V *vs.* SCE at a scan rate of 60 mV s^{-1}. All solutions were deoxygenated by bubbling gas argon for 30 min before applying potential and were blanketed with argon atmosphere during the entire experimental period to protect the solution from oxygen. The glucose experiments were done in oxygen saturated PBS, aliquots of glucose (500 mM) in 0.1 M phosphate buffer solution (pH 6.8) were added then the solution in the electrochemical cell was mixed using magnetic stirrer and CVs reported after each addition at a scan rate of 60 mV s^{-1} vs. SCE. All experiments were performed in thermostated electrochemical cell at 24 °C.

2.5.2 Determination of the pH dependent redox potential of glucose oxidase

Cyclic voltammetry measurements for GC/MWCNT/GOx electrodes were carried out in 0.1 M buffers, pH values (4.5 – 8.5). Measurements were performed in buffer (depending on pH sodium citrate, sodium phosphate, or tris (hydroxymethyl) aminomethane (TRIS)-buffer were

used) with 0.1 M potassium chloride and 5 mM magnesium chloride. Buffer solutions were deoxygenated by purging with Ar gas for at least 30 min prior to electrochemical measurements by CV.

Table 2.2. *Composition of the buffers used in the determination of the pH dependent redox potential of glucose oxidase as reported by Vogt et al.*[144]

pH	Buffer(s)
4.5	0.1 M citrate buffer, 0.1 M KCl, 5 mM $MgCl_2$
5.0	
5.5	
6.0	0.1 M citrate buffer, 0.1 M KCl, 5 mM $MgCl_2$; in other measurements: 0.1 M phosphate buffer, 0.1 M KCl, 5 mM $MgCl_2$
6.5	0.1 M phosphate buffer, 0.1 M KCl, 5 mM $MgCl_2$
7.0	
7.4	
7.6	
7.8	
8.0	0.1 M Tris buffer, 0.1 M KCl, 5 mM $MgCl_2$
8.5	

2.6 Stepwise modification of GC, BDD and GC/MWCNT electrodes with maleimide

Working carbon electrodes used in this study, GC, BDD and MWCNT were modified with a mixture of two primary amines, Scheme 2.1. A solution containing *N*-Boc-1,6-hexanediamine (2 mM), *N*-(2-aminoethyl) acetamide (18 mM) and TBATFB (0.1 M) in acetonitrile was prepared and deoxygenated with argon (20 min) in the electrochemical cell. The covalent attachment of the primary amines onto GC/MWCNT electrodes was carried out by chronoamperometry holding the electrode potential at +2 V *vs.* SCE for 180 s. Then the

electrode was washed with acetonitrile, and the BOC-linker was de-protected in 4 M HCl in dioxane (45 min) under gently stirring. For the coupling of 6C-spacer, a solution containing *N*-Boc-6-aminohexanoic acid (10 mM), NHS (60 mM) and EDC (0.1 M) in DMF was prepared and stirred for 15 min. Electrodes were immersed for 16 h, then washed with acetonitrile and water and dried. The 6C-spacer was de-protected in 4 M HCl in dioxane (45 min) under gently stirring. For the coupling of maleimide, a solution containing *N*-maleoyl-β-alanine (25 mM), NHS (60 mM) and EDC (0.1 M) in DMF was prepared and stirred for 15 min. Electrodes were immersed for 16 h, then washed with acetonitrile and water and dried.

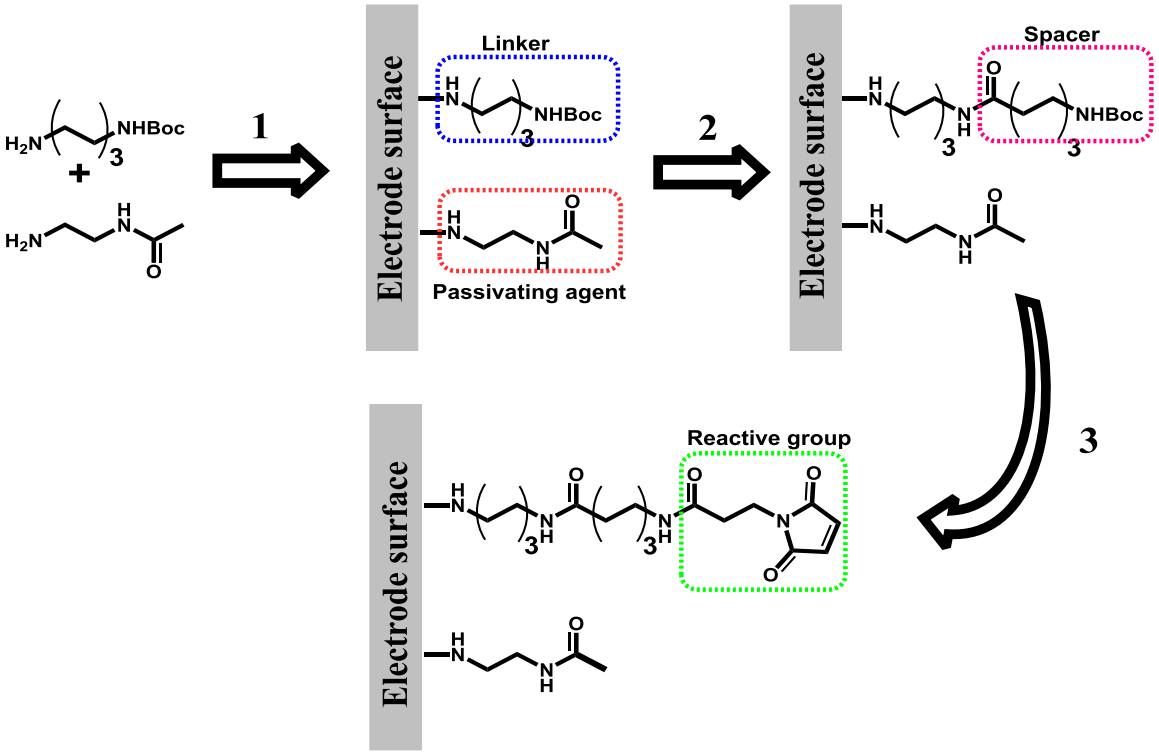

Scheme 2.1. *Sequential electrochemical and solid-phase preparation of maleimide-modified working electrodes. Reagents and conditions: 1) Attachment of linker and capping group at the electrode surface via electrochemical oxidation of N-Boc-1, 6-hexanediamine and N-(2-aminoethyl) acetamide in acetonitrile containing TBATFB, applying a constant potential of 2 V vs. SCE for 180 s. 2) Boc-deprotection of the linker in 4 M HCl in dioxane (45 min), followed by EDC/NHS coupling of 6C- spacer in DMF (16 h). 3) Boc–deprotection of the spacer in 4 M HCl in dioxane (45 min), followed by EDC/NHS coupling of maleimide group in DMF (16 h).*

2.7 Immobilization of *Mt*CDH variants

The variants were supplied in 50 mM acetate buffer (pH 5.5) and stored in the freezer at -30 °C. The storage buffer of the enzyme was exchanged from a pH 5.5 acetate (50 mM) to a pH 7.0 phosphate buffer (50 mM) using mini dialysis devices provided with a PES membrane (Fisher Scientific) with 10 kDa cut off. 10 µL of enzyme solution were placed in each membrane and the dialysis devices were immersed in gently stirred phosphate buffer (250 mL) for 10

minutes; 250 mL of fresh buffer were then put in and the dialysis units were immersed for 20 minutes; finally the dialysis units were immersed in 500 mL of fresh buffer in the fridge for 2 hours. After dialysis, 3 µL of the CDH variant of choice were placed on each maleimide-modified electrode, which was then stored in the fridge (4 °C) overnight.

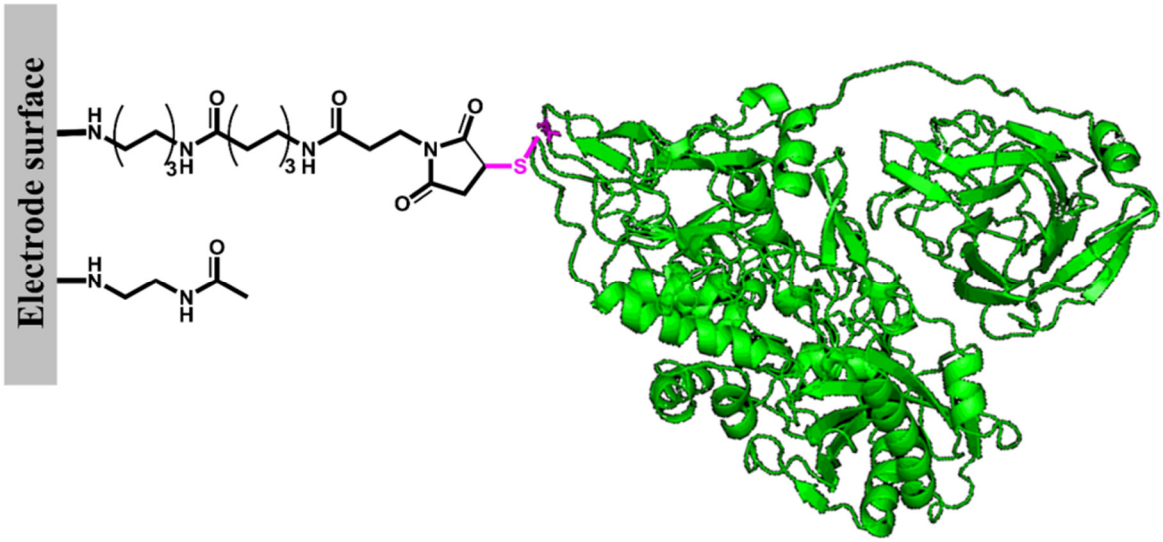

Scheme 2.2. *Immobilization of the CDH variant of choice from a pH 7.0 solution on the maleimide-modified working (GC, BDD, and MWCNT) electrodes.*

2.7.1 Analysis of CDH-modified GC/MWCNT electrodes

Cyclic voltammetry measurements of CDH-modified electrodes were performed in 50 mM Tris buffer (pH 7.4), containing 30 mM $CaCl_2$. All solutions were deoxygenated by bubbling gas argon for 30 min before applying potential, and for two minutes after every addition of glucose from a 1 M stock solution (in the same buffer used for the measurement). CVs were performed utilising the software Nova 1.10, usually sweeping the potential at 1 mV/s from -0.35 to 0.1 V *vs.* SCE in direct electron transfer (DET) experiments. Electrodes were also tested for mediated electrochemistry in deoxygenated 50 mM tris buffer (pH 7.4), in the presence of 0.2 mM ferrocenecarboxylic acid and 30 mM $CaCl_2$ at 2 mV s^{-1} by cycling the potential from 0.0 to 0.4 V *vs.* SCE. Aliquots of glucose (1 M) in deoxygenated 50 mM tris buffer (pH 7.4) in the presence of 0.2 mM ferrocenecarboxylic acid, and 30 mM $CaCl_2$ were added and CVs reported after each addition. The data were analysed using the software Origin 9.

2.8 Immobilization of *Mo*BOD variants

The variants were supplied in 25 mM sodium phosphate buffer (pH 6.0) and stored in the freezer at -80 °C. The storage buffer of the enzyme was exchanged from a pH 6.0, 25 mM NaPi

buffer to a pH 7.0, 50 mM phosphate buffer using the same method which has been described in Section 2.7. After dialysis, 3 µL of the BOD variant of choice were placed on each maleimide-modified electrode, which was then stored in the fridge (4 °C) overnight.

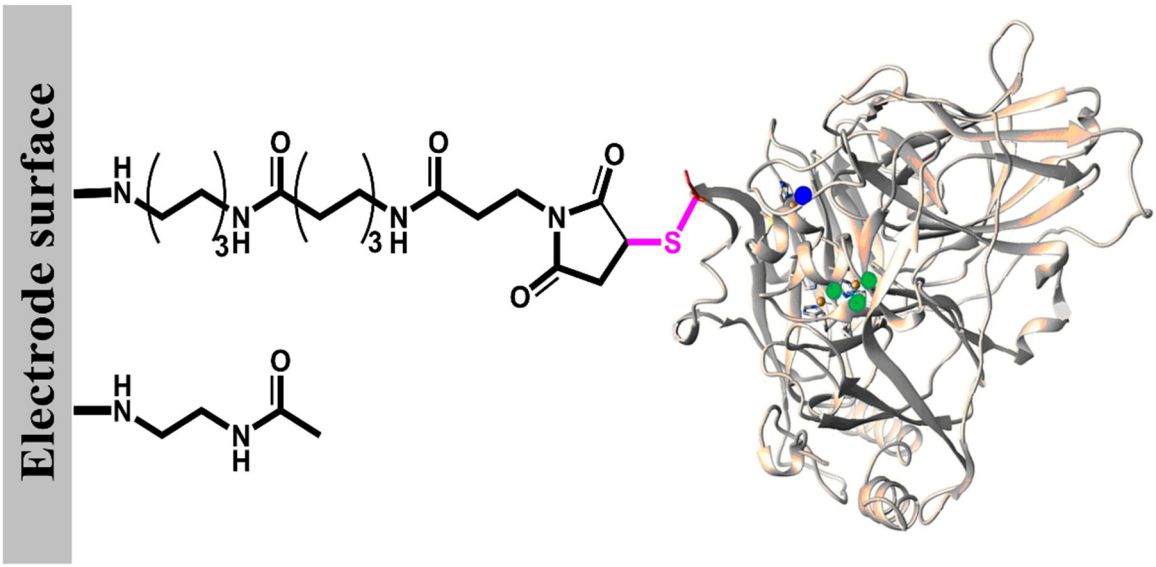

Scheme 2.3. *Immobilization of the BOD variant of choice from a pH 7.0 solution on the maleimide-modified GC/MWCNT electrodes.*

2.8.1 Oxygen reduction studies on the BOD-modified GC/MWCNT electrodes

For oxygen reduction reaction on the BOD-modified GC/MWCNT electrodes, oxygen was purged through the cell containing 10 ml of buffer solution for 8 minutes. This was optimized by bubbling oxygen for different durations such as 3, 5, 8 and 10 minutes. 8 min was adopted as it gives a maximum ORR limiting current. Therefore, no more oxygen purging was employed.

Chapter 3 Native glucose oxidase (GOx) does not undergo direct electron transfer (DET) at carbon nanotube electrodes

3.1 Overview

Glucose oxidase (GOx) (E.C. 1.1.3.4) has been a long-standing field of research for electrochemical applications, dating back to the 1960s when Clark and Lyons pioneered the development of oxygen electrode based enzyme electrodes.[145-146] The employment of the GOx in the field of the biosensors is gaining increasing popularity because it is it is readily available and highly active, it is a very stable and robust enzyme and, most significantly, the monitoring of its substrate, β-D-glucose, *in vivo* is vital for the management of diabetes. Therefore, a huge number of studies on electrochemical glucose biosensors using GOx have performed since Clark's initial publication. These electrochemical glucose biosensors can be categorised into three classes. So-called "first generation"[92] glucose biosensors, it is either a layer of GOx entrapped over an oxygen electrode, measurements are made based on the monitoring of a co-reactant (oxygen), or electrode consists of a metallic sensing layer covered by immobilized glucose oxidase, measurements are made based on the monitoring of product (hydrogen peroxide) of the natural enzymatic reaction.[147] The "second generation" glucose biosensors have been designed by replacing the oxygen with diffusive artificial redox mediator in the enzymatic reaction, the notable example being the work of Cass *et al.*[148] using ferrocenes. The "third generation" glucose biosensors, in which, the electron gained from glucose oxidation is transferred directly to the electrode via the active site of the enzyme; direct electrochemical oxidation of the flavin active site of glucose oxidase occurs. It is this last case that we consider in this Chapter.

It has often been suggested that native GOx undergoes direct electron transfer (DET) at nanostructured electrodes. Over the past 15 years, DET has been reported in the case of electrodes based on the enzyme GOx and carbon nanotubes (CNT).[111, 113-114, 118, 121, 123, 138, 149-185] The redox active centre of GOx is shielded from the electrodes by a glycoprotein coat preventing efficient electron tunnelling.[186-188] The claimed DET of GOx at these nanocarbon materials is often ascribed to some "special", but not clearly specified, properties of the nanostructured materials or possibly some specific interaction of the enzyme and the carbon nanotubes. The present study focuses on the indications that stand against the claimed DET of the GOx modified CNT electrode. Our argument is that in the vast majority, if not all, of the research papers which claim such DET to GOx there is no evidence to support the claim and

that the results support an entirely different explanation. GOx and MWCNTs are not simple, pure, well defined, reagents; both can contain significant amounts of impurities, and both can be subject to batch to batch variations. In this study, four different suppliers/sources of glucose oxidase and two of MWCNTs have been used to examine the claimed DET of GOx at these nanocarbon materials.

3.2 Aim of the work

The claimed DET of the GOx that has been reported in the literature is debatable and arguably incorrect. In this chapter, we present expermental results for GOx adsorbed on MWCNTs, which show that the results can be explained by adsorption of enzymatically active GOx at the electrode surface. The presented data indicate that DET may not be happening for any GOx/CNT-based electrode. The electrodes were sensitive to D-glucose in oxygenated solutions indicating the O_2-mediated enzymatic oxidation of D-glucose. The experimental evidence that are common in the literature (when DET of glucose oxidase is claimed) are critically examined to point out the fallacies and errors in a logical manner. The results that will be shown in this chapter are essentially identical to those in many papers in the literature that claim DET to GOx for CNTs. We will show how these results can be critically analysed to support an entirely different conclusion.

3.3 Glucose oxidase (GOx)

Glucose oxidase from *Aspergillus niger* is a homodimer, containing two non-covalently bound flavin adenine dinucleotide (FAD) cofactors, one per subunit.[189] The enzyme is heavily glycosylated, with a carbohydrate content of 16 - 25%.[190] Its molecular weight varies from approximately 130 to 175 kDa depending on the level of glycosylation.[191] GOx belongs to the glucose/methanol/ choline (GMC) oxidoreductase family. A significant feature of GOx from *Aspergillus niger* is its very high substrate specificity for the β-anomer of D-glucose.[192] The enzyme catalyses the oxidation of β-D-glucose to gluconic acid by employing molecular oxygen as an electron acceptor. Its catalytic reaction occurs via a "ping-pong" mechanism in which one of the oxidised flavin active sites (FAD) in the GOx reacts with the D-glucose to give the reduced flavin ($FADH_2$) and the product D-glucono-1,5-lactone.

β-D-glucose ($C_6H_{12}O_6$) + GOx(FAD) →

D-glucono-1,5-lactone ($C_6H_{10}O_6$) + GOx($FADH_2$) (*Eq.* 3.1)

The reduced flavin in the GOx is then oxidised by reaction with oxygen

$GOx(FADH_2) + O_2 \rightarrow GOx(FAD) + H_2O_2$ (*Eq.* 3.2)

The two flavin active sites are buried deeply within the structure of GOx and there is no evidence for redox communication between them.[190] Despite the fact that the amino acid content of GOx has been investigated and explained on a number of publications, but little was known about its crystal structure until the early 1990s.[189] Indeed, the early work in the field of glucose biosensors was performed without the knowledge of the crystal structure of the enzyme. The crystal structure was produced and published by Hecht *et al.* in 1993.[190, 193] Figure 3.1 shows the cartoon representation of secondary structure of GOx. The access to the flavin active site is down a narrow channel developed at the interface between the two homodimers. Such structure serves to insulate the flavin active sites from non-specific electron transfer with redox species in the biological system and controls the local environment around the flavin ensuring high selectivity towards β-anomer of D-glucose[194] and no activity with L-glucose.

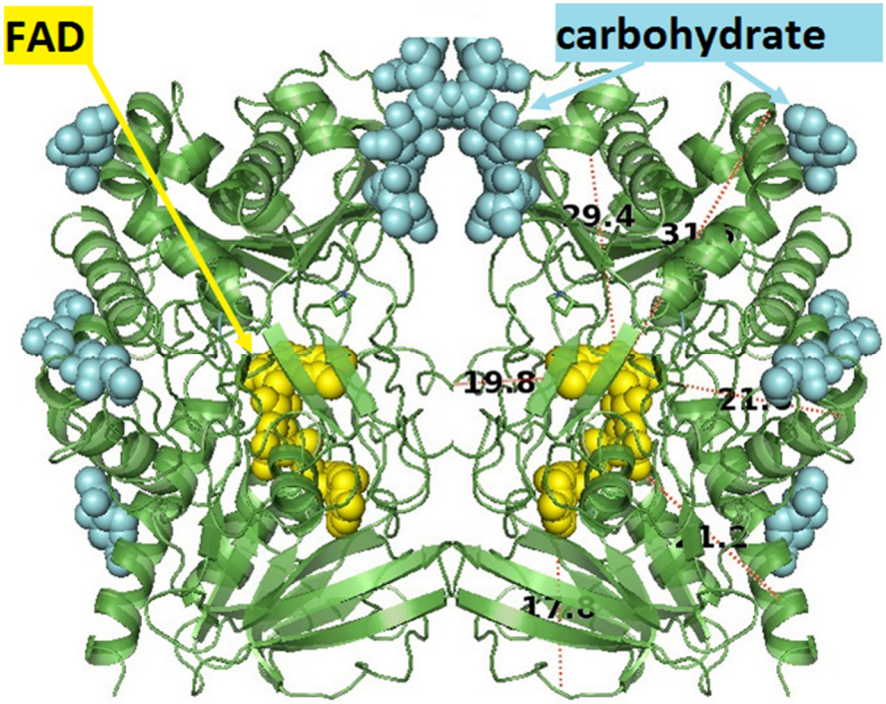

Figure 3.1. *Cartoon representation of secondary structure of GOx. The image was obtained with PyMol software, PyMol visualizations are based on the crystal structure of GOx from Aspergillus niger, PDB code 1gal.*[192]

The crystal structure for the de-glycosilylated GOx in Figure 3.1 also reveals that the flavin active sites are at least 17 Å from the surface of the protein. Thus, in reality this distance will be rather longer for the native enzyme where the carbohydrate makes more than 16% of the mass of the enzyme.[195-197] There have been numerous investigations of electron transfer through enzymes.[198-201] Although they may differ in some details, these reports all agree that the rate of electron transfer through the protein drops off exponentially with distance and that fast electron transfer through proteins can only be achieved if the distance between the

electrode and the enzyme redox sites is 8 Å or less. The direct electron transfer DET rates should decrease by *ca.* 10^4 when the distance is increased from 8 to 17 Å.[186] This makes the observation of DET for native glucose oxidase rather unlikely.

3.4 A selection of papers claim DET to GOx

In spite of the issue of the large electron transfer distance (Figure 3.1), there are continuing attempts to demonstrate DET between the active site joined FAD cofactor of GOx and carbon nanotubes and more recently with other additives, Table 3.1 shows an extensive list of examples that claim DET to GOx. DET for GOx at different nanostructured materials is discussed in a number of recent reviews.[123-124, 126, 138, 163] The evidence presented to support these claims of DET for GOx are (see Table 3.1): i) the appearance of a pair of surface redox peaks at around -0.46 V *vs.* SCE at pH 7, assumed to be the flavin within the enzyme, and ii) changes in the current on addition of glucose that correlate with the glucose concentration. The claimed DET of GOx at these nanocarbon materials is often described using two theories. It is either a CNT "plug into" a GOx's active site, or that GOx partially unfolds enabling the charge transfer between the FAD cofactor and CNT. The vast majority of these claims of DET for GOx are supported by a "me too" argument that the data presented closely resemble that already in the literature in papers that claim DET.

Table 3.1. *A selection of papers that claim direct electron transfer (DET) to glucose oxidase (GOx)*

Authors	Title	Reference	Surface redox peaks	Effect of pH	Effect of scan rate	Glucose/O_2 current	Comments
B. Kowalewska, K. Jakubow	"The impact of immobilization process on the electrochemical performance, bioactivity and conformation of glucose oxidase enzyme"	Sens. Actuat. B-Chem. 238 (2017) 852-61	-0.438 and -0. 440 V *vs*. Ag/AgCl, pH 7.0	✓	✓	✓	4-(pyrrole-1-yl) benzoic acid modified MWCNT EIS
Z.P. Kang, K.L. Jiao, C. Yu, J. Dong, R.Y. Peng, Z.Q. Hu, S.Q. Jiao,	"Direct electrochemistry and bioelectrocatalysis of glucose oxidase in CS/CNC film and its application in glucose biosensing and biofuel cells"	RSC Adv. 7 (2017) 4572-9	-0.454 V *vs*. Ag/AgCl, pH 7.2	✓	✓	✓	Carbon nanochips (CNCs) and chitosan (CS)
X. Zhong, W. Yuan, Y. Kang, J. Xie, F. Hu, C.M. Li	"Biomass-derived hierarchical nanoporous carbon with rich functional groups for direct-electron-transfer-based glucose sensing"	ChemElectroChem 3 (2016) 144-51	ca. -0.45 V *vs*. SCE, pH 7.4		✓	✓	
Y. Zhao, W.B. Li, L.J. Pan, D.Y. Zhai, Y. Wang, L.L. Li, W.	"ZnO-nanorods/graphene heterostructure: a direct electron transfer glucose biosensor"	Sci. Rep. 6:32327 (2016)	ca. -0.39 V *vs*. SCE, pH 5.8		✓	✓	

K. Vijayaraj, S.W. Hong, S.-H. Jin, S.-C. Chang, D.-S. Park	"Fabrication of a novel disposable glucose biosensor using an electrochemically reduced graphene oxide–glucose oxidase biocomposite"	Anal. Methods 8 (2016) 6974-81	-0.46 V *vs*. Ag/AgCl, pH 7.0			✓	
Y.H. Song, X.P. Lu, Y. Li, Q.H. Guo, S.L. Chen, L.Q. Mao, H.Q. Hou, L. Wang	"Nitrogen-doped carbon nanotubes supported by macroporous carbon as an efficient enzymatic biosensing platform for glucose"	Anal. Chem. 88 (2016) 1371-7	-0.384 V *vs*. Ag/AgCl sat. KCl, pH 7.0	✓	✓	✓	GOx/CT/ZnS-CdS/PGE EIS
O. Saglam, B. Kizilkaya, H. Uysal, Y. Dilgin	"Biosensing of glucose in flow injection analysis system based on glucose oxidase-quantum dot modified pencil graphite electrode"	Talanta 147 (2016) 315-21	ca. -0.42 V *vs*. Ag/AgCl sat. KCl, pH 6.0	✓		✓	
M. Qi, Y. Zhang, C.M. Cao, Y. Lu, G.Z. Liu	"Increased sensitivity of extracellular glucose monitoring based on AuNP decorated GO nanocomposites"	RSC Adv. 6 (2016) 39180-7	-0.481 V *vs*. SCE, pH 7.0		✓	✓	GC/GOx-Ph-AuNPs
A. Muthurasu, V. Ganesh	"Glucose oxidase stabilized fluorescent gold nanoparticles as an ideal sensor matrix for dual mode sensing of glucose"	RSC Adv. 6 (2016) 7212-23	-0.464 V *vs*. Ag/AgCl, pH 7.0		✓		H_2O_2 detection on Au
D.B.T. Mascagni, C.M. Miyazaki, N.C. da Cruz, M.L. de Moraes, A. Riul, M. Ferreira	"Layer-by-layer assembly of functionalized reduced graphene oxide for direct electrochemistry and glucose detection"	Mater. Sci. Eng. C Mater. Bio. App. 68 (2016) 739-45	-0.415 V *vs*. SCE, pH 6.3				glucose measurement at -0.3 V

Y.G. Liu, X.M. Zhang, D.N. He, F.Y. Ma, Q. Fua, Y. Hu	"An amperometric glucose biosensor based on a MnO_2/graphene composite modified electrode"	RSC Adv. 6 (2016) 18654-61	-0.39 V *vs*. SCE, pH 6.0	✓	✓	✓	
J. Liu, Z.M. He, S.Y. Khoo, T.T.Y. Tan	"A new strategy for achieving vertically-erected and hierarchical TiO_2 nanosheets array/carbon cloth as a binder-free electrode for protein impregnation, direct electrochemistry and mediator-free glucose sensing"	Biosens. Bioelectron. 77 (2016) 942-9	-0.479 V *vs*. SCE, pH 7.4	✓	✓	✓	EIS
Z.J. Li, L.Y. Sheng, A. Meng, C.C. Xie, K. Zhao	"A glassy carbon electrode modified with a composite consisting of reduced graphene oxide, zinc oxide and silver nanoparticles in a chitosan matrix for studying the direct electron transfer of glucose oxidase and for enzymatic sensing of glucose"	Microchim. Acta 183 (2016) 1625-32	-0.513 V *vs*. SCE, pH 7.4	✓	✓		GOx/rGO-Zn-Ag/GCE DPV measurement of glucose with O_2 in solution
X. Li, Y. Jiang, B. Xu, L.T. Qu, Y.J. Shi, H.B. Shao	"Glucose oxidase immobilization by volume shrinkage of graphene as "Door-Function" microelectrode"	J. Electrochem. Soc. 163 (2016) B169-B75	-0.525 V *vs*. SCE, pH 6.76	✓	✓	✓	GOx@ERGO mocroelectrode
J. Li, M.M. Lu, Z.N. Tan, Y.B. Xu, Y.C. Zhang, X.Y. Hu, Z.J. Yang	"One-step solvothermal preparation of silver-ZnO hybrid nanorods for use in enzymatic and direct electron-transfer based biosensing of glucose"	Microchim. Acta 183 (2016) 1705-12	-0.357 V *vs*. SCE, pH 7	✓	✓	✓	Silver-ZnO/GOx/Nafion/GCE EIS
S.W. Lee, K.Y. Lee, Y.W. Song, W.K. Choi, J. Chang, H. Yi	"Direct electron transfer of enzymes in a biologically assembled conductive nanomesh enzyme platform"	Adv. Mater. 28 (2016) 1577-84	-0.38 V *vs*. Ag/AgCl ssat. KCl, pH 7.2		✓	✓	GOx/PEI/nanomesh/Au

K.T. Lee, Y.C. Liang, H.H. Lin, C.H. Li, S.Y. Lu	"Exfoliated SnS_2 nanoplates for enhancing direct electrochemical glucose sensing"	Electrochim. Acta 219 (2016) 241-50	-0.45 V *vs*. Ag/AgCl, pH 7.4		✓	✓	MWCNT/e-SnS_2/GOx
S. Kumar-Krishnan, A. Hernandez-Rangel, U. Pal, O. Ceballos-Sanchez, F.J. Flores-Ruiz, E. Prokhorov, O.A. de Fuentes, R. Esparza, M. Meyyappan	"Surface functionalized halloysite nanotubes decorated with silver nanoparticles for enzyme immobilization and biosensing"	J. Mater. Chem. B 4 (2016) 2553-60	-0.455 V *vs*. SCE, pH 7.4				HNT/AgNP-GOx glucose measurement by H_2O_2 detection in O_2 sat. soln.
S. Kumar-Krishnan, S. Chakaravarthy, A. Hernandez-Rangel, E. Prokhorov, G. Luna-Barcenas, R. Esparza, M. Meyyappan	"Chitosan supported silver nanowires as a platform for direct electrochemistry and highly sensitive electrochemical glucose biosensing"	RSC Adv. 6 (2016) 20102-8	-0.455 -0.55? V *vs*. SCE, pH 7.4		✓		CS/AgNWs/GOx/GCE H_2O_2 detection
S. Gupta, C.R. Prabha, C.N. Murthy	"Functionalized multi-walled carbon nanotubes/polyvinyl alcohol membrane coated glassy carbon electrode for efficient enzyme immobilization and glucose sensing"	J. Environ. Chem. Eng. 4 (2016) 3734-40	-0.426 V *vs*. Ag/AgCl 3 M KCl, pH 7.0	✓	✓	✓	PVA-MWCNT/GAD/GOx
V.R. Gonçales, R.N.P. Colombo, M.A.O.S. Minadeo, E.Y. Matsubara, J.M. Rosolen, S.I. Córdoba de Torresi	"Three-dimensional graphene/carbon nanotubes hybrid composites for exploring interaction between glucose oxidase and carbon based electrodes"	J. Electroanal. Chem. 775 (2016) 235-42	-0.46 V *vs*. Ag/AgCl sat. KCl, pH 7.4		✓	✓	

L.X. Fang, B. Liu, L.L. Liu, Y.H. Li, K.J. Huang, Q.Y. Zhang	"Direct electrochemistry of glucose oxidase immobilized on Au nanoparticles-functionalized 3D hierarchically ZnO nanostructures and its application to bioelectrochemical glucose sensor"	Sens. Actuat. B-Chem. 222 (2016) 1096-102	-0.426 V *vs.* SCE, pH 7.0		✓	✓	Au-ZnO/GCE
R.A. Escalona-Villalpando, A. Dector, D. Dector, A. Moreno-Zuria, S.M. Durón-Torres, M. Galván-Valencia, L.G. Arriaga, J. Ledesma-García	"Glucose microfluidic fuel cell using air as oxidant"	Int. J. Hydrogen Energy 41 (2016) 23394-400	-0.48 V *vs.* SCE, pH 7.0	✓	✓		GOx/MWCNT-GA Ferrocynanide used as mediator for glucose response
R.X. Zhao, X.Q. Liu, J.M. Zhang, J. Zhu, D.K.Y. Wong	"Enhancing direct electron transfer of glucose oxidase using a gold nanoparticle|titanate nanotube nanocomposite on a biosensor"	Electrochim. Acta 163 (2015) 64-70	-0.41 V *vs.* Ag/AgCl 3 M KCl, pH 7.4		✓	✓	TNT-GNP/[Demin]Br/Nafion /GOx/GCE DPV glucose measurements
M. Zhao, Y. Gao, J.Y. Sun, F. Gao	"Mediator less glucose biosensor and direct electron transfer type glucose/air biofuel cell enabled with carbon nanodots"	Anal. Chem. 87 (2015) 2615-22	-0.463 V *vs.* Ag/AgCl, pH 7.2	✓	✓		glucose response in deoxygenated buffer, oxidation current
X.P. Zhang, D. Liu, L.B. Li, T.Y. You	"Direct electrochemistry of glucose oxidase on novel free-standing nitrogen-doped carbon nanospheres@carbon nanofibers composite film"	Sci. Rep. 5:09885 (2015)	-0.43 V *vs.* Ag/AgCl sat. KCl, pH 7.0				GOx/NCNSs@CNFs uniform shift in CV for glucose in N_2 sat buffer

L. Zhang, C.S. Zhou, J.J. Luo, Y.Y. Long, C.M. Wang, T.T. Yu, D. Xiao	"A polyaniline microtube platform for direct electron transfer of glucose oxidase and biosensing applications"	J. Mater. Chem. B 3 (2015) 1116-24	-0.393 V *vs.* SCE, pH 5.5		✓	✓	
Z.H. Yu, Y.N. Kou, Y. Dai, X.Y. Wang, H. Wei, D.G. Xia	"Direct electrochemistry of glucose oxidase on a three-dimensional porous zirconium phosphate-carbon aerogel composite"	Electrocatalysis 6 (2015) 341-7	-0.483 V *vs.* SCE, pH 7.0	✓	✓	✓	
Y.K. Ye, S. Ding, Y.W. Ye, H.C. Xu, X.D. Cao, S. Liu, H.J. Sun	"Enzyme-based sensing of glucose using a glassy carbon electrode modified with a one-pot synthesized nanocomposite consisting of chitosan, reduced graphene oxide and gold nanoparticles"	Microchim. Acta 182 (2015) 1783-9	-0.418 V *vs.* Ag/AgCl, pH 7.0		✓	✓	
Z.J. Yang, Y.B. Xu, J. Li, Z.Q. Jian, S.H. Yu, Y.C. Zhang, X.Y. Hu, D.D. Dionysiou	"An enzymatic glucose biosensor based on a glassy carbon electrode modified with cylinder-shaped titanium dioxide nanorods"	Microchim. Acta 182 (2015) 1841-8	-0.422 V *vs.* SCE, pH 7.0	✓	✓	✓	
Z.J. Yang, Y. Cao, J. Li, Z.Q. Jian, Y.C. Zhang, X.Y. Hu,	"Platinum nanoparticles functionalized nitrogen doped graphene platform for sensitive electrochemical glucose biosensing"	Anal. Chim. Acta 871 (2015) 35-42	-0.296 V *vs.* SCE, pH 6.0	✓	✓	✓	
L. Xia, J.F. Xia, Z.H. Wang	"Direct electrochemical deposition of polyaniline nanowire array on reduced graphene oxide modified graphite electrode for direct electron transfer biocatalysis"	RSC Adv. 5 (2015) 93209-14	-0.447 V *vs.* SCE, pH 7.4		✓		GOx/PANi/rGO/GE detect oxidation current with glucose in N_2 sat. buffer

M. Velmurugan, S. Sakthinathan, S.M. Chen, C. Karuppiah	"Direct electron transfer of glucose oxidase and electrocatalysis of glucose based on gold nanoparticles/electroactivated graphite nanocomposite"	Int. J. Electrochem. Sci. 10 (2015) 6663-71	-0.404 V *vs.* Ag/AgCl, pH 7.0	✓	✓	✓	GOx/AuNPs-EGr/SPCE
T. Terse-Thakoor, K. Komori, P. Ramnani, I. Lee, A. Mulchandani	"Electrochemically functionalized seamless three-dimensional graphene-carbon nanotube hybrid for direct electron transfer of glucose oxidase and bioelectrocatalysis"	Langmuir 31 (2015) 13054-61	-0.459 V *vs.* Ag/AgCl 3 M KCl, pH 7.0	✓	✓	✓	
Q.Q. Sun, Y.N. Yu, J.J. Li, S.J. Bao	"*In situ* growth of metallic silver on glucose oxidase for a highly sensitive glucose sensor"	RSC Adv. 5 (2015) 34486-90	-0.474 V, no Ref. given, pH 7.4			✓	Au-GOx/Nafion
Y.H. Song, J.Y. Chen, H.Y. Liu, Y.G. Song, F.G. Xu, H.L. Tan, L. Wang	"Conformation, bioactivity and electrochemical performance of glucose oxidase immobilized on surface of gold nanoparticles"	Electrochim. Acta 158 (2015) 56-63	ca. -0.47 V *vs.* SCE, pH 7.0			✓	AuNPs-GOx/GCE AuNPs-MHA-GOx/GCE AuNPs-MUA-GOx/GCE
Y.J. Shi, X. Li, M.H. Ye, C.G. Hu, H.B. Shao, L.T. Qu	"An imperata cylindrical flowers-shaped porous graphene microelectrode for direct electrochemistry of glucose oxidase"	J. Electrochem. Soc. 162 (2015) B138-B44	-0.489 V *vs.* SCE, pH 6.86	✓	✓		DPV measurement of glucose in air sat. buffer
A.A. Sehat, A.A. Khodadadi, F. Shemirani, Y. Mortazavi	"Fast immobilization of glucose oxidase on graphene oxide for highly sensitive glucose biosensor fabrication"	Int. J. Electrochem. Sci. 10 (2015) 272-86	-0.521 V *vs.* Ag/AgCl sat. KCl, pH 7.0	✓	✓	✓	glucose measured in O_2 sat. solution

V. Mani, R. Devasenathipathy, S.M. Chen, B. Subramani, M. Govindasamy	"A novel glucose biosensor at glucose oxidase immobilized graphene and bismuth nanocomposite film modified electrode"	Int. J. Electrochem. Sci. 10 (2015) 691-700	-0.427 V *vs.* Ag/AgCl sat. KCl, pH 7.0		✓		Graphene-Bi/GOx/SCE Glucose measured with FcMCA mediator
Y.Y. Liu, T.D. Dolidze, S. Singhal, D.E. Khoshtariya, J.J. Wei	"New evidence for a quasi-simultaneous proton-coupled two-electron transfer and direct wiring for glucose oxidase captured by the carbon nanotube-polymer matrix"	J. Phys. Chem. C 119 (2015) 14900-10	ca. -0.43 V *vs.* Ag/AgCl, pH 7.0	✓	✓		use hydroquinone mediator
B. Liang, X.S. Guo, L. Fang, Y.C. Hu, G. Yang, Q. Zhu, J.W. Wei, X.S. Ye	"Study of direct electron transfer and enzyme activity of glucose oxidase on graphene surface"	Electrochem. Commun. 50 (2015) 1-5	-0.48 V *vs.* Ag/AgCl, pH 7.4	✓		✓	FCA mediator use
K. Hyun, S.W. Han, W.-G. Koh, Y. Kwon	"Direct electrochemistry of glucose oxidase immobilized on carbon nanotube for improving glucose sensing"	Int. J. Hydrogen Energy 40 (2015) 2199-206	-0.41 V *vs.* Ag/AgCl, pH 8.25	✓	✓	✓	
N. Huang, S. Zhang, L.Q. Yang, M.L. Liu, H.T. Li, Y.Y. Zhang, S.Z. Yao	"Multifunctional electrochemical platforms based on the Michael addition/Schiff base reaction of polydopamine modified reduced graphene oxide: construction and application"	ACS Appl. Mater. Interfaces 7 (2015) 17935-46	-0.468 V *vs.* SCE, pH 7.4				GOx-PDA-rGO/GCE

H. Hu, M. Feng, H. Zhan	"A glucose biosensor based on partially unzipped carbon nanotubes"	Talanta 141 (2015) 66-72	-0.470 V *vs*. SCE, pH 7.0		✓	✓	PUCNT/GOx/GCE DPV glucose measurement EIS
J.X. Guo, T. Zhang, C.G. Hu, L. Fu	"A three-dimensional nitrogen-doped graphene structure: a highly efficient carrier of enzymes for biosensors"	Nanoscale 7 (2015) 1290-5	-0.478 V *vs*. SCE, pH 7.4		✓	✓	
E. Ghasemi, E. Shams, N.F. Nejad	"Covalent modification of ordered mesoporous carbon with glucose oxidase for fabrication of glucose biosensor"	J. Electroanal. Chem. 752 (2015) 60-7	-0.45 V *vs*. Ag/AgCl 3 M KCl, pH 7.0	✓	✓	✓	
K. Eskandari, H. Zarei, H. Ghourchian, S.M. Amoozadeh	"The electrochemical study of glucose oxidase on gold-coated magnetic iron oxide nanoparticles"	J. Anal. Chem. 70 (2015) 1254-60	-0.270 V *vs*. Ag/AgCl, pH 6.8	✓	✓		GOx/NH_2-Fe@Au GOx oxidied with periodate glucose measured by SWV in air sat. soln.
R. Devasenathipathy, V. Mani, S.M. Chen, S.T. Huang, T.T. Huang, C.M. Lin, K.Y. Hwa, T.Y. Chen, B.J. Chen	"Glucose biosensor based on glucose oxidase immobilized at gold nanoparticles decorated graphene-carbon nanotubes"	Enz. Microb. Technol. 78 (2015) 40-5	-0.40 V *vs*. Ag/AgCl sat.KCl, pH 7	✓	✓	✓	GR-MWTs/AuNPs/GOx
H.C. Chen, Y.M. Tu, C.C. Hou, Y.C. Lin, C.H. Chen, K.H. Yang	"Direct electron transfer of glucose oxidase and dual hydrogen peroxide and glucose detection based on water-dispersible carbon nanotubes derivative"	Anal. Chim. Acta 867 (2015) 83-91	-0.44 V *vs*. Ag/AgCl sat.KCl, pH 7.0		✓	✓	H_2O_2 detection

G.Q. Chen, Y.X. Liu, Y. Liu, Y. Tian, X. Zhang	"Nitrogen and sulfur dual-doped graphene for glucose biosensor application"	J. Electroanal. Chem. 738 (2015) 100-7	-0.445 V *vs.* Ag/AgCl, pH 7.4	✓	✓	✓	GOx/NS-G/GCE
Y. Yu, Z. Chen, S. He, B. Zhang, X. Li, M. Yao	"Direct electron transfer of glucose oxidase and biosensing for glucose based on PDDA-capped gold nanoparticle modified graphene/multi-walled carbon nanotubes electrode"	Biosens. Bioelectron. 52 (2014) 147	-0.454 V *vs.* Ag/AgCl sat. KCl, pH 7.0	✓	✓	✓	
Q. Xu, S.-X. Gu, L. Jin, Y.-e. Zhou, Z. Yang, W. Wang, X. Hu	"Graphene/polyaniline/gold nanoparticles nanocomposite for the direct electron transfer of glucose oxidase and glucose biosensing"	Sens. Actuat. B-Chem. 190 (2014) 562	-0.477 V *vs.* SCE, pH 7.0	✓	✓	✓	
S. Palanisamy, S. Cheemalapati, S.-M. Chen	"Amperometric glucose biosensor based on glucose oxidase dispersed in multiwalled carbon nanotubes/graphene oxide hybrid biocomposite"	Mater. Sci. Eng. C-Materials for Biological Applications, 34 (2014) 207	-0.420 V *vs.* Ag/AgCl, pH 7.0	✓	✓	✓	EIS
M. V. A. Martins, A. R. Pereira, R. A. S. Luz, R. M. Iost, F. N. Crespilho	"Evidence of short-range electron transfer of a redox enzyme on graphene oxide electrodes"	Phys. Chem. Chem. Phys. 16 (2014) 17426	-0.43 V and -0.55 V *vs*. Ag/AgCl sat. KCl, pH 7 for FCF-Gox and FCF-GO-Gox	✓	✓		oxidation current for glucose at -0.3 V in N_2 sat. buffer
L.-M. Liu, J. Wen, L. Liu, D. He, R.-y. Kuang, T. Shi	"A mediator-free glucose biosensor based on glucose oxidase/chitosan/alpha-zirconium phosphate ternary biocomposite"	Anal. Biochem. 445 (2014) 24	-0.389 V *vs.* SCE, pH 5.5		✓	✓	
C. Karuppiah, S. Palanisamy, S.-M.	"A novel enzymatic glucose biosensor and sensitive non-enzymatic hydrogen	Sens. Actuat. B-Chem. 196 (2014) 450	-0.441 V *vs.* Ag/AgCl, pH 7	✓	✓	✓	

Chen, V. Veeramani, P. Periakaruppan	peroxide sensor based on graphene and cobalt oxide nanoparticles composite modified glassy carbon electrode"						
M.Y. Elahi, A.A. Khodadadi, Y. Mortazavi	"A glucose biosensor based on glucose oxidase immobilized on ZnO/Cu_2O graphene oxide. nanocomposite electrode"	J. Electrochem. Soc. 161 (2014) B81	-0.523 V *vs.* Ag/AgCl, pH 7.0		✓		DPV measurement of glucose EIS
X. Cao, Y. Sun, Y. Ye, Y. Li, X. Ge	"Macroporous ordered silica foam for glucose oxidase immobilisation and direct electrochemical biosensing"	Anal. Methods 6 (2014) 1448	-0.528 V *vs.* Ag/AgCl, pH 7.0		✓	✓	EIS
Y.-F. Bai, T.-B. Xu, J.H.T. Luong, H.-F. Cui,	"Direct electron transfer of glucose oxidase-boron doped diamond interface: a new solution for a classical problem"	Anal. Chem. 86 (2014) 4910	-0.42 V *vs.* Ag/AgCl 3 M, pH 7.0		✓	?	APTES treated BDD
H. Zhao, S.H. Yu, P.J. Yoo, J.H. Park, J.Y. Lee	"Glucose sensing by glucose oxidase/PEDOT thin film electrode"	Mol. Cryst. Liq. Cryst. 580 (2013) 22	ca. -0.45 V *vs.* Ag/AgCl sat. KCl, pH 7.4			✓	poorly defined peaks
K. Won, Y.-H. Kim, S. An, H.J. Lee, S. Park, Y.-K. Choi, J.H. Kim, H.-I. Hwang, H.J. Kim, H. Kim, S.H. Lee	"Glucose oxidase/cellulose-carbon nanotube composite paper as a biocompatible bioelectrode for biofuel cells"	App. Biochem. Biotechnol. 171 (2013) 1194	-0.464 V *vs.* Ag/AgCl sat. KCl, pH 7.0		✓	✓	
M. Vesali-Naseh, Y. Mortazavi, A.A. Khodadadi, P.	"Plasma thiol-functionalized carbon nanotubes decorated with gold nanoparticles for glucose biosensor"	Sens. Actuat. B-Chem. 188 (2013) 488	-0.47 V *vs.* Ag/AgCl, pH 7.0		✓		detects H_2O_2

H. Razmi, R. Mohammad-Rezaei	"Graphene quantum dots as a new substrate for immobilization and direct electrochemistry of glucose oxidase: Application to sensitive glucose determination"	Biosens. Bioelectron. 41 (2013) 498	-0.509 V *vs.* SCE, pH 7.4	✓	✓	✓	EIS
H.-P. Peng, R.-P. Liang, L. Zhang, J.-D. Qiu	"Facile preparation of novel core-shell enzyme-Au-polydopamine-Fe_3O4 magnetic bionanoparticles for glucose sensor"	Biosens. Bioelectron. 42 (2013) 293	-0.458 V *vs.* SCE, pH 6.98	✓	✓	✓	
Z. Nasri, E. Shams	"A glucose biosensor based on direct electron transfer of glucose oxidase immobilized onto glassy carbon electrode modified with nitrophenyl diazonium salt"	Electrochim. Acta 112 (2013) 640	-0.48 V *vs.* Ag/AgCl, pH 7.0		✓	✓	also used FcMeOH mediator EIS
Rochefort M. Moumene, D., M. Mohamedi	"Electrochemical functionalization as a promising avenue for glucose oxidase immobilization at carbon nanotubes: enhanced direct electron transfer process"	Int. J. Electrochem. Sci. 8 (2013) 2009	-0.451 V *vs.* Ag/AgCl, pH 7.2				SWV with glucose
R. D. Milton, J. Baur, J. R. Varcoe, A. E. Thumser, R. C. T. Slade	"An optimised glucose oxidase bioelectrode exhibiting high performance direct electron transfer"	Phys. Chem. Chem. Phys., 14 (2012) 9582	-0.389 V *vs.* Ag/AgCL, pH 6.0		✓	✓	GC, MWCNT/GOx/MWCNT, cellulose
B. Liang, L. Fang, G. Yang, Y. Hu, X. Guo, X. Ye	"Direct electron transfer glucose biosensor based on glucose oxidase self-assembled on electrochemically reduced carboxyl graphene"	Biosens. Bioelectron. 43 (2013) 131	-0.467 V *vs.* Ag/AgCl, pH 7.4			✓	ERCGr-GOX/GCE EIS

S.-J. Li, T.-W. Chen, N. Xia, Y.-L. Hou, J.-J. Du, L. Liu	"Direct electrochemistry of glucose oxidase on sulfonated graphene/gold nanoparticle hybrid and its application to glucose biosensing"	J. Solid State Electrochem. 17 (2013) 2487	-0.481 V *vs.* SCE, pH 7.0		✓	✓	
M. Li, B. Feng, Y. Ding, J. Fei	"Direct electrochemistry of glucose oxidase in beta-cyclodextrin covalently functionalized single-walled carbon nanotubes-cetyltrimethyl ammonium bromide hybrid film and its biosensing"	Nanosci. Nanotechnol. Lett. 5 (2013) 712	-0.415 V *vs.* SCE, pH 7.0	✓	✓	✓	EIS
J. Li, Z. Yang, Y. Tang, Y. Zhang, X. Hu	"Carbon nanotubes-nanoflake-like SnS_2 nanocomposite for direct electrochemistry of glucose oxidase and glucose sensing"	Biosens. Bioelectron. 41 (2013) 698	-0.454 V *vs.* SCE, pH 6.0		✓	✓	
Y.-H. Kim, S. Park, K. Won, H.J. Kim, S.H. Lee	"Bacterial cellulosecarbon nanotube composite as a biocompatible electrode for the direct electron transfer of glucose oxidase"	J. Chem. Technol. Biotechnol. 88 (2013) 1067	-0.496 V *vs.* Ag/AgCl, pH 7.0			✓	
H. Jianing, C. Jiewu, X. Guangqing, S.B. Adeloju, W. Yucheng	"Direct electrochemistry of glucose oxidase based on Nafion-Graphene-GOD modified gold electrode and application to glucose detection"	Mater. Lett. 108 (2013) 88	-0.456 V *vs.* Ag/AgCl 3 M KCl, pH 7.4		✓	✓	
C. Hui-Fang, Z. Kuan, Z. Yong-Fang, S. Yu-Long, W. Jia, Z. Wei-De, J.H.T. Luong	"Immobilization of glucose oxidase into a nanoporous TiO_2 film layered on metallophthalocyanine modified vertically-aligned carbon nanotubes for efficient direct electron transfer"	Biosens. Bioelectron. 46 (2013) 113	-0.483 V *vs.* Ag/AgCl 3 M KCl, PBS pH 7.4		✓		detects glucose at +0.5 V

Z. Luo, L. Yuwen, Y. Han, J. Tian, X. Zhu, L. Weng, L. Wang	"Reduced graphene oxide/PAMAM-silver nanoparticles nanocomposite modified electrode for direct electrochemistry of glucose oxidase and glucose sensing"	Biosens. Bioelectron. 36 (2012) 179	-0.381 V *vs.* Ag/AgCl sat. KCl, pH 7.0	✓	✓	✓	uses guanidine hydrochloride
L. Liu, Y. Cheng, F. Sun, J. Yang, Y. Wu	"Enhanced direct electron transfer of glucose oxidase based on a protic ionic liquid modified electrode and its biosensing application"	J. Solid State Electrochem. 16 (2012) 1003	-0.476 V *vs.* SCE, pH 7.0	✓	✓	✓	
S. Lee, B.S. Ringstrand, D.A. Stone, M.A. Firestone	"Electrochemical activity of glucose oxidase on a poly(ionic liquid)-Au nanoparticle composite"	ACS App. Mater. Interfaces 4 (2012) 2311	-0.472 V *vs.* Ag/AgCl sat KCl pH 7.4		✓	✓	detects H_2O_2
M.V. Jose, S. Marx, H. Murata, R.R. Koepsel, A.J. Russell	"Direct electron transfer in a mediator-free glucose oxidase-based carbon nanotube-coated biosensor"	Carbon 50 (2012) 4010	-0.447 V *vs.* Ag/AgCl sat. KCl, pH 7.0	✓	✓	✓	H_2O_2 detected at +0.8 V
Y. Jiang, Q. Zhang, F. Li, L. Niu	"Glucose oxidase and graphene bionanocomposite bridged by ionic liquid unit for glucose biosensing application"	Sens. Actuat. B-Chem. 161 (2012) 728.	-0.45 V *vs.* Ag/AgCl sat. KCl, pH 7.4		✓	✓	
F. Gutierrez, M.D. Rubianes, G.A. Rivas	"Dispersion of multi-wall carbon nanotubes in glucose oxidase: Characterization and analytical applications for glucose biosensing"	Sens. Actuat. B-Chem. 161 (2012) 191	-0.490 V *vs.* Ag/AgCl 3 M NaC, pH 7.4		✓		Uses FcMeOH mediator
C.-J. Cai, M.-W. Xu, S.-J. Bao, C. Lei, D.-Z. Jia	"A facile route for constructing a graphene-chitosan-ZrO_2 composite for direct electron transfer and glucose sensing"	RSC Adv. 2 (2012) 8172	-0.445 V *vs.* Ag/AgCl sat. KCl, pH 7	✓	✓	✓	

Q. Zhang, S. Wu, L. Zhang, J. Lu, F. Verproot, Y. Liu, Z. Xing, J. Li, X.-M. Song	"Fabrication of polymeric ionic liquid/graphene nanocomposite for glucose oxidase immobilization and direct electrochemistry"	Biosens. Bioelectron. 26 (2011) 2632	ZrO_2/GOx -0. 380 V; ER-GO/ZrO_2/GOx -0.417 V; ER-GO/CS/ZrO_2/GOx -0.437 V *vs.* Ag/AgCl, pH 7.4		✓	✓	3 systems studied
P. Wu, Q. Shao, Y. Hu, J. Jin, Y. Yin, H. Zhang, C. Cai	"Direct electrochemistry of glucose oxidase assembled on graphene and application to glucose detection"	Electrochim. Acta, 55 (2010) 8606	-0.454 V *vs*. SCE, pH 6.9			✓	GOx-graphene/GC
K. Wang, Q. Liu, Q.-M. Guan, J. Wu, H.-N. Li, J.-J. Yan	"Enhanced direct electrochemistry of glucose oxidase and biosensing for glucose via synergy effect of graphene and CdS nanocrystals"	Biosen. Bioelectron. 26 (2011) 2252	-0.442 V *vs.* Ag/AgCl, pH 6.5	✓	✓	✓	Polymeric ionic liquid/graphene
B.C. Janegitz, R. Pauliukaite, M.E. Ghica, C.M.A. Brett, O. Fatibello-Filho	"Direct electron transfer of glucose oxidase at glassy carbon electrode modified with functionalized carbon nanotubes within a dihexadecylphosphate film"	Sens. Actuat.B-Chem. 158 (2011) 411	-0.418 V *vs.* Ag/AgCl 3 M KCl, pH 7.0	✓	✓		SWV for glucose in N_2 sat. solution
J.H. Kim, H.J. Lee, H. Jung, H-K. Song, H.H. Yoon, K. Won	"Direct electron transfer of glucose oxidase and carbon nanotubes entrapped with biocompatible organic materials"	Mol. Cryst. Liq. Cryst. 519 (2010) 82-9	-0.450 V *vs.* Ag/AgCl 3 M KCl, pH 7.0		✓	✓	
J. Ryu, H. Kim, S. Lee, H.T. Hahn, D. Lashmore	"Carbon nanotube mat as mediator-less glucose sensor electrode"	J. Nanosci. Nanotechnol. 10 (2010) 941	-0.425 V *vs.* Ag/AgCl, pH 7.4		✓	✓	
K.-P. Lee, S. Komathi, N.J. Nam, A.I. Gopalan	"Sulfonated polyaniline network grafted multi-wall carbon nanotubes	Microchem. J. 95 (2010) 74	-0.815 V *vs.* Ag/AgCl, pH 7.0		✓		H_2O_2 detected with glucose and O_2

	for enzyme immobilization, direct electrochemistry and biosensing of glucose"						
C. Deng, J. Chen, Z. Nie, S. Si	"A sensitive and stable biosensor based on the direct electrochemistry of glucose oxidase assembled layer-by-layer at the multiwall carbon nanotube-modified electrode"	Biosens. Bioelectron. 26 (2010) 213	-0.45 V *vs.* SCE, pH 7.0	✓	✓	✓	
X. Wu, F. Zhao, J.R. Varcoe, A.E. Thumser, C. Avignone-Rossa, R.C.T. Slade	"Direct electron transfer of glucose oxidase immobilized in an ionic liquid reconstituted cellulose-carbon nanotube matrix"	Bioelectrochemistry 77 (2009) 64	-0.371 V *vs.* Ag/AgCl, pH 6.0	✓	✓	✓	
K. Wang, H. Yang, L. Zhu, Z. Ma, S. Xing, Q. Lv, J. Liao, C. Liu, W. Xing	"Direct electron transfer and electrocatalysis of glucose oxidase immobilized on glassy carbon electrode modified with Nafion and mesoporous carbon FDU-15"	Electrochim. Acta 54 (2009) 4626	-0.436 V *vs.* Ag/AgCl, pH 7.1	✓	✓	✓	
C. Shan, H. Yang, J. Song, D. Han, A. Ivaska, L. Niu	"Direct electrochemistry of glucose oxidase and biosensing for glucose based on graphene"	Anal. Chem. 81 (2009) 2378	-0.43 V *vs.* Ag/AgCl sat. KCl, pH 7.4		✓	✓	
J. Li, F. Zhao, G. Wang, Z. Gui, F. Xiao, B. Zeng	"Novel composite of multiwalled carbon nanotubes and gold nanoparticles stabilized by chitosan and hydrophilic ionic liquid for direct electron transfer of glucose oxidase"	Electroanalysis 21 (2009) 150	-0.463 V *vs.* SCE, pH 7.0	✓	✓	✓	

F. Li, J. Song, F. Li, X. Wang, Q. Zhang, D. Han, A. Ivaska, L. Niu	"Direct electrochemistry of glucose oxidase and biosensing for glucose based on carbon nanotubes@SnO_2-Au composite"	Biosens. Bioelectron. 25 (2009) 883	ca. -0.42 V *vs.* Ag/AgCl, pH 7		✓		
X. Kang, J. Wang, H. Wu, I.A. Aksay, J. Liu, Y. Lin	"Glucose oxidase-graphene-chitosan modified electrode for direct electrochemistry and glucose sensing"	Biosens. Bioelectron. 25 (2009) 901	-0.477 V *vs.* Ag/AgCl 3 M KCl, pH 7.4	✓	✓	✓	
D.R.S. Jeykumari, S.S. Narayanan	"Functionalized carbon nanotube-bienzyme biocomposite for amperometric sensing"	Carbon 47 (2009) 957	-0.47 *vs.* SCE, pH 7.4		✓		H_2O_2 detected with HRP and mediator
R. Gao, J. Zheng	"Amine-terminated ionic liquid functionalized carbon nanotube-gold nanoparticles for investigating the direct electron transfer of glucose oxidase"	Electrochem. Commun. 11 (2009) 608.	-0.501 V *vs.* SCE, pH 7.0	✓	✓	✓	
C. Fu, W. Yang, X. Chen, D.G. Evans	"Direct electrochemistry of glucose oxidase on a graphite nanosheet-Nafion composite film modified electrode"	Electrochem. Commun. 11 (2009) 997	-0.425 V *vs.* Ag/AgCl sat. KCl, pH 7.0		✓	✓	
S. Deng, G. Jian, J. Lei, Z. Hu, H. Ju,	"A glucose biosensor based on direct electrochemistry of glucose oxidase immobilized on nitrogen-doped carbon nanotubes"	Biosens. Bioelectron. 25 (2009) 373	-0.459 V *vs.* SCE, pH 7.0		✓	✓	
Y. Zhou, H. Yang, H.-Y. Chen,	"Direct electrochemistry and reagentless biosensing of glucose oxidase immobilized on chitosan	Talanta 76 (2008) 419	-0.460 V *vs.* SCE, pH 7.4		✓		glucose response reduction current at -0.4 V

	wrapped single-walled carbon nanotubes"						
F. Jia, C. Shan, F. Li, L. Niu	"Carbon nanotube/gold nanoparticles/polyethylenimine-functionalized ionic liquid thin film composites for glucose biosensing"	Biosens. Bioelectron. 24 (2008) 945	-0.42 V *vs.* Ag/AgCl, pH 7.4		✓	✓	
D. Ivnitski, K. Artyushkova, R.A. Rincon, P. Atanassov, H.R. Luckarift, G.R. Johnson,	"Entrapment of enzymes and carbon nanotubes in biologically synthesized silica: Glucose oxidase-catalyzed direct electron transfer"	Small 4 (2008) 357	-0.406 V *vs.* Ag/AgCl, pH 6.2		✓	✓	
C. Deng, J. Chen, X. Chen, C. Mao, L. Nie, S. Yao	"Direct electrochemistry of glucose oxidase and biosensing for glucose based on boron-doped carbon nanotubes modified electrode"	Biosens. Bioelectron. 23 (2008) 1272	-0.477 V *vs.* SCE, pH 6.98	✓	✓	✓	
G. Wang, N.M. Thai, S.T. Yau	"Preserved enzymatic activity of glucose oxidase immobilized on unmodified electrodes for glucose detection"	Biosens. Bioelectron. 22 (2007) 2158	-0.435 V *vs.* Ag/AgCl, pH 7.0	✓	✓	✓	Edge plane HOPG SiO_2/Si
H. Tachikawa, Z. Jingdong, F. Manliang	"Layer-by-layer fabrication and direct electrochemistry of glucose oxidase on single wall carbon nanotubes"	Biosens. Bioelectron. 22 (2007) 3036	-0.46 V *vs.* Ag/AgCl, pH 7.0	✓	✓	✓	
A. Salimi, E. Sharifi, A. Noorbakhsh, S. Soltanian	"Immobilization of glucose oxidase on electrodeposited nickel oxide nanoparticles: Direct electron transfer and electrocatalytic activity"	Biosens. Bioelectron. 22 (2007) 3146.	-0.43 V *vs.* Ag/AgCl, pH 7.0	✓	✓	✓	FeMeOH mediation

O. Nadzhafova, M. Etienne, A. Walcarius	"Direct electrochemistry of hemoglobin and glucose oxidase in electrodeposited sol-gel silica thin films on glassy carbon"	Electrochem. Commun. 9 (2007) 1189	-0.390 V *vs.* Ag/AgCl, pH 6.5			✓	co-immobilized Hb
Q. Liu, X. Lu, J. Li, X. Yao, J. Li	"Direct electrochemistry of glucose oxidase and electrochemical biosensing of glucose on quantum dots/carbon nanotubes electrodes"	Biosens. Bioelectron. 22 (2007) 3203	-0.372 V *vs.* Ag/AgCl, pH 6.0		✓	✓	Nafion CdTe/CNT
H. Liu, N. Hu	"Study on direct Electrochemistry of glucose oxidase stabilized by cross-linking and immobilized in silica nanoparticle films"	Electroanalysis 19 (2007) 884.	-0.48 V *vs.* SCE, pH 7.0			✓	GOx/GA/SiO_2. FcMA mediator
Y.J. Yin, Y.F. Lu, P. Wu, C.X. Cai,	"Direct electrochemistry of redox proteins and enzymes promoted by carbon nanotubes"	Sensors 5 (2005) 220	-0.466 V *vs.* SCE, pH 6.9	✓	✓		3 M guanidinium hydrohloride no glucose results
C.X. Cai, J. Chen, T.H. Lu	"Direct electron transfer of glucose oxidase on the carbon nanotube electrode"	Sci. China Ser. B-Chem. 47 (2004) 113	-0.456 V *vs.* SCE, pH 6.9	✓			3 M guanidinium hydrohloride FcMA mediator
C.X. Cai, J. Chen	"Direct electron transfer of glucose oxidase promoted by carbon nanotubes"	Anal. Biochem. 332 (2004) 75	-0.466 V *vs.* SCE, pH 6.9	✓	✓		Nafion GOx CNT/GC 3 M guanidinium hydrochloride FcMA mediator
A. Guiseppi-Elie, C.H. Lei, R.H. Baughman	"Direct electron transfer of glucose oxidase on carbon nanotubes"	Nanotechnol. 13 (2002) 559	-0.441 V *vs.* Ag/AgCl, pH 7.0			✓	

Abbreviations:

AuNPs – gold nanoparticles
AgNWs – silver nanowires
ATPES – 3-aminopropyltriethoxysilane
BDD – boron doped diamond
CS – chitosan
MWCNT – multi walled carbon nanotube
EIS – electrochemical impedance spectroscopy
DPV – differential pulse voltammetry
ERCGr – electrochemically reduced carboxy-graphene
ERGO – electrochemically reduced grapheme oxide
EGr – electroactivated graphite
e-SnS_2 – exfoliated tin disulphide
Fc – ferrocene
FCA – ferrocene carboxylic acid
FCF – flexible carbon fibre
FcMA –ferrocene monocarboxylic acid
FcMeOH – ferrocene methanol
GA – glutaraldehyde
GO – exfoliated graphene oxide
GR-MWCNTs – graphene-multiwalled carbon nanotubes
Hb – hemoglobin
MHA – mercaptohexadecyl acid
MUA – mercaptoundecanoic acid
GE – graphite electrode
NCNs@CNFs-nitrogen-doped carbon nanospheres@carbon nanofibres
NCNT – nitrogen-doped carbon nanotube
NS-G – nitrogen, sulfur dual-doped graphene
PANi – poly(aniline)
PDA – polydopamine
PEI – poly(ethylenimine)
PGE – pencil graphite electrode
PVA – polyvinyl alcohol
rGO – reduced graphene oxide
SPCE – screen printed carbon electrode
SWV – square wave voltammetry
TNT-GNP – titanate nanotube-gold nanoparticle

3.5 Electrochemistry of carbon nanotube electrodes with adsorbed GOx

In order to evaluate the electrochemistry of carbon nanotube electrodes with adsorbed GOx, cyclic voltammograms were performed in deoxygenated phosphate buffer solution (PBS) at a scan rate of 60 mV s-1. Figure. 3.2 shows cyclic voltammograms recorded at bare glassy carbon (GC) (a), glassy carbon with adsorbed glucose oxidase (GC/GOx) (b), glassy carbon drop coated with carboxylate functionalised multiwall carbon nanotubes (GC/MWCNT) (c), and glassy carbon drop coated with carboxylate functionalised multiwall carbon nanotubes and adsorbed glucose oxidase (GC/MWCNT/GOx) (d) obtained in deoxygenated 0.1 M phosphate buffer solution, pH 6.8. The glucose oxidase was adsorbed on the GC and GC/MWCNT electrodes by incubation for 12 h in a solution containing 1 kU GOx dissolved in 0.1 M phosphate buffer solution (pH6.8).

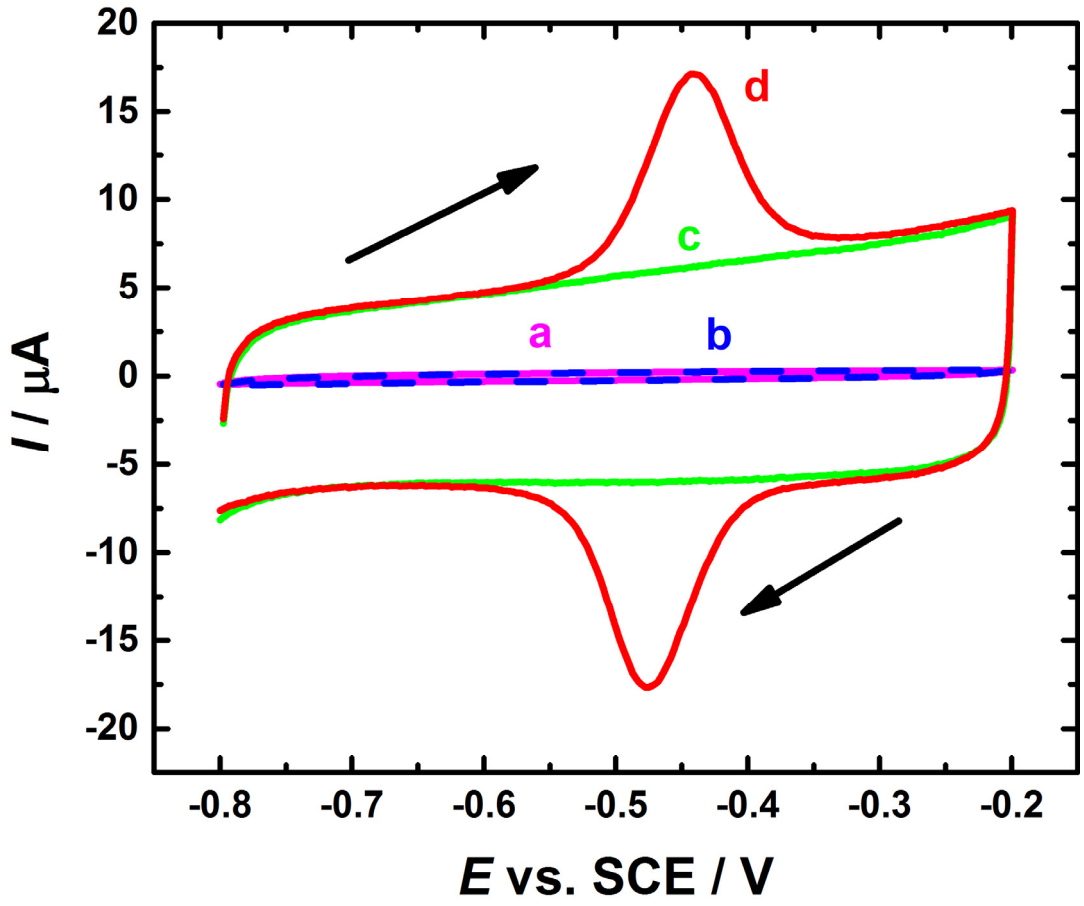

Figure 3.2. *Cyclic voltammograms of different electrodes in 0.1 M deoxygenated phosphate buffer solution (PBS) (pH 6.8) at the scan rate of 60 mV s^{-1} (a) Bare GC, (b) GC/GOx, (c) GC/MWCNT and (d) GC/MWCNT/GOx. The GC/MWCNT electrode was prepared by drop casting of a 5 µL aliquot of 1 mg mL^{-1} MWCNT (carboxylic acid functionalized) dispersion onto the cleaned surface of GC. GOx was immobilized using incubation in a solution of 1 kU GOx dissolved in 0.1 M phosphate buffer solution (pH 6.8) for 12 h.*

In the absence of adsorbed GOx the voltammetry of the bare GC electrode (a) and the GC/MWCNT multiwall carbon nanotube electrode (c) are featureless. The background double layer charging current is considerably larger for the GC/MWCNT electrode due to the much greater surface area; the surface area of the GC/MWCNT electrode is ca. 100 times more than bare GC electrode. An estimated area of ca. 14 cm^2 was calculated using the method suggested by Peigney *et.al* [202] for 9.5 nm MWCNTs with 7-9 walls. For the two electrodes after incubation in the GOx solution there is a very clear pair of redox peaks in the case of the GC/MWCNT/GOx electrode (d) but no obvious change for the GC electrode (compare (a) and (b)). For the pair of redox peaks at the GC/MWCNT/GOx electrode at 60 mV s^{-1} the formal potential (E°) is *ca.* -0.459 V vs. SCE with a peak-to-peak separation (ΔE_p) of 0.021 V, the cathodic and anodic peak currents and charges are approximately equal.

The results shown in Figure 3.2 are basically identical to those in the literature reported for GOx at carbon nanotube electrodes and are frequently taken as evidence of direct electron transfer to flavin in the redox active site of GOx (for examples see Table 3.1). However, the crystal structure of GOx (Figure 3.1) makes it clear that the electron transfer distance from the enzyme's cofactor FAD to an electrode surface is large and thus, no effective and fast DET should be expected. Therefore, the symmetrical and well-defined peaks shown in Figure 3.2 (d) could be attributed to the presence of free FAD within the commercial GOx,[203-205] which seems to be sufficient to produce those peaks taking into account the dramatic increase of the enzyme loading as a result of the significant increase in the electrode surface area; the surface area of the GC / CNT electrode is ca. 100 times more than bare GC electrode.[202] This conclusion is discussed further in Section 3.14.

3.6 Effect of scan rate on voltammetry of GC/MWCNT/GOx

The effect of scan rate on the voltammetry performance has been employed in the vast majority of the literature reported for GOx at carbon nanotube electrodes (see Table 3.1 for examples). The linear dependence of the anodic peak current and cathodic peak current on the scan rate are taken as evidence for a quasi-reversible surface-controlled process for the redox reaction. To investigate the electrochemistry of the adsorbed species, different scan rate studies were first performed at the GC/MWCNT/GOx electrode which was prepared using pure carboxylate functionalised MWCNTs and the results are shown in Figure 3.3. The second different scan rate studies were done at the GC/MWCNT/GOx electrode which was prepared using impure MWCNTs (the metallic impurities in these MWCNTs are discussed in Section 3.13) and the results are shown in Figure 3.4. The voltammetry on the two different electrodes is very similar. In both cases the redox peak currents (I_{pa} and I_{pc}) increase linearly with increasing scan rates from 10 to 1000 mV s^{-1} indicative of a surface adsorbed redox species. The peak-to-peak

separation (ΔE_p) increase linearly with increasing scan rates with the cathodic (E_{pc}) and anodic (E_{pa}) peak potentials shifting in positive and negative directions respectively. For the carboxylate functionalised MWCNTs the redox charge is 4.3 µC and for the impure MWCNTs 4.2 µC. Assuming a surface area of 14 cm^2 and a two electron process this corresponds to a coverage of around 1.5 pmol cm^{-2}.

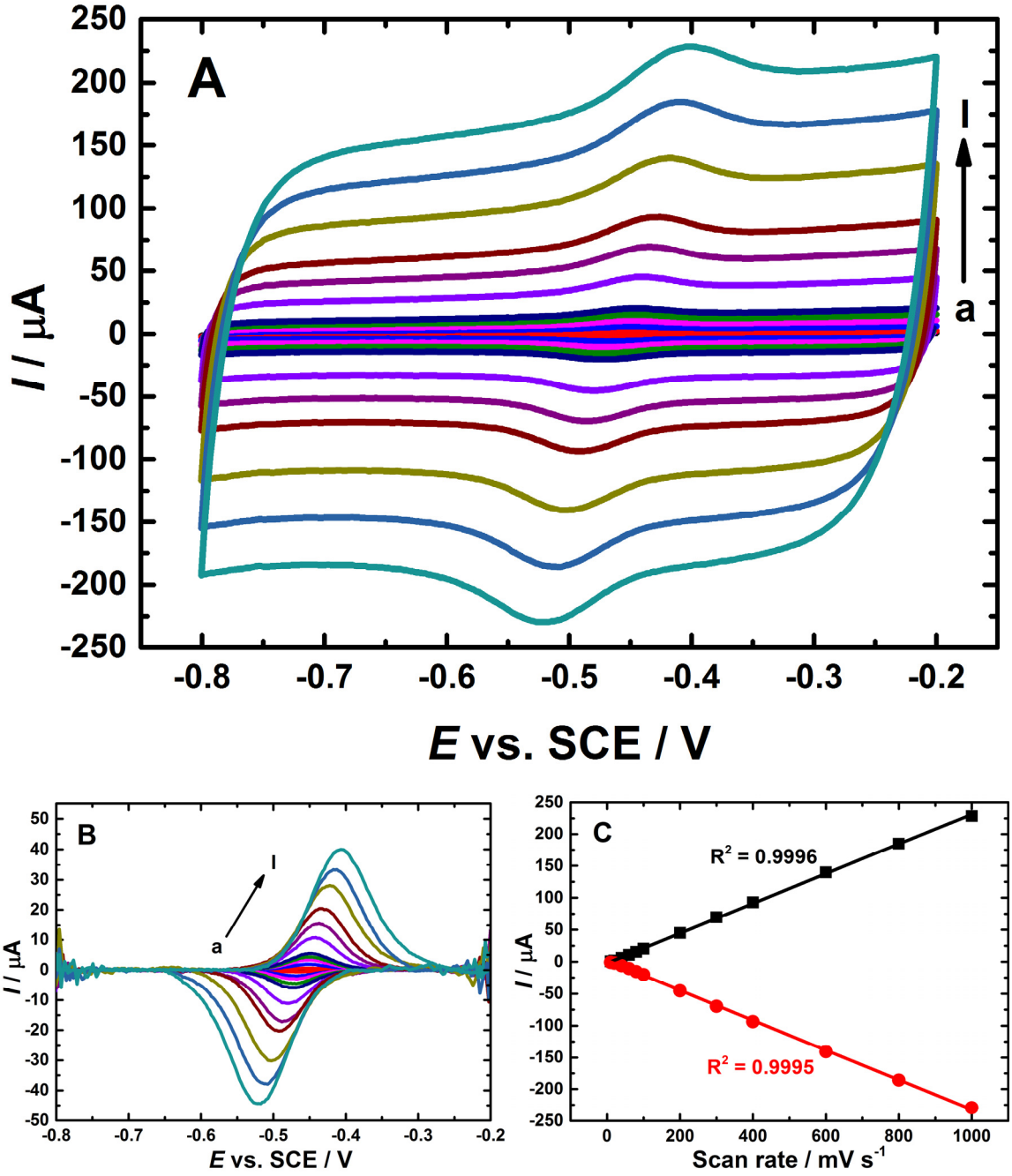

Figure 3.3. *(A) Cyclic voltammograms of GC/MWCNT/GOx electrode in deoxygenated 0.1 M PBS (pH 6.8) at different scan rates (from (a) to (l): 10, 20, 40, 60, 80, 100, 200, 300, 400, 600, 800 and 1000 mV s^{-1}). (B) After background current subtraction. (C) Shows the linear dependence plot of peak currents with scan rate. The GC/MWCNT electrode was prepared by drop casting of a 5 µL aliquot of 1 mg mL^{-1} MWCNT (pure, carboxylic acid functionalized) dispersion onto the cleaned surface of GC. GOx was immobilized using incubation in a solution of 1 kU GOx dissolved in 0.1 M phosphate buffer solution (pH 6.8) for 12 h.*

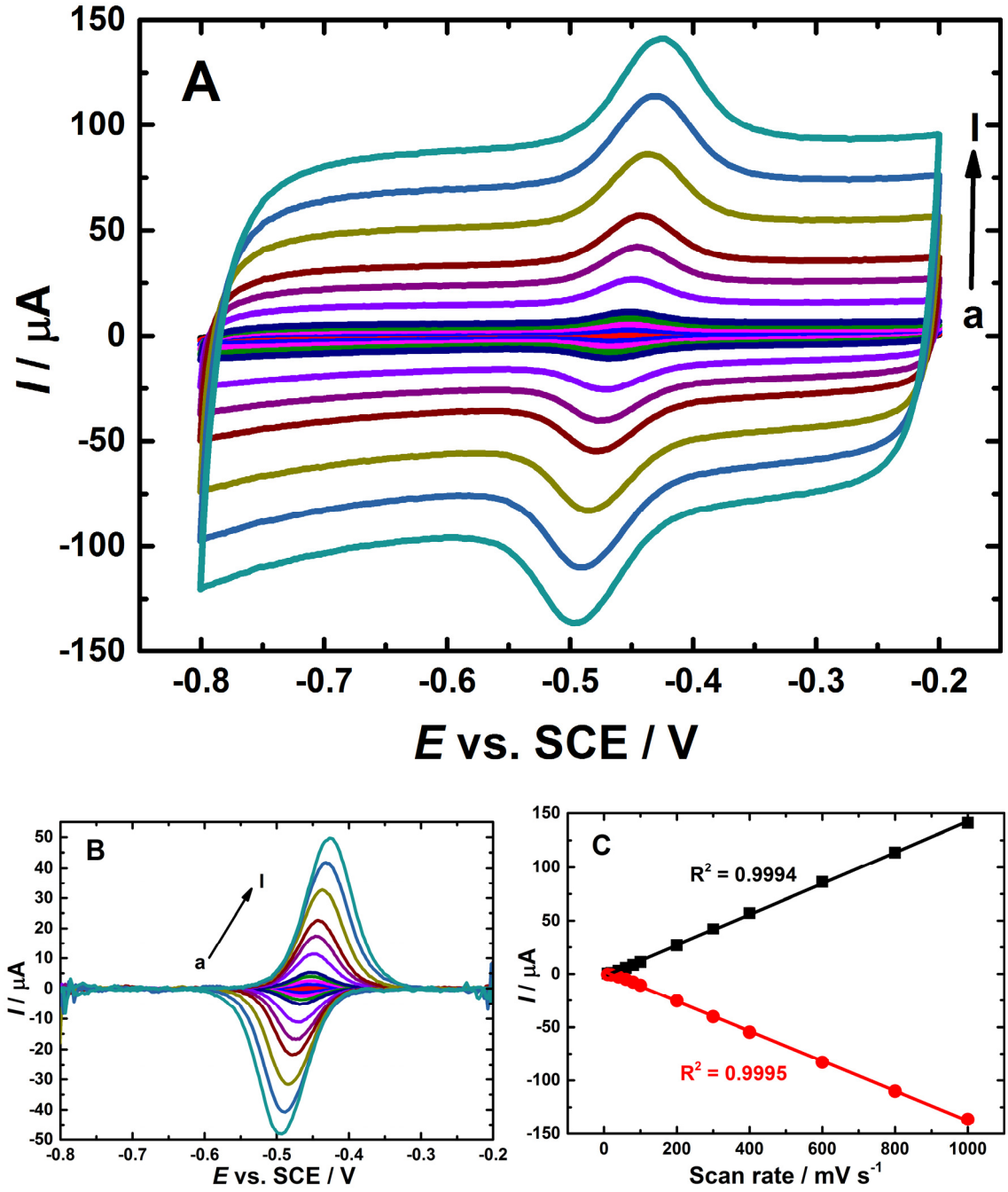

Figure 3.4. *(A) Cyclic voltammograms of GC/MWCNT/GOx electrode in deoxygenated 0.1 M PBS (pH 6.8) at different scan rates (from (a) to (l): 10, 20, 40, 60, 80, 100, 200, 300, 400, 600, 800, 1000 mV s^{-1}). (B) After background current subtraction. (C) Shows the linear dependence plot of peak currents with scan rate. The GC/MWCNT electrode was prepared by drop casting of a 5 µL aliquot of 1 mg mL^{-1} impure MWCNT dispersion onto the cleaned surface of GC. GOx was immobilized using incubation in a solution of 1kU GOx dissolved in 0.1 M phosphate buffer solution (pH 6.8) for 12 h.*

The background currents were subtracted (Figure 3.3B and Figure 3.4B) using a baseline (subtract baseline) created in Origin 9.0. The baselines were created individually for each half

of the voltammograms (anodic and cathodic) using 300 points automatically placed on the curve through the potential range, points were then deleted from the potential range of the peak. The remaining points were interpolated using B-spline function to produce the baseline.

To further reveal the behaviour of the carbon nanotube electrodes with adsorbed GOx, such performance can be modelled by the Laviron equation[206] for estimation of the transfer coefficient (α) and the heterogeneous electron transfer rate constant (k_s). This equation was chosen as it is widely used in publications that claim to observe DET for GOx. In order to evaluate the effect of the residual metallic impurities present within the CNTs on the heterogeneous electron transfer rate constant for the species immobilised on the GC/MWCNT electrode, the kinetic analysis for the electrodes used in Figure 3.3 and Figure 3.4 were accomplished by processing the cyclic voltammograms within the Laviron model. This mathematical approach uses the ΔE_p, namely,the overpotential / (cathodic–anodic) peak potential separation as a way to determine the heterogeneous electron-transfer rate constant (k_s), which should be a function of the scan rate.[207]

The standard rate constant (k_s) for 2 electron transfer, and the transfer coefficients for anodic (α_a) and cathodic (α_c) reaction were determined using the equation of Laviron derived for linear potential scan and based on the Butler-Volmer approximation. Overpotentials (Ep-Emid) are the only experimental data required to employ this Butler-Volmer method.[8] α generally lies between 0.3 to 0.7 but 0.5 is normally taken as the value of α in the absence of actual measurements. However, the α value is not always 0.5.[208] Therefore, the determination of α is crucial in order to estimate the apparent rate constant (k_s). Thus, $E_{pa/pc}$-E_{mid} was plotted separately as a function of log v, which gives two branches, in order to determine the value of α. Hence, using a Laviron trumpet plot of peak separations ($E_{pa/pc}$-E_{mid}) versus log scan rate (v) in a linear fitting for the anodic and cathodic branches at high scan rate yields two straight lines.[206] Both of the linear fits should be obtained where $\Delta E_{peak} > 200/n$ mV, where n is the number of electrons exchanged.[209] These allow us to determine the k_s value using equations 3.3 and/or 3.4

$$k_s = \frac{\alpha_c n F V_c}{RT} \qquad (Eq.\ 3.3)$$

$$k_s = \left(1 - \alpha_a\right)\frac{nFV_a}{RT} \qquad (Eq.\ 3.4)$$

where V_c and V_a at zero overpotential are the intercept points of the extrapolated lines for the cathodic and anodic branches, respectively.[207] α_a and α_c values can be calculated from the slopes of linear parts of the $E_{pa/pc}$ - E_{mid} *vs.* Log v dependence using the equations 3.5 and 3.6.

$$Cathodic\ slope = \frac{-2.3\ RT}{\alpha_c\ nF} \qquad (Eq.\ 3.5)$$

$$Anodic\ \ slope = \frac{2.3\ RT}{(1-\alpha_a)nF} \qquad (Eq.3.6)$$

where R is the gas constant, T is the temperature in Kelvin (K), n = 2 is the number of electrons transferred, F is the Faraday constant, α_c and α_a are transfer coefficient of anodic and cathodic, respectively. Figure 3.5A shows the Laviron plots of $E_{pa/pc}$ - E_{mid} versus logarithm of the scan rate used to estimate the charge transfer rate constant of the GC/MWCNT/GOx electrode which was constructed using pure MWCNTs. Figure 3.5B displays the Laviron plots of $E_{pa/pc}$ - E_{mid} versus the logarithm of the scan rate used to estimate the charge transfer rate constant of the GC/MWCNT/GOx electrode which was fabricated using impure MWCNTs. The results shown in Table 3.2 confirmed a significant increase in the charge transfer rate constant of the GC/MWCNT/GOx electrode (prepared using impure MWCNTs when compared with the charge transfer rate constant of the GC/MWCNT/GOx electrode (prepared using pure MWCNTs).

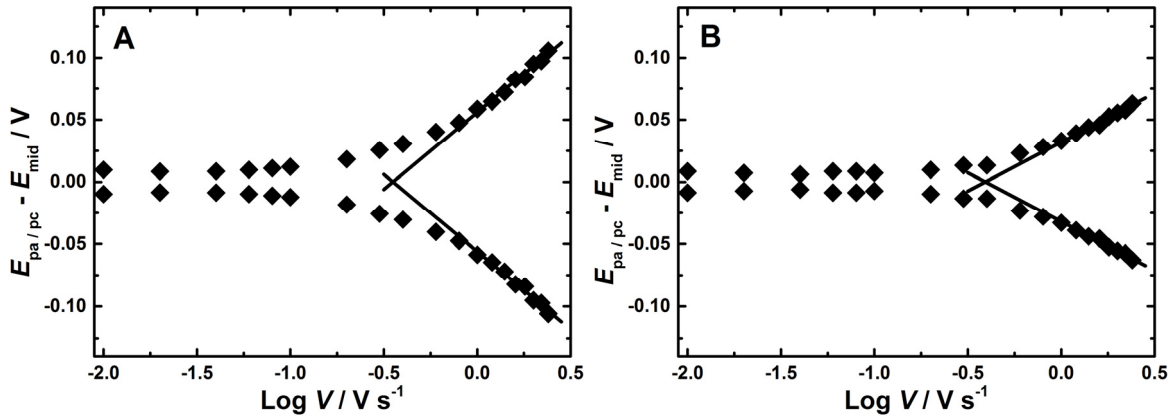

Figure 3.5. *Laviron trumpet plot of the logarithm of the scan rate versus $E_{pa/pc}$ - E_{mid} used to estimate the transfer coefficient and charge transfer rate constant of the GC/MWCNT/GOx electrode in deoxygenated 0.1 M PBS (pH 6.8) at different scan rates (10-2400 mV s^{-1}). The electrodes were prepared as in Figure 3.2 (A) using pure carboxylic acid functionalized MWCNTs; (B) using impure MWCNTs.*

Table 3.2. *Electron transfer coefficient (α) and heterogeneous electron transfer rate constant (ks) for GC / MWCNT / GOx electrodes.*

CNT type	Transfer coefficient for anodic (α_a)	Transfer coefficient for cathodic (α_c)	Rate constant (k_s) / s^{-1}
Pure MWCNTs (carboxylic acid functionalized)	0.3±0.2	0.3±0.2	6.7±0.2
Impure MWCNTs	0.4±0.2	0.4±0.2	11.0±0.2

The Laviron equation was developed from the Butler-Volmer expressions.[208] In the Butler-Volmer equation, α is defined for one electron transfer process in which $\alpha_a + \alpha_c = 1$. Therefore, in the case of α for a 2 electron transfer process such as for FAD, the α for anodic and cathodic branches does not add to 1 because they might refer to different transition states.

Figure 3.6 shows Laviron "trumpet plots"[206] for the two sets of voltammograms (Figure 3.3 and Figure 3.4). These trumpet plots can also be analysed to extract estimates of the electron transfer kinetics for the adsorbed species, however there are some complications in this analysis because the original Laviron equations refer to a reaction which includes one electron and because the results in the voltammetry can be affected by iR drop[210] that will increase the peak separations, particularly at high scan rate when the peak current is largest. In addition, in common with results for many surface redox couples, the trumpet plots show a residual peak separation at low scan rate that is not accounted for in the Laviron theory.[174, 211-212]

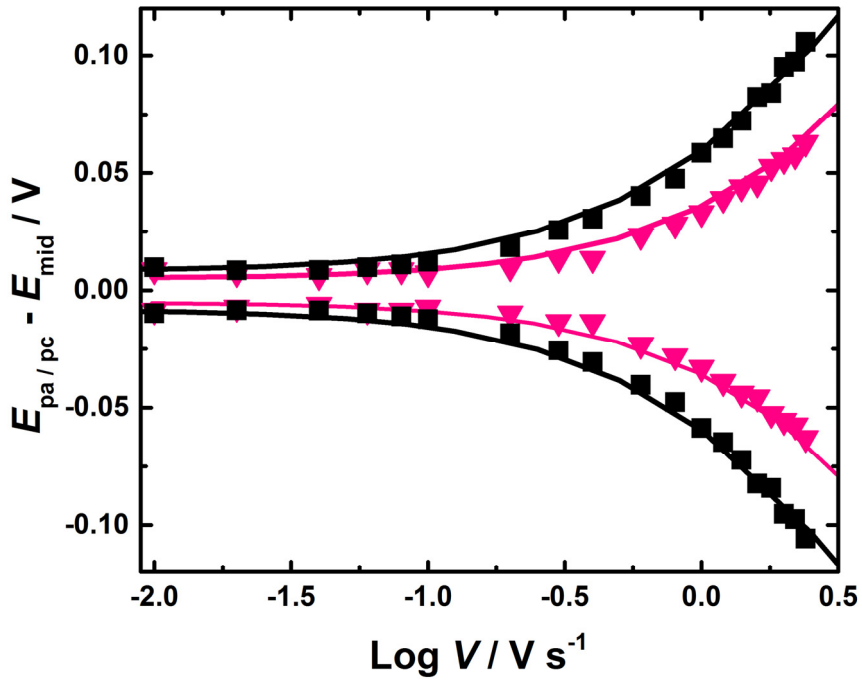

Figure 3.6. *Plots of $E_{pa/pc}$ - E_{mid} against log scan rate for GC/MWCNT/GOx electrodes in deoxygenated 0.1 M PBS (pH 6.8) at different scan rates (10-2400 mV s^{-1}). The lines are calculated using the theoretical expression of Laviron with α = 0.4 for anodic and cathodic curves. The electrodes were prepared as in Figure.3.2. Black line, squares: using pure carboxylic acid functionalized MWCNTs; pink line, triangles: using impure MWCNTs.*

Regardless of the precise details of the Laviron analysis it is clear that the electron transfer kinetics for the surface bound redox species are fast (at least 6.5 s^{-1}) and this is inconsistent with long range electron transfer over 17 Å as would be required by the crystal structure of GOx. Thus although these redox peaks appear in a region that might be consistent with oxidation/reduction of the flavin in the GOx active site it seems much more likely that there is some other explanation for the voltammetric peaks.

3.7 Denaturation using guanidine hydrochloride

One piece of evidence that has been suggested in the literature[150-152, 213] to support the assumption that the redox peaks are due to DET to GOx is the effect of guanidine hydrochloride. It has often been suggested that guanidine hydrochloride at high concentration can easily dissociate FAD from the active site of GOx and/or denature GOx and displace it from the electrode surface.[150-151, 214-216] It is also known that high concentrations of guanidine hydrochloride have little effect on FAD directly adsorbed at electrode surfaces.[150-152, 213] Figure 3.7 shows the results of this type of experiment for our GC/MWCNT/GOx electrode. After incubation of the electrode in 3 M guanidine hydrochloride solution for 12 h, the redox peak has approximately halved in size. Indeed, these results appear to support the idea that the redox peaks are due to DET to GOx. Nonetheless, the situation is more complex. High concentrations of guanidine hydrochloride are known to denature proteins.[217]

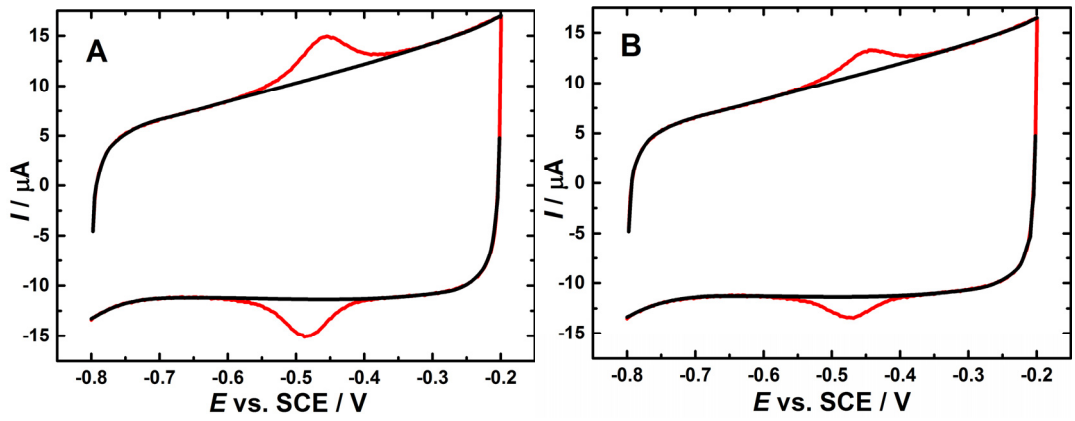

Figure 3.7. *Cyclic voltammograms in 0.1 M deoxygenated PBS (pH 6.8) at a scan rate of 60 mV s^{-1} for the GC/MWCNT/GOx electrode (red lines) before (A) and after (B) incubation in 3 M guanidine hydrochloride solution for 12 h, the black lines are the corrected baseline. The GC/MWCNT electrode was prepared by drop casting drop casting of a 5 µL aliquot of 1 mg mL^{-1} MWCNT (carboxylic acid functionalized) dispersion onto the cleaned surface of GC. GOx was immobilized using incubation in a solution of 1 KU GOx dissolved in 0.1 M PBS (pH 6.8) for 12 h.*

To evaluate the effect of the guanidine hydrochloride on the free FAD which may have dissociated away from the enzyme due to conformational changes during immobilization, a control experiment was performed. To that aim, the GC/MWCNT electrode was modified with flavin and human serum albumin, a 65 kDa heart shaped, soluble protein with no redox centres of its own.[218] In this case, the GC/MWCNT electrode was immersed in a mixture of human serum albumin and FAD for 4 h and then the electrode was incubated in 3 M guanidine hydrochloride for 12 h. Figure 3.8A shows the voltammetry for the GC/MWCNT/(albumin + FAD) electrode before incubation in 3 M guanidine hydrochloride solution. Surface redox peaks for the adsorbed flavin are clearly visible around -0.454 V *vs.* SCE. After incubation with

guanidine hydrochloride these peaks are significantly reduced, again nearly half of the redox peak has disappeared (Figure 3.8B). Thus we cannot conclude, based on the effect of guanidine hydrochloride that the redox peaks must be associated with DET to GOx. They could as readily be explained as due to free flavin at the electrode surface that is significantly reduced in coverage when incubated with guanidine hydrochloride when a protein, GOx or human serum albumin, is also present on the surface. Most probably this is caused by co-desorption of the flavin with the denatured protein.

The importance of this experiment is that the albumin + FAD mixture has been used as a model for the commercial GOx because it contains protein and free FAD. Thus, the experiment done in guanidine hydrochloride as reported in the literature is not convincing evidence to support the claimed direct electron transfer between the GOx and the CNT electrodes.

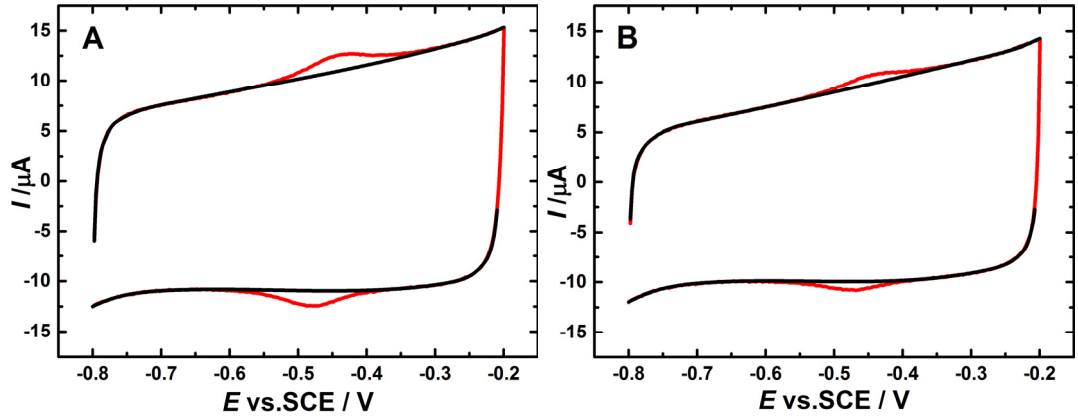

Figure 3.8. *Cyclic voltammograms in 0.1 M deoxygenated PBS (pH 6.8) at a scan rate of 60 mV s^{-1} for the GC/MWCNT/albumin + FAD electrode (red lines) before (A) and after (B) incubation in 3 M guanidine hydrochloride solution for 12 h, the black lines are the corrected baseline. The GC/MWCNT electrode was prepared by drop casting drop casting of a 5 µL aliquot of 1 mg mL^{-1} MWCNT (carboxylic acid functionalized) dispersion onto the cleaned surface of GC. (Albumin + FAD) was immobilized using incubation in a solution of 0.6 x 10^{-6} M FAD in 1.9 mg mL^{-1} human serum albumin for 4 h.*

3.8 Adsorbed flavin

An obvious candidate for the adsorbed redox species seen on the GC/MWCNT/GOx electrodes is flavin adsorbed directly on the electrode surface, but where could this free flavin come from? There are two obvious sources, free flavin as an impurity in the original enzyme solution[203-205] or flavin that dissociates from the enzyme during the incubation of the electrode with the enzyme. The presence and gradual release of free FAD from commercially available glucose oxidase were investigated using a GC electrode covered by a dialysis membrane (Sigma No. D9777) during incubation with the GOx solution. To avoid the dialysis membrane displacing

the drop coated MWCNTs, the GC electrode was employed rather than the GC/MWCNT electrode. This membrane has a typical molecular weight cut-off of 14,000 Dalton. Therefore only the FAD can penetrate through the membrane but GOx, with a relative molecular weight around 160 kD, cannot. Figure 3.9 displays the cyclic voltammograms of the glucose oxidase immobilised on the GC electrode covered by dialysis membrane in 0.1 M PBS (pH 6.8) at a scan rate of 70 mV s^{-1}. For the GC electrode incubated with the freshly prepared solution of as-received, commercial GOx (Figure 3.9A) weak anodic and cathodic peaks around -0.452 V vs. SCE can be seen. For the dialysis membrane covered GC incubated in an aged solution of the same GOx (Figure 3.9B) the same redox peaks are clearly visible but in this case the intensity is larger. The adsorbed redox peaks in these experiments are significantly less prominent than those at the GC/MWCNT electrodes (compare Figure 3.2 and 3.9) but this is because: i) the dialysis membrane acts as a diffusional barrier to the flavin reaching the GC surface, and ii) the area of the GC electrode is much less than that for the GC/MWCNT electrode. Nonetheless, the experiment clearly indicates that free flavin is present in solution, that it is there in greater amounts in the aged enzyme solution, showing that the flavin does dissociate from the GOx over time,[203] and that it adsorbs at the electrode surface to give redox peaks in the same region as seen for the GC/MWCNT/GOx electrode. The flavin in GOx is known to be strongly bound and not to be removed by dialysis at neutral pH[219] but it is also know that flavin is adsorbed to the enzyme. The importance of this observation lies in its implications for direct electron transfer of glucose oxidase electrode that have been claimed in many research papers (see Table 3.1 for examples). Therefore, it is clear that the pair of well-defined redox peaks obtained in Figure 3.2 was indeed due to free FAD electrochemistry.

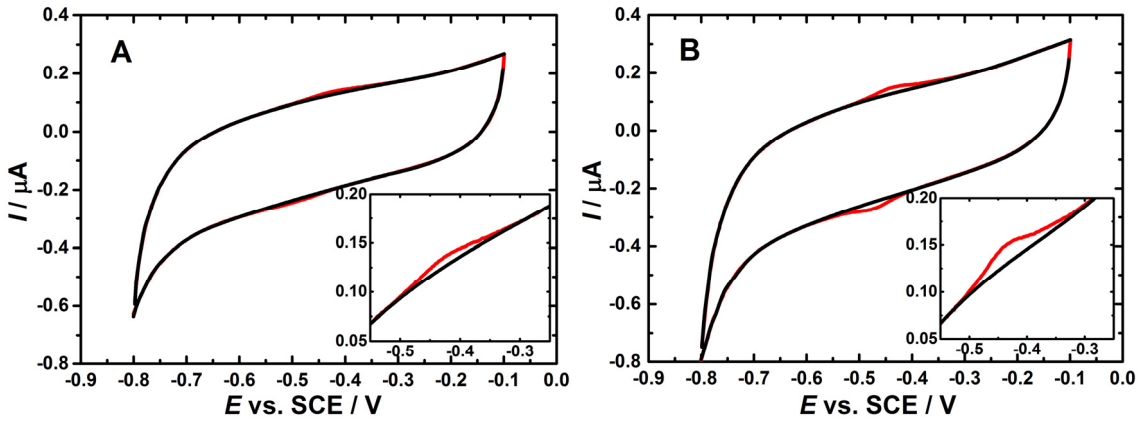

Figure 3.9. *Cyclic voltammograms of the glucose oxidase immobilised on the GC electrode covered by dialysis membrane in 0.1 M PBS (pH 6.8) at a scan rate of 70 mV s^{-1} (red lines), the black lines are the corrected baselines. The GC electrode was incubated in a solution of 1 kU GOx dissolved in 0.1 M phosphate buffer solution (PH 6.8) for 3 h. (A) The GOx solution was freshly prepared, (B) the glucose oxidase solution was prepared 48 h prior to incubation.*

An attempt has been made to overcome the problem of the presence of free FAD in commercial glucose oxidase. The idea was to block the adsorption of FAD onto the surface of the GCE by

passivating the surface using a molecule that has a higher affinity to the surface than FAD. Two molecules have been tested; pyranine (8-hydroxypyrene-1, 3, 6-trisulfonic acid trisodium salt) was drop cast onto GCE. Then the electrode was incubated in FAD. The same experiment was carried out using 1-pyrencarboxylic acid (see Figure 3.10 for structures). Figure 3.11 shows the cyclic voltammograms of GC/FAD, GC/ pyranine/FAD and GC/1-pyrencarboxylic acid/FAD electrodes. The surface concentration of electroactive FAD on the surface of these electrodes, Γ (in mol/cm^2), was estimated using the Faraday's Law:

$$\Gamma = \frac{Q}{nFA\rho} \qquad (Eq.3.7)$$

where Q is the charge consumed in coulombs, obtained from integrating the anodic (or cathodic) peak area in cyclic voltammograms under the background correction, F is the Faraday constant, n =2 is the number of electrons transferred, A is the geometric area of the glassy carbon electrodes (0.071 cm^2) and ρ is the roughness of the cleaned electrode. As 1 and 0.3 μm alumina slurries were employed in GCE polishing, a value of 2 was used for ρ in this calculation.[220] Table 3.3 shows the surface coverage for the adsorbed FAD at the surface of GC, GC / pyranine and GC / 1-pyrencarboxylic acid electrodes.

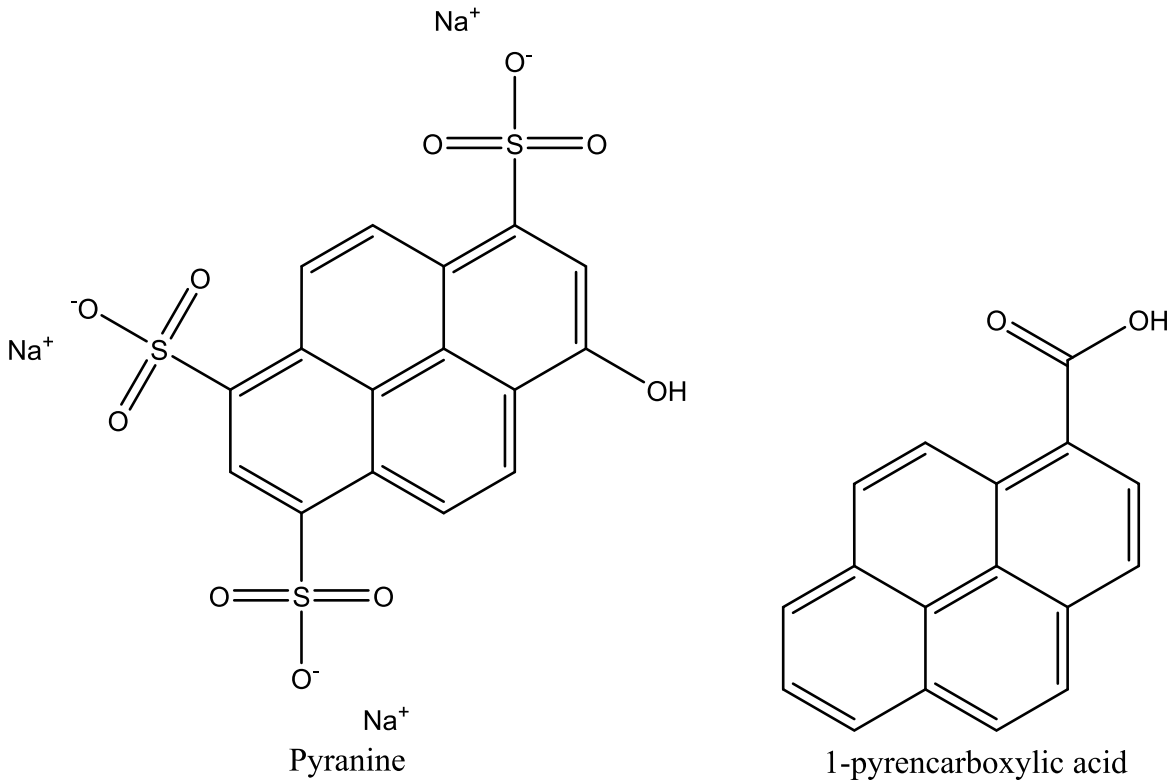

Figure 3.10. *Molecular structures of the pyranine and 1-pyrencarboxylic acid.*

Table 3.3. *The surface coverage for the adsorbed FAD at the surface of bare GC, GC/ pyranine and GC/1-pyrencarboxylic acid electrodes.*

Electrode	GC	GC / pyranine	GC / 1-pyrencarboxylic acid
Surface coverage/ mol cm^{-2}	(1.05± 0.2) x 10^{-12}	(0.14±0.04) x 10^{-12}	(0.03±0.01) x 10^{-12}

The results shown in Table 3.3 confirmed a significant decrease in the concentration of the FAD adsorbed onto the surface of GC / pyranine and GC / 1-pyrencarboxylic acid electrode when compared with the FAD adsorbed onto bare GC electrode. This shows that both pyranine and 1-pyrencarboxylic acid have the ability to block the FAD adsorption onto the surface of the GC electrode. Indeed, those experiments were not further investigated because the pyranine and 1-pyrencarboxylic acid were expected to block the adsorption of the GOx as well.

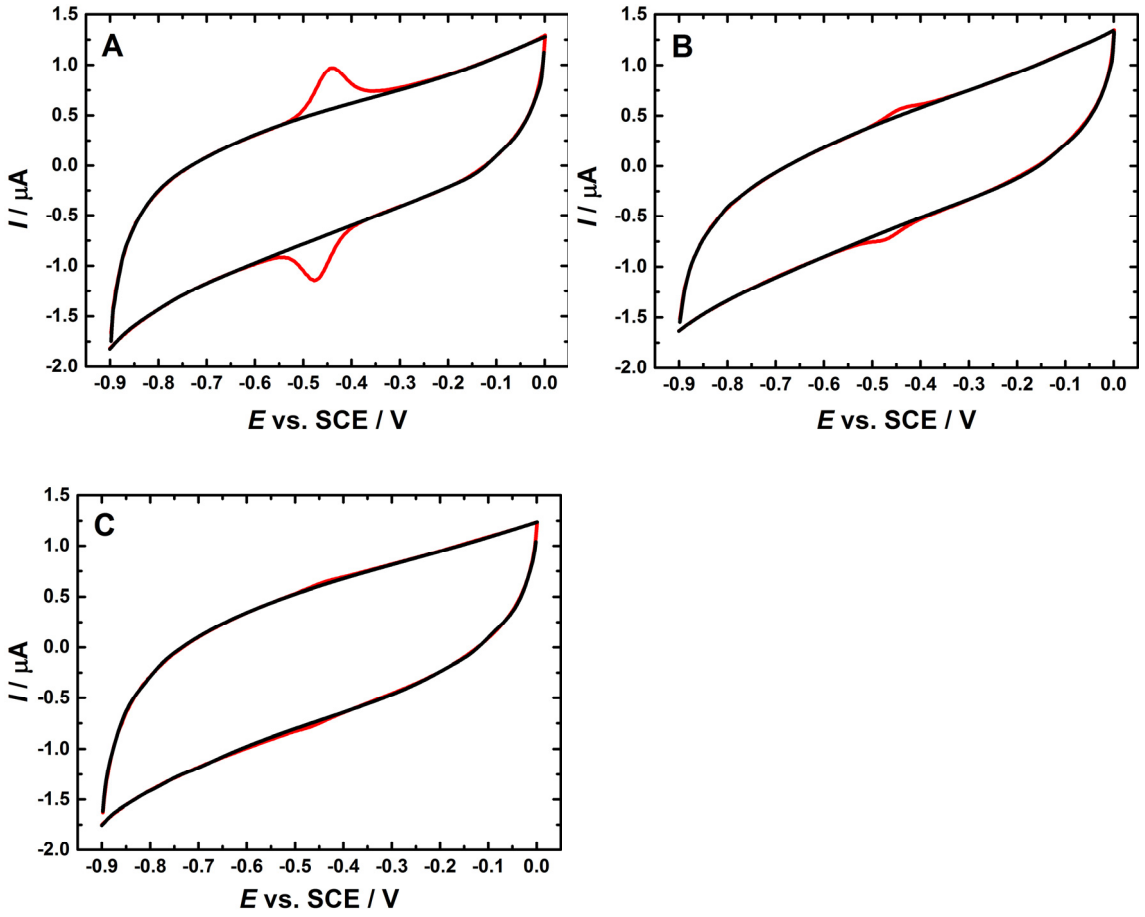

Figure 3.11. *(A) Cyclic voltammograms of the GC electrode in 0.1 M PBS (pH 6.8) at a scan rate of 70 mV s^{-1} after incubation in 10^{-5} M FAD for 30 min. (B) Cyclic voltammograms of the GC/ pyranine electrode in 0.1 M PBS (pH 6.8) at a scan rate of 70 mV s^{-1} after incubation in 10^{-5} M FAD for 30 min. (C) Cyclic voltammograms of the GC/pyrencarboxylic acid electrode in 0.1 M PBS (pH 6.8) at a scan rate of 70 mV s^{-1} after incubation in 10^{-5} M FAD for 30 min.*

3.9 Catalase (CAT) Interference in Glucose Oxidase Electrode

Free flavin is not the only impurity in commercial samples of GOx that can complicate interpretation of the voltammetry. A survey of seventy reported articles [23, 33, 100, 102-103, 106, 112-121, 149, 153, 155-158, 160-161, 164, 167-171, 175-177, 179-186, 205, 213, 221-247] on GOx-immobilised electrodes shows that *ca.* 90% of these papers have employed as supplied glucose oxidase obtained from Sigma Aldrich with no further purification. The main problems in the manufacture of glucose oxidase are the low yield and/or the parallel production of catalase (CAT).[191] According to the specification sheet given by Sigma, it can be seen that the different grades of GOx have different ratios of GOx / CAT. The ratio of GOx / CAT for type VII is about 15, which was used by about 17% of these papers; the ratio for type X-S is about 30, which was used by approximately 27% of these papers; and the ratio is about 7.5 for type II, which was used by 46% of those papers. On the other hand, nearly 10% of the papers used a pure glucose oxidase acquired from other suppliers. In this section, the effects of the presence of catalase in the commercially available as received glucose oxidase purchased from different suppliers was studied.

Catalase (EC 1.11.1.6) is a tetrameric enzyme that catalyses the decomposition of hydrogen peroxide and peroxidatively oxidises alcohol, formate or nitrate using hydrogen peroxide.[248] The four subunits of the enzyme are identical with a relative molecular weight of 57 kDa. Each sub-unit contains a high spin ferriprotoporphyrin IX redox group.[249-250] Many groups have studied the electrochemistry of catalase immobilised on electrode surfaces.[251] Immobilisation of catalase at nanostructured electrode surfaces such as carbon nanotube electrodes shows evidence of a well-defined pair of surface redox peaks at around -0.47 V vs. SCE.[252-253] These redox peaks shift by around 59 mV pH^{-1} and are close to the redox potential expected for the haem Fe(II)/Fe(III) redox centre.[27, 254]

Figure 3.12 shows the cyclic voltammogram of GC/MWCNT/CAT electrode in 0.1 M deoxygenated PBS (pH 6.8) at a scan rate of 60 mV s^{-1}. CVs were recorded in the potential range of -0.8 to -0.2 V vs. SCE. A pair of well-defined and reversible redox peaks can be observed for GC/MWCNT/CAT electrode. The anodic peak potential (E_{pa}) and the cathodic peak potential (E_{pc}) of the redox peaks of the CAT are located at -0.43 and -0.47 V, respectively. Thus, the formal potential calculated was -0.45 V ± 1 mV vs. SCE and the peak potential separation (ΔE_p) was found to be 46 mV at 60 mV s^{-1}. The charge associated with this redox process (5.0 μC) is very similar to that seen for the adsorbed GOx in Figure 3.3 and 3.4. These results are very similar to those in the literature for catalase.[251-253] Interestingly, the formal potential for the surface redox couple on the GC/MWCNT/GOx electrode prepared using GOx from Sigma (Figure 3.2) was also -0.46 V *vs.* SCE.

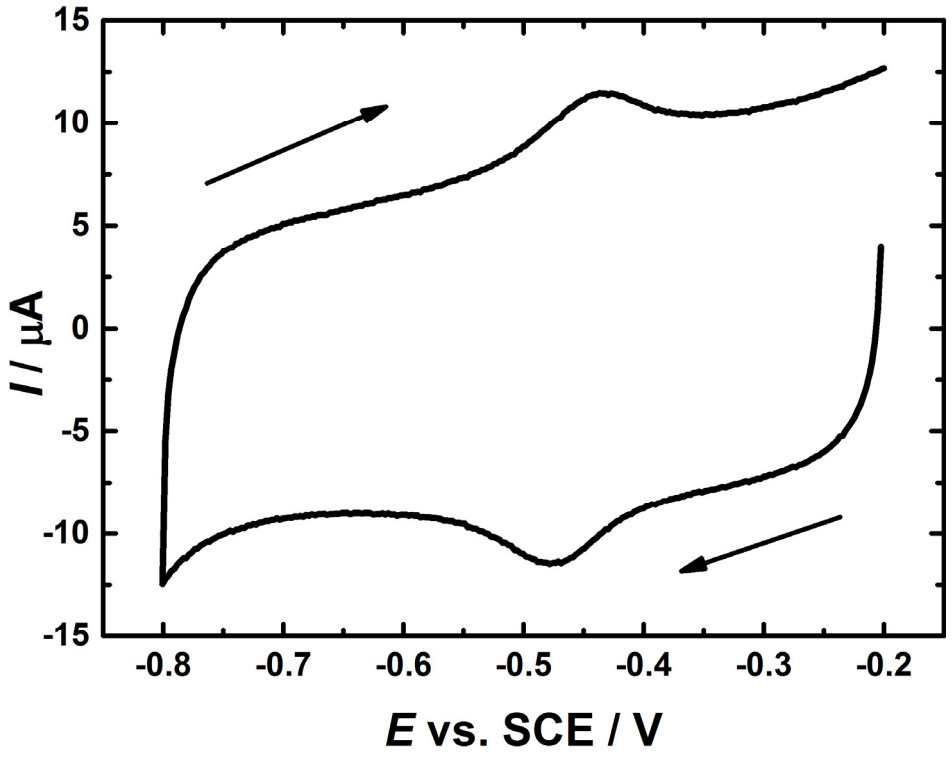

Figure 3.12. *Cyclic voltammograms of GC/MWCNT/CAT electrode in 0.1 M deoxygenated PBS (pH 6.8) at the scan rate of 60 mV s^{-1}. The GC/MWCNT electrode was prepared by drop casting of a 5 µL aliquot of 1 mg mL^{-1} MWCNTs (carboxylic acid functionalized) dispersion onto the cleaned surface of GC. CAT was immobilized using incubation in a solution of 1 kU CAT dissolved in 0.1 M phosphate buffer solution (pH 6.8) for 12 h.*

It could be argued that the effects of CAT on the voltammetry of the adsorbed GOx was not taken into consideration in most, if not all, of already published papers that claimed DET of the GOx. In this study, the effect of the presence of CAT in GOx from Sigma was investigated. To this purpose, we compared results for three different GC/MWCNT/GOx electrode preparations. The first electrode was prepared using a purified GOx (purchased from BBI) with a GOx/CAT ratio ≥ 27500, the second electrode was prepared using type II GOx from Sigma with a GOx/CAT ratio of 7.5, the third electrode (control experiment) was prepared using the purified GOx but with CAT added so the ratio of GOx/CAT was 7.5 to mimic the Sigma type II enzyme. In all cases the electrodes were treated in the same way with the GOx immobilized by incubating the electrodes in a solution of 1 kU mL^{-1} GOx in 0.1 M phosphate buffer solution (pH 6.8) for 12 h. The results are shown in Figure 3.13.

For the electrode prepared with the purified GOx the redox peaks are still present but are much smaller than those for the other two electrodes. Significantly, the redox peaks in the case of the type II enzyme and for the purified GOx mixed with CAT are very similar. From this we conclude that catalase, present as an impurity in many commercial GOx samples can contribute to the redox peaks seen in the voltammetry at around -0.46 V *vs.* SCE in pH 6.8 solution.

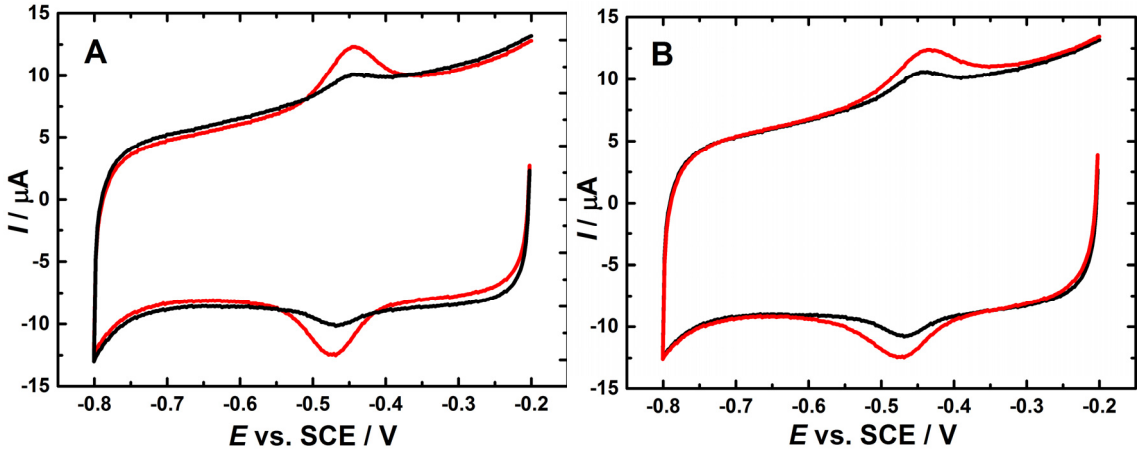

Figure 3.13. *Cyclic voltammograms in 0.1 M deoxygenated PBS (pH 6.8) at a scan rate of 60 mV s^{-1}. A) For the GC/MWCNT/GOx electrode (prepared using pure GOx from BBI) (black line) and GC/MWCNT/GOx electrode (prepared using GOx from Sigma) (red line). B) For the GC/MWCNT/GOx electrode (black line) and GC/MWCNT/GOx+CAT electrode (red line).) The MWCNT electrode was prepared as in Figure 3.2 using carboxylic acid functionalized MWCNTs.*

The importance of the control experiment is that the mixture (pure GOx + CAT) was used as a model for the commercial GOx from Sigma because it contains CAT. Hence, the CAT is the second candidate for the adsorbed redox species seen on the GC/MWCNT/GOx when GOx from Sigma is employed.

3.10 Drop casting GOx

Pure GOx was used to prepare the GC/MWCNT/GOx electrode for the result shown in Figure 3.13 (black lines). However, small peaks can be seen in the CVs. As the incubation in the GOx solution was done for 12 h, those small peaks can be attributed to the dissociation of the FAD from the active site of the GOx. An alternative method to adsorb the GOx on the GC/MWCNT electrode is to drop cast a solution of the enzyme onto the surface rather than incubating the electrode in a solution of GOx for 12 h. In the drop casting experiments, 5 µL of GOx solution (5 U of enzyme) was put onto the GC/MWCNT electrode and then left to dry in the refrigerator at 4°C for one hour before use. The results are shown in Figure 3.14. For the type II GOx from Sigma, the drop casting method still produces surface redox peaks around -0.46 V vs. SCE but they are somewhat less pronounced (redox charge 1.7 µC) than those from the 12 h incubation method (compare with Figure 3.2). In contrast, for the purified GOx from BBI, the redox peaks produced by the drop casting method are very small (redox charge 0.46 µC).

These results strongly suggest that the surface redox peaks seen around -0.46 V *vs.* SCE are not associated with DET of GOx but rather arise from the impurities in the enzyme solution and/or flavin that dissociates from the GOx.

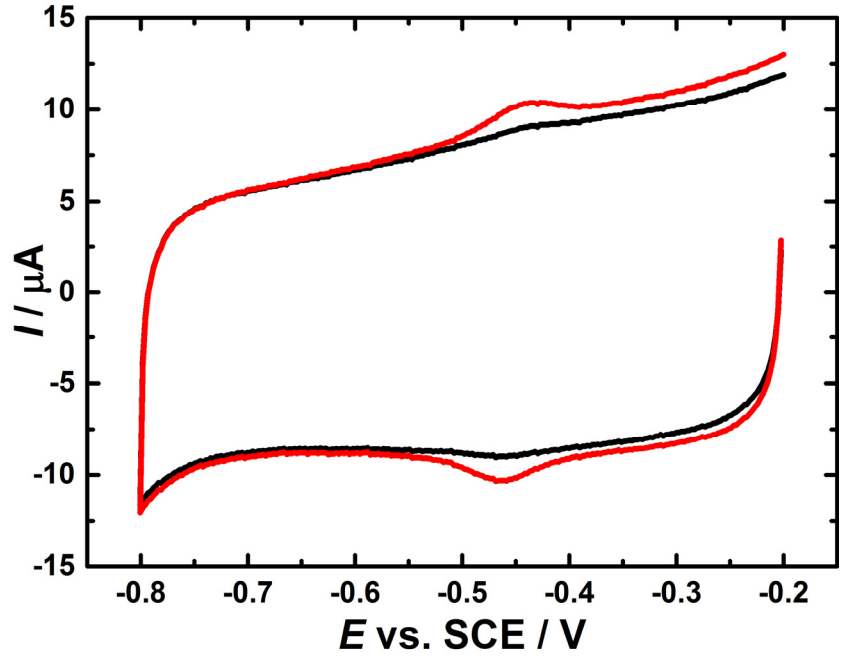

Figure 3.14. *Cyclic voltammograms in 0.1 M deoxygenated PBS (pH 6.8) at a scan rate of 60 mV s^{-1} for the GC/MWCNT/GOx electrode (using pure GOx) (black line) and GC/MWCNT/GOx electrode (using GOx from Sigma) (red line). The MWCNT electrode was prepared as in Figure 3.2 using carboxylic acid functionalized MWCNTs. GOx was immobilized by drop casting of 5 µL (5 U) GOx solution.*

3.11 Effect of solution pH

The pH dependence of the voltammetry has been employed in the vast majority of the literature reported for GOx at carbon nanotube electrodes. The slope of linear regression equation which is in close agreement with the theoretical value of -58.5 mV pH^{-1} is taken (in the literature) as an evidence for the participation of two protons and two electrons in the redox reaction. The electrochemistry of the carbon nanotube electrodes with adsorbed GOx could be due to redox reaction of FAD, which is bound to the enzyme molecule or not (free FAD), and can be expressed as:

$$GOx\text{-}FADH_2 \longrightarrow GOx\text{-}FAD + 2H^+ + 2e^- \qquad Eq.\ 3.8$$

Hence, we studied the effect of pH on the GC/MWCNT/GOx electrode in different deoxygenated pH solutions at a scan rate of 60 mV s^{-1}. Figure 3.15 shows the pH dependence of the voltammetry for GOx at carbon nanotube electrodes in various buffer solutions (pH 4.5-8.5). It can be seen here that a pair of stable and well-defined redox peaks for GOx is observed in each pH solution. Both the E_{pa} and E_{pc} move to negative and positive directions with increasing and decreasing pH. The redox potentials shift by ~50 mV per pH unit. The results shown in Figure 3.15 are basically identical to those in the literature described for GOx at carbon nanotube

electrodes and are frequently taken as evidence of direct electron transfer to flavin in the redox active site of the enzyme (for examples see Table 3.1).

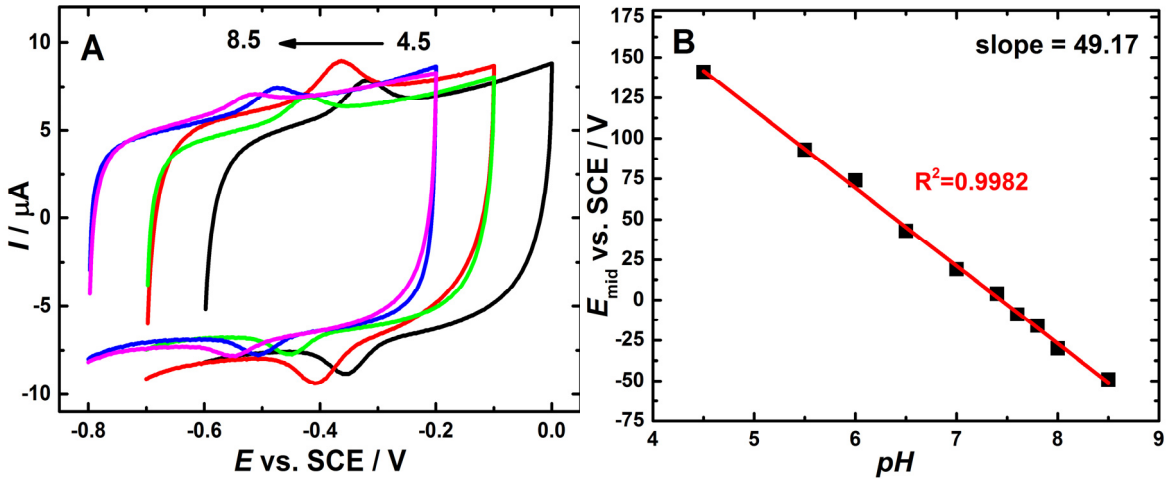

Figure 3.15. *(A) Cyclic voltammograms of the GC/MWCNT/GOx electrode in various deoxygenated pH solutions (4.5 to 8.5) at a scan rate of 60 mV s^{-1}. The MWCNT electrode was prepared as in Figure 3.2 using carboxylic acid functionalized MWCNTs. GOx was immobilized using incubation in a solution of 1 kU GOx dissolved in 0.1 M phosphate buffer solution (pH 6.8) for 12 h. (B) Shows the linear dependence of peak potential with pH.*

In order to explore the origin of the surface redox peaks, the pH dependence of the voltammetry was reviewed comprehensively. The two flavin redox groups in GOx are deeply buried within the protein[190, 193] and their environment should not be changed upon immobilisation of the enzyme at the electrode surface. However, it could be affected if there is a significant perturbation to the enzyme structure which could be caused by the immobilisation of the enzyme. Any significant disruption would, of necessity, substantially disrupt the catalytic activity of the enzyme. The redox potentials of flavins in flavoproteins are known to change depending on the conditions around the flavin and the extent of solvent exposure.[255] Thus, it is expected that the redox behaviour pH dependence of the flavin in the adsorbed GOx to be unchanged from that of the solution enzyme. The determination of the redox potential of flavin in GOx in solution is difficult because the two flavin redox groups are deeply buried inside the protein shell. The features of GOx-bound FAD cannot be determined by cyclic voltammetry because the exchange current is too low. Therefore, it is crucial to perform a classical redox titration[256] in which a mediator creates electrochemical equilibrium with both the GOx and the electrode. Vogt *et al.*[144] recently overcame this problem using UV/vis spectroelectrochemistry. In this section, a comparison between the results of our study of the pH dependence of the surface redox peaks to their recent results for GOx in solution, was conducted. To this aim, the pH dependent redox potentials for the couple observed for glucose oxidase immobilised on the surface of GC / CNT, were measured between pH 4.5 and 8.5 using cyclic voltammetry. Figure 3.16 shows a plot of the mid peak potentials for two replicates of

the GC/MWCNT/GOx electrodes plotted as a function of pH (curves (c) and (d) in the figure). For comparison, the results for the pH dependence of the redox potentials of flavin and GOx in the solution which were provided by Vogt *et al.* were also plotted in Figure 3.16. On one hand, there is a significant difference between our experimental data and the redox potential for GOx in solution (curves a, c and d). On the other hand, the curves for the surface-bound redox process and flavin in the solution (curves b, c and d) are reasonably close with a notable deviation in the lines occurring above pH 7. For flavin which is present in the solution, in their paper Vogt *et al.* also showed that the pH dependence changes from -50 mV pH^{-1} below pH 7 to -27 mV pH^{-1} above pH 7. This change corresponds to a pK_a for the flavohydroquinone of around 6.8 which is in agreement with the literature.[257] A similar shift in the redox potential of the enzyme-bound FAD from that of the free FAD at pH 7 was also reported by Liu *et al.*[129] for the experiments where the apo-enzyme was reconstituted around surface immobilised FAD. Thus, it can be concluded that the redox peaks for the couple observed at carbon nanotube electrodes with adsorbed GOx are from FAD adsorbed on the electrode surface and not from FAD that is deeply buried in enzyme active site.

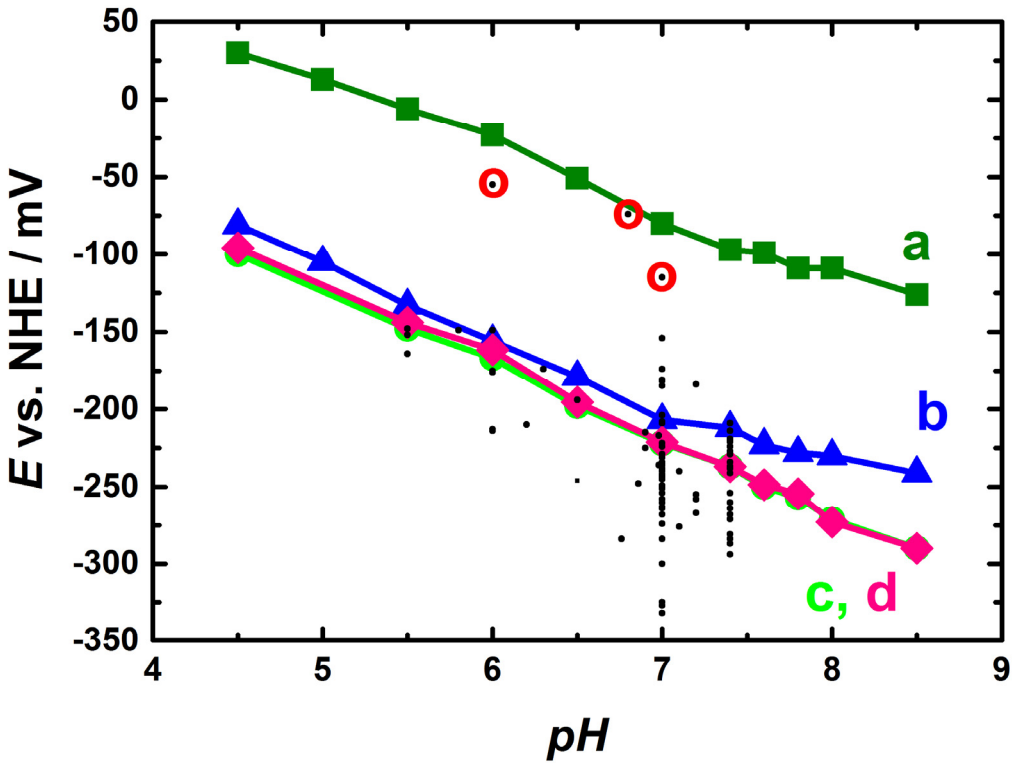

Figure 3.16. *Redox potentials of GOx (a) and FAD (b) investigated using UV/vis. spectroelectrochemistry as reported by Vogt et al.[144] compared with replicate experimental data (c, d) obtained from cyclic voltammetry of GC/MWCNT/GOx electrodes in the pH range between pH 4.5 and 8.5. Measurements were performed in deoxygenated 0.1 M buffers (depending on pH sodium citrate, sodium phosphate, or tris (hydroxymethyl) aminomethane (TRIS)-buffer were used) with 0.1 M potassium chloride and 5 mM magnesium chloride at a scan rate of 60 mV s^{-1}. The overlaid points (black dots) are the redox potentials take from the literature given in Table 3.1. In all cases, the values have been converted to the NHE scale.*

The potentials and pH dependent redox potential obtained in Figure 3.16 for electrodes with adsorbed GOx are in agreement with literature data for flavin adsorbed on GC[258] and CNT electrodes.[174]

Figure 3.16 also shows a plot of the different redox potentials reported in the literature (taken from Table 3.1). It is clear that the vast majority of the results matches with the curve corresponding to adsorbed FAD and are considerably shifted (>100 mV) from the potential expected for GOx-bound FAD. Nonetheless, only three publications, the three circled points, fall close to the potential expected for GOx-bound FAD. These correspond to Yang *et al.*,[259] Eskandari *et al*.[260] and Li *et al.*[261] It is not clear why these three are outliers. However, it is obvious in each case that there is no evidence for the catalytic DET from the responses to glucose. Li and Yang both utilised as- supplied GOx from Amresco and in both cases Nafion was employed in the preparation of the modified electrodes. In Li's case the GOx was adsorbed on a glassy carbon electrode modified with silver-ZnO hybrid nanorods. In Yang's case the GOx was adsorbed together with platinum nanoparticle functionalized nitrogen doped graphene. In both cases glucose was detected at negative potentials through the decrease in the oxygen reduction current upon addition of glucose to oxygen saturated buffer. In the work of Eskandari *et al.* the enzyme was covalently immobilised on gold coated magnetic iron oxide and these were held (using a permanent magnet) at the surface of a gold plate electrode. In the latter study, the non-catalytic measurement and the response to glucose experiment were performed in oxygen saturated buffer.

Therefore, it can be concluded that the redox peaks shown in the literature (see Table 3.1) for the surface bound redox couple cannot be taken as evidence for DET to the flavin in the active site of GOx. Rather they almost certainly arise from free FAD adsorbed directly on the electrode surface.

3.12 Response to glucose

Figure 3.17 shows a typical set of data for the voltammetry of the GC/MWCNT/GOx electrode with different concentrations of glucose. These results are representative of those reported in the literature by many groups for GOx adsorbed on MWCNTs and a variety of other nanomaterial electrode surfaces for which direct electron transfer to glucose oxidase has been claimed (see Table 3.1 for examples).

It is widely claimed in the literature that the surface redox peaks seen on the MWCNT electrodes with adsorbed GOx are due to direct electron transfer to the active site of the enzyme. However, in our study, the results presented so far have confirmed that the observed

redox peaks are due to the adsorption of some impurity, possibly free flavin, onto the electrode surface. If this is the case how does the glucose response of these electrodes arise?

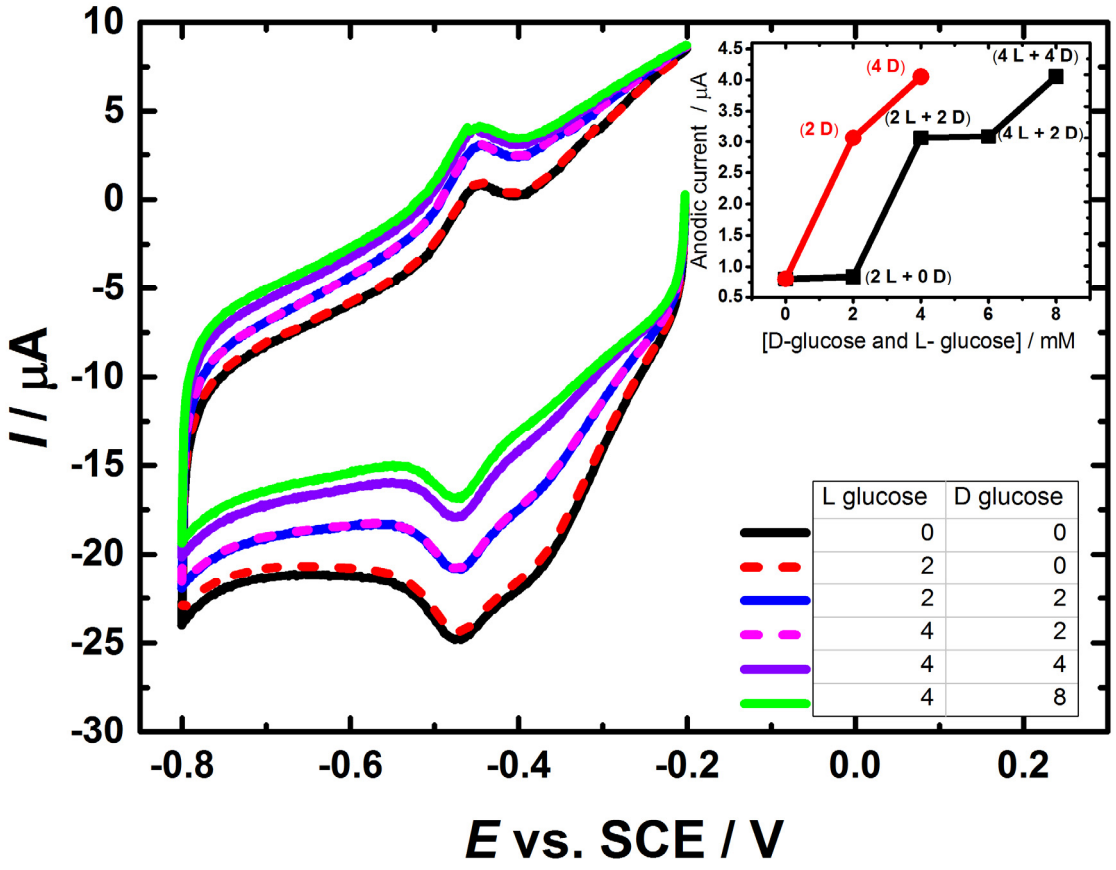

Figure 3.17. *Cyclic voltammograms showing oxygen reduction on a GC/MWCNT/GOx electrode in oxygen saturated 0.1 M PBS pH 6.8 containing different concentration of L and D glucose recorded at 60 mV s^{-1}. The GC/MWCNT/GOx electrode was prepared as in Figure 3.2 using pure carboxylic acid functionalized MWCNTs. Inset relative current for the CV experiments; total glucose (black line), D-glucose (red line).*

Figure 3.17 also reveals the impact of adding aliquots of L-glucose to the solution in the electrochemical cell. The addition of L-glucose is an excellent control experiment to show whether the response arises from the enzymatic reaction or comes about in some other way although it is scarcely ever used in the literature. In this case (Figure 3.17), where upon addition of aliquots to increase the concentration of L-glucose in the cell there is no change in the current (compare each pair of dashed and solid curves), whereas upon each addition of an aliquots of D-glucose to increase its concentration in the cell the current changes (compare the solid curves). This rules out changes in the current because of purely physical effects, such as changes in solution viscosity etc. caused by addition of glucose, and non-specific electrochemical reactions, and clearly shows that the process is in some way enzyme catalysed; L-glucose experiment has also been used to indicate that the immobilized GOx is still active and specific to D-glucose.

The results shown in Figure 3.17 are often taken as evidence for DET of GOx at carbon nanotube electrodes. Nevertheless, there are a number of serious problems with this analysis. First, the current response corresponds to a decrease in the reduction current arising at the electrode not the oxidation current expected to correspond to enzymatically catalysed electrochemical oxidation of glucose. Second, the surface redox peaks around -0.46 V vs SCE are unaffected by addition of D-glucose with both oxidation and reduction peak clearly present throughout and simply moving with the changing background. Third, the position of the onset of the reduction current on addition of D-glucose starts at -0.25 V vs SCE, far-off from the potential of the surface redox peaks.

The behaviour observed in Figure 3.17 can be explained by the fact that there is oxygen dissolved in the solution. Therefore, it is the reduction of oxygen that starts at -0.25 V vs SCE at the MWCNT electrode. Accordingly, the change in current on addition of D-glucose corresponds to a decrease in the oxygen reduction current. This change can be attributed to the decline in oxygen reduction current owing to the depletion of oxygen in GC/MWCNT/GOx electrode; the oxygen at the electrode surface is consumed by the enzyme catalysed reaction with glucose according to the following mediated enzymatic processes:

$$\text{GOx (FAD)} + \beta\text{-D-glucose} \longrightarrow \text{GOx (FADH}_2\text{)} + \text{D-glucono-1, 5-lactone} \qquad (Eq.\ 3.9)$$

$$\text{GOx (FADH}_2\text{)} + \text{O}_2 \longrightarrow \text{GOx (FAD)} + \text{H}_2\text{O}_2 \qquad (Eq.\ 3.10)$$

Depending on the electrode material and the solution composition, the oxygen reduction reaction (ORR) proceeds by a two-electron mechanism or via “direct” four-electron mechanism. For most carbon electrode materials, the indirect peroxide pathway is more likely to be the mechanism of ORR, which involves two sequential 2- electron-transfer steps where peroxide is produced as an intermediate.[262] On CNT electrodes, the ORR proceeds to give H_2O_2[263] and there is a large overpotential region over which the H_2O_2 is unreactive.[264] However, in the cases where metal nanoparticles such as Au nanoparticles are incorporated at the electrode, it is possible to detect the H_2O_2 produced by the enzymatic reaction (see Table 3.1 for examples). Thus, the results in Figure 3.17 indicate that there is enzymatically active GOx immobilised at the electrode surface. However, it is not able to undergo DET at the electrode at any considerable rate. In the next section, the ORR at MWCNT electrodes is further discussed.

3.13 The oxygen reduction reaction at carbon nanotube electrodes

It is widely believed that the oxygen reduction reaction is very sensitive to impurities and there are many research papers that have highlighted the fact that carbon nanotubes, which are created from metallic catalyst, contain residual metallic impurities.[132, 265-266] This unavoidable presence of the metallic impurities would confuse the researchers when analysing the

performance of the carbon nanotubes, especially in their application on biosensor and biofuel cell.[267] The removal of such residual metallic impurities is practically hard to achieve. Even after attempting several acid washing methods, the impurities concentration is in the range of several wt%.[265, 268]

In this section, two types of carbon nanotubes have been used; multi-walled carbon nanotubes (30 ± 10 nm in diameter and 1 - 5 μm in length from NanoLab Inc.), and carboxylic-acid-functionalized multi-walled carbon nanotubes (> 8% carboxylic-acid-functionalized, average 9.5 nm in diameter and 1.5 μm in length from Sigma-Aldrich). According to the specification sheet given by the suppliers, the carboxylic-acid-functionalized carbon nanotubes should have higher purity than the other nanotubes. This has also been supported by the energy dispersive spectroscopy (EDS) spectra presented in Figure 3.18.

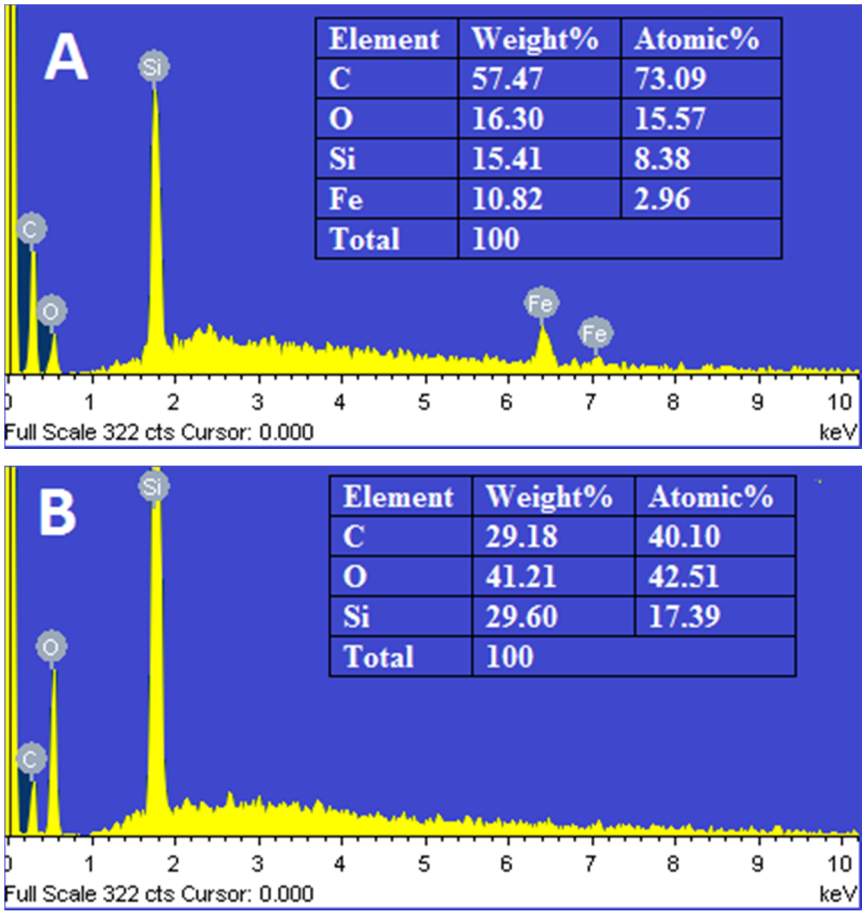

Figure 3.18. *EDS spectra of the MWCNT on the GC electrodes, magnification: 5000x, accelerating voltage: 20.0 kV. The GC/MWCNT electrodes were prepared by drop casting of 5 μL of 1 mg mL^{-1} MWCNT onto the cleaned surface of GC. A) MWCNTs from NanoLab Inc. B) carboxylic acid functionalized MWCNTs from Sigma-Aldrich.*

For the MWCNTs from NanoLab Inc, the spectrum shown in Figure 3.18A confirmed the existence of residual iron impurities with the multi-walled carbon nanotubes. On the other

hand, the carboxylic-acid-functionalized multi-walled carbon nanotubes from Sigma-Aldrich, Figure 3.18B, show no evidence by EDS for metallic impurities. However, the oxygen fraction is much higher, consistent with carboxylic acid functionalization. Several electrochemical experiments were conducted, the ORR and the response to glucose were studied using GC electrodes modified with the two different types of MWCNTs. The results are shown in Figure 3.19 and 3.20.

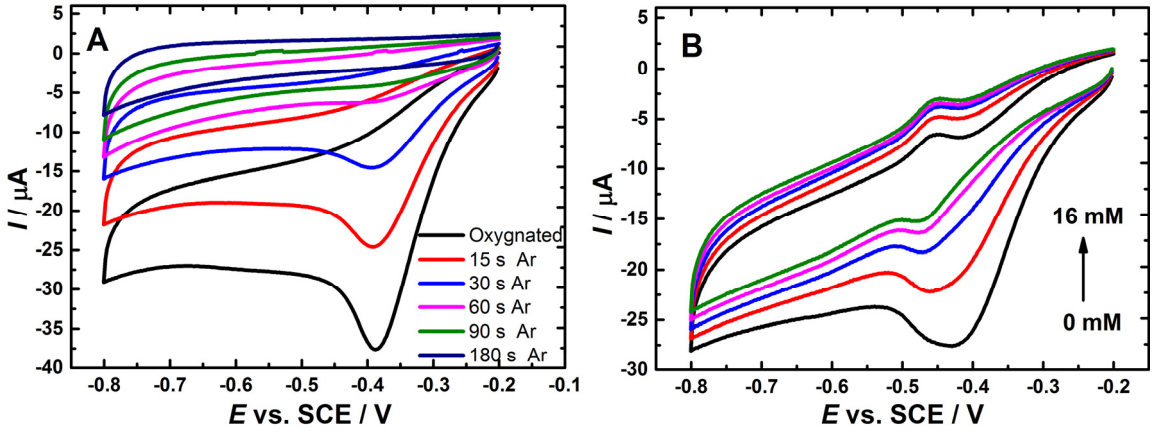

Figure 3.19. *Cyclic voltammograms recorded at 60 mV s^{-1} showing the response of (A) GC/MWCNT electrode in different oxygen concentration and(B) GC/MWCNT/GOx in oxygen saturated 0.1 M PBS pH 6.8 containing 0, 4, 8, 12 and 16 mM of glucose. The GC/MWCNT/GOx was prepared as in Figure 3.2 using impure MWCNTs from NanoLab, Inc.*

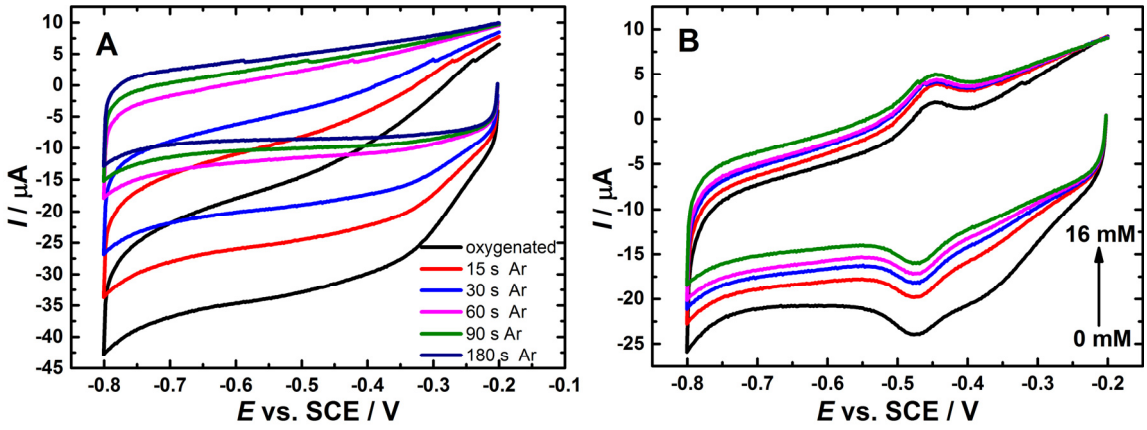

Figure 3.20. *Cyclic voltammograms recorded at 60 mV s^{-1} showing the response of (A) GC/MWCNT electrode and (B) GC/MWCNT/GOx in oxygen saturated 0.1 M PBS pH 6.8 containing 0, 4, 8, 12 and 16 mM of glucose. The GC/MWCNT/GOx was prepared as in Figure 3.2 using carboxylic acid functionalized pure MWCNTs.*

ORR occurs in both cases (Figure 3.19A and Figure 3.20A). The current onset starting at around -0.25 V vs SCE. This current is clearly dependent on the concentration of dissolved oxygen in solution as it decreases with the increasing length of time that the solution is deoxygenated by

purging with Ar. When all the oxygen is removed from solution the current disappears. Comparing the two electrodes, the currents are about the same in both cases but for the MWCNTs with the Fe impurity, Figure 3.19A, there is an obvious peak in the current around -0.4 V vs SCE which is not seen for the purified carboxylate modified MWCNTs. This is probably because the impurity acts as an electrocatalyst for the ORR.[265] As a carbon nanotube modified electrode is used, even for purified MWCNTs, it is very difficult to prove that no traces of the metal catalyst which is used for the creation of the nanotubes are remaining.[266]

Figure 3.19B and 3.20B show the response of GC/MWCNT/GOx electrodes which were constructed using impure (from NanoLab, Inc.) and pure MWCNTs (from Sigma-Aldrich) respectively. Compared to the results for ORR on the different MWCNT electrodes observed in Figure 3.19A and 3.20A, it is clear that the oxygen reduction current is less at the corresponding electrodes with adsorbed GOx indicating that the enzyme partially blocks the catalytic sites for oxygen reduction at the surface. It is also obvious that the onset potential and potential dependence of the reduction current is very similar in the corresponding cases (compare panels A and B in each case).

Interestingly, these results highlight the fact that the differences in performance of different GOx carbon nanotube electrode preparations (in the literature) are likely due to the different levels of impurity present in each case. In light of these conclusions, it is very likely that the claimed bioelectrocatalytic oxidation of glucose on the GC/MWCNT/GOx electrode is in fact an ORR which is catalysed by residual metallic impurities present within the CNTs.

3.14 The suggestions of these results

A new hypothesis, different from the general viewpoint, is put forward in this study; DET may not be happening for any GOx/MWCNT-based electrode. Indeed, the GOx immobilized on the surface of MWCNTs-modified electrode is unable to demonstrate DET with the electrode. However, it retains its catalytic activity. The results obtained show that the appearance of surface redox peaks around -0.46 V vs SCE is unconvincing evidence for DET to GOx but rather is explained by adsorption of impurities, most probably free flavin as well as catalase, onto the nanostructured-electrode material. The high surface area of the nanoelectrode material plays a role here in increasing the magnitude (charge) of these surface redox peaks. Nonetheless, the enzyme is also immobilised at the electrode surface and this immobilised enzyme remains enzymatically active. Therefore, the electrochemical response to glucose observed at potential cathodic of around -0.25 V vs SCE is due to the decrease in dissolved oxygen concentration at the electrode surface due to the enzyme catalysed oxidation of D-glucose. This behaviour is consonant with the “first generation” glucose electrode rather than a “third generation” behaviour with DET to the GOx. Four different suppliers/sources of glucose oxidase and two of

MWCNTs have been used to evaluate the claimed DET of GOx at these nanocarbon materials. Significantly the behaviour of the GOx/CNT system is dominated by the effects of impurities in both the enzyme preparation used, flavin and catalase in the GOx, and in the MWCNTs, Fe impurities that catalyse oxygen reduction. These impurities are not taken into account by many authors.

The conclusions in this chapter here have answered the questions that have been raised by several authors in regards to the evidence for DET of GOx. An investigation of GOx which was immobilised in chitosan on MWCNTs by Wang *et al.*[172] led to a conclusion where there was no evidence for DET even though surface redox peaks were observed and the presence of enzymatically active GOx at the surface of the electrode mediated by ferrocene was shown. They concluded that the redox peaks came from an adsorbed form of enzymatically inactive GOx. However, it is more likely that adsorbed free flavin was present considering that they employed as-received GOx. Goran *et al.*[174] used carbon nanotubes and nitrogen-doped carbon nanotubes using type X-S GOx from Sigma Aldrich in order to study GOx. They concluded that adsorbed GOx was enzymatically active when a redox mediator (1, 4-benzoquinone) was added or oxygen was present and that the surface redox peak was the result of flavin that was not enzymatically active. Wooten *et al.*[184] used GOx (from Sigma-Aldrich) immobilized in chitosan on MWCNTs and found no evidence for DET. They concluded that the electroactive flavin seen in the voltammetry was not part of enzymatically active GOx.

Thus, a similar effect could be seen on any GOx electrodes regardless of electrode materials such as other nanomaterials which include graphene, gold nanoparticles or with various different “additives” namely chitosan or Nafion.

3.15 Do MWCNTs show “special” properties?

Carbon nanotubes (CNTs) were first discovered in the early 1990s.[130] Extensive research on CNTs was initiated in the 1990s. Indeed, this was preceded in 1980 by the first industrial creation of some products now known as CNTs and also the recorded observations of hollow carbon nanofibers in the early 1950s.[131] CNTs have a tubular structure and composed of hexagonal honeycomb lattices built from sp^2 carbon units.[132] The diameters of CNTs are usually several nanometres and the length is several micrometres. Basically , there are two forms of CNT, single-walled carbon nanotubes (SWCNTs) and multi-walled carbon nanotubes (MWCNTs).[133-134] CNTs are interesting for use in electrochemical biosensors. It is widely believed that they have “special” electrochemical properties.[137] Furthermore, it has been suggested that the ET features of CNTs can be enhanced by producing surface groups such as amino groups, NO_2, carboxyl groups or oxygen. However, a question that arises from this study is to what extent carbon nanotubes show “special” properties with regard to their

electrochemistry in applications in glucose electrodes. Taking a closer look at our results, it is clear that there is nothing specific about the use of MWCNTs that enhances the performance of the electrode beyond the fact that the MWCNT layer deposited on the glassy carbon supporting electrode provides a high real surface area, estimated in this case to be 14 cm^2. Moreover, the charging current in the phosphate buffer solution at the GC electrode is much greater per unit real area (100 $\mu F\ cm^{-2}$) than that at the MWCNT surface (8 $\mu F\ cm^{-2}$), Figure 3.2. This difference can be ascribed to the difference in the electronic structure of the two materials and the consequent difference in the density of states (DOS) at the Fermi level.[269-270] Thus, the MWCNTs and carbon nanomaterials do have a "special" property but it has nothing to do with their ability to transfer electrons to/from native GOx.

3.16 Conclusions

In this chapter, it has been demonstrated that the evidence presented in the literature for the vast majority of cases in support of direct electron transfer (DET) to glucose oxidase at electrodes constructed for various nanomaterials, particularly carbon nanotubes (CNTs) of various forms, is unconvincing, arguable or debatable. The present study has shown that the surface redox peaks usually observed in these cases are due to free, adsorbed flavin and not, as claimed to be, due to DET to flavin within the enzyme. In most cases, this free flavin comes predominantly from impurities present in the commercial enzyme when it is used without purification. In addition, the continuing release of FAD from the enzyme's active site has also been recorded. We have also shown that catalase, also present in significant amounts in commonly used commercial sources of GOx, is a concern.

The redox potential of the GOx-bound FAD cannot be determined by conventional voltammetry. Recently, a parallel set of such redox potentials, over a range of pH, has been determined by Vogt *et al.*[144] for both free and GOx-bound FAD. At pH 7.0, the redox potentials were -0.32 V and -0.44 V vs. SCE for GOx-bound FAD and free FAD, respectively. The peaks corresponding to GOx-bound FAD were not seen in the previously published papers that claimed DET of GOx because DET did not take place. Thus, the observed electrochemistry was due to adsorbed free FAD.

The obtained results have also confirmed that the commonly reported response to glucose seen in the presence of oxygen is due to the consumption of oxygen by adsorbed GOx, which should be enzymatically active but electrochemically inactive, that is present at the electrode surface and that metal impurities present in the MWCNTs play an important role in providing the response associated with the oxygen reduction. In this respect, it is ironic that the commonly reported results that claim DET for GOx, as given in Table 3.1, are largely

contributed by impurities. Therefore, our clear conclusion is that there is no evidence for direct electron transfer to native glucose oxidase.

Up to now, numerous types of enzymes have been studied for their electrochemical properties. The enzymes with coupled redox centers have shown an encouraging performance as they can facilitate interaction between the electrode and the active redox center. The next generation biosensors require new enzymes, designed and made by genetic engineering.[271] Indeed, it is crucial to develop a new strategy for the enzyme's immobilisation by employing genetically engineered enzymes with specific surface groups to allow a more targeted approach. In the next Chapter, the focus will be on cellobiose dehydrogenase (CDH) which could have the added advantage of oxygen independent response and structures supporting intramolecular electron transfer between the catalytically active center and an electrode.

Chapter 4 Amperometric cellobiose dehydrogenase electrode

4.1 Overview

Electrodes modified with redox proteins and enzymes are fundamental in the construction of biosensors and biofuel cells. The extraordinary advantages of the enzymes' employment in such applications are moderate working temperature, operation close to the physiological pH, and in addition high activity and excellent selectivity toward the enzyme's substrate.[272] Furthermore, devices that utilise enzymes can be entirely biocompatible and/or biodegradable, making them an ideal choice in the field of implantable medical devices or environmental, self-powered biosensors.[18-19] Nevertheless, the lack of long-term operational stability, as well as the short shelf-storage life of enzymes have not been solved yet.[68] In addition, direct electron transfer (DET) to redox enzymes, which are close to the electrode surface is usually very slow. It may even prove impossible because of the shielding of the prosthetic group (redox-active cofactors) of the enzyme by the surrounding insulating apoprotein shell.[32, 110] The key factor for DET is that the redox-active centre of the enzyme is orientated properly and is within the assumed electron tunnelling distance of less than 8 Å from the electrode surface.[2] Therefore, effective DET between the electrode surface and the enzyme is not always achieved; it has been shown for less than 10% of the known redox enzymes.[32, 273] This problem was resolved by introducing external redox mediators (artificial electron shuttles).[274-276] However, the mediator not only adds an extra step to the electron transfer chain but also introduces interferences in a biosensor and reduces the potential in a biofuel cell. In some cases, these issues can be defeated by the optimal immobilisation of enzymes at electrode surfaces. Clearly, the immobilised enzyme should be strongly bound, keep its structure, and maintain its activity.[277-278] Thus, the intrinsic, short lifetime of enzymes can be increased by immobilisation.[279] The ideal immobilisation procedure would be applicable to a broad range of enzymes and electrode types. Also, enzymes should be immobilised in such a way as to control the orientation of the enzyme on the electrode surface in order to optimise DET without using any redox mediators. The work in this Chapter attempts to meet this challenge.

4.2 Aim of the work

A part of this study, which has been recently published by Bartlett and co-workers in 2017,[22] aims to develop a flexible method for a stable, site-specific covalent immobilisation of redox

proteins and enzymes at electrode surfaces. To that end, an approach has been described based on the use of site-directed mutagenesis, to introduce cysteine residues at specific locations on the protein surface, followed by reaction between the free thiol and a maleimide group on the electrode surface to attach the mutated enzymes. As a model enzyme, cellobiose dehydrogenase (CDH), was covalently attached to carbon nanotube electrodes. The electrode surfaces were first modified with maleimide groups following a modular approach based on an electrochemical attachment of two primary amines at the electrode surface and application of solid state synthesis procedure. The key advantage of this electrode modification procedure is its modular approach that allows the single elements of the modification to be varied independently.[24] The CDH-modified electrodes were tested for DET, showing high catalytic currents, excellent selectivity, and a great long-term storage stability.

Another aim for this study was to investigate the kinetics and electrocatalytic behaviour of cellobiose dehydrogenase from *Myriococcum thermophilum* (*Mt*CDH). Five *Mt*CDH variants have been used in this work, engineered to bear a free cysteine residue in different positions at the surface of the enzyme, allowing fast and selective attachment to maleimide-modified electrodes. Cyclic voltammetry experiments with the *Mt*CDH-modified electrodes were carried out in buffered solutions at pH 7.4 (physiological pH), at increasing concentrations of glucose, showing direct electron transfer (DET) between the enzyme and the electrode surface and allowing discrimination between the different *Mt*CDH variants. Calibration curves for glucose were recorded, and the data were fitted to the Michaelis-Menten equation, enabling the determination of kinetic parameters for the immobilised *Mt*CDH variants. Moreover, the effect of solution pH was studied, and experiments in the presence and absence of calcium chloride were carried out to reach a better understanding of the DET and MET mechanism of this enzyme.

4.3 Immobilisation of cysteine-modified genetically engineered proteins

There are many procedures to immobilise redox proteins and enzymes at electrodes in the literature.[32] However, in most cases, they do not allow control over the orientation of the enzyme on the electrode surface. Enzymes can be immobilised on a support using a variety of methods, ranging from physical adsorption and ionic binding to stable covalent bonds.[66-69] The covalent immobilisation of enzymes onto electrode surfaces is made possible via the reaction between strong nucleophilic groups on the enzyme surface and an electrode modified with functional groups.[66] Despite the enormous amount of research accomplished and ongoing in the field of enzyme immobilisation,[32] there are still limitations. For instance, the use of the amino acid chain for coupling is not specific; there is always the possibility for more than one

amino acid in the protein which to react with the modified electrode surface. As a consequence, the protein may be imperfectly orientated on the modified electrode, giving inefficient direct electron transfer. Moreover, the active cite of the enzyme may become blocked by the immobilisation and/or the conformation may be changed by the immobilisation on the electrode. Under those circumstances, it is fundamental to develop a new strategy for enzyme immobilisation by employing the genetically engineered enzyme with specific target groups to allow a more controlled approach.

This study suggests a flexible, selective immobilisation method based on the covalent attachment of cysteine-modified genetically engineered enzymes at maleimide modified electrodes, which utilises the coupling of a thiol amino acid residue, namely cysteine, with maleimide (unsaturated carbonyls), to form stable thioether bonds (Scheme 4.1). It has often been suggested that unsaturated carbonyls (particularly maleimide) strongly undergo conjugate addition with thiols at neutral pH (6.5-7.5), without the requirement of catalyst or any other reagent,[280-281] making it an excellent choice for the selective attachment of cysteine-modified biomolecules. On the contrary, under these conditions amines are principally protonated and thus, unreactive.[24, 68]

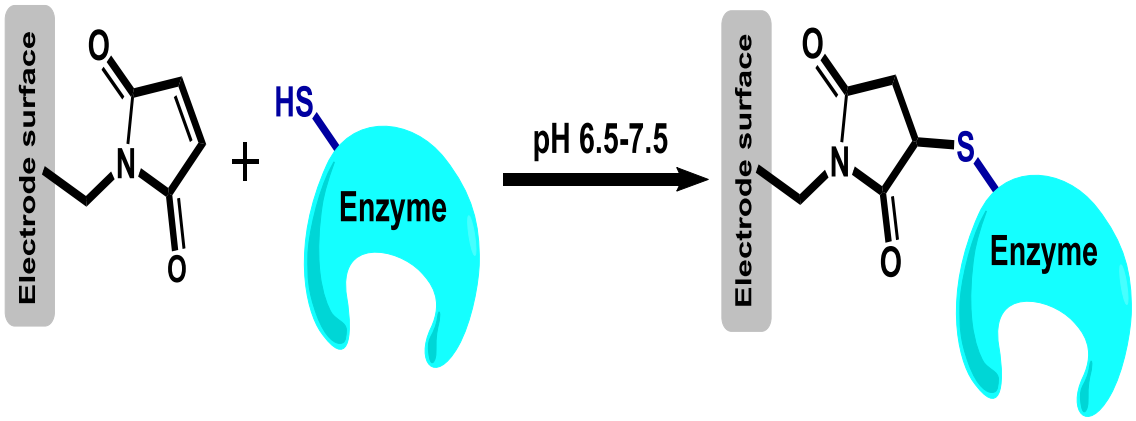

Scheme 4.1. *The reaction of a maleimide group immobilised onto an electrode surface with the thiol of a cysteine residue.*

4.4 Key elements of the modification composition

The carbon-based electrodes of interest were modified with maleimide groups following a study by Bartlett *et al.*[24] Our suggested procedure includes the creation of a modified electrode surface by building up the construction of the surface in a stepwise manner, allowing the key components of the structure to be separately changed. In this case, these elements are an "electrode", a "linker", a "spacer", a "reactive group" and a "passivating group", Scheme 4.2. For the "electrode" element, carbon-based electrodes were used in this modification; carbon

material was chosen as it is a relatively cheap and widely available material. The "linker" is used to provide a link between the electrode surface and the rest of the modification connecting to the enzyme; a mono-Boc protected diamine was used for this purpose; it has two functionalities that enables it to be electrochemically grafted on the electrode surface and then chemically linked with other molecules. The "spacer" could then be coupled to the linker (using conventional solid-phase synthesis methodology) to lengthen the linkage; it has two functional groups, one to react with the linker and the other with the reactive group, and it can be of different length. The "reactive group" is the final component in the linkage that can be chemically coupled to the spacer (or the linker if a spacer is not used) through one of its functionalities and has a second functional group suitable to react with the target group on the desired genetically engineered protein. Finally, the "passivating group" which is a small molecule that can be attached to the electrode surface together with the linker, thus forming a mixed two-component monolayer. This gives a controlled partial coverage of the reactive group on the surface, compatible with the surface of the enzyme around the attachment point and suitable for accommodating big biomolecules such as enzymes, thus to reduce denaturation of the protein.

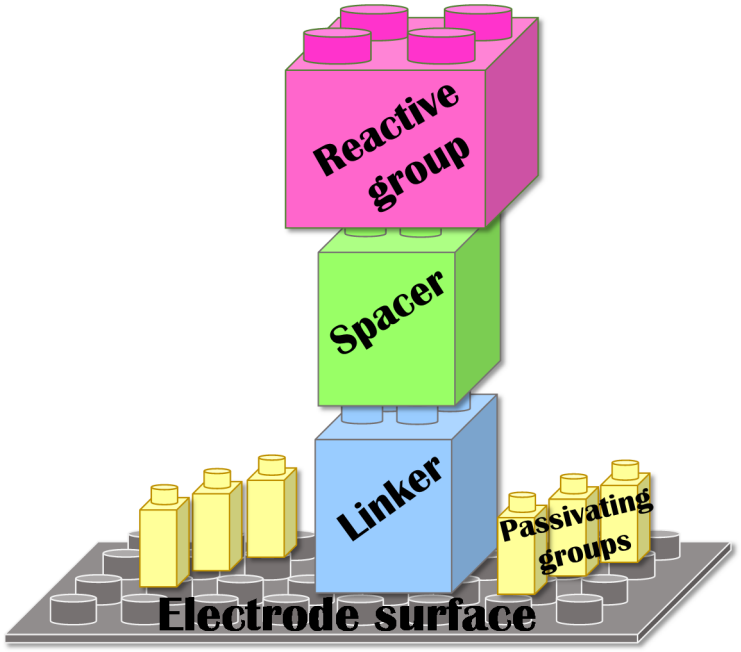

Scheme 4.2. *Schematic representation of the stepwise modified electrode, with key elements highlighted.*

4.5 Cellobiose dehydrogenase (CDH)

As a consequence of the obvious drawbacks with GOx (see Chapter three); there has been a continuous search for alternative carbohydrate-oxidation enzymes. Cellobiose dehydrogenase (CDH) (EC 1. 1. 99. 18) [282] was selected as the model redox enzyme system in this study. CDH

is an extracellular enzyme secreted by several of the fungi involved in wood degradation.[283] It catalyses the oxidation of carbohydrates, and CDH can be used as a versatile bio-recognition element in the detection of saccharides such as glucose.[284] As a flavocytochrome, CDH has been used as a model enzyme for glucose biosensors because of its exceptional properties.[283, 285] It is a monomeric protein, between 85 and 101 kDa in mass depending on the degree of glycosylation, consisting of two separate domains with different structures linked together by a polypeptide linker of around 20 amino acids that allows the two to come in close contact for internal electron transfer (IET).[286] CDH consists of a larger flavin-containing domain (DH), and a smaller haem-associated domain (CYT), the natural cofactors are FAD and haem b, respectively.[285] CDH is represented by a phylogenetic classification of class I and class II CDHs.[287] Class I CDHs have a pH optima in the acidic pH range. Class II CDHs have longer amino acid sequences than class I, can have pH optima around pH 7.4 (physiological pH), and are able to oxidize mono and disaccharides, although with lower efficiencies.[284]

The crystal structure of the CDH is known,[288] Figure 4.1 shows the cartoon representation of the secondary structure of *Myriococcum thermophilum* cellobiose dehydrogenase (*Mt*CDH) which belongs to Class II CDHs. The crystal structure of the DH fragment of CDH shows that it is closely related to that of glucose-methanol-choline (GMC) family of oxidoreductases. Another member of GMC oxidoreductase family GOx is similar in overall structure and active-site architecture to the DH domain.[289] However, the structure of the catalytic-site in the DH domain around the flavin ring has two conserved residues, histidine and asparagine in a similar conformation and geometry relative to the flavin N5. In GOx, the asparagine is replaced by a histidine residue.[290]

As a typical dehydrogenase, CDH displays the properties of both oxidative and reductive half-reactions that can be investigated separately. The oxidative half-reaction exhibits an oxidation at the C1 position of a carbohydrate, which is converted to a lactone that can undergo hydrolysis spontaneously to a carboxylic acid.[290-291] Compared to GOx, few research groups have been focussed on the catalytic mechanism of the immobilised CDH, particularly, the individual roles of the two prosthetic groups. GOx catalyses the oxidation of D-glucose to D-glucono-1, 5-lactone. Therefore, GOx and CDH perform similar reductive half-reactions. The vast majority of the published results for CDH indicates that the oxidation of a saccharide is carried out by the FAD group, which is reduced to $FADH_2$.[291] Hence, $FADH_2$ is oxidised back by donating electrons to an electron acceptor, or to the haem cofactor. In other words, the electrons obtained by carbohydrate oxidation can be transferred directly from the flavin domain to different one or two-electron acceptors. On the contrary, the electrons can be transferred by an interdomain electron transfer (IET) to the haem domain and then to one-electron acceptors such as cytochrome c or rather to an electrode surface in a direct

electron transfer (DET) reaction.[283, 292] Common artificial electron acceptors include quinones, osmium complexes, Fe^{3+}, Cu^{2+}, and triiodide ion.[291] In general, the CDH is unaffected by molecular oxygen. Its higher affinity for artificial electron acceptors than for oxygen[293-294] and the low-spin character of the haem in the oxidized and reduced states[295], confirm that the electron acceptor of this enzyme is not molecular oxygen. On the contrary, in GOx-based electrodes the oxygen turnover decreases the electrode efficiency and yields hydrogen peroxide (H_2O_2) which degrades the enzyme.[296]

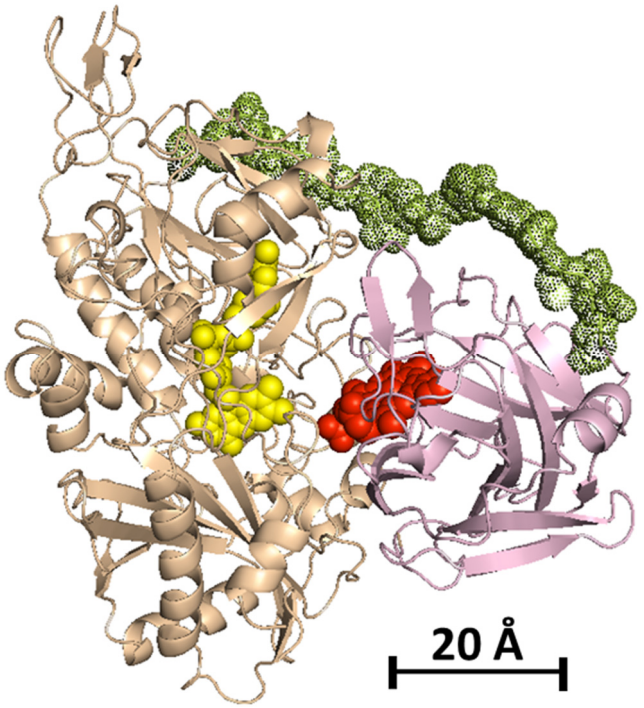

Figure 4.1. *Cartoon representation of the secondary structure of* Myriococcum thermophilum *cellobiose dehydrogenase. The sites of the flavin domain with the FAD group in beige/yellow and cytochrome domain with the haem group in pink/red. The polypeptide chain linking the two domains is highlighted in lime green. (The image was obtained with PyMol software, PyMol visualisations are based on the crystal structure of* Mt*CDH, PDB code 4QI6).*[288]

4.6 Engineered *Mt*CDH

There is no evidence that *Mt*CDH has any surface cysteines,[288] making it an ideal nominee for site-directed mutagenesis to place cysteines at a specific surface site for immobilisation. Five genetically engineered *Mt*CDH variants, D813C, D574C, E522C, E674C and T701C have been used in this study. The five variants of the *Mt*CDH were provided by Dr Su Ma and Dr Roland Ludwig, University of Natural Resources and Life Sciences, BOKU, in Vienna. They were modified to bear a free single cysteine residue in different positions on the enzyme surface (Figure 4.2) allowing site-specific attachment to the maleimide-modified electrodes. To refresh the memory, the key aspect for the DET of the immobilised CDH is that the electrons are

transferred from FAD in the catalytic flavin domain to haem in a mobile cytochrome domain, which acts as a built-in mediator.[286] Thus, the mobility of the haem domain is fundamental for direct electron transfer of our proposed electrode.[297] Accordingly, the positions of cysteine residues at a particular site on the surface of the flavin domain were chosen to obtain the desired mobility of the haem domain after immobilisation.

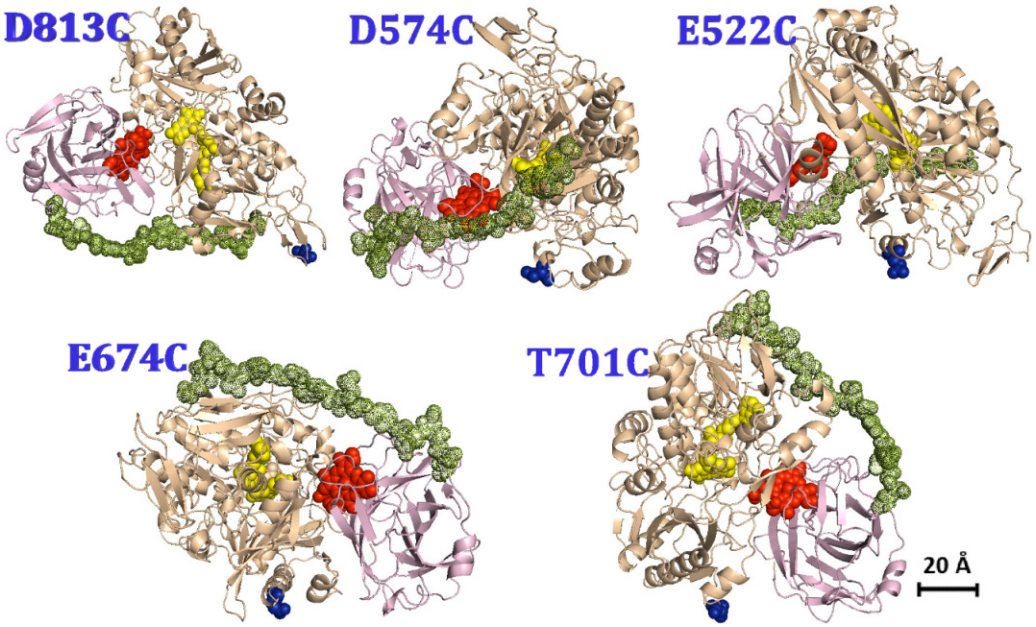

Figure 4.2. *Cartoon representation of the secondary structure of the five* Mt*CDH variants. The free cysteine residues on the surface of the flavin domain are highlighted in blue. (PyMol visualisations are based on the crystal structure of* Mt*CDH, PDB code 4QI6).*[288]

4.7 Electrode modification and *Mt*CDH immobilization

Multiwall carbon nanotube modified glassy carbon electrodes (GC/MWCNT) were selected as a template for carbon-based electrodes owing to their high surface area combined with comparatively low capacitance. Herein, we describe an innovative procedure for the covalent, site-specific immobilization of cysteine-modified genetically engineered *Mt*CDH onto the maleimide-modified multiwall carbon nanotube electrodes.

GC/MWCNT electrodes were modified with a mixture of two primary amines, (Scheme 4.3 a), in order to dilute the final number of maleimide groups in the ultimate film. The linker (*N*-Boc-1,6-hexanediamine) and the passivating group (*N*-(2-aminoethyl) acetamide) were oxidised onto the surface of GC/MWCNT electrodes through electrochemical grafting from an acetonitrile solution with a ratio of one linker to nine passivating groups. The electrode potential was held at +2 V *vs.* SCE for 180 s; this potential was chosen because both amines are oxidised and, therefore, stoichiometric amounts of the corresponding amine radicals should be produced. Assuming similar reactivity for the two amine radicals produced, one might expect

that the ratio of their surface coverages to be similar to the ratio of their solution concentrations. After electrografting, Boc-deprotection of the linker was performed (Scheme 4.3 b1), then a six carbon-long spacer (*N*-Boc-6-aminohexanoic acid) was introduced to the linker in order to lengthen the tether. It has been proposed that the use of such length of spacer should provide an approximately 3 nm long linkage at the end of the modification, making it more flexible and accessible for the cysteine residue at the CDH surface, (Scheme 4.3 c). Eventually, the Boc-protecting group of the spacer was removed (Scheme 4.3 b2) and *N*-maleoyl-β-alanine was coupled to the amino-modified surface to produce the maleimide-modified multiwall carbon nanotube electrode (Scheme 4.3 d). Scheme 4.3 illustrates the sequential electrochemical and solid-phase preparation of maleimide-modified GC/MWCNT electrodes. The maleimide group was chosen because it undergoes spontaneous reaction with free thiols in aqueous solution at neutral pH [19,20] and room temperature, allowing efficient use of small quantities of the cysteine-modified genetically engineered enzyme.

Coupling of the *Mt*CDH variants was performed by drop casting 3 µL of CDH solution (at pH 7.0) on the surface of the maleimide-modified GC/MWCNT electrode which was then covered and stored in the fridge (4 °C) overnight, electrodes were then washed with 50 mM pH7 tris buffer, but not allowed to dry, before electrochemical measurements. Scheme 4.4 shows the immobilisation of the *Mt*CDH variant of choice on the maleimide-modified GC/MWCNT electrode.

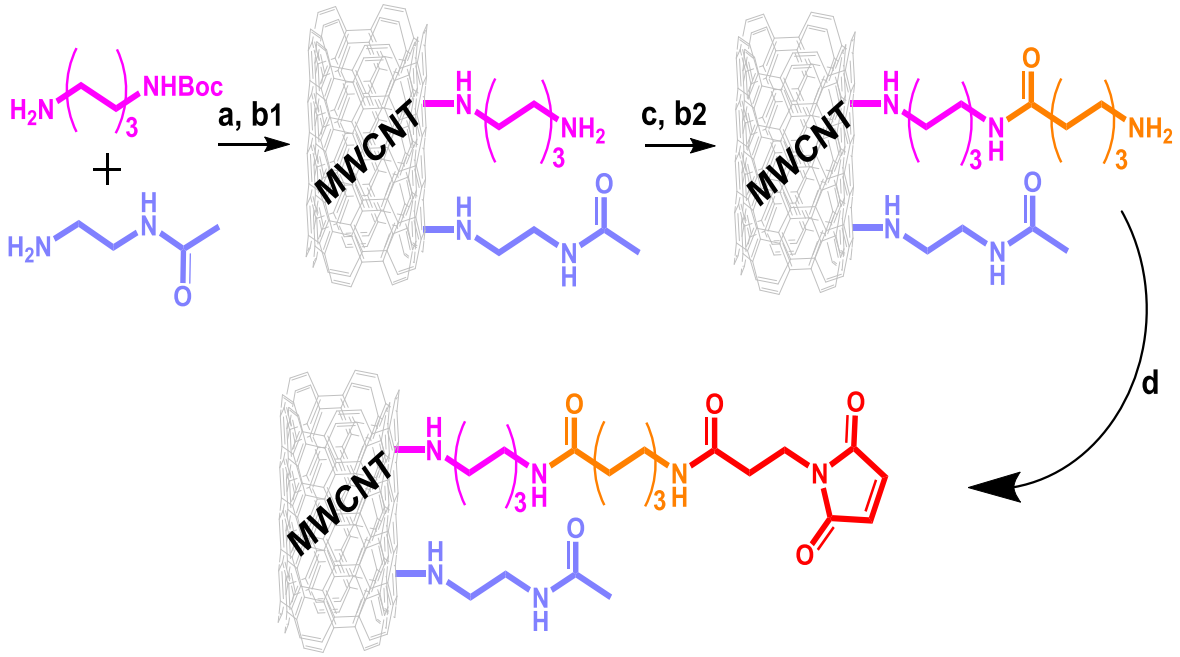

Scheme 4.3. *Sequential electrochemical and solid-phase preparation of maleimide-modified GC/MWCNT electrodes. Reagents and conditions: a) 2 mM N-Boc-1,6-hexanediamine, 18 mM N-(2-aminoethyl) acetamide, 0.1 M TBATFB in deoxygenated acetonitrile, constant potential of 2 V vs. SCE for 180 s; b1, b2) 4 M HCl in 1,4-dioxane (45 min); c) 10 mM N-Boc-6-aminohexanoic acid, 0.1 M EDC, 60 mM NHS in DMF (16 h); d) 25 mM N-maleoyl-β-alanine , 0.1 M EDC, 60 mM NHS in DMF (16 h).*

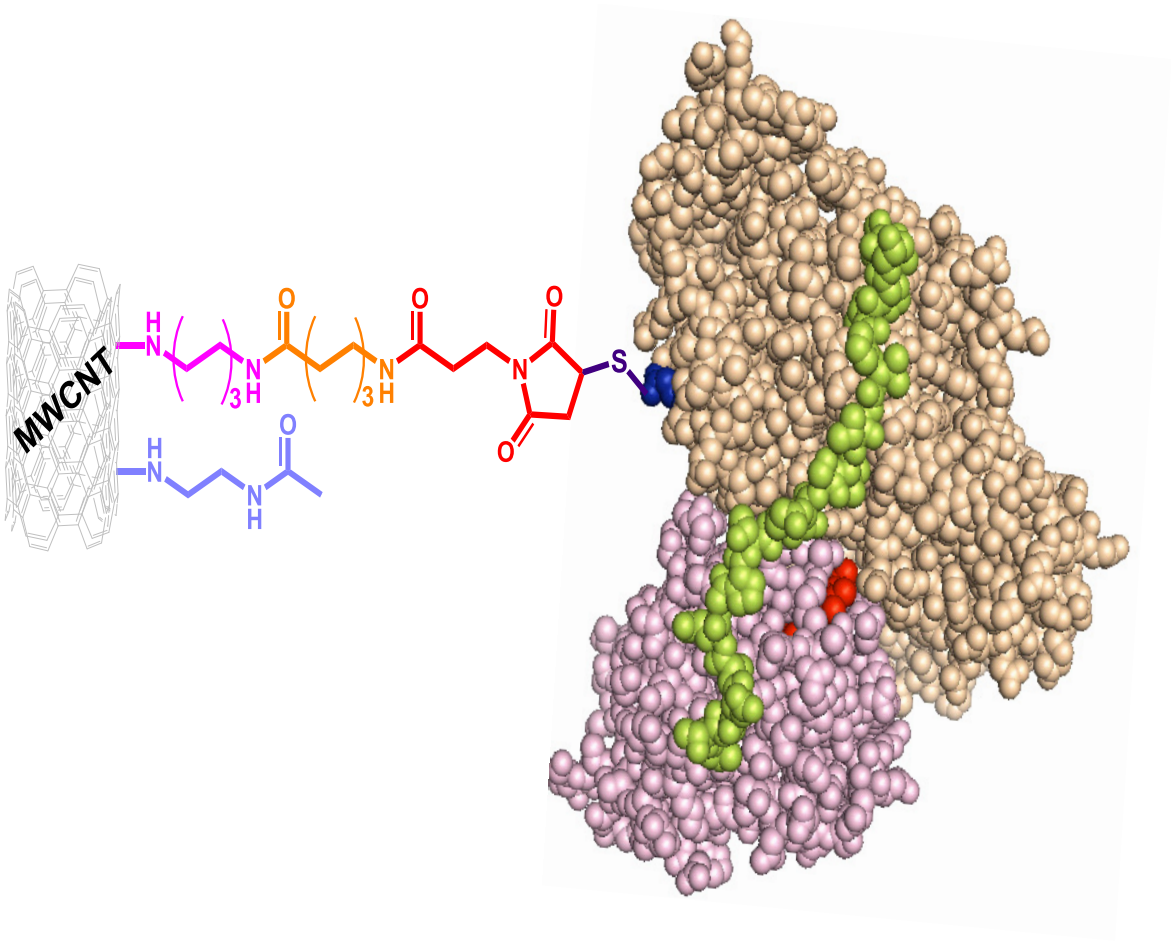

Scheme 4.4. *Immobilisation of the* Mt*CDH variant of choice on maleimide-modified GC/MWCNT electrode. The MtCDH image was obtained with PyMol software, PyMol visualisations are based on the crystal structure of* Mt*CDH, PDB code 4QI6.*[288]

The genetically engineered proteins require some time and effort to prepare and are often available only in small quantities. Thus, the E522-*Mt*CDH variant was selected as a model variant to examine and improve our suggested electrode modification method because it was available in larger amount than the other variants.

4.7.1 Direct electron transfer at *Mt*CDH-modified electrodes

GC/MWCNT electrodes modified with the CDH variants E522 (see Figure 4.2 for the structure) were first tested for DET by cyclic voltammetry in deoxygenated 50 mM Tris/30 mM $CaCl_2$ buffer (pH 7.4) at 10 mV s^{-1}. Figure 4.3 shows that, the anodic and cathodic peaks as a consequence of the oxidation and reduction of the redox centre (most probably, the haem cofactor) of the enzyme are clearly visible above the capacitive background current. The redox electrode potential (E_{mid}) of about -0.135 V *vs.* SCE is consistent with results from other studies of DET of class II CDHs at pH 7.4.[283-284, 298]

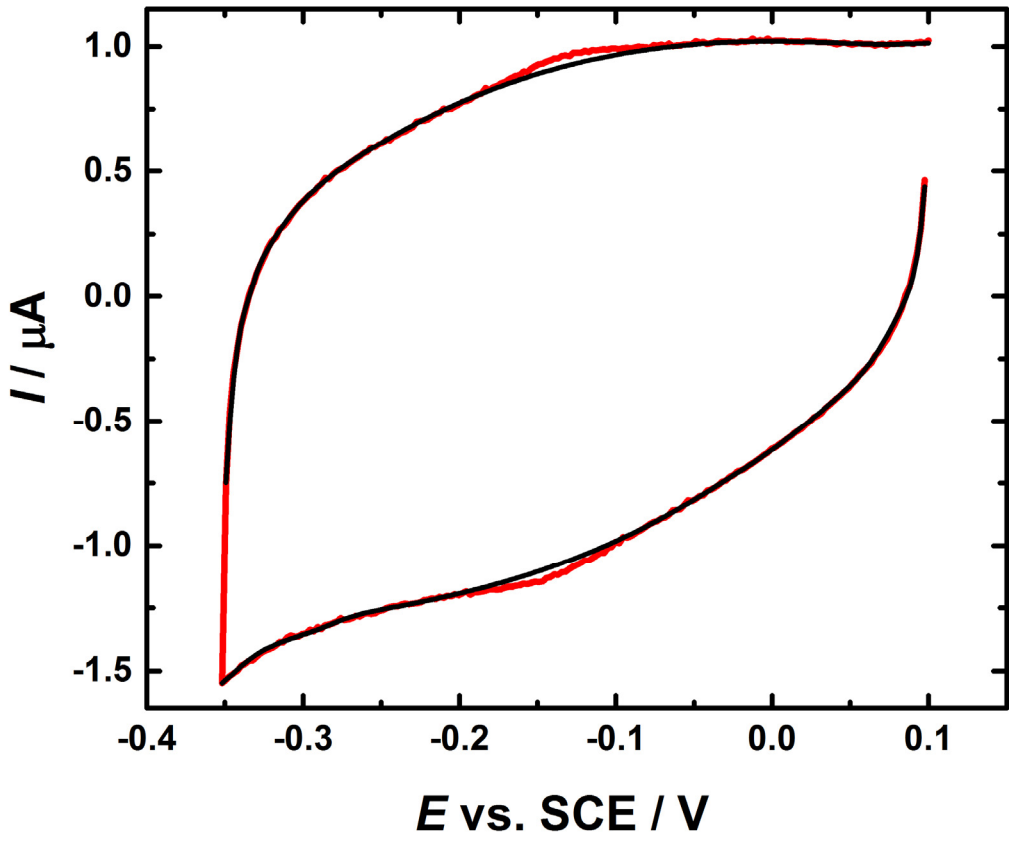

Figure 4.3. *Cyclic voltammogram for CDH-modified GC/MWCNT electrode (E522-CDH) in deoxygenated 50 mM Tris buffer (pH 7.4), containing 30 mM $CaCl_2$ (red line). The GC/MWCNT electrode was prepared by drop casting of a 5 µL aliquot of 1 mg mL^{-1} MWCNT (carboxylic acid functionalized) dispersion onto the cleaned surface of GC. The black line is the calculated baseline. The electrode potential was swept at 10 mV/s from -0.35 to 0.1 V vs. SCE.*

DET of the GC/MWCNT electrodes modified with the *Mt*CDH E522 variant were also tested indirectly by monitoring the catalytic current caused by glucose oxidation. Slow scan cyclic voltammetry experiments were carried out in deoxygenated 50 mM tris buffer (pH 7.4) and after the addition of different concentrations of D-glucose. Figure 4.4 shows an increase in the catalytic current as the concentration of D-glucose in the solution was increased up to 70 mM. The current started to increase at *ca.* -0.2 V *vs*. SCE reaching a catalytic current plateau at around -0.05 V. The position of the onset of the catalytic current agrees with that reported in the literature for immobilised *Mt*CDH at silver, graphite and single-walled carbon nanotubes electrodes and corresponds to DET from the haem to the electrode.[283, 299-300] The non-catalytic voltammetry and the electrocatalytic behaviour of the *Mt*CDH variant E522C are discussed in more detail in Section 4.9.1.

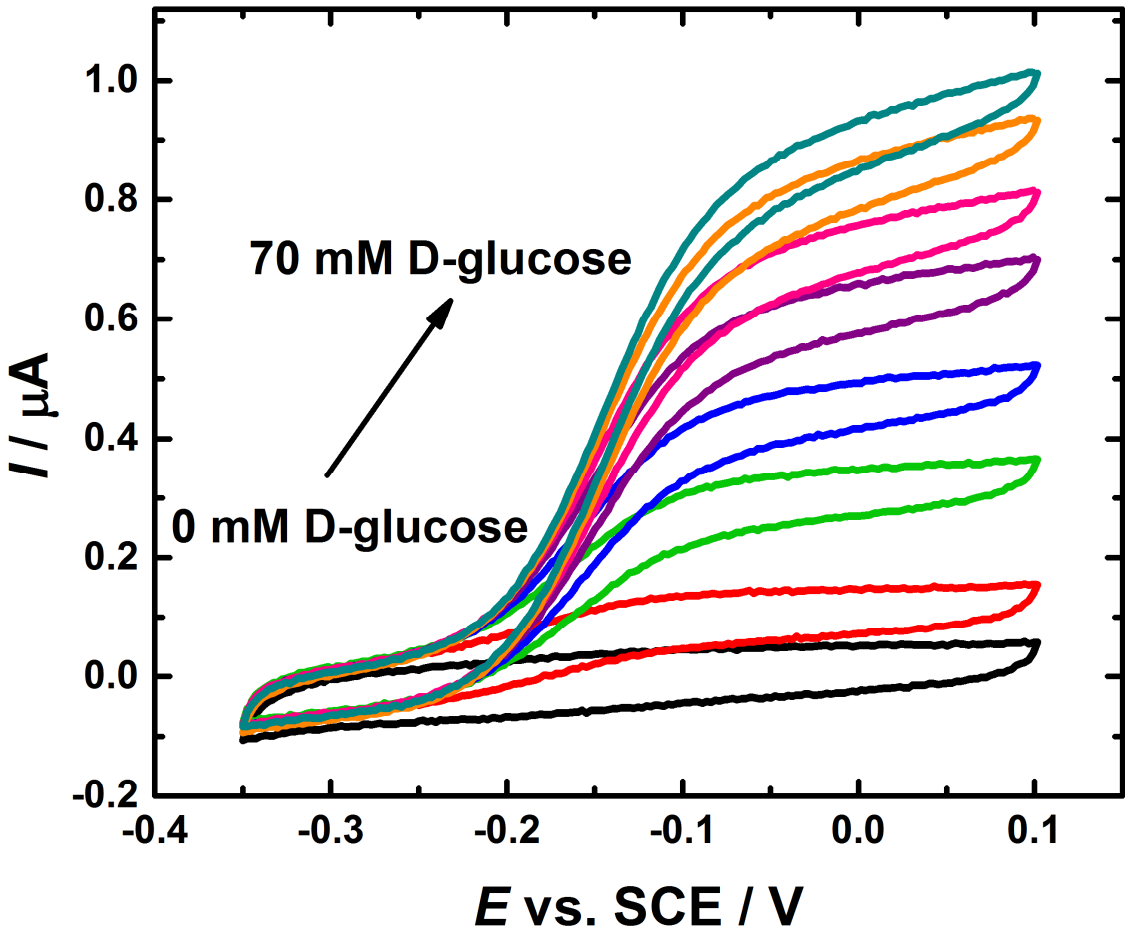

Figure 4.4. *Typical cyclic voltammograms for CDH-modified GC/MWCNT electrode (E522-CDH) in deoxygenated 50 mM Tris buffer (pH 7.4), containing 30 mM $CaCl_2$ and increasing concentrations of D-glucose. The GC/MWCNT electrode was prepared by drop casting of a 5 µL aliquot of 1 mg mL^{-1} MWCNT (carboxylic acid functionalized) dispersion onto the cleaned surface of GC. The electrode potential was swept at 1 mV/s from -0.35 to 0.1 V vs. SCE.*

4.7.2 Control experiments

It is important to note that in many literature examples of "covalent methods for enzyme immobilisation" the evidence presented is often incomplete and unconvincing as there are insufficient controls reported. In this study several control experiments have been attempted. The control experiments were designed to confirm that the DET observed is due to the selective oxidation of D-glucose catalysed by the enzyme, the enzyme is irreversibly immobilised through the thioether bond, to demonstrate long-term stability of the enzyme on maleimide modified GC/MWCNT electrodes and the reproducibility of the approach.

4.7.2.1 L-glucose experiment

One piece of evidence that the catalytic current (observed in Figure 4.4) is due to the oxidation of glucose by the immobilised enzyme is delivered by the control experiment using L-glucose,

the DET experiment was repeated using L-glucose and D-glucose. L-glucose is not oxidised by CDH.[301-302] Therefore, the addition of L-glucose should not cause any increase in the catalytic current. However, if the current were to be due to direct oxidation of glucose on the electrode surface (not by the enzyme) L-glucose should cause the same increase in the current as D-glucose. Figure 4.5 shows the cyclic voltammograms of the CDH-modified GC/MWCNT electrode (E522-CDH) in deoxygenated 50 mM Tris buffer (pH 7.4) and after the addition of different concentrations of L and D-glucose. Upon addition of aliquots to increase the concentration of L-glucose in the cell there is no change in the current (compare each pair of dotted and solid curves), whereas upon each addition of an aliquot of D-glucose, the current increases (compare the solid curves). This chiral selectivity can only be explained by catalysis of the reaction by the enzyme. Thus, the increase in current was due to the specific oxidation of D-glucose (excellent selectivity).

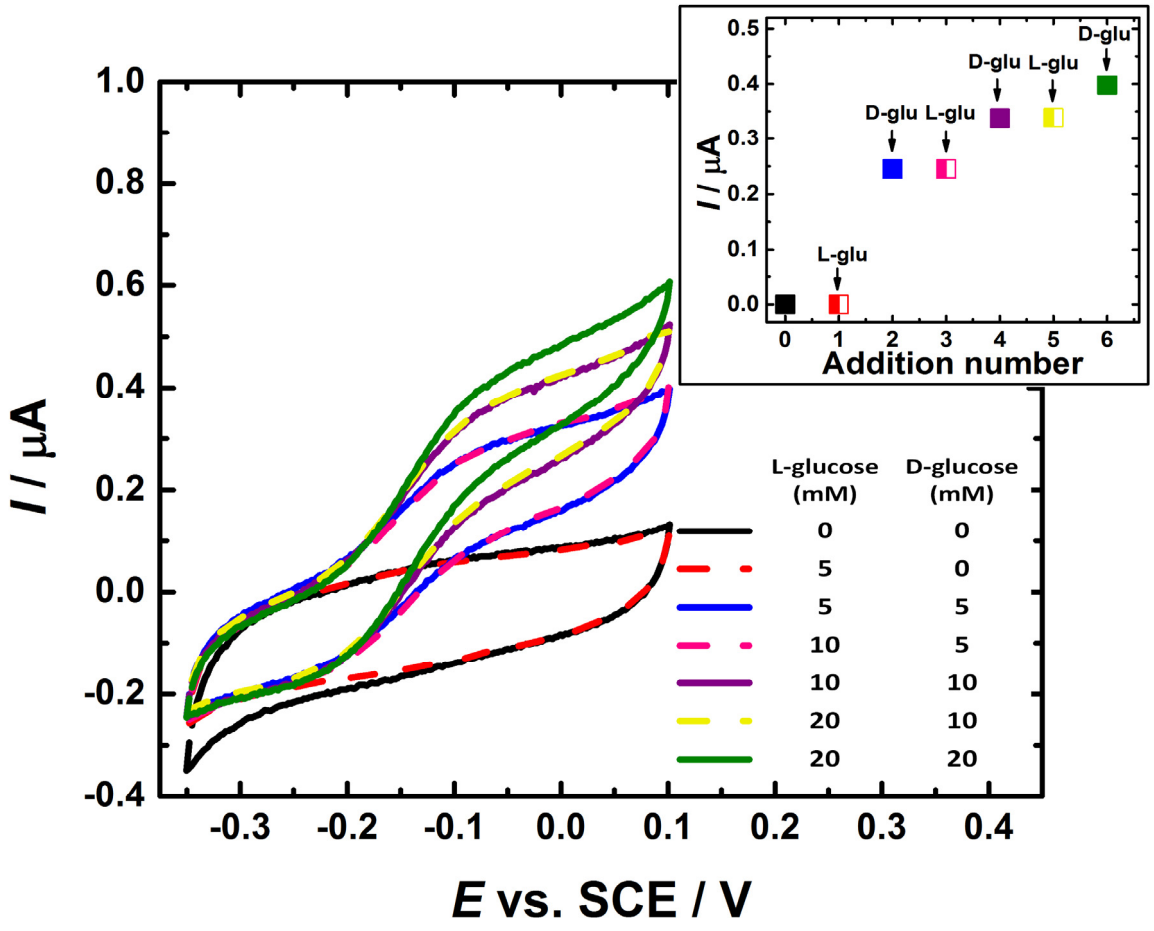

Figure 4.5. *Cyclic voltammograms for a CDH-modified GC/MWCNT electrode (CDH variant E522) in deoxygenated 50 mM Tris buffer (pH 7.4), containing 30 mM $CaCl_2$ (black line) and after the addition of different concentrations of L- and D-glucose. The GC/MWCNT electrode was prepared by drop casting of a 5 µL aliquot of 1 mg mL^{-1} MWCNT (carboxylic acid functionalized) dispersion onto the cleaned surface of GC. The electrode potential was swept at 1 mV/s. Inset: plot of the background subtracted currents measured at 0.0 V for all the additions.*

4.7.2.2 Covalent immobilization vs. physical adsorption

So as to verify that *Mt*CDH was successfully attached to the maleimide-modified GC/MWCNT electrode through the thioether bond, a comparison between the covalently bound and physically adsorbed *Mt*CDH E522 variant on the GC / MWCNT electrodes was performed. For the covalent immobilization, the maleimide-modified electrode was prepared using the procedure described in Section 4.7, while the physically-modified one was prepared by drop casting 3 µL of the *Mt*CDH solution onto a bare GC/MWCNT electrode. Both electrodes were tested for DET using slow scan cyclic voltammetry in deoxygenated 50 mM Tris buffer (pH 7.4) and increasing concentrations of D-glucose (Figure 4.6 A, B), and calibration curves for glucose were plotted (Figure 4.7). Direct electron transfer was observed for both modification methods. However, the catalytic currents for physically adsorbed CDH (Figure 4.7 b) were clearly lower than those for covalently immobilised CDH (Figure 4.7 a): in particular, the current decreased by about 60 %. In the same context, a maleimide-modified GC/MWCNT electrode was modified with a pH 5.5 enzyme solution (variant E522 dissolved in 50 mM acetate buffer, pH 5.5) instead of the pH 7 enzyme solution which is typically used in the immobilization procedure. This electrode was also evaluated by monitoring the catalytic current caused by glucose oxidation using cyclic voltammetry (Figure 4.6 C). The calibration curve of such an electrode (Figure 4.7 c) is similar to the one for the physically-modified electrodes (Figure 4.7 b), showing that in such condition the covalent binding has not occurred. This can be explained by the fact that the coupling reaction between the free thiols and maleimide only occurs at neutral pH (6.5-7.5); at acidic pH the thiol group is not nucleophilic enough to react with maleimide[303-304](the pK_a of the cysteine side chain in folded proteins is around 6.8).[305]

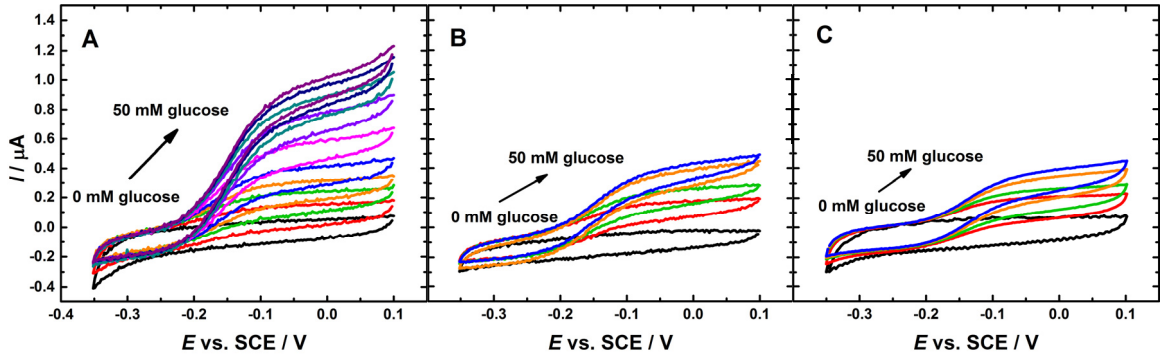

Figure 4.6. *Typical cyclic voltammograms recorded at maleimide-modified electrodes (A, C) and unmodified GC/MWCNT electrodes (B) with CDH variant E522. The CDH immobilisation was made at pH 7 for the electrodes in (A) and (B). For the electrode in (C) the CDH was drop cast from a pH 5.5 solution. CVs were carried out in deoxygenated 50 mM Tris buffer (pH 7.4), containing 30 mM $CaCl_2$ and increasing concentrations of D-glucose, sweeping the potential at 1 mV/s from -0.35 to 0.1 V vs. SCE. The GC/MWCNT electrode was prepared by drop casting of a 5 µL aliquot of 1 mg mL^{-1} MWCNT (carboxylic acid functionalized) dispersion onto the cleaned surface of GC.*

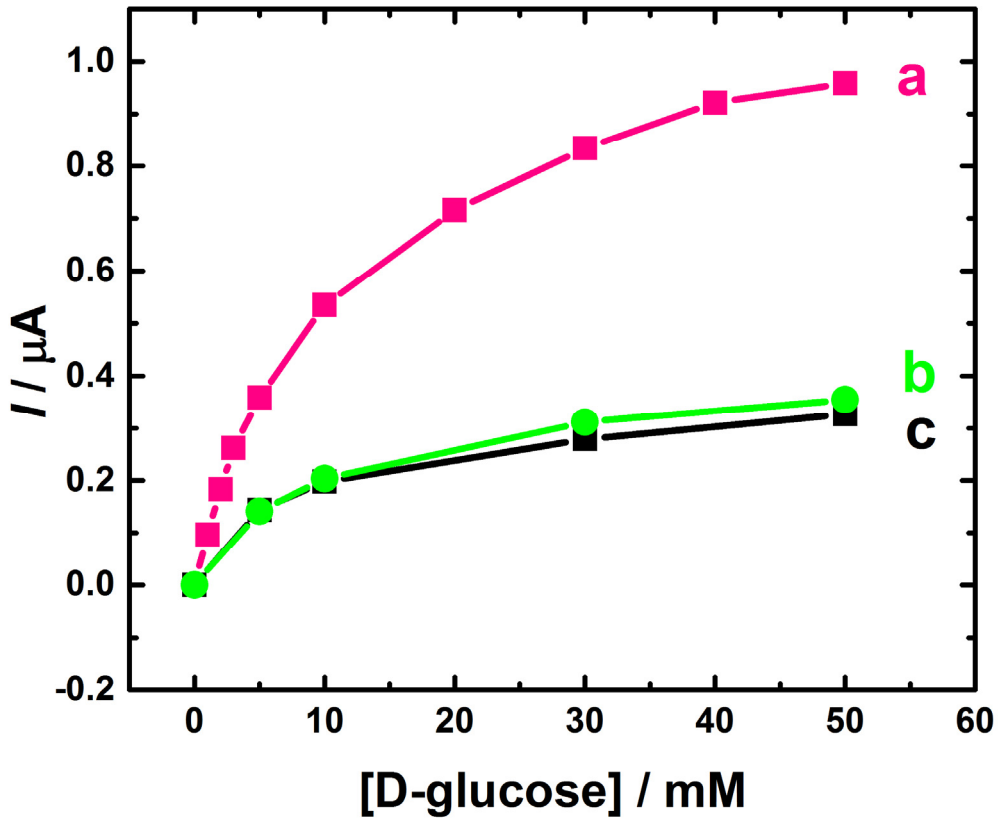

Figure 4.7. *Background subtracted currents measured at 0.0 V vs. SCE in cyclic voltammograms recorded at maleimide-modified electrodes (a, c) and unmodified GC/MWCNT electrodes (b) with CDH variant E522. The CDH immobilisation was performed at pH 7 for the electrodes in (a) and (b). For the electrode in (c) the CDH was drop cast from a pH 5.5 solution. CVs were carried out in deoxygenated 50 mM Tris buffer (pH 7.4), containing 30 mM $CaCl_2$ and increasing concentrations of D-glucose, sweeping the potential at 1 mV/s from -0.35 to 0.1 V vs. SCE.*

The higher catalytic currents obtained with covalently-modified electrode (Figure 4.7 a) can be attributed to a greater quantity of enzyme molecules immobilised onto the electrode and/or the fact that the covalently bound enzyme is held in a more suitable orientation for DET as compared to the randomly oriented, physically adsorbed CDH.

So as to rule out the probability that the different catalytic currents in Figure 4.7 might be obtained from different amounts of the enzyme molecules on the electrodes surfaces, mediators were introduced (see Section 4.9.3.4). The mediator in the solution should react with all the active enzyme molecules on the surface of the electrode.[36] Therefore, the mediated electron transfer (MET) experiment can be employed as a valid method to relate the currents observed in Figure 4.7 to the real coverage of the CDH-variant on each electrode. To that purpose, the same three electrodes were re-tested by monitoring the catalytic current caused by glucose oxidation in the presence of ferrocene monocarboxylic acid as a mediator. From the results obtained (Figure 4.8) it can be assumed that the amount of active enzyme on the surface

of the electrodes is about the same. However, it was slightly higher (about 10%) in the case of the covalently bound enzyme, which is to be expected in such a comparison.

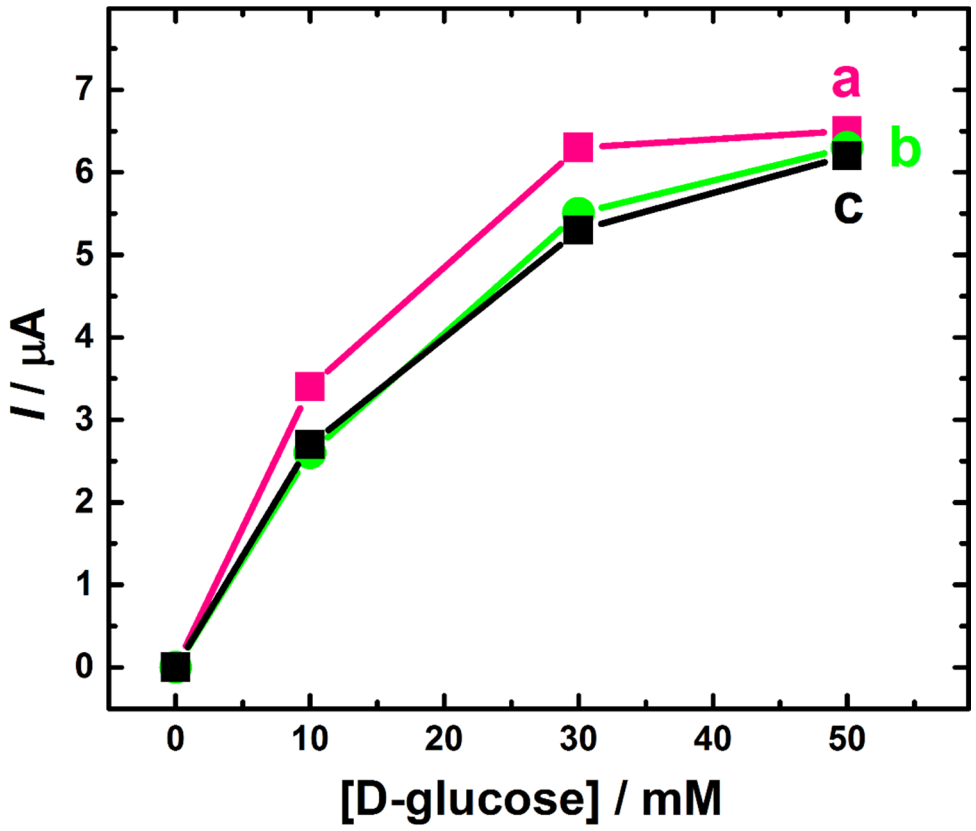

Figure 4.8. *Background subtracted currents measured at 0.3 V vs. SCE in cyclic voltammograms recorded at maleimide-modified electrodes (a, c) and unmodified GC/MWCNT electrodes (b) with CDH variant E522. The CDH immobilisation was performed at pH 7 for the electrodes in (a) and (b). For the electrode in (c) the CDH was drop cast from a pH 5.5 solution. CVs were carried out in deoxygenated 50 mM tris buffer (pH 7.4), containing 0.2 mM ferrocene monocarboxylic, 30 mM $CaCl_2$ and increasing concentrations of D-glucose, sweeping the potential at 1 mV/s from -0.35 to 0.1 V vs. SCE.*

Thus, it can be concluded that the results achieved in Figure 4.7 are consistent with covalent binding of CDH at the maleimide-modified electrode that occurred in more appropriate orientation for DET as compared to the randomly oriented physically adsorbed CDH.

4.7.2.3 Stability of the CDH-modified electrodes

The DET of the CDH immobilised through maleimide is stable when the GC/MWCNT electrodes modified with the CDH variant E522 were scanned continuously in 50 mM tris buffer (pH 7.4) in the presence of 30 mM $CaCl_2$ and the glucose concentrations of interest at 1 mV s^{-1}. Figure 4.9 illustrates this; the response on the second cycle is identical with the response on the first cycle, showing high stability for the immobilised enzyme.

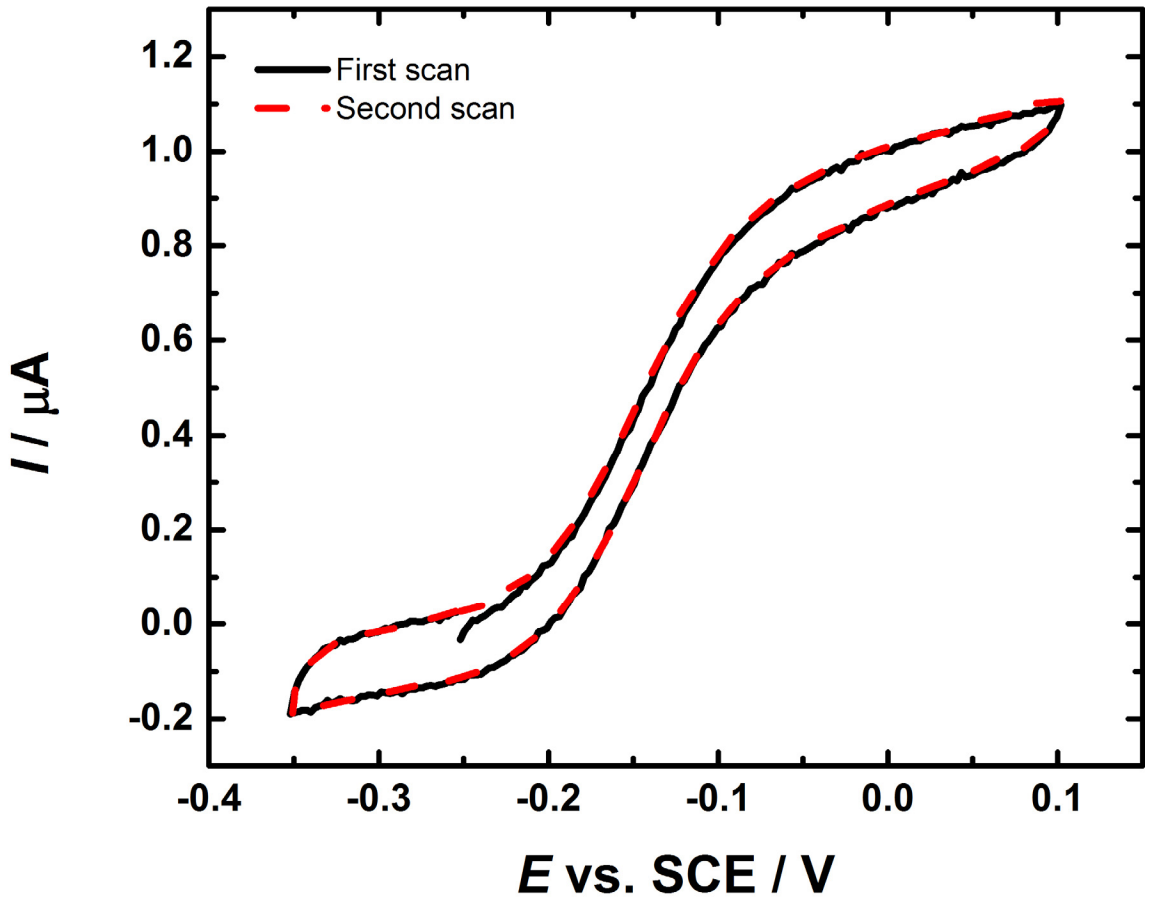

Figure 4.9. *Typical cyclic voltammogram for CDH-modified GC/MWCNT electrode (E522-CDH), first scan (black line) and second scan (red dashed line) in deoxygenated 50 mM Tris buffer (pH 7.4), containing 30 mM $CaCl_2$ and 70 mM D-glucose. The electrode potential was swept at 1 mV/s from -0.35 to 0.1 V vs. SCE.*

The stability over time of the bio-electro-catalytic activities of the CDH-modified GC/MWCNT electrodes (E522-CDH) to oxidation of glucose was also studied. To this purpose, a comparison between the stability of the CDH immobilised through maleimide and a physically adsorbed CDH on unmodified GC/MWCNT were performed. Figure 4.10 illustrates this; the enzyme immobilised at the maleimide electrode is much more stable than the control for the adsorbed variant E522 at an unmodified GC/MWCNT electrode, where the catalytic response decays much more rapidly. Compared to the physically-modified electrode, the covalently-modified electrodes were found to be very stable for long periods showing the same activity after two months (about 40% of the initial activity) as after one week from preparation. The stability of the modified electrodes was investigated by keeping the electrodes in a wet condition with the same buffer used for the tests (50 mM Tris/30 mM $CaCl_2$, pH 7.4) in the refrigerator (4 °C), for several weeks. It may be the case that the small variations in the activity observed during the test are due to experimental factors, such as slightly different temperatures or concentrations of glucose.

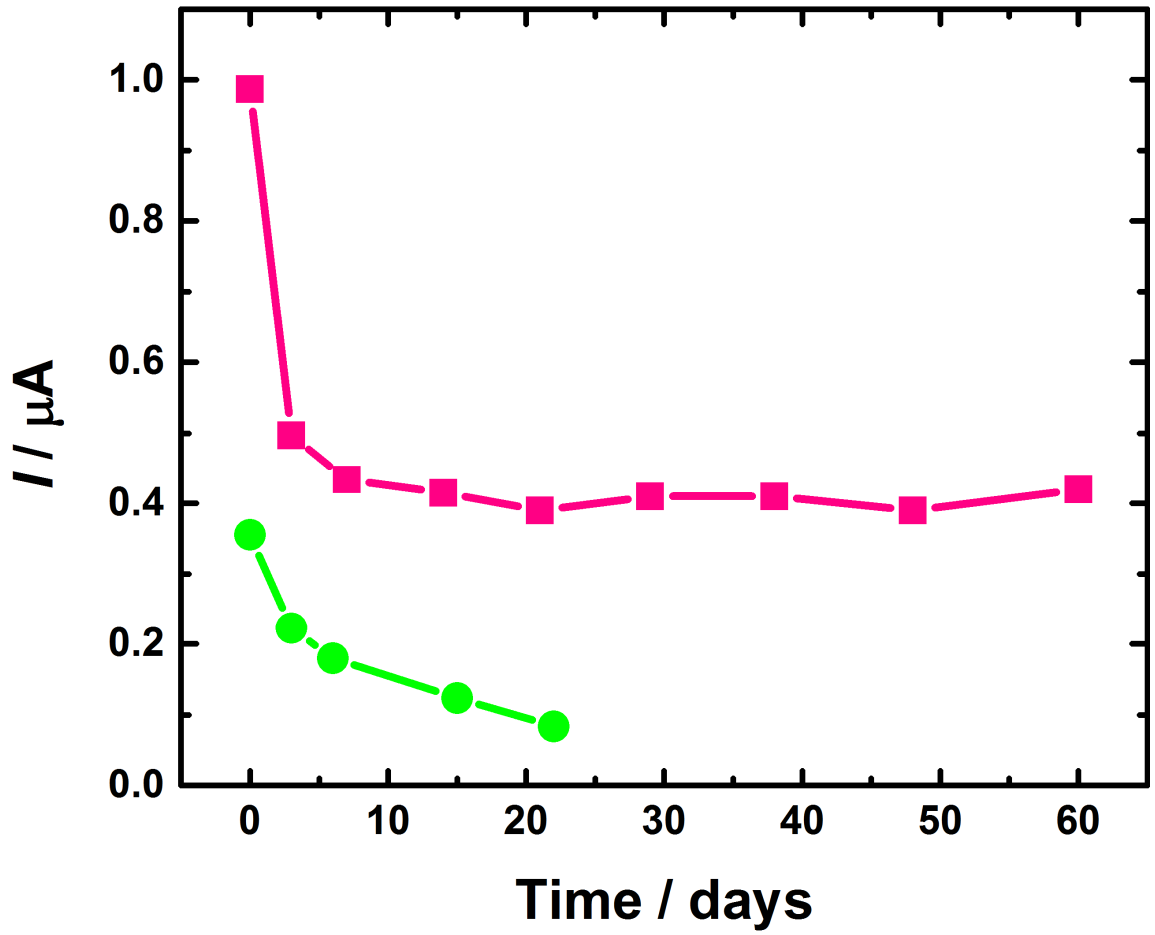

Figure 4.10. *Background subtracted currents measured at 0.1 V vs. SCE in cyclic voltammograms recorded at CDH-modified GC/MWCNT electrodes (CDH variant E522 in deoxygenated 50 mM Tris buffer (pH 7.4), containing 30 mM $CaCl_2$ and 50 mM D-glucose. Pink squares: enzyme immobilised through maleimide. Green circles: control, physically adsorbed enzyme on unmodified GC/MWCNT. The electrodes were stored in wet condition at 4 °C for two months.*

The significant initial decrease in activity during the first week for the maleimide immobilised enzyme can be accounted for by desorption of physically adsorbed CDH, which diffuses away from the electrode surface within a few days. It is also important to note that, the decrease in the catalytic response of modified electrodes can be due to a potential loss of MWCNTs from the GC electrode surface. Nevertheless, separate experiments (using the same electrodes used for the stability experiment in Figure 4.10) showed no change in the capacitive background currents for the electrodes over the same period (Figure 4.11); the background currents do not change significantly with the storage times and are very similar for the two types of electrode. Therefore it could be argued that the electrodes did not lose a significant amount of carbon nanotubes during storage and repeated cycling; two months for the enzyme immobilised through maleimide and 22 days for the physically adsorbed enzyme. The slight differences in the background currents at cathodic potentials (around -0.35 V) are due to traces of oxygen remaining in the deoxygenated solutions.

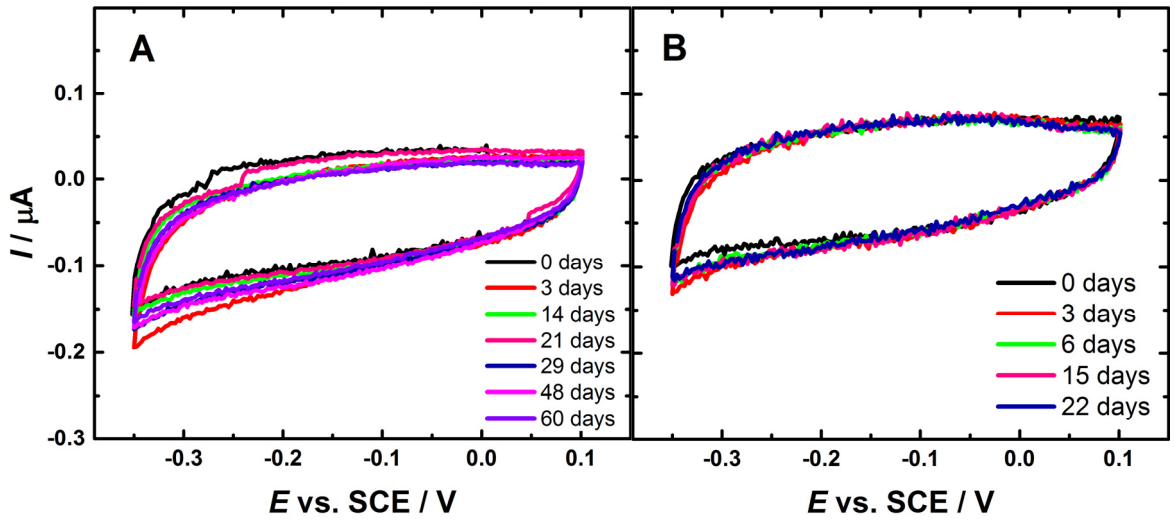

Figure 4.11. *Cyclic voltammograms for the background of GC/MWCNT electrodes covalently-modified (A) and physically-modified (B) with E522 CDH, recorded after different times from the preparation. CVs were recorded in deoxygenated 50 mM Tris buffer (pH 7.4), containing 30 mM $CaCl_2$, sweeping the electrode potential at 1 mV/s. The electrodes were stored in the same buffer used for the analysis, at 4 °C. The GC/MWCNT electrodes were prepared by drop casting of a 5 µL aliquot of 1 mg mL^{-1} MWCNT (carboxylic acid functionalized) dispersion onto the cleaned surface of GC.*

4.7.2.4 Stability of the CDH-modified electrodes in pH 3

The control experiments mentioned above have verified that the reaction of maleimide with the cysteine led to a covalent immobilisation of the enzyme at the electrode surface. In order to further test the stability of the CDH immobilised through the thioether bond, a final test has been performed (Figure 4.12). In this experiment the physically and the covalently modified electrodes were incubated in citrate buffer solution at pH 3.5 and periodically tested for their response to glucose. Figure 4.13 decidedly confirms a very significant difference between the physically adsorbed enzyme and the enzyme attached through the thiol-maleimide. The thiol-maleimide linked enzyme shows excellent stability when compared with the physically adsorbed enzyme; the activity of the electrode with physically adsorbed enzyme drops to 8% in 6 h whereas that for the enzyme immobilised through maleimide the activity remains at 84% over the same period. This difference arises because the physical, non-covalent, binding of the enzyme to the MWCNT electrode surface is strongly pH dependent due to the carboxylic acid groups on the surface of the MWCNTs. Indeed, changing the pH to 3.5 leads to protonation of the carboxylic acid groups on the MWCNTs (p*K*a ~ 4.5) and CDH (p*I* ~ 3.8)[284] which should significantly alter the strength of the physical adsorption of the CDH. At pH 7 the carboxylic groups are ionised, at pH 3.5 they are protonated, and this change influences the strength of the adsorption.[66]

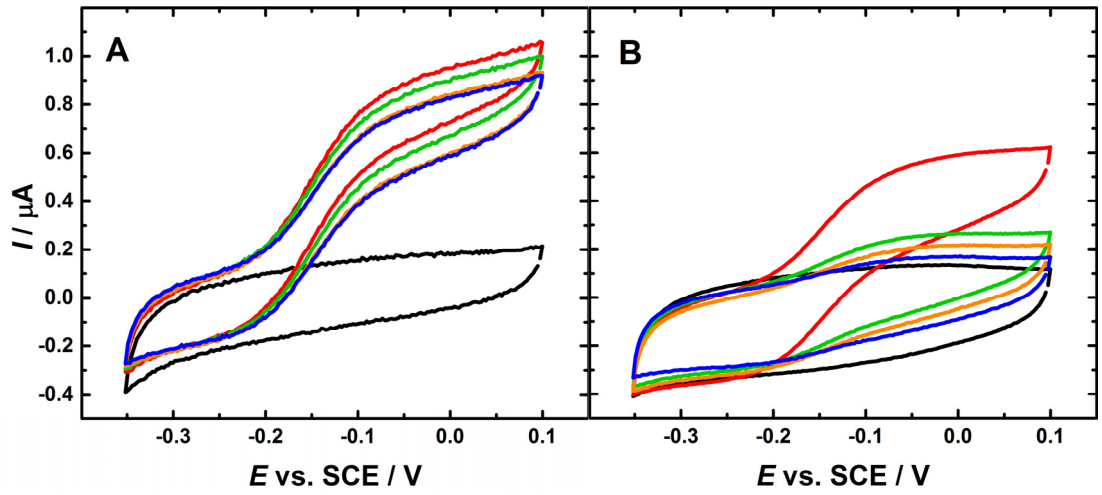

Figure 4.12. *Typical cyclic voltammograms for CDH-modified GC/MWCNT electrode (E522-CDH) in deoxygenated 50 mM Tris buffer (pH 7.4), containing 30 mM $CaCl_2$ and 70 mM D-glucose (red lines) and after incubation the electrodes in 50 mM citrate buffer (pH 3.5) for 2 (green lines), 4 (orange lines) and 6 (blue lines) hours. (A): enzyme immobilised through maleimide. (B): control, physically adsorbed enzyme on unmodified GC/MWCNT. The electrode potential was swept at 1 mV/s from -0.35 to 0.1 V vs. SCE. The GC/MWCNT electrode was prepared by drop casting of a 5 μL aliquot of 1 mg mL^{-1} MWCNT (carboxylic acid functionalized) dispersion onto the cleaned surface of GC.*

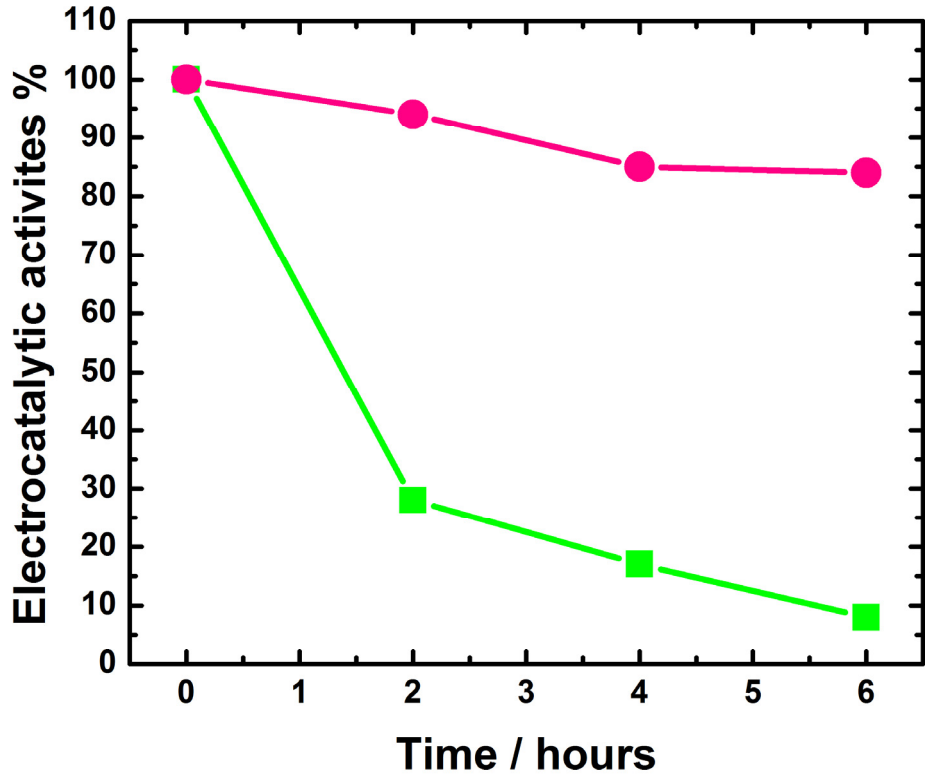

Figure 4.13. *The electrocatalytic activities in % measured at 0 V vs. SCE (after background current subtraction) in cyclic voltammograms recorded at CDH-modified GC/MWCNT electrodes (CDH variant E522 in deoxygenated 50 mM Tris buffer (pH 7.4), containing 30 mM $CaCl_2$ and 70 mM D-glucose. Pink circles: enzyme immobilised through maleimide. Green squares: control, physically adsorbed enzyme on unmodified GC/MWCNT. The electrodes were incubated in 50 mM citrate buffer (pH 3.5) whilst stirring for 2, 4 and 6 hours at 24 °C.*

4.8 Covalent immobilization of CDH on flat carbon-based electrodes

The use of carbon-based electrodes became very popular because of the wide potential window, low cost and good mechanical and dimensional stability. Carbon materials of note include carbon fibers, glassy carbon, graphite, vapor deposited carbon and carbon nanotubes.[270]

The key advantage of the electrode modification procedure described in Section 4.7, is its modular approach that allows the single elements of the modification to be varied independently. Therefore, the next study was attempted using boron doped diamond (BDD) electrodes rather than glassy carbon electrodes modified with multiwall carbon nanotubes (GC/MWCNT). However, the other modification elements, the linker, spacer, passivating group and reactive group (maleimide) were utilised as described before.

Indeed, our suggested electrode modification approach (Section 4.7) was previously applied on glassy carbon (GC) electrodes; the DET of the GC electrodes covalently modified with the *Mt*CDH variant E522 were tested by monitoring the catalytic current caused by glucose oxidation using cyclic voltammetry at 1 mV/s. Nonetheless, no catalytic current was observed. The poor performance of the CDH-modified GC electrodes has been related to the quantity of immobilised enzyme on a bare GC electrodes (geometric surface area = 0.071 cm^2) which was insufficient to generate a catalytic current higher than the electrode capacitive current, so as to be detected. Alternatively, glassy carbon electrodes modified with multiwall carbon nanotubes (GC/MWCNT) were chosen as a model for carbon-based electrodes because of their high surface area (estimated surface area = 14 cm^2)[202] combined with relatively low capacitance. Using one variant of *Mt*CDH we have shown that this approach leads to stable attachment of the enzyme to the GC/MWCNT electrode surface and that the immobilised enzyme is active for the electrochemical oxidation of D-glucose without added redox mediators. Nevertheless, we reasoned that flat electrodes could be investigated by choosing low capacitance electrode materials. Thus boron doped diamond (BDD) electrodes were introduced.[63] The BDD electrodes were purchased from Windsor Scientific. The covalent immobilisation of *Mt*CDH variant E522C on the maleimide-modified BDD electrodes were performed using the method explained in Section 4.7. DET at the CDH-modified BDD electrodes was tested by cyclic voltammetry in deoxygenated 50 mM Tris-HCl buffer, pH 7.4. Figure 4.14 shows that, with increasing concentration of D-glucose in solution up to 10 mM, an increasing catalytic current is visible starting from about -0.2 V vs. SCE and reaching a plateau around -0.05 V. The position of the electro-catalytic wave agrees with that obtained for the

CDH-modified GC/MWCNT electrode (Figure 4.4) and corresponds to DET from the haem to the electrode.[299-300]

Compared to the catalytic current obtained with the CDH-modified GC/MWCNT electrode (Figure 4.4) the catalytic current shown in Figure 4.14 is very low (in the order of nA) which is expected in such comparison. Indeed, the quantity of enzyme which can be immobilised at surface of the BDD electrode is much lower than that immobilised at the GC/MWCNT electrodes, generating a much lower current.

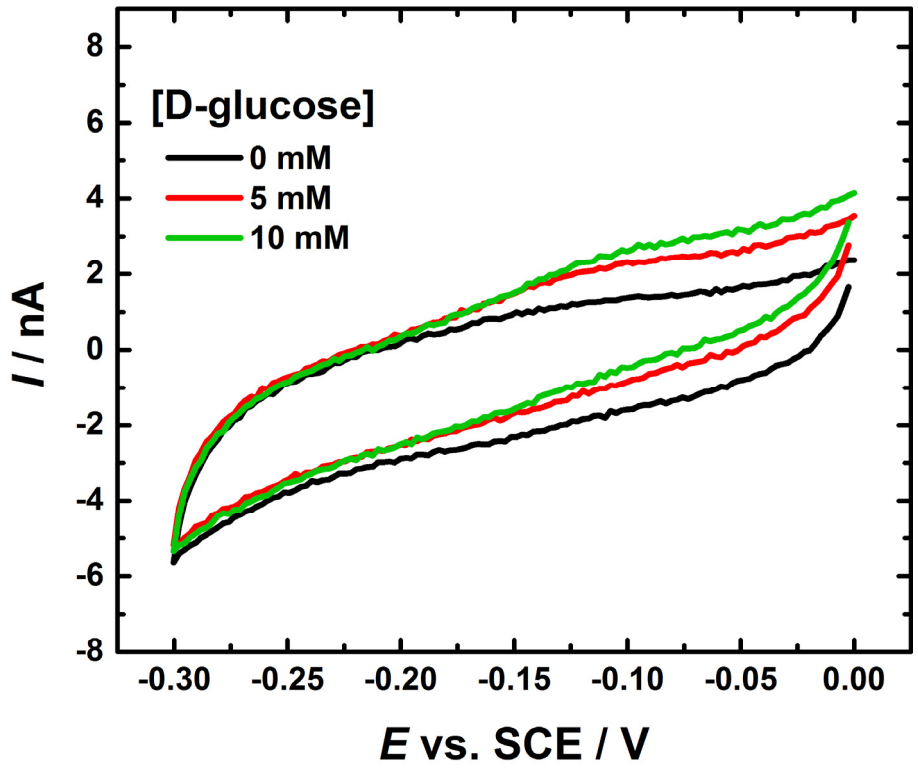

Figure 4.14. *Typical cyclic voltammograms for CDH-modified BDD electrode (E522-CDH) in deoxygenated 50 mM Tris buffer (pH 7.4), containing 30 mM $CaCl_2$ and increasing concentrations of D-glucose. The electrode potential was swept at 1 mV/s from -0.3 to 0.0 V vs. SCE.*

Despite the small quantity of the immobilised enzyme on the surface of the BDD electrode (geometric surface area = 0.071 cm^2) it is able to produce an electrochemical oxidation of D-glucose. Therefore, it could be argued that the poor performance of the CDH-modified GC electrodes was not because of their small surface area (small quantity of the immobilised enzyme), it is most probably because of their relatively high capacitance.

4.8.1 Direct electron transfer of *Mt*CDH-modified GC electrode

The experimentally measured current density includes two components i) the Faradaic current density, $j_{Faradaic}$ that is associated with the electrons crossing the electrode-solution interface

and leading to the chemical change and ii) the non-Faradaic current density, $j_{charging}$, ensuing from the electrons required to alter the surface charge. Using cyclic voltammetry to demonstrate the impact of charging currents (double layer charging) on electrochemical experiments it is straightforward to compare the amounts of the Faradaic and non-Faradaic current densities. For cyclic voltammetry, the potential changes continuously; hence, the obtained current always has a component of charging current. The charging current density is given by:[306]

$$j_{charging} = vC_{dl} \qquad (Eq.4.1)$$

Where v is the scan rate and C_{dl} the double layer capacitance. According to equation (4.1), it can be seen that the non-Faradaic current density is a minor factor at low scan rate but becomes a major feature at high scan rate. Thus, the relatively high capacitance current of an electrode such as GC might be reduced by optimising the potential scan rate of the cyclic voltammetry. At this point it is also helpful to explain about the electrochemical reversibility. For the reduction of an oxidized form (Ox) of a species, the electron transfer can be represented by:

$$Ox + ne^- \rightleftharpoons Red$$

For a reversible system, the concentrations of the oxidized and reduced species C_O and C_R at the electrode surface ($x = 0$) are at equilibrium with the applied potential as determined by the Nernst equation:

$$E = E^{0`} + \frac{RT}{nF} ln \frac{C_O(x=0)}{C_R(x=0)} \qquad (Eq.4.2)$$

Where $E^{0`}$ is the formal potential of the electrochemical reaction, R is the gas constant, T is the temperature, and F is the Faraday constant. The electrochemical reaction that obeys this equation is called reversible.[32] However, the reversibility is affected by the parameters employed during the electrochemical measurement. From equation (4.2), when the applied potential (E) is varied, the ratio between oxidized and reduced species has to be adjusted instantly.[307] For protein film voltammetry (PFV), the DET kinetics must be relatively fast to change the ratio between oxidized and reduced protein molecules according to the electrode potential. Hence, the electrochemical reversibility relies on the scan rate. The ratio between oxidised and reduced protein molecules may not be in equilibrium with the applied potential when faster scan rates are employed.[32] Thus, slower sweep rates should be employed.

Our electrode modification procedure was re-attempted on GC electrodes. The covalent immobilisation of *Mt*CDH variant E522C on the maleimide-modified GC electrodes were done using the method described in Section 4.7. However, the DET of the CDH-modified GC electrodes were examined by a slower scan cyclic voltammetry (0.5 mV/s) in 50 mM Tris-HCl

buffer, pH 7.4. Figure. 4.15 shows that, with increasing concentration of D-glucose in solution up to 10 mM, an increasing catalytic current is visible (compare the solid curves) starting from about -0.2 V vs. SCE and reaching a plateau around -0.05 V. The position of the electrocatalytic wave agrees with that obtained for the CDH-modified GC/MWCNT electrode (Figure 4.4) and corresponds to DET from the haem to the electrode.[299-300] A valid proof that the catalytic current is due to the oxidation of the glucose by the immobilised enzyme is delivered by the control experiment using L-glucose (Figure 4.15); upon addition of aliquots to increase the concentration of L-glucose in the cell there is no change in the current (compare each pair of dotted and solid curves). This excellent selectivity can only be described by the catalysis of the reaction by the enzyme.

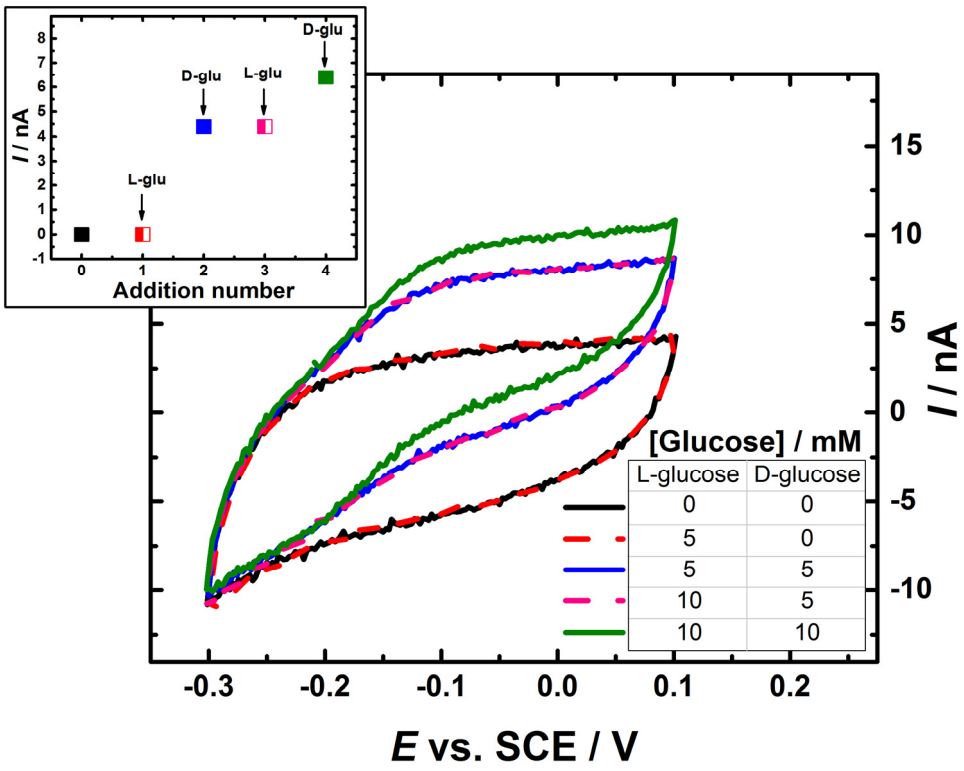

Figure 4.15. *Cyclic voltammograms for a CDH-modified GC electrode (CDH variant E522) in deoxygenated 50 mM Tris buffer (pH 7.4), containing 30 mM $CaCl_2$ (black line) and after the addition of different concentrations of L- and D-glucose. The electrode potential was swept at 0.5 mV/s. Inset: plot of the background subtracted currents measured at 0.0 V for all the additions.*

4.8.2 Covalent immobilization *vs.* physical adsorption of the *Mt*CDH onto GC electrodes

To verify that the CDH was immobilized at the GC electrode surface through covalent bonding to the surface cysteine, we carried out a comparison between the covalently bound and physically adsorbed *Mt*CDH. To this end, three different electrodes were prepared in which the

covalent immobilisation method, as described in Section 4.7, and the physical adsorption method were employed. The covalent immobilisation of *Mt*CDH variant E522C was performed on a maleimide-modified GC electrode. Meanwhile, the physical adsorption was done on the two different electrodes; i) *Mt*CDH variant E522C was adsorbed onto a bare unmodified GC electrode, and ii) *Mt*CDH variant E522C was adsorbed onto a succinimide-modified GC electrode. The succinimide was chosen as it has almost the same molecular structure of the maleimide (Figure 4.16). However, it is classified as a cyclic imide. The thiol-ene reaction, is, simply, the hydrothiolation of a C=C. Therefore, by using succinimide, no thioether bond should be obtained with the surface cysteine of the engineered enzyme. Indeed, unsaturated carbonyls, namely, maleimide is the most common substrate for such thiol-ene reactions because it has two activating cis-carbonyl groups coupled with ring-strain/bond angle distortion, the C=C bond in maleimide is specifically reactive and such thiol-ene reaction occur very rapidly.[280-281] The physical adsorption was made simply by drop casting 3 µL of the *Mt*CDH variant E522C onto the aforementioned electrodes.

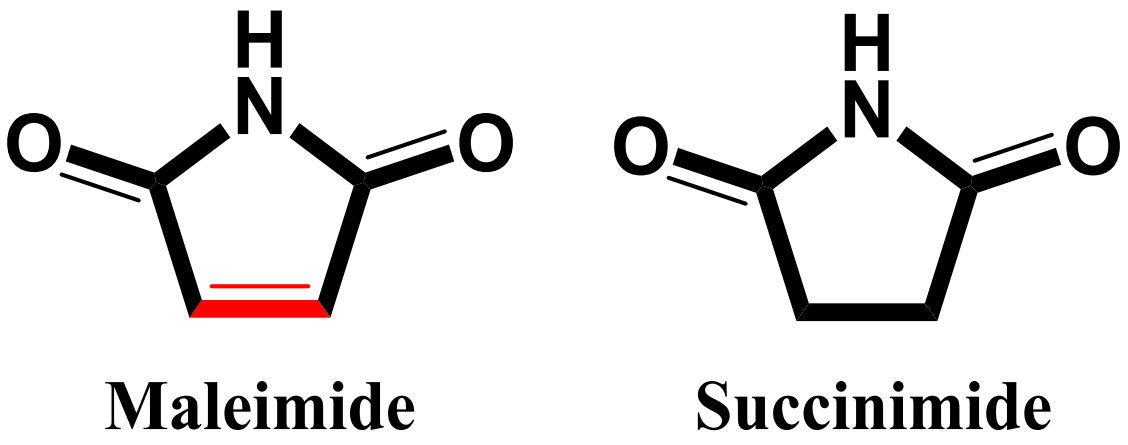

Figure 4.16. *Molecular structures of the maleimide group and succinimide group.*

The three GC electrodes modified with the *Mt*CDH E522 variant were tested for DET by cyclic voltammetry in 50 mM Tris-HCl buffer, pH 7.4 at 0.5 mV s^{-1} (Figure 4.17). DET was observed for both modification methods (physical and covalent) in the presence of D-glucose. However, the catalytic currents for physically adsorbed *Mt*CDH (Figure 4.18, b and c) were decidedly lower than the one for the covalently immobilized *Mt*CDH (Figure 4.18, a): in particular, the current was about 50% less for (b) and 75% less for (c). The results in Figure 4.18 are consistent with covalent binding of CDH at the maleimide-modified GC electrode. The higher catalytic currents obtained with the covalently-modified electrode can be explained by the fact that the covalently immobilized enzyme is held in a more suitable orientation for DET as compared to the randomly oriented, physically adsorbed CDH.

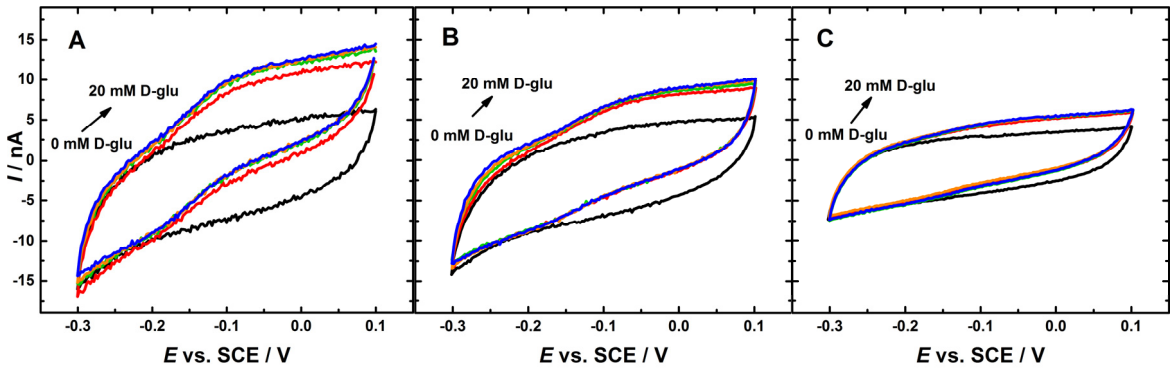

Figure 4.17. *Typical cyclic voltammograms recorded at CDH-modified GC electrodes. (a) CDH variant E522 was covalently immobilised at maleimide-modified GC electrode, (b) CDH variant E522 was physically adsorbed on succinimide-modified GC electrode, and (c) CDH variant E522 was physically adsorbed on bare unmodified GC electrode. CVs were carried out in deoxygenated 50 mM Tris buffer (pH 7.4), containing 30 mM $CaCl_2$ and increasing concentrations of D-glucose, sweeping the potential at 0.5 mV/s from -0.3 to 0.1 V vs. SCE.*

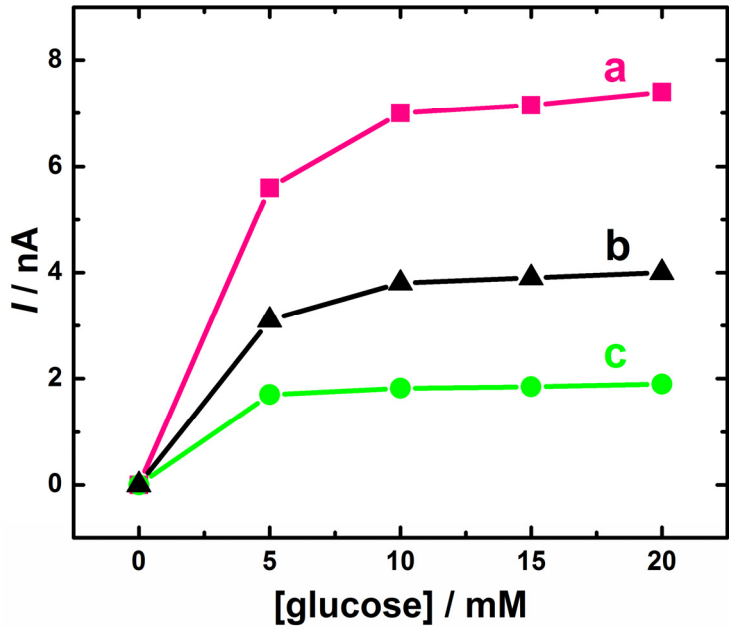

Figure 4.18. *Background subtracted currents measured at 0.0 V vs. SCE in cyclic voltammograms recorded at CDH-modified GC electrodes. (a) CDH variant E522 was covalently immobilised at maleimide-modified GC electrode, (b) CDH variant E522 was physically adsorbed on succinimide-modified GC electrode, and (c) CDH variant E522 was physically adsorbed on bare unmodified GC electrode. CVs were carried out in deoxygenated 50 mM Tris buffer (pH 7.4), containing 30 mM $CaCl_2$ and increasing concentrations of D-glucose, sweeping the potential at 0.5 mV/s from -0.3 to 0.1 V vs. SCE.*

Note that the capacitive background current for the succinimide-modified electrode is higher than the one of the bare unmodified electrode. Thus, the higher catalytic currents obtained with succinimide-modified GC electrode (Figure 4.18, b) compared to the currents achieved with bare unmodified GC electrode (Figure 4.18, c) can be explained by the adsorption of a greater quantity of enzyme molecules at the succinimide-modified GC electrode surface.

4.8.3 Stability of the CDH-modified GC electrodes

The *Mt*CDH-modified GC electrode (through the thioether bond) were found to be extraordinary stable for long periods showing after one month the same activity (about 80 % compared to the initial activity) as after four days from preparation (Figure 4.19, a). Note that the enzyme immobilised at the maleimide modified GC electrode is much more stable than the first control for the adsorbed *Mt*CDH at succinimide-modified GC electrode; 25% after one month (Figure 4.19, b), and the second control for the adsorbed *Mt*CDH at bare unmodified GC electrode; 0% after one month (Figure 4.19, c), where the catalytic response decays much more rapidly. The slight decrease in activity for the covalently modified electrode during the first four days can be accounted for by desorption of physically adsorbed CDH, which diffuses away from the electrode surface over a few days. However, the covalently modified electrode maintained roughly the same activity for a period of at least one month when stored at 4 °C wet with the same buffer used for the tests (50 mM Tris/30 mM $CaCl_2$, pH 7.4). The small fluctuations in the activity observed during the experiment are probably due to experimental factors, such as a slightly different temperatures or concentrations of glucose.

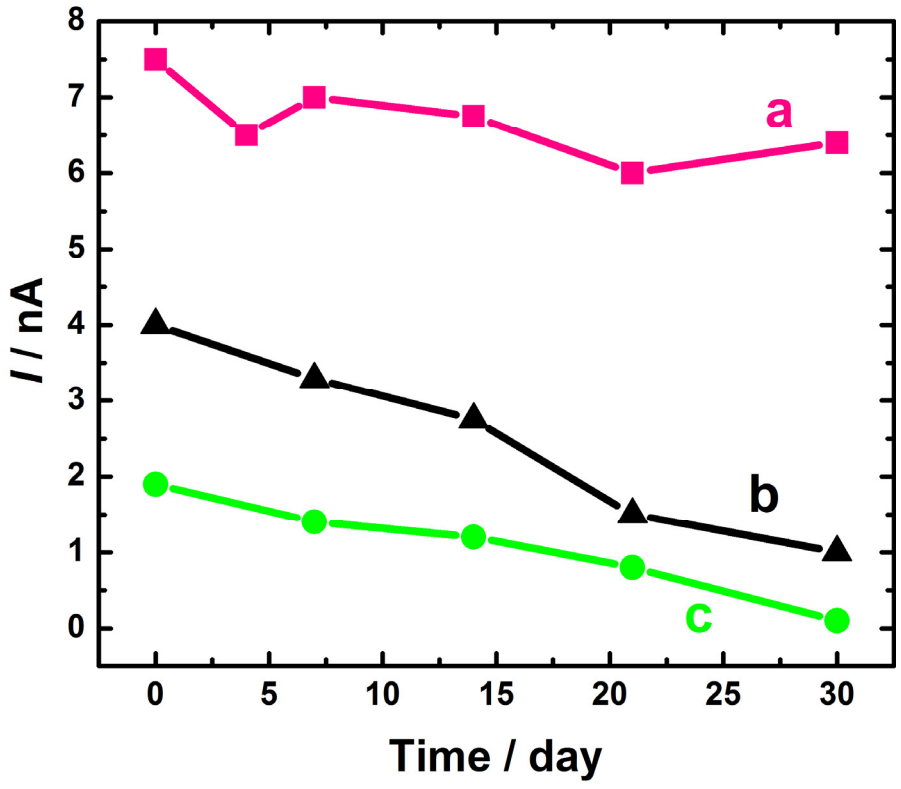

Figure 4.19. *Background subtracted currents measured at 0.0 V vs. SCE in cyclic voltammograms recorded at CDH-modified GC electrodes in deoxygenated 50 mM Tris buffer (pH 7.4), containing 30 mM $CaCl_2$ and 20 mM D-glucose. (a) CDH variant E522 was covalently immobilised at maleimide-modified GC electrode, (b) CDH variant E522 was physically adsorbed on succinimide-modified GC electrode, and (c) CDH variant E522 was physically adsorbed on bare unmodified GC electrode. The electrodes were stored in wet condition at 4 °C for one month.*

With the *Mt*CDH variant E522C (as a model for the cysteine-modified genetically engineered protein), we have shown that our immobilisation approach leads to an extraordinary stable attachment of the enzyme to the electrode surface and the fact that the immobilised enzyme is active for the electrochemical oxidation of D-glucose without added redox mediators. With these promising results, a wide range of engineered enzymes could now be electro-kinetically investigated in such a novel strategy; a detailed study of the enzyme kinetics of the immobilised *Mt*CDH mutants of interest are discussed in the next sections.

4.9 Kinetics and electrocatalytic behaviour of *Mt*CDH

Redox enzymes can be classified into extrinsic and intrinsic enzymes according to the mechanism of the ET reaction.[36] Intrinsic enzymes, such as glucose oxidase (GOx), have one region, namely, the vicinity of the prosthetic group, where the ET reaction between the substrate and redox active sites of the redox enzyme happens. Since there is no natural requirement for long range ET pathways to the surface of the protein,[308] DET is very difficult to achieve.[32] With extrinsic redox enzymes such as CDH, an electron-accepting or donating center is essential which binds to the enzyme in some protein fragment or at a site not extremely close to the active site and hence there are an electron pathway to the surface and/or additional active site on the surface for another protein to connect to, making them an excellent choice for DET.[36] For CDH the electrons are transported via internal electron transfer (IET) from the catalytically active flavin domain to the haem domain which is able to communicate with electrodes in a DET reaction.[32]

There have been many reports of direct electron transfer (DET) with flavoproteins and most of those have been concerned with glucose oxidase (GOx).[108] However, further investigations of these systems (see Chapter three) confirm that it is the electrochemistry of the free FAD and/or impurities that is being observed rather than that of the enzyme. Following the successful immobilisation of the E522-CDH variant on the maleimide modified GC/MWCNT electrodes via the thioether linkage, the next aim was to investigate the kinetics and electrocatalytic behaviour of *Mt*CDH. To this objective, five different *Mt*CDH variants (Figure 4.2) genetically engineered to bear a free cysteine in different positions at the surface of the flavin domain were investigated.

4.9.1 Electrochemistry of E522-*Mt*CDH on maleimide-modified MWCNT electrodes

GC/MWCNT electrodes covalently modified with the *Mt*CDH variants E522 were previously tested for DET (Section 4.7.1) by cyclic voltammetry. Figure 4.3 showed that in the absence of

substrate, sweeping across the potential range at 10 mV/s produces redox peaks due to DET between the electrode and the redox centre of the enzyme. The redox electrode potential (E_{mid}) observable at *ca.* -0.137 V vs. SCE (Figure 4.3) is consistent with other studies of DET to CDH class II at pH 7.4,[283-284, 298] and can be attributed to the one-electron transfer of the haem group, one of the two CDH active sites, identified in two distinct domains of the enzyme.[284, 309] In this Section, a further analysis is conducted. After the background current subtraction (Figure 4.20A), the area under the resulting faradaic voltammogram can be integrated to estimate the charge and, subsequently, the absolute amount of electroactive enzyme on the surface of the modified electrode, the average amount of electroactive CDH was calculated (using Faraday's law) to be ≈ 5.0 pmol. The surface coverage (Γ) of CDH cannot be calculated because the precise active area for a carbon nanotubes electrode is not known or practically accessible. However, an estimated area of *ca.* 14 cm^2 was obtained using the mathematical method described by Peigney [202] for 9.5 nm MWCNTs with 7-9 walls. Assuming a surface area of 14 cm^2 and a one electron process this (4.5 pmol) corresponds to a coverage of around 0.36 x 10^{-12} mol cm^{-2}.

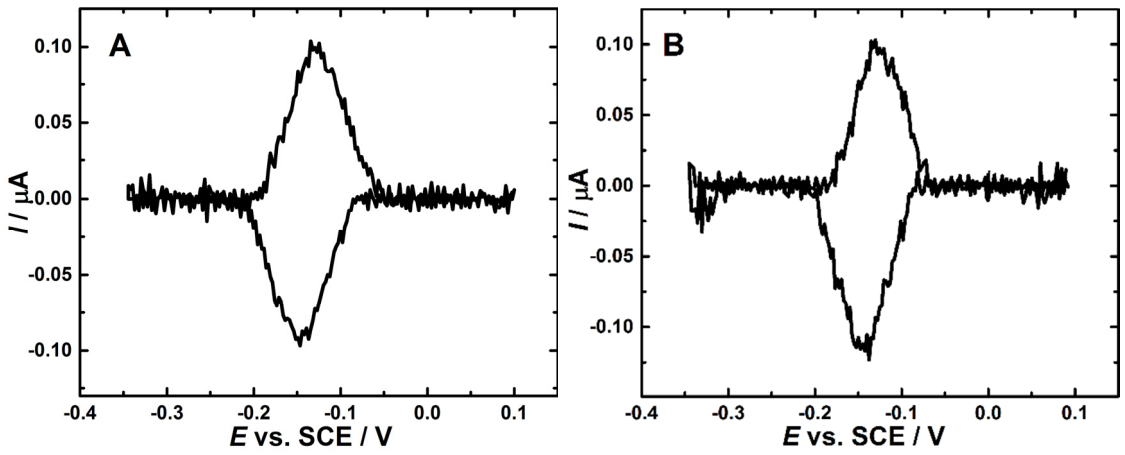

Figure 4.20. *Cyclic voltammograms (after background current subtraction) for the CDH-modified GC/MWCNT electrode (E522C). (A) The CV was recorded in deoxygenated 50 mM Tris buffer (pH 7.4) at 20 mV/s. (B) The CV was recorded in deoxygenated 50 mM acetate buffer pH 5.5 at 20 mV/s.*

4.9.1.1 Haem vs. FAD

To rule out the possibility that the redox peaks shown in Figure 4.20A were due to exchange of electrons with the deeply buried FAD active site the same electrode was retested for DET in more acidic solution at pH 5.5. Figure 4.20B shows the cyclic voltammogram (after background current subtraction) for the CDH-modified GC/MWCNT electrode in deoxygenated 50 mM acetate buffer pH 5.5. The cyclic voltammogram recorded at pH 5.5 displays a redox peaks at a potential close to that recorded at pH 7.4 (Figure 4.20A). Indeed, if the redox peaks observed in Figure 4.20 were due to the redox reaction of the FAD active site a pH dependent redox

potential should be obtained.[310] According to the Nernst equation for a 2 proton-2 electron redox process a shift of 59 mV should be achieved per pH unit. Consequently, moving from pH 7.4 to pH 5.5 should increase the redox potential by *ca.* 120 mV. For GOx bound FAD, Vogt *et al.*[144] showed that a dependence of the midpoint potential by a change of 50 mV pH^{-1} in the pH range between 4.5 and 7.4, indicating a $2H^+/2e^-$ redox mechanism of the FAD cofactor, for the pH region between 7.6 and 8.5 the slope declined to 27 mV pH^{-1}, implying a $1H^+/2e^-$ redox mechanism for FAD. Gorton *et al.*[309] have suggested that the switch from a $2H^+/2e^-$ to a $1H^+/2e^-$ redox reaction for FAD happens at lower pH in the case of class I CDHs (note that our model enzyme, *Mt*CHD, is a class II CDH), demonstrating structural differences of the catalytic site. Despite the fact that the DH domain of CDH is similar to GOx and both are members of the GMC family of oxidoreductase. However, the structure of the catalytic site in the CDH around the flavin ring has two conserved residues, histidine and asparagine in a similar conformation, in GOx there are two histidines instead.[290] It has been suggested that the asparagine in CDH is further facilitate the proton abstraction from the substrate by the histidine residue.[290, 309] In their work Gorton *et al.*[309] have also confirmed that the DET of class II, CDHs, such as *Mt*CDH, by exchange electrons with the FAD active site is not possible at all. The *ca.* 5 mV difference in the redox potential obtained in Figure 4.20 between the two pHs is most probably due to experimental error. Hence, it can be concluded that the haem group exchanges electrons with the electrode surface in the DET mechanism.

At a scan rate of 20 mV s^{-1} the peak to peak separation (ΔE_p) was also calculated to be 0.02 V (Figure 4.20), such a small value of ΔE_p reveals that a fast and reversible electron transfer process occurs at the surface of the CHD modified electrodes.[306] For a surface-bound reversible redox couple, the theoretical width at half height, $W_{1/2}$ for the wave at 298 K is 90.6 $/n$ in mV, where n is the number of exchanged electrons.[309, 311] The values for $W_{1/2}$ of around 80± 5 mV for the CDH-modified GC/MWCNT electrode (E522C) further support a $1e^-$ transfer process originating from the haem cofactor located in the CYT domain.

4.9.1.2 Effect of scan rate on voltammetry of *Mt*CDH-modified electrode

Different scan rate studies were also performed at the CDH-modified electrode. Figure 4.21A shows the cyclic voltammograms (after background current subtraction) for the CDH-modified GC/MWCNT electrode (E522C) at different scan rates. The anodic peak potential (E_{pa}) shifted to a more positive direction and the cathodic peak potential (E_{pc}) shifted to a more negative direction with the increasing scan rate in the range of 5 to 150 mV / s. Nonetheless, the formal (redox) potential ($E^{0`}$) is nearly not changed. The integrated redox peaks provide a nearly constant charge Q (*ca.* 0.55 µC) at different scan rates. In addition, the redox peak currents (I_{pa} and I_{pc}) increase linearly with increasing scan rates (Figure 4.21B), showing that the redox

reaction of the immobilized *Mt*CDH at maleimide-modified electrode is a surface-confined reversible electron transfer process.

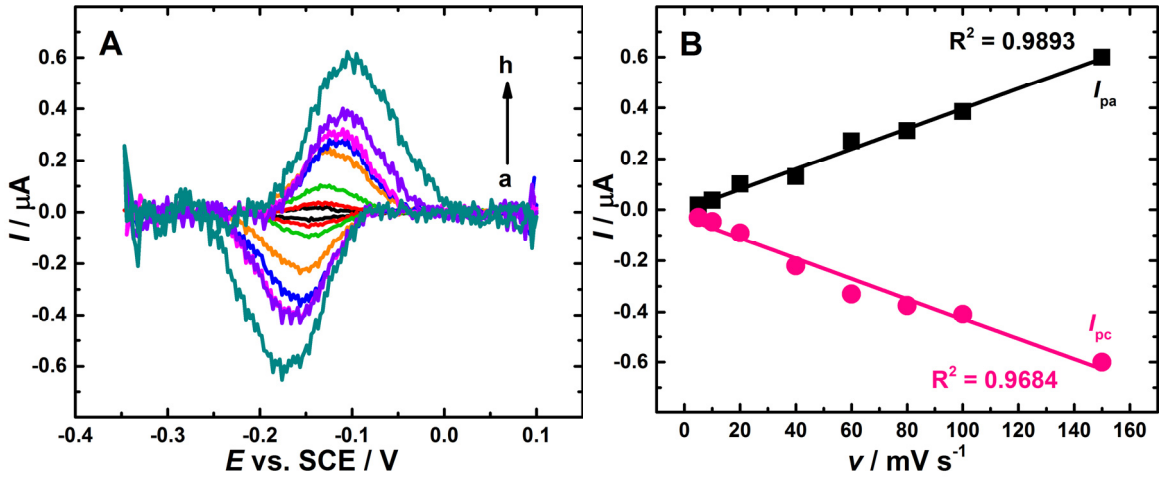

Figure 4.21. *(A) Cyclic voltammograms (after background current subtraction) for the CDH-modified GC/MWCNT electrode (E522C) recorded at 25 °C in deoxygenated 50 mM Tris buffer (pH 7.4), containing 30 mM $CaCl_2$ at different scan rates (from (a) to (h): 5, 10, 20, 40, 60, 80, 100 and 150 mV s^{-1}). (B) Shows the linear dependence plot of peak currents with scan rate.*

To further reveal the nature of DET of the immobilized *Mt*CDH, the kinetic analysis of the DET reactions proceeding in the *Mt*CDH-modified electrodes was accomplished by processing the cyclic voltammograms in Figure 4.21A within the Laviron model.[206] This mathematical approach uses the ΔE_p, namely, the overpotential / (cathodic–anodic) peak potential separation as a way to determine the heterogeneous electron-transfer rate constant (k_s), which should be a function of the scan rate.[207] When n ΔE_p < 200 mV, the k_s could be estimated according to the following equation[178]

$$k_s = \frac{mnFv}{RT} \qquad (Eq. 4.3)$$

Where *n* is the number of transferred electron, *F* is the Faraday constant, *R* is the universal gas constant, *T* is the temperature, *v* the scan rate and *m* values are presented in Laviron's paper (1979)[206] and depend on the peak to peak separation related to the number of electrons ($n\Delta E_p$) involved in the DET reaction.[207] It should be noted that Laviron[206] has provided some values of $n\Delta E_p$ as a function of $1/m$ for the charge transfer coefficient (α) = 0.5. Table 4.1 illustrate the heterogeneous electron transfer rate constant (k_s) for *Mt*CDH-modified electrode estimated at different scan rate. The average k_s value registered for *Mt*CDH-modified electrode (variant E522) was calculated to be ca. 1.9 s^{-1}. The k_s value is discussed in Section 4.9.3.5.

Table 4.1. *The heterogeneous electron transfer rate constant (k_s) for MtCDH-modified electrode (variant E522). The k_s values were estimated at 25 °C using equation 4.3.*

Scan rate (v) / V s^{-1}	Peak separation (ΔE_p) / mV	m	k_s / s^{-1}
0.02	20±2	2	1.5±0.05
0.04	28±2	1.3	2.0±0.05
0.06	41±2	0.8	1.9±0.05
0.08	48±2	0.65	2.0±0.05
0.1	57±2	0.55	2.1±0.05

4.9.2 Electrocatalytic behaviour of E522-*Mt*CDH on maleimide-modified MWCNT electrodes

DET of the GC/MWCNT electrodes modified with the *Mt*CDH E522 variant was previously tested by monitoring the catalytic current caused by glucose oxidation. Figure 4.4 showed an increase in the catalytic current as the concentration of D-glucose in the solution was increased. The position of the onset of the catalytic current agrees with that reported in the literature and corresponds to DET from the haem to the electrode.[283, 299-300] Herein, the electrocatalytic behaviour of the *Mt*CDH variant E522C is analysed in greater detail to reach a better understanding for the DET mechanism before introducing the other four *Mt*CDH variants. Figure 4.22A shows a voltammogram recorded for the same CDH-modified GC/MWCNT electrode in deoxygenated 50 mM Tris buffer (pH 7.4) solution containing 70 mM D-glucose. The scan rate is an important parameter which controls the time-scale of the cyclic voltammetry experiment and consequently the time required for the electrochemical processes under investigation.[306] Therefore, a slow scan rate was used (1 mV/s) to ensure steady state; in a voltammetric experiment, this corresponds to a steady-state flux of electrons from a substrate in solution to the electrode, via the immobilised redox enzyme, which is measured as a steady-state current. The voltammogram shown in (Figure 4.22, black line) is a "direct read-out" of the rate of the catalysis as a function of the applied potential.[16] At a driving force higher than the CDH equilibrium potential, electrons flow from glucose to the electrode via the FAD and haem active centres. The recorded current is directly proportional to the rate of glucose oxidation for that given concentration of substrate. Particularly, when re-oxidation of the haem active centre by the electrode is not the rate determining step.

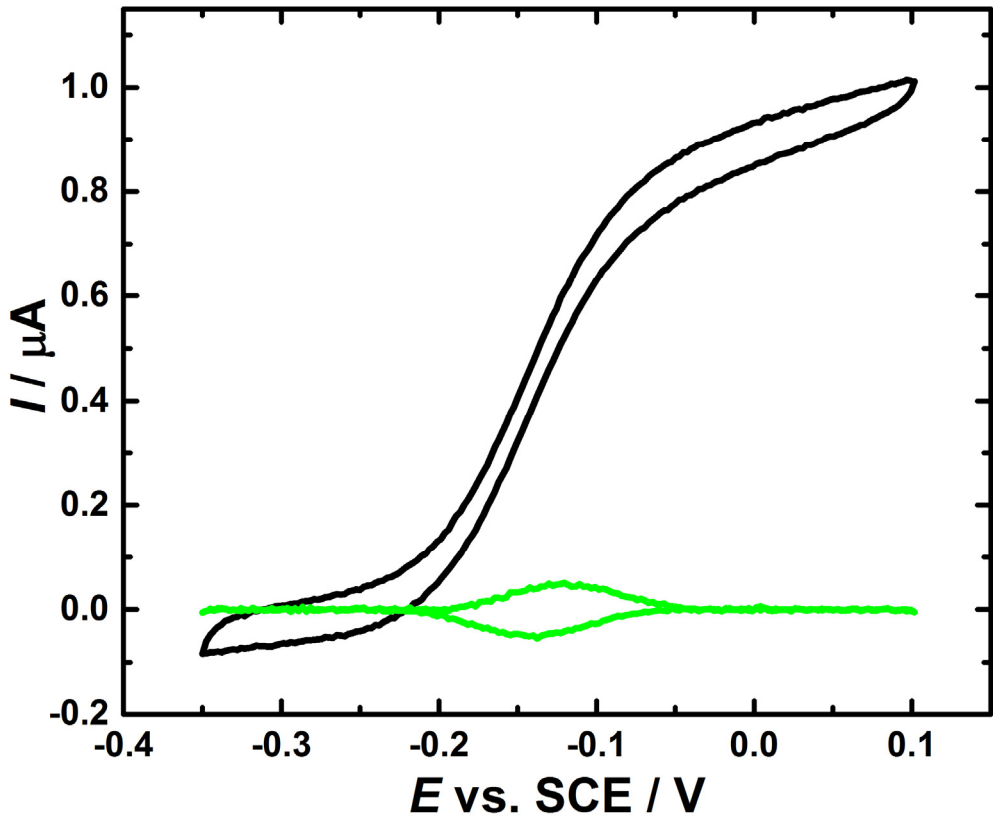

Figure 4.22. *Cyclic voltammograms for the CDH-modified GC/MWCNT electrode (E522-CDH), in presence of 70 mM glucose (black line), the CV was recorded in deoxygenated 50 mM Tris buffer (pH 7.4), containing 30 mM $CaCl_2$ by scanning the potential at 1 mV/s. The green line is the cyclic voltammogram (after background current subtraction) which was recorded in deoxygenated 50 mM Tris buffer (pH 7.4) at 10 mV/s in the absence of glucose.*

In the absence of glucose, the immobilised *Mt*CDH onto the maleimide-modified electrode produces peak-like signals resulting from the reversible electrochemical transformation of its haem redox centre (Figure 4.22, green line). Upon adding glucose, the non-turnover peaks are transformed to a significant "catalytic wave" (Figure 4.22, black line). Therefore, it can be concluded that the reaction with glucose transforms the active sites, which are regenerated by electron transfer with the electrode in a progression of catalytic cycles. The magnitude of the current is proportional to the concentration of the immobilised enzyme, and to the turnover rate, and hence the driving force could relate to the catalytic activity of a redox enzyme by conducting a voltammetric experiment.[312]

4.9.2.1 FAD vs. haem

The vast majority of the results for DET for CDH in the literature indicate that the oxidation of the carbohydrate at the flavin domain of CDHs is followed by IET to the haem domain, which is able to donate the electrons to the electrode.[283, 297, 313] However, a study by Gorton *et al.* [309] claimed DET between the glycosylated, FAD-containing domain of class I CDHs, and the

electrode. The authors showed the corresponding catalytic waves obtained from cyclic voltammetric measurements. Nonetheless, they indicate that the DET from the FAD group is only possible under acidic conditions (pH 3 to 5), whereas the catalytic currents are visible even at pH values above pH 5 via DET through the haem group, implying that the flavin-containing domain is still catalytically active, but that DET via the flavin is not possible.

In the present study, to rule out that the catalytic wave obtained in Figure 4.22 (black line) was due to the exchange of electrons with the FAD active site, the same electrode was retested for DET by sweeping in a wider potential window (from -0.6 to 0.4 V). Taking a closer look at the voltammograms in Figure 4.23, we can notice that the oxidation process starts at about -0.2 V vs. SCE. Several publications report that this potential should be the redox potential of the haem group,[283-284] whereas enzyme-bound FAD should be oxidised at more negative potentials.[144, 314] In their work Gorton *et al.*[309] have concluded that DET from the DH domain (of class I CDHs) occurs at potentials roughly 130 mV more negative than the usually observed DET of CYT. Accordingly, if the DET was due to the exchange of electrons with the FAD group, we would have observed the catalytic wave in Figure 4.23 at a redox potential of *ca.* – 0.35 mV (vs. SCE.), which did not occur. This should confirm that the DET from DH domain of our *Mt*CDH (class II CDH) is not feasible.

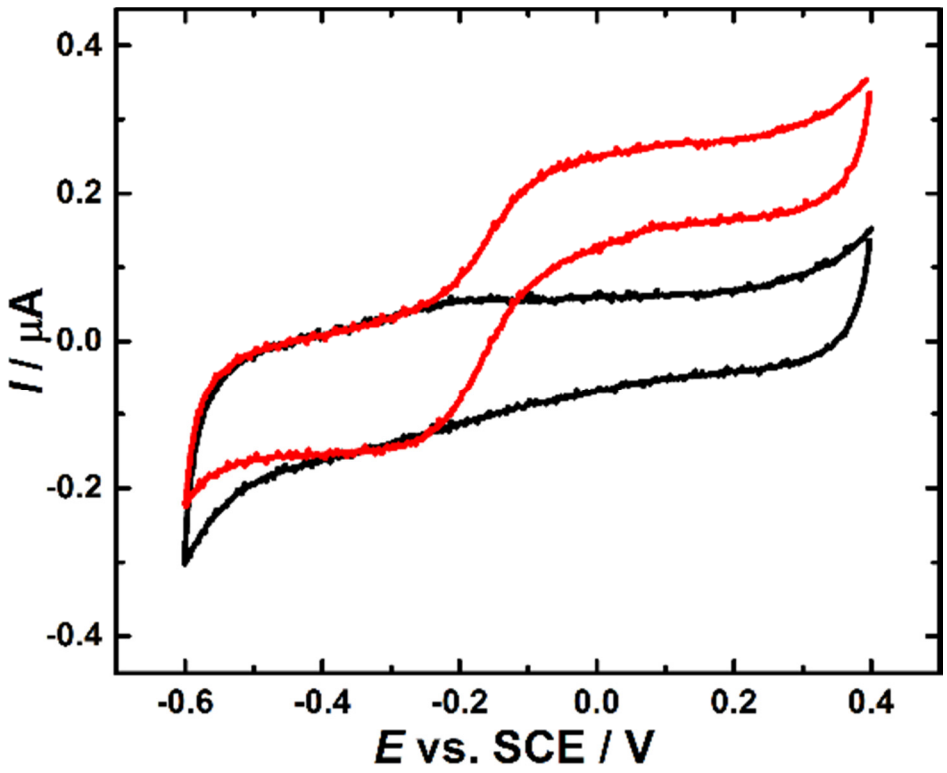

Figure 4.23. *Cyclic voltammograms for the CDH-modified GC/MWCNT electrode (E522-CDH) in deoxygenated 50 mM Tris buffer (pH 7.4), containing 30 mM $CaCl_2$ (black line) and after the addition of 3 mM D-glucose (red line). The electrode potential was swept at 1 mV/s from -0.6 to 0.4 V vs. SCE.*

To further prove that the haem group exchanges electrons with the electrode surface (1 e- transfer process) in the DET mechanism, a deeper analysis can be carried out using the following modified form of the Nernst equation:

$$E = E^0 + \frac{0.059}{n} Log\left(\frac{i_L - i}{i}\right) \qquad (Eq.\ 4.4)$$

Where E^0 is the formal potential, n the number of exchanged electrons and i_L the limiting current. Firstly, equation (4.4) has been employed, in order to estimate the number of the electrons transferred in DET for the CDH-modified GC/MWCNT electrode. Applying this equation to some points taken in the middle part of the steady-state catalytic voltammograms subtracted for the background current (Figure 4.24.A), a linear relation between the applied potential and Log (i_L - i/i) was obtained. Linear fits of such plots (Figure 4.24.B) give a more accurate value for the E^0, about -0.14 V vs. SCE, as well as the number of exchanged electrons (slope = 0.059 / n), which was calculated to be *ca.* 0.8 and can be approximated at 1. This is a further proof that the haem group interacts with the electrode surface in the DET mechanism, as its redox process involves one electron, while FAD would need two electrons to be oxidised.[144, 309]

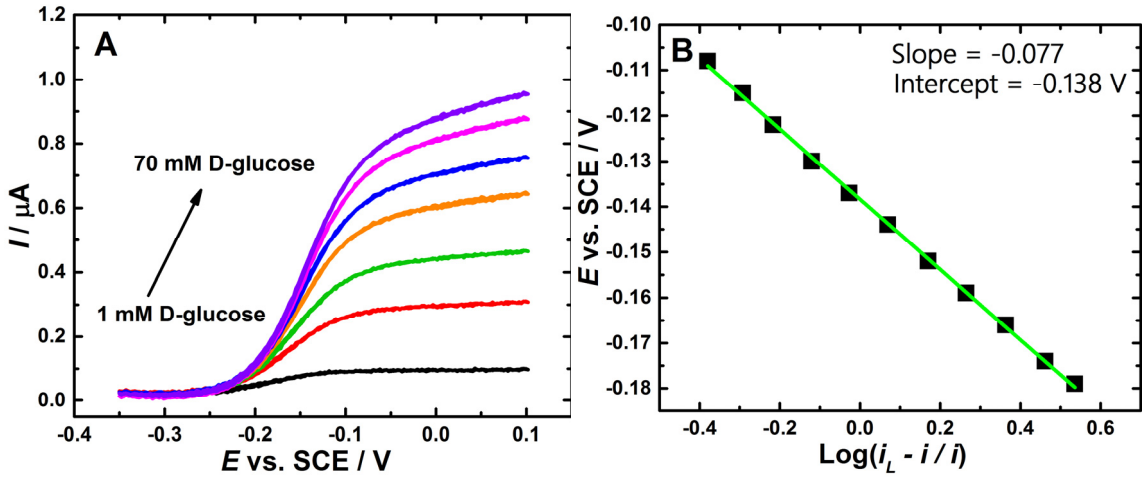

Figure 4.24. *A) Background current subtracted cyclic voltammograms for a CDH- modified GC/MWCNT electrode (E522-CDH): The original CVs are shown in Figure 4.4 which were recorded in deoxygenated 50 mM Tris buffer (pH 7.4), containing 30 mM $CaCl_2$ and increasing concentrations of glucose, scanning the potential at 1 mV/s from -0.35 to 0.1 V vs. SCE. B) Some potential points taken in the middle region of CV recorded for 70 mM glucose (in A) plotted against the Log (i_L-i/i). Data were fitted with the linear fitting (green line) to determine the intercept (E^0) and the slope (-0.059/n).*

4.9.2.2 Papain experiment

As a final control experiment to verify that the haem group exchanges electrons with the electrode surface in the DET mechanism, papain was introduced (the experiment was done by

my collaborator, M. Meneghello). Papain (EC 3.4.22.2) exhibits proteolytic activity towards proteins, short-chain peptides and amide links and is used widely in the field of food and medicine .[315-316] CDH consisting of two separate domains (CYT and DH) linked together by a polypeptide linker (of around 20 amino acids) that allows the two to come in close contact for internal electron transfer (IET).[286] A recent study by Tan *et al.*[288] has employed papain for the proteolytic cleavage in the linker of the *Mt*CDH to obtain the individual DH and CYT domains. It is widely believed that papain can be used to detach the two CDH domains in the solution.[317-320] Indeed, no convincing evidence have been shown to demonstrate that the papain favours cleavage of the polypeptide linker that connects the CDH domains. The treatment of the CDH-modified GC/MWCNT electrode with papain would remove the CYT domain from the electrode surface (Scheme 4.5), and consequently no electrons exchanging via the haem group should be expected. On the other hand, the electrons obtained by glucose oxidation at the DH domain can still be transferred from the FAD group to different electron acceptors (mediators).

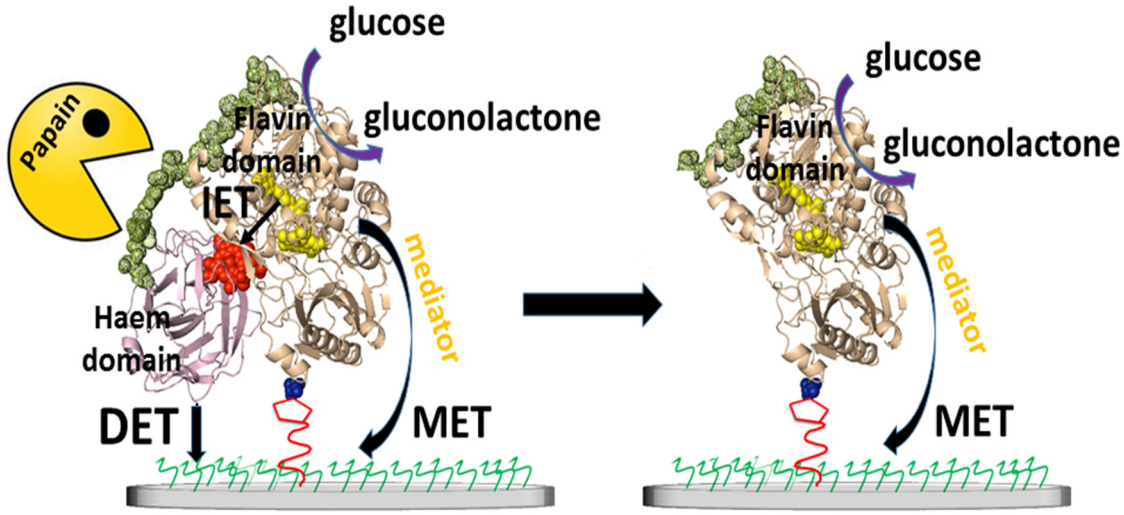

Scheme 4.5. *Schematic representation of the presumed papain (Pacman) effect on the immobilised MtCDH. The CDH was immobilised at the electrode surface via the thioether bond.*

*Mt*CDH-modified GC/MWCNT electrode (E522C) was tested for DET and MET by cyclic voltammetry before and after the papain treatment; the aforementioned electrode was immersed in deoxygenated acetate buffer pH 5.5, containing 30 mM $CaCl_2$ and 0.3 mg / ml papain for 24 hours. Figure 4.25A shows the cyclic voltammograms of the GC/MWCNT electrode modified with E522-CDH in deoxygenated 50 mM acetate buffer (pH 5.5), containing 30 mM $CaCl_2$ (black lines), after the addition of 50 mM glucose (green lines) and 0.2 mM ferrocenecarboxylic acid (pink lines). By adding glucose in the solution, the DET catalytic onset starts at *ca.*-0.2 V vs. SCE and reaches a catalytic current plateau at around -0.05 V, whereas after the addition of the mediator, the DET catalytic onset was also obtained at the same potential, meanwhile, the MET catalytic current starts at *ca.* 0.13 V. After the papain treatment,

the electrode was retested for DET and MET. Figure 4.25B illustrates that both DET and MET currents decreased. However, by significantly different ratios.

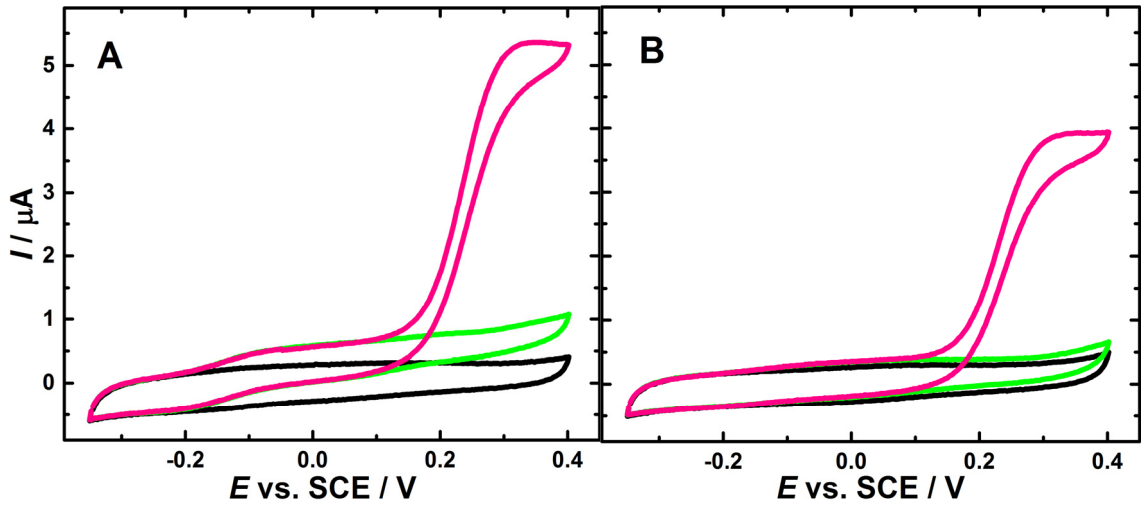

Figure 4.25. *Cyclic voltammograms of the GC/MWCNT electrode modified with E522-CDH in deoxygenated 50 mM acetate buffer (pH 5.5), containing 30 mM $CaCl_2$ (black lines), after the addition of 50 mM glucose (green lines) and 0.2 mM ferrocenecarboxylic acid (pink lines). The CVs were recorded before (A) and after (B) the papain treatment. The experiment was done by my collaborator, M. Meneghello.*

The results shown in Figure 4.25B were almost as expected, showing that the DET current decreased by (80%) after the treatment with papain, most probably due to the loss of the haem group from the CDH after the papain cleaves the amino acid linker between the two domains. However, the MET current was also decreased, even if to a lesser extent (30%). This behaviour may be explained by the fact that the papain not only breaks the polypeptide linker of the CDH, but is also expected to hydrolyse the flavin domain as well. However, it can be argued that the 50% difference in the lessened catalytic currents between the DET and MET was due to the removal of the vast majority of the haem domain from the electrode surface. Therefore, this supports the conclusion that the DET mechanism only occurs via the haem group.

4.9.3 Direct electron transfer for the five CDH variants

The correct orientation of an immobilized enzyme on the electrode surface is fundamental, when the enzyme molecules are oriented with their active centre is facing the electrode surface the pathway for ET is straightforward. Efficient DET requires a good connection between the electrode and enzyme with the correct orientation and favourable distance as suggested by Marcus theory.[7, 21] Therefore, the electrochemical performance of the five *Mt*CDH variants (see Figure 4.2 for the structures) was investigated. As described, the five *Mt*CDH variants were engineered to bear a free cysteine residue in different positions at the surface of the enzyme, allowing fast, selective and site-specific attachment to maleimide-modified electrodes. In this

way, we would expect the different CDH variants to be immobilised with different orientations on the electrode surface, depending on the location of their free cysteine residue (Figure 4.26). Hence, the different variants would have different electron transfer distances or different internal electron transfer distances and, consequently, different electron transfer rates. For instance, the position of the cysteine mutation for the variant D813C molecule would requires the haem domain to move far away from the flavin domain to be close to the electrode surface. With regard to the E522C and D574C variants, the haem domain not only needs to move away from the flavin domain but also to rotate to contact the electrode surface. On the contrary, the other enzyme orientations T701C and E674C require only a small movement of haem domain and no reorientation of the haem towards the electrode surface. However, the results showed later (see Section 4.9.3.5) make it clear that the electron transfer kinetics for the haem/electrode are fast for the five variants (The internal electron transfer (IET) has been shown to be the rate determining step in the proposed mechanism). To investigate this, maleimide-modified GC/MWCNT electrodes were used to immobilise the five different CDH variants. The electrodes were constructed using the method described in Section 4.7.

DET of the CDH-modified GC/MWCNT electrodes (of each variant) were tested by monitoring the catalytic current caused by glucose oxidation. The maximum catalytic current (i_{max}) that can be reached upon saturation depends on the total amount of electroactive enzyme present, *vide supra*. Assuming the active area of our GC/MWCNT electrodes to be almost the same every time as well as the surface coverage of the enzyme, we could use the maximum catalytic current to measure the amount of electroactive CDH, more precisely the number of CDH molecules able to undergo efficient direct electron transfer to an electrode surface. Figure 4.27 shows the cyclic voltammograms of the CDH-modified GC/MWCNT electrodes for the various variants: (A) D813C, (B) D574C, (C) E522C, (D) T701C and (E) E674C in deoxygenated 50 mM tris buffer (pH 7.4) and after the addition of different concentrations of D-glucose. The addition of the glucose increases the anodic current at around -0.2 V (*vs.* SCE) and the current reaches a catalytic plateau at around 0.0 V *vs.* SCE, showing the direct electron transfer between the enzyme and the electrode. Note that for all variants the $E_{1/2}$ is the same, indicating that the immobilisation does not change the haem potential. Calibration curves for glucose were plotted. Figure 4.27F shows that increasing the concentration of D-glucose up to 70 mM, the catalytic currents increased up to 0.73 µA for the D813C variant, 1.73 µA for the D574C variant, 1.03 µA for the E522C variant, 1.83 µA for the T701C variant and 1.33 µA for the E674C variant, showing that each variant exhibits different maximum catalytic currents. Indeed, more precise values of i_{max} were calculated (Section 4.10.1) by fitting the experimental data in Figure 4.27F with the electrochemical form of the Michaelis-Menten equation (*Eq.* 4.7).

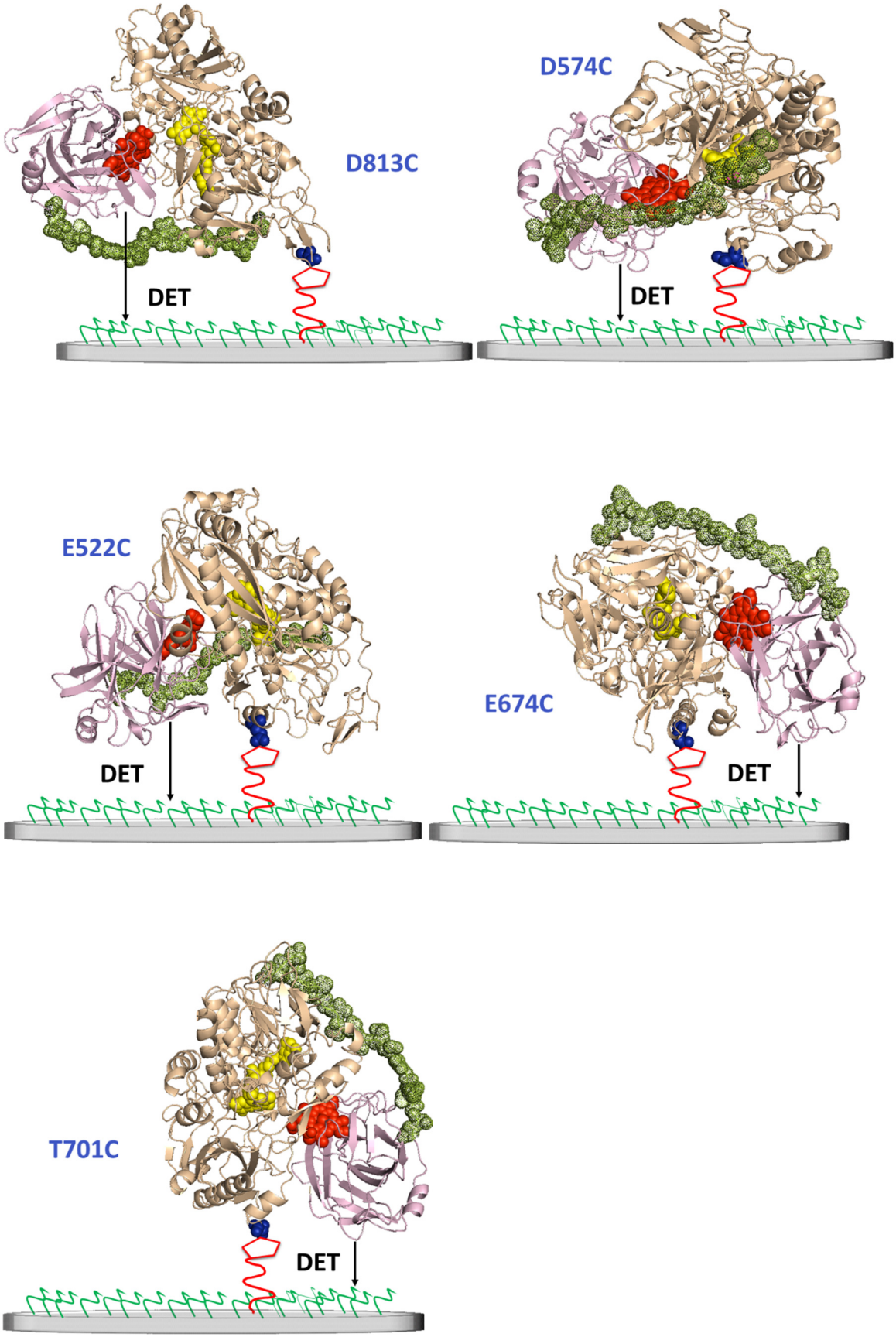

Figure 4.26. *The presumed orientations for the five MtCDH variants on to maleimide-modified electrodes. The variants images was obtained with PyMol software, PyMol visualisations are based on the crystal structure of MtCDH, PDB code 4QI6.*[288]

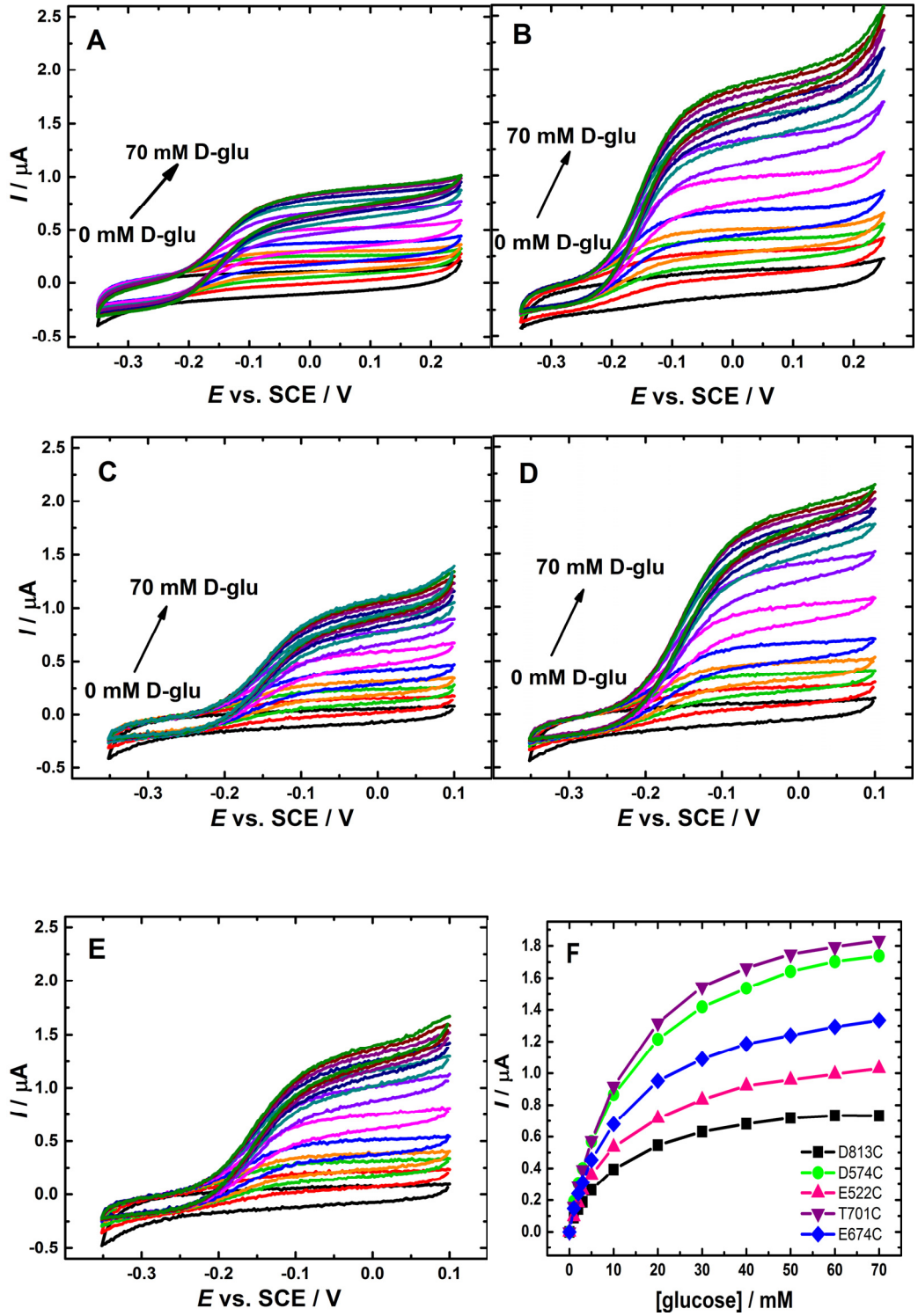

Figure 4.27. *Cyclic voltammograms of the CDH-modified GC/MWCNT electrodes for various variants: (A) D813C, (B) D574C, (C) E522C, (D) T701C, (E) E674C in deoxygenated 50 mM tris buffer (pH 7.4) in the presence of 30 mM $CaCl_2$ at 1 mV s^{-1}, Black lines: background current without glucose; coloured lines: after the addition of 1, 2, 3, 5, 10, 20, 30, 40, 50, 60 70 mM D-glucose. (F) Relative background subtracted currents for the CV experiments, the current was taken at 0 V vs. SCE and the background current were subtracted.*

In order to understand why the different variants give different currents we need to understand whether the different responses are because of differences in active area of our

GC/MWCNT electrodes, differences in the surface coverage of the enzyme or if it is because of differences in enzyme kinetics.

So as to verify that a different orientation for each *Mt*CDH variant was successfully achieved, several control experiments were attempted. The control experiments were designed to confirm that: i) the CDH variants were successfully attached with different enzyme immobilization orientations to GC/MWCNT through the thioether bond, ii) the *Mt*CDH variants immobilized on the surface of MWCNT electrodes retain their bioelectrocatalytic activity to the specific oxidation of D-glucose, and iii) good stability of each variant on the maleimide modified GC/MWCNT electrodes. In addition, MET experiments were employed as a method to relate the current observed in the DET of each variant (Figure 4.27F) to the real coverage of that variant on the electrode surface.

4.9.3.1 Covalent immobilization vs. physical adsorption

To verify that the CDH variants were immobilized at the electrode surface through covalent bonding to the surface cysteine, we carried out a comparison using three different *Mt*CDH variants covalently bound and physically adsorbed at GC/MWCNT electrodes. For the covalent immobilization, maleimide-modified electrodes were prepared using the procedure described in Section 4.7, while the physically-modified ones were prepared by simply drop casting 3 µL of the *Mt*CDH solution onto a bare (unmodified) GC/MWCNT electrode. Direct electron transfer was observed for both modification methods in the presence of D-glucose (Figure 4.28). However, the catalytic currents for physically adsorbed *Mt*CDH (Figure 4.28, blue, pink and purple squares) were decidedly lower than the ones for covalently immobilized CDH (Figure 4.28, blue, pink and purple circles): in particular, the current was about 60% less for the variant E522, 70% less for the variant E574 and 80% less for the variant T701. Moreover, we can see that the curves of current *vs.* glucose concentration are the same for the electrodes physically-modified with the three different *Mt*CDH variants. In contrast, for the three covalently-modified electrodes the curves are different, as expected if the three variants are immobilized with different orientations through the cysteine residues located in different positions on the enzyme surface (see Figure 4.26). The higher catalytic currents obtained with covalently-modified electrodes can be explained by immobilization of a greater quantity of enzyme molecules at the surface and/or the fact that the covalently immobilized enzyme is held in a more suitable orientation for DET as compared to the randomly orientated physically adsorbed CDH. The differences between the covalently immobilized variants E522, E674 and T701 reflect differences in the enzyme kinetics (IET rate) for different enzyme immobilization orientations, this will be discussed later in Section 4.10. Thus, it can be concluded that CDH variants have been effectively attached to the GC/MWCNT electrodes through covalent binding, and different orientations for the CDH variants have been successfully discriminated.

Another important key outcome becomes apparent in Figure 4.28; the catalytic currents for the three physically adsorbed *Mt*CDH are almost the same showing that the different immobilized variants have the same enzymatic activity toward glucose oxidation (assuming the same coverage).

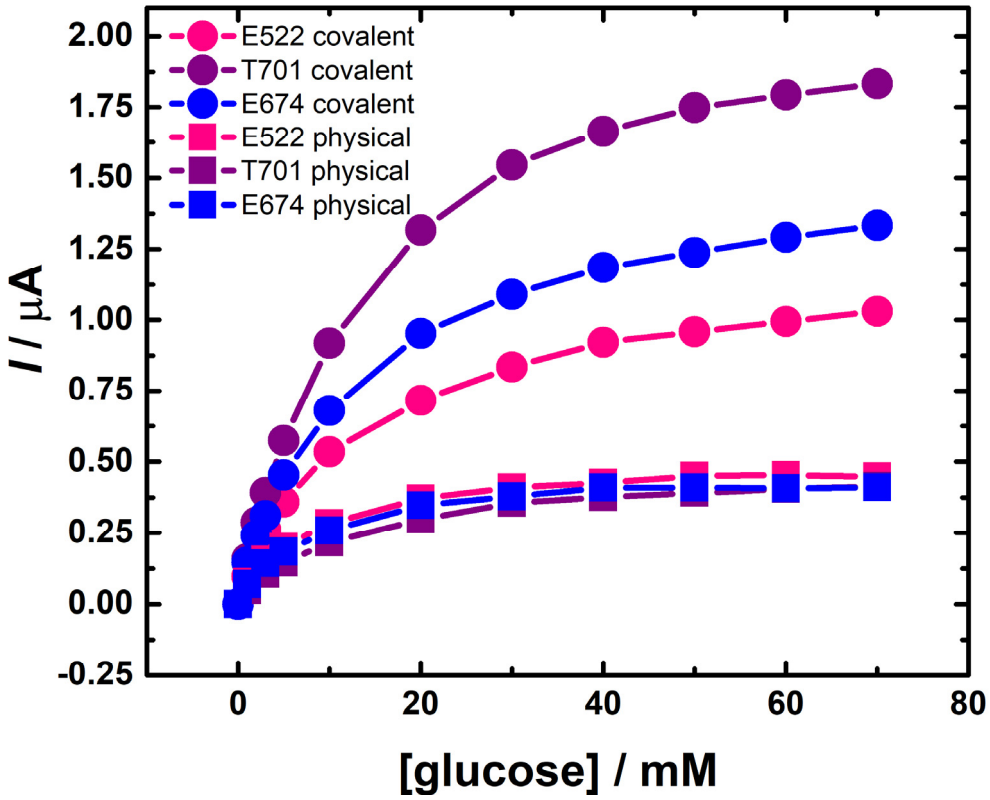

Figure 4.28. *Background subtracted currents measured at 0.0 V vs. SCE in cyclic voltammograms recorded at maleimide-modified electrodes (circles) and unmodified GC/MWCNT electrodes (squares) with the three different CDH variants E522, E674 and T701. CVs were carried out in deoxygenated 50 mM Tris buffer (pH 7.4), containing 30 mM $CaCl_2$ and increasing concentrations of D-glucose, sweeping the potential at 1 mV/s from -0.35 to 0.1 V vs. SCE.*

4.9.3.2 Selectivity of the CDH variants towards D-glucose

In order to investigate whether the *Mt*CDH variants immobilized on the surface of MWCNT electrodes retain their bioelectrocatalytic activity to the specific oxidation of D-glucose, the DET experiments (Section 4.9.3) were repeated using L-glucose and D-glucose. Figure 4.29 shows the cyclic voltammograms of the CDH-modified GC/MWCNT electrodes for various variants: (A) D813, (B) D574, (C) E522, (D) T701 and (E) E574 in deoxygenated 50 mM tris buffer (pH 7.4), with different concentrations of L and D-glucose. Upon each addition of an aliquot of D-glucose to increase its concentration the current increases (compare the solid curves), whereas upon addition of an aliquot to increase the concentration of L-glucose there is no change in the current (compare the pairs of dashed orange and solid green curves). Indeed, the key outcome of the L-glucose experiment in this Section was that direct electron

transfer (in the presence of L-glucose) was ruled out, as the increases in currents were not seen on addition of L-glucose (Figure 4.29), which is not oxidised by CDH.[302] Thus, the increase in currents were due to the specific oxidation of D- glucose catalysed by the CDH variants.

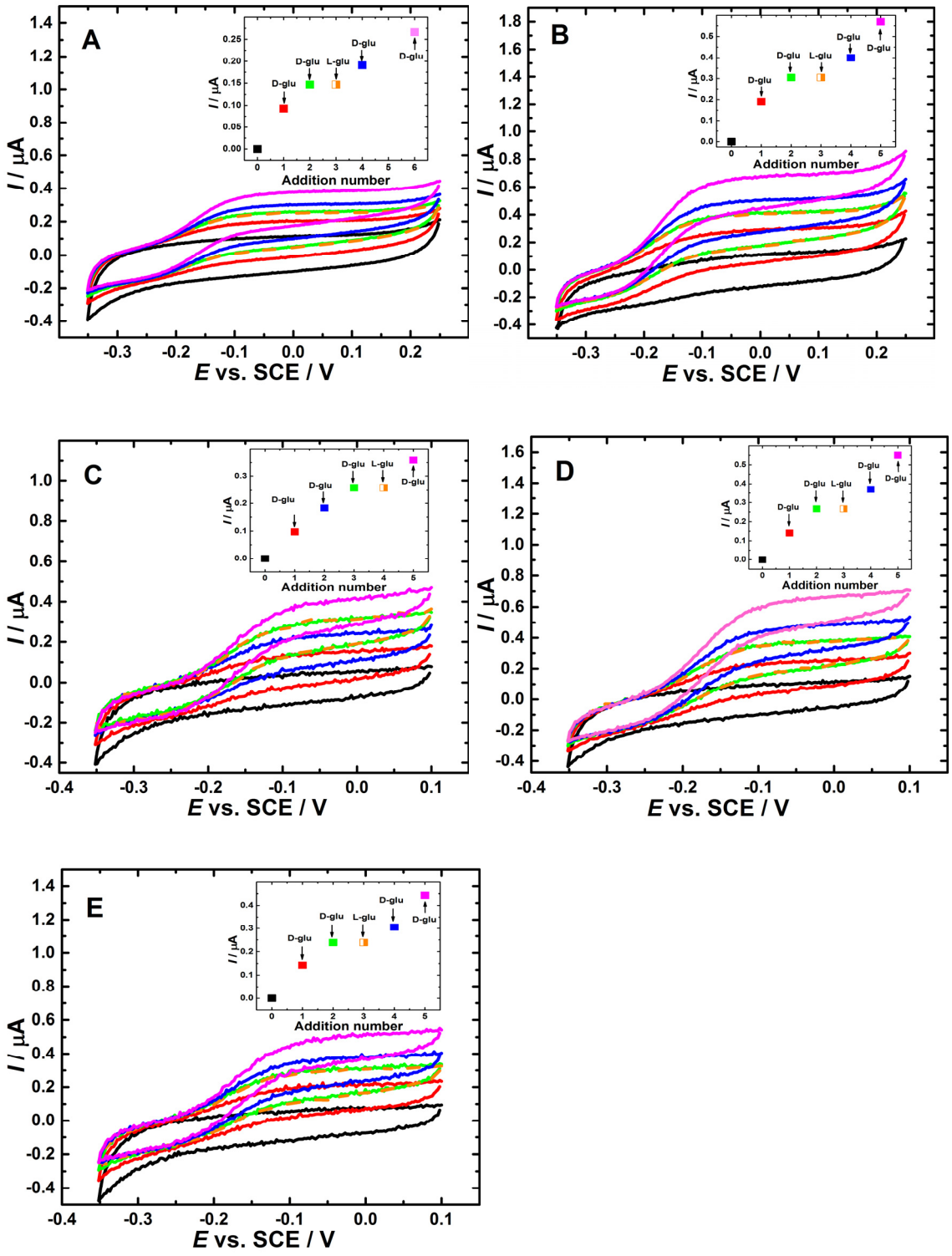

Figure 4.29. *Cyclic voltammograms of CDH-modified GC/MWCNT electrodes for some variants: (A) D813C, (B) D574C, (C) E522C, (D) T701C and (E) E674C in deoxygenated 50 mM Tris buffer (pH 7.4) in the presence of 30 mM $CaCl_2$ at 1 mV s^{-1}, with different concentrations of L and D-glucose. The electrodes potential was swept at 1 mV/s. Insets: plot of the background subtracted currents measured at 0.0 V for all the additions.*

4.9.3.3 Stability of the CDH variants on the GC/MWCNT electrodes

The direct electron transfer of CDH-modified GC/MWCNT electrodes is stable when the electrodes were tested continuously by cyclic voltammetry in solution for one full day. The storage stability of the CDH-modified GC/MWCNT electrodes was previously investigated (Section 4.7.2.3) showing that the catalytic current of covalently-modified CDH-electrodes (variant E522), stored in wet conditions at 4 °C, was the same after one week as after two months from the preparation. Nonetheless, the storage stability of the GC/MWCNT electrodes modified with the other four CDH variants was also studied by keeping the electrodes (used in Figure 4.27) in a wet condition at 4 °C. After one week, the same electrodes were retested for DET using cyclic voltammetry, Figure 4.30 shows the background subtracted currents measured at 0.0 V vs. SCE in cyclic voltammograms recorded in deoxygenated 50 mM tris buffer (pH 7.4) in the presence of 30 mM $CaCl_2$ with different concentration of D-glucose at 1 mV s^{-1}. Compared to the catalytic currents obtained on the day of preparation (Figure 4.27) a decrease in the currents during the first week was obtained. However, the electrodes can still retain ca. 60 % of the initial response after 7 days except for the D574 variant, which was about 10 %. These results indicate that the bioelectrocatalytic activities of the CDH variants (D813, E522, T701 and E674) covalently immobilized on the surface of CNT have excellent stability. Therefore, the different catalytic currents observed for each variant in Figure 4.27 were not due to a different catalytic activity because of difference in long/short-term stability of that variant. Indeed, the stability of a new GC/MWCNT electrode modified with D574 variant was re-attempted. Unfortunately, the bad performance was obtained again and consequently, it was excluded from the rest of this work.

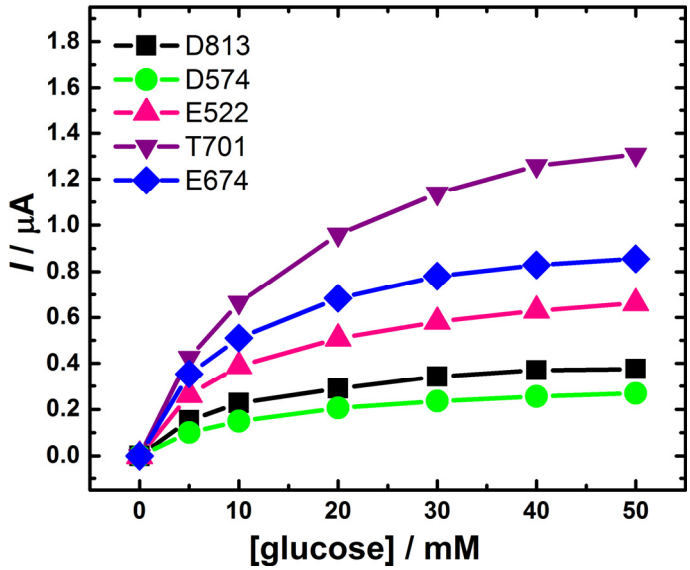

Figure 4.30. *Background subtracted currents measured at 0.0 V vs. SCE in cyclic voltammograms recorded at GC/MWCNT electrodes modified with five different CDH variants in deoxygenated 50 mM Tris buffer (pH 7.4) in the presence of 30 mM $CaCl_2$ at 1 mV s^{-1}. The measurements were done one week after the preparation of the modified electrodes.*

4.9.3.4 Mediated electron transfer for the five CDH variants

To exclude the fact that the different catalytic currents observed for the different CDH variants in Figure 4.27, was due to different amounts of CDH molecules immobilised on each GC/MWCNT electrode, the same electrodes (used in Figure 4.27) were retested for mediated electron transfer (MET), using a mediator dissolved in solution. Indeed, the mediator in the solution should react with all the active enzyme molecules on the surface of the electrode, shuttling electrons between the enzyme and the electrode surface.[36] Mediated electron transfer can, therefore, be employed to relate the current observed in the DET of each variant (Figure 4.27) to the real coverage of that CDH-variant on the electrode surface.

In this study, ferrocenecarboxylic acid was employed as a soluble mediator. Many research groups utilised ferrocene derivatives as electron acceptors for GOx.[41, 275, 321-323] With CDH instead, most research groups have used quinone derivatives as mediators.[324-325] To employ a mediator its redox potential should be more positive than the redox potential of the redox enzyme. In the case of CDH the redox potential was found to be about -0.135 V *vs.* SCE at pH7.4 (Section 4.9.1), whilst the redox potential of ferrocenecarboxylic acid is at about +0.3 V *vs.* SCE. Therefore, ferrocenecarboxylic acid was selected as a mediator to be used with CDH. It is important to note that, in the case of CDH, the FAD group is expected to exchange electrons with the mediator. Therefore, we should not look at the redox potential of the CDH found by DET, since this is due to the haem group of CDH as demonstrated before. However, the redox potential of the CDH-bound FAD was shown to be at potentials more negative than the usually observed DET of the haem group.[309]

Figure 4.31 shows the cyclic voltammograms of the CDH-modified GC/MWCNT electrodes for the variants: (A) D813C, (B) E522C, (C) T701C and (D) E674C in deoxygenated 50 mM tris buffer (pH 7.4) in the presence of 0.2 mM ferrocene carboxylic acid and 30 mM $CaCl_2$ and increasing concentrations of D-glucose. The addition of the glucose increases the anodic current at around -0.1 V *vs.* SCE (*vide infra*), showing the mediated electron transfer between the enzyme and the electrode. Calibration curves for glucose were plotted (Figure 4.32E). By increasing the concentration of D-glucose until 70 mM, the background subtracted catalytic currents increased up to 6.9 μA for the D813C variant, 7.1 μA for the E522C variant, 7.2 μA for the T701C variant and 7.4 μA for the E674C variant, showing that the four variants exhibit almost the same MET current. Hence, we can conclude that the quantity of CDH molecules immobilised on each electrode was basically the same. From the results obtained, one might expect that the different catalytic currents observed for each variant in Figure 4.27 were not due to the immobilization of a greater / smaller quantity of that variant at the electrode surface.

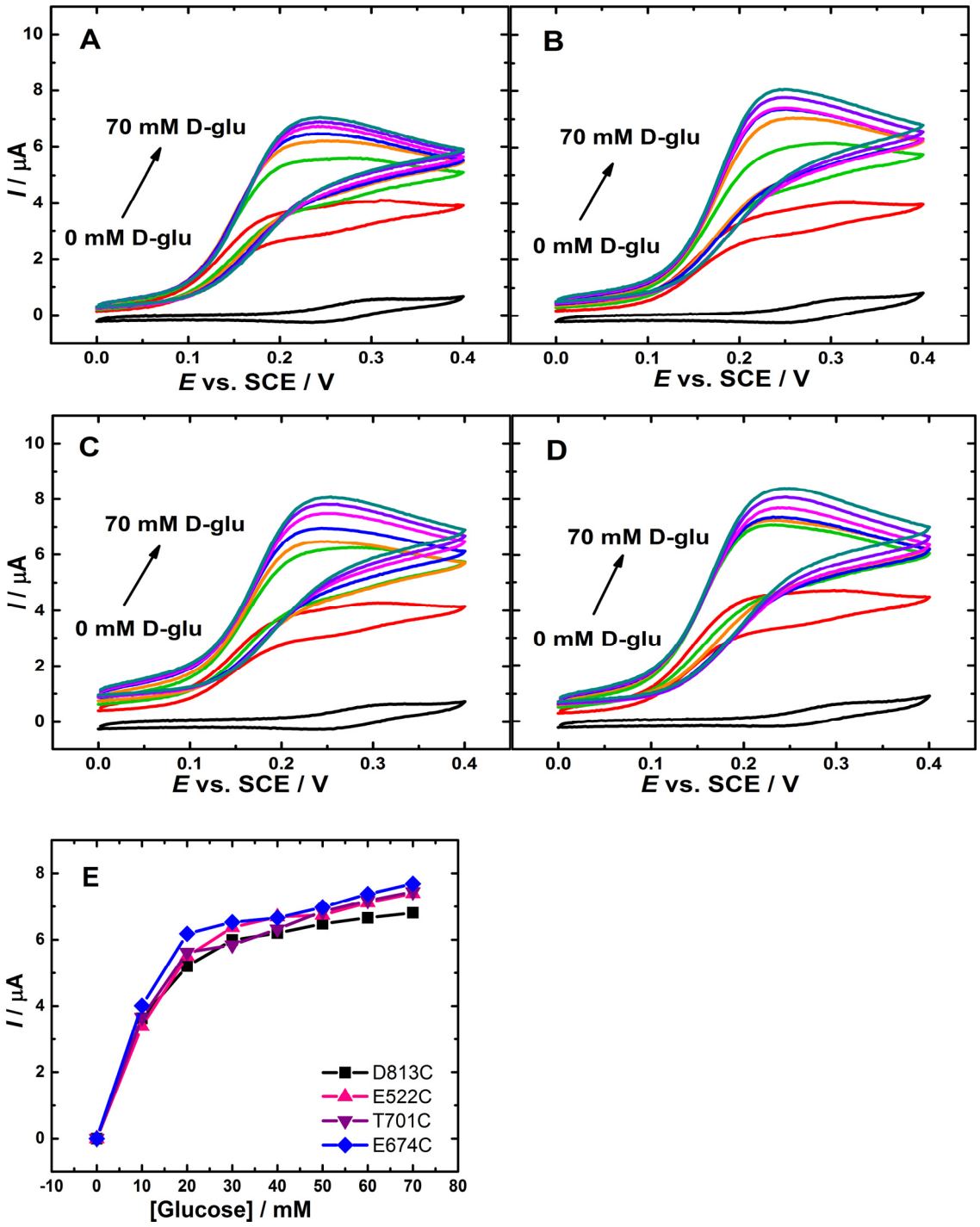

Figure 4.31. *Cyclic voltammograms of the CDH-modified GC/MWCNT electrodes for various variants: (A) D813C, (B) E522C, (C) T701C and (D) E674C in deoxygenated 50 mM tris buffer (pH 7.4) in the presence of 0.2 mM ferrocenecarboxylic acid and 30 mM $CaCl_2$ at 2 mV s^{-1}, Black lines: background current without glucose; coloured lines: after the addition of 10, 20, 30, 40, 50, 60 70 mM D-glucose. (E) Relative background subtracted currents for the CV experiments, the current was taken at 0.3 V vs. SCE and the background current were subtracted.*

The system under study in this section (Figure 4.31) should follow an *ec'* mechanism, [41] in which the oxidation reaction at the electrode is followed by a heterogeneous reaction that regenerates the reduced reactant. However, at first sight the cyclic voltammograms do not look

quite as usually found in such a case. As shown in Figure 4.31A, the maximum oxidation peak current for ferrocenecarboxylic acid at the CDH-modified GC/MWCNT electrode (D813) occurs at 0.3 V *vs.* SCE. In the presence of glucose, the MET currents started to increase at 0.1 V *vs.* SCE, which is 200 mV before the oxidation peak of the ferrocenecarboxylic acid. This shift in the onset potential also occurred with the other three variants (Figure 4.31B, C and D). To understand this behaviour, an experiment was performed using lower concentrations of the ferrocenecarboxylic acid. Figure 4.32A displays the cyclic voltammograms of CDH-modified GC/MWCNT electrode (E674C) in deoxygenated 50 mM tris buffer (pH 7.4) in the presence of 10 mM D-glucose, and increasing concentrations of ferrocenecarboxylic acid. Interestingly, the oxidation peak can still be observed even by employing 1 µM of ferrocenecarboxylic acid. Nonetheless, the oxidation peaks are shifted to a more positive potential at lower ferrocenecarboxylic acid concentration. The same shifting in the onset potential was also obtained when the same experiment was repeated using another ferrocene derivative, ferrocenemethanol (Figure 4.32B), indicating that the reaction between the Fc^+ and CDH is very fast, *vide infra.*

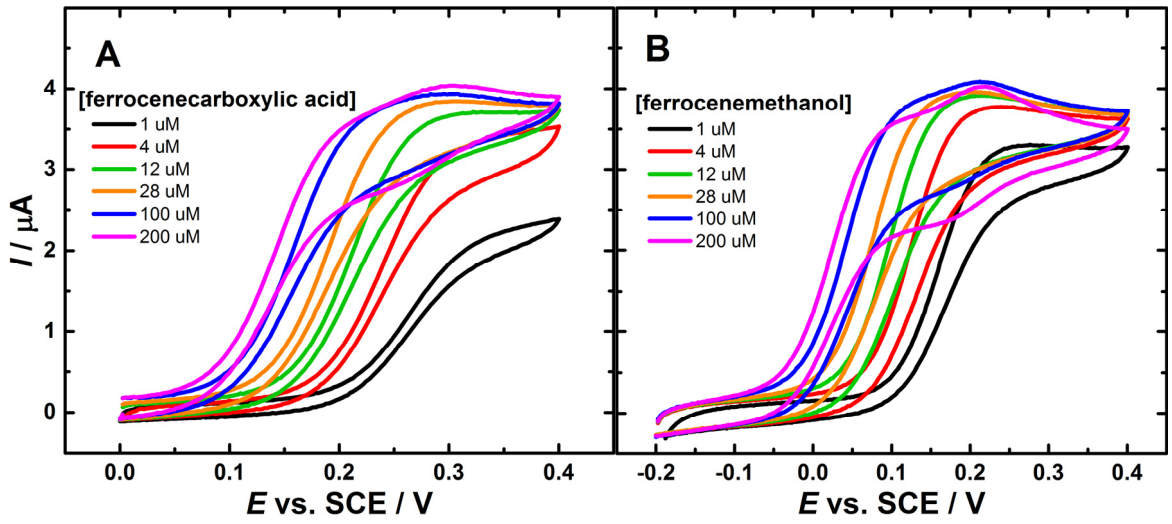

Figure 4.32. *Cyclic voltammograms for a CDH-modified GC/CNT electrode (variant E674) in deoxygenated 50 mM tris buffer (pH 7.4), containing 30 mM $CaCl_2$, 10 mM glucose and increasing concentrations of (A) ferrocenecarboxylic acid and (B) ferrocenemethanol. The electrode potential was swept at 2 mV/s from 0.0 to 0.4 V vs. SCE.*

The half-wave potential ($E_{1/2}$) for each voltammogram in Figure 4.32 was determined using the Nernst equation (*Eq.* 4.4). Applying this equation to some points taken in the middle part of the each voltammograms in Figure 4.32A, a linear relation between the applied potential and Log (i_L - i/i) was obtained. Linear fits of such plots give an accurate value for the ($E_{1/2}$). The half-wave potential is correlated to the concentration of ferrocene and ferrocenium through the following equation:

$$E = E^0 + \frac{0.059}{n} log \frac{[Fc^+]}{[\text{Med}] - [Fc^+]} \qquad (Eq.\ 4.5)$$

Where E is the $E_{1/2}$ determined for each voltammogram in Figure 4.32A, n is the number of electrons exchanged in the electrochemical process (1 e^-), [Fc^+] and [Med] are the concentrations of ferrocenium and ferrocene, respectively. Plotting the values of $E_{1/2}$ versus the concentration of ferrocene ([Med] >>[Fc^+]) added in solution, and fitting with a logarithmic function (Figure 4.33), we can obtain the following parameters:

$$A = E^0 + \frac{0.059}{n} log[Fc^+] \ = \ 0.265 \text{ V}$$

$$B = \frac{0.059}{n} \ = 0.055 \text{ V}$$

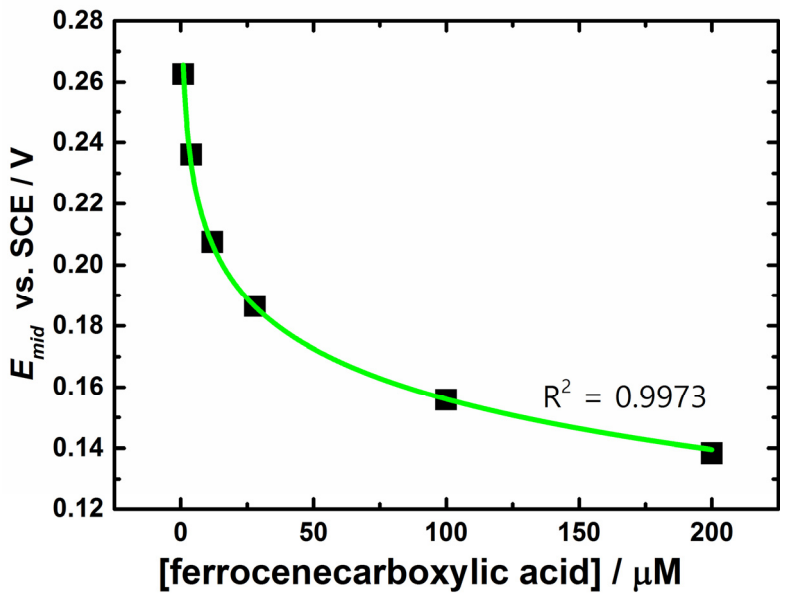

Figure 4.33. *Plot of half-wave potential determined for each voltammogram in Figure 4.32A vs. ferrocene concentration. The data were fitted with Nernst equation expression shown in Eq. 4.5 (green line).*

As shown in Figure 4.33, the potential at which the catalytic current starts is shifted to a more negative potential at higher ferrocene carboxylic acid concentration. This occurs because the MET reaction involves the oxidised form of ferrocene, ferrocenium, which oxidises the enzyme active site (FAD group) that in turn, oxidises the glucose. According to Nernst equation (*Eq.* 4.5) the concentration of ferrocenium ions, at each concentration of ferrocene, depends on the applied potential. Consequently, by increasing the ferrocene concentration in solution, a less positive potential value is required to have the minimum sufficient concentration of ferrocenium ions to support the MET reaction. The concentration of ferrocenium ions required was calculated using parameter A and found to be ca. 0.4 μM. In this calculation, the E^0 value of 0.275 V *vs.* SCE determined experimentally (in the absence of glucose) from the voltammogram recorded in the same conditions was used. This is somewhat unusual MET behaviour occur because the reaction between the Fc^+ and CDH is very fast ($k \sim 4 \times 10^6$ L mol^{-1} s^{-1}).

4.9.3.5 Electrochemistry of the *Mt*CDH variants

The non-catalytic DET of the GC/MWCNT electrodes covalently modified with the *Mt*CDH variant E522 was previously tested for DET (Section 4.9.1) by cyclic voltammetry. Figure 4.20A showed that, in the absence of substrate, sweeping across the potential range produces redox peaks at E_{mid} *ca.* -0.137 V vs. SCE due to DET between the electrode and the haem group in the CYT_{CDH}. In this section, the CDH-modified GC/MWCNT electrodes for the variants D813C, T701C and E674C were also tested for DET in the absence of the substrate. Figure 4.34 shows the cyclic voltammograms (after background current subtraction) of the CDH-modified GC/MWCNT electrodes for the variants: (A) D813C, (B) E522 (C) T701C and (D) E674C recorded in deoxygenated 50 mM tris buffer (pH 7.4). Sweeping across the potential range at 40 mV/s produces redox peaks at E_{mid} of *ca.* -0.138 V vs. SCE, indicating that the different orientations of the different variants does not influence the redox electrode potential of the haem. Therefore, it can be concluded that the DET for the CDH variants under investigation always occurs via the haem group located in CYT_{CDH} domain. Theoretically for a reversible process, $W_{1/2}$ at 298 K is 90.6 /n in mV, where n is the number of exchanged electrons.[309, 311] The obtained values of around 85± 5 mV for the CDH-modified GC/MWCNT electrode of the D813, E522, T701, and E674 variants further support a $1e^-$ transfer process originating from the haem cofactor. Assuming an electrode surface area of 14 cm^2 and a one electron process, the surface coverages (T) of the D813, E522, T701, and E674 variants on the different electrodes, shown in Figure 4.34, were calculated to be 0.42, 0.41, 0.4 and 0.39 pmol cm^{-2} respectively, indicating that the amount of CDH molecules capable of undergoes DET immobilised on each electrode was almost the same. This shows that the orientation does not affect the kinetics of the haem /electrode reaction. Hence, one might expect that the different catalytic currents observed for each variant in Figure 4.27 were due to difference in the IET rate for the different variants.

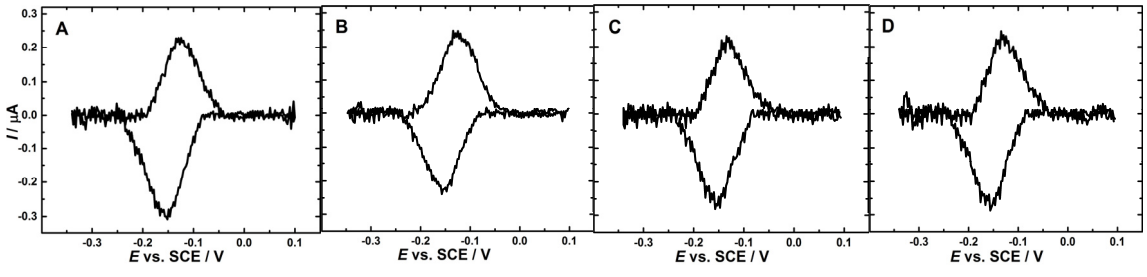

Figure 4.34. *Cyclic voltammograms (after background current subtraction) for the CDH-modified GC/MWCNT electrode for the variants: (A) D813C, (B) E522 (C) T701C and (D) E674C. The CVs were recorded in deoxygenated 50 mM Tris buffer (pH 7.4) at 40 mV/s.*

The effect of the scan rate on voltammetry of *Mt*CDH-modified electrodes for the variants D813 and T701 was also investigated. Figure 4.35 shows that the anodic peak potentials (E_{pa}) shifted to a more positive direction and the cathodic peak potentials (E_{pc}) shifted to a more negative

direction with the increasing scan rate in the range of 20 to 100 mV / s. However, the shifting is more pronounced in the case of D813 variant (Figure 4.35 A). This suggests some possible kinetic effect.

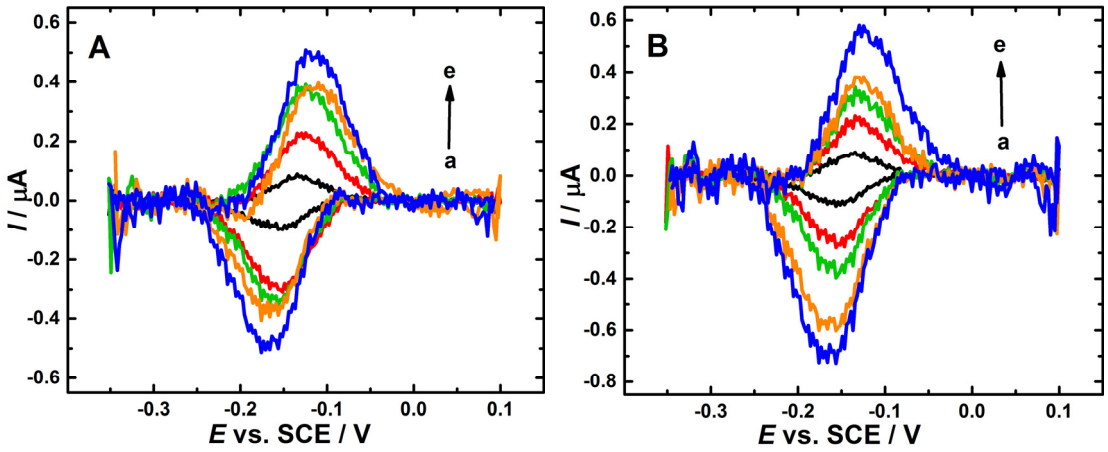

Figure 4.35. *Cyclic voltammograms (after background current subtraction) for the CDH-modified GC/MWCNT electrode for the variants: (A) D813C and (B) T701C recorded at 25 °C in deoxygenated 50 mM Tris buffer (pH 7.4), containing 30 mM $CaCl_2$ at different scan rates (from (a) to (e): 20, 40, 60, 80, 100 mV s^{-1}).*

To uncover the nature of DET of the immobilized *Mt*CDH, the kinetic analysis of the DET reactions proceeding in the *Mt*CDH-modified electrodes was performed by processing the cyclic voltammograms in Figure 4.35A, B within the Laviron model.[206] This mathematical approach was described in Section 4.9.1.2. As n ΔE_p < 200 mV, the k_s could be estimated according to *Eq.* 4.3.[178] Table 4.2 illustrates the heterogeneous electron transfer rate constant (k_s) for *Mt*CDH-modified electrodes (D813 and T701 variants) estimated at different scan

Table 4.2. *The heterogeneous electron transfer rate constant (k_s) for MtCDH-modified electrodes for the variants: D813C and T701C. The k_s values were estimated at 25 °C using equation 4.3.*

Scan rate (v) (V s^{-1})	Peak separation (ΔE_p) (mV)		m		k_s (s^{-1})	
	D813	T701	D813	T701	D813	T701
0.02	23±2	15±2	1.6	2.5	1.2±0.05	2.0±0.05
0.04	31±2	22±2	1.2	1.65	1.7±0.05	2.7±0.05
0.06	44±2	27±2	0.74	1.35	1.7±0.05	3.1±0.05
0.08	55±2	37±2	0.60	0.95	1.8±0.05	2.9±0.05
0.1	62±2	44±2	0.5	0.75	1.9±0.05	2.9±0.05

The average k_s values registered for *Mt*CDH-modified electrodes for the variants D813 and T701 were calculated to be *ca.* 1.65 and 2.7 s^{-1} respectively. One important factor that influences electron transfer is the distance between the redox cofactor and the surface of the electrode.[21] The average k_s value for *Mt*CDH-modified electrode for variant E522 was previously calculated to be ca. 1.9 s^{-1} (Section 4.9.1.2), indicating that different variants exhibit different k_s values. Independent of the precise details of the Laviron analysis, it is clear that the electron transfer kinetics for the haem/electrode are fast for the three variants.

The cyclic voltammograms of the steady-state catalysis for the variants D813C, T701C and E674C (Figure 4.27A, D, E) were further analysed using the modified form of the Nernst equation (*Eq.* 4.4). Applying this equation to some points taken in the middle part of the steady-state catalytic voltammograms subtracted for the background current (Figure 4.36A, C, and E), a linear relations between the applied potential and Log (i_L - i/i) were obtained, indicating a fast reversible DET reaction. Linear fit of such plots (Figure 4.36B, D, and F) give good estimates for the E^0 values at about -0.141, -0.143 and -0.145 V vs. SCE for the variants D813, T701, and E674 respectively. The E^0 of the variant E522 was previously calculated to be -0.138 vs. SCE (Figure 2.24). The E^0 values are consistent with other studies of DET to *Mt*CDH at pH 7.4[283-284, 298] and can be attributed to the one-electron transfer of the haem group. Thus, the catalytic currents observed for each variant in Figure 4.27 are most probably due to the DET process originating from the haem cofactor located in the CYT domain. To date, no efficient direct communication with the FAD group of the class II CDH has been shown.[326] This would have been expected to occurred at redox potentials of ca. −0.435 V vs SCE.[325]

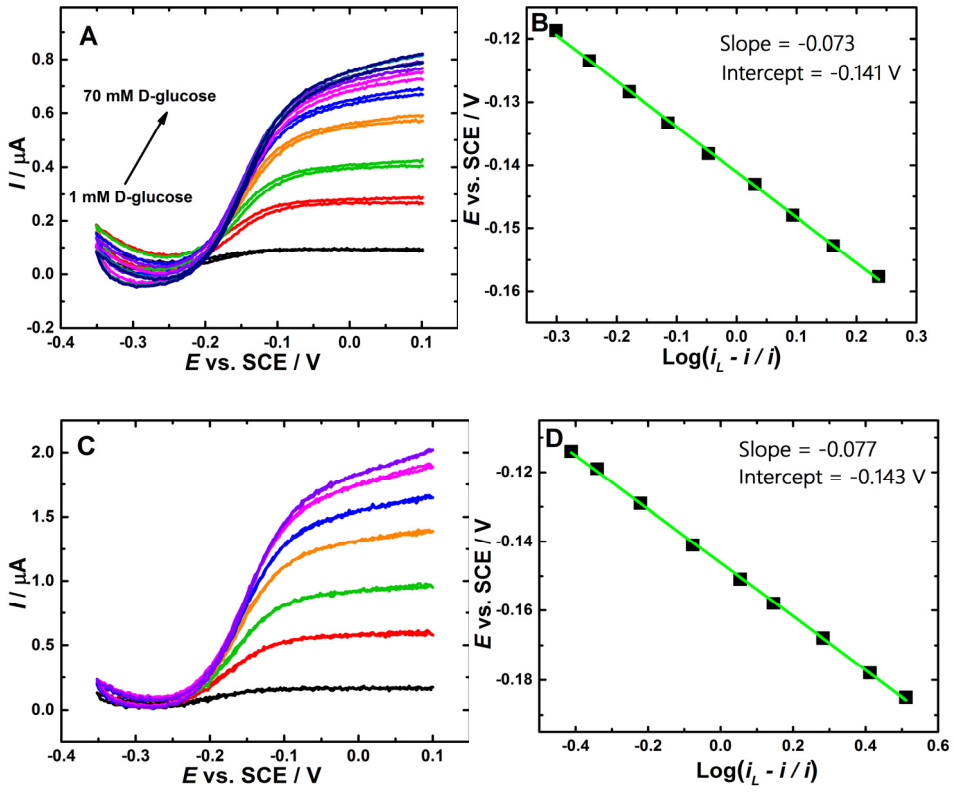

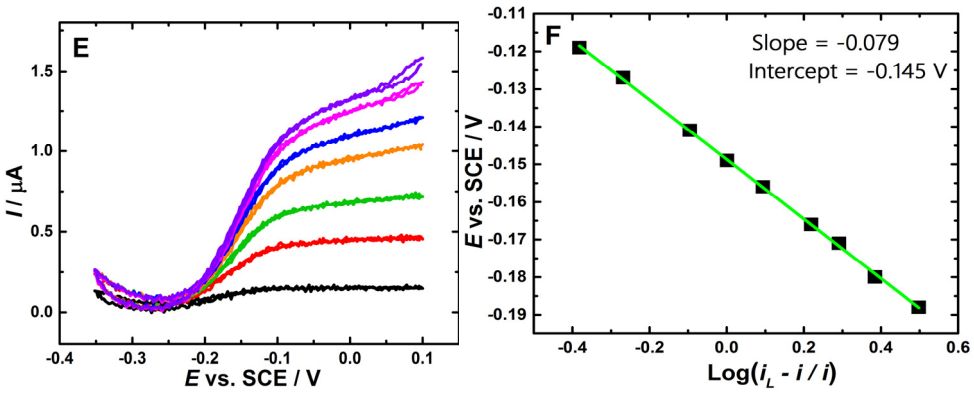

Figure 4.36. *Background current subtracted cyclic voltammograms for a CDH-modified GC/MWCNT electrode for the variants: D813C (A), T701C (C) and E674C (E). The original CVs are shown in Figure 4.27A, D, E which were recorded in deoxygenated 50 mM Tris buffer (pH 7.4), containing 30 mM $CaCl_2$ and increasing concentrations of glucose, at 1 mV/s. (B), (D) and (F) are Heyrovsky-Ilkovich plots performed* using *some potential points taken in the middle region of CV recorded for 70 mM glucose in (A), (C) and (E) respectively plotted against the Log (i_L-i/i). Data were fitted with a linear fitting (green line) to determine the intercept (E^0) and the slope (-0.059/n).*

The number of exchanged electrons (slope = -0.059 / *n*) for the D813, T701, and E674 variants on the different electrodes, shown in Figure 4.36, were also calculated to be *ca.* 0.8 and can be approximated at 1. This is a further proof that the haem group of the CDH variants under investigation interact with the electrode surface in the DET mechanism, as its redox process involves one electron, whereas the FAD group would need two electrons to be oxidised.[144, 309] A second important key outcome becomes apparent in the corresponding Heyrovsky-Ilkovich plots shown in Figure 4.24B and Figure 4.36B, D and F. This plot of log [(i_L - i)/i] versus E is often utilized to analyze the entire current-potential curve obtained under steady-state conditions.[16] For an *n*-electron electrochemical process that obeys Nernst equation, the plot is linear. Obviously, Figure 4.24B and Figure 4.36B, D and F show a significant linear relationship, indicating thus, a fast DET mechanism (haem /electrode reaction). Hence, the different catalytic currents observed for each variant in Figure 4.27 were due to difference in the IET rate for the different variants.

4.9.4 Effect of calcium chloride

The results presented so far were all been obtained in buffer solutions with $CaCl_2$. Indeed, GC/MWCNT electrodes modified with the *Mt*CDH variants were previously tested for DET by slow scan cyclic voltammetry in the absence of $CaCl_2$. Figure 4.37 shows that, increasing the concentration of D-glucose in solution up to 20 mM, an increasing catalytic current is visible starting from about -0.2 V *vs.* SCE and reaching a plateau around 0.0 V. However, the catalytic

currents observed were too small and the electrodes seem to already be saturated at 20 mM glucose, making the next planned experiments practically complicated. For this reason $CaCl_2$ was added to the buffer solutions in all the experiments described above.

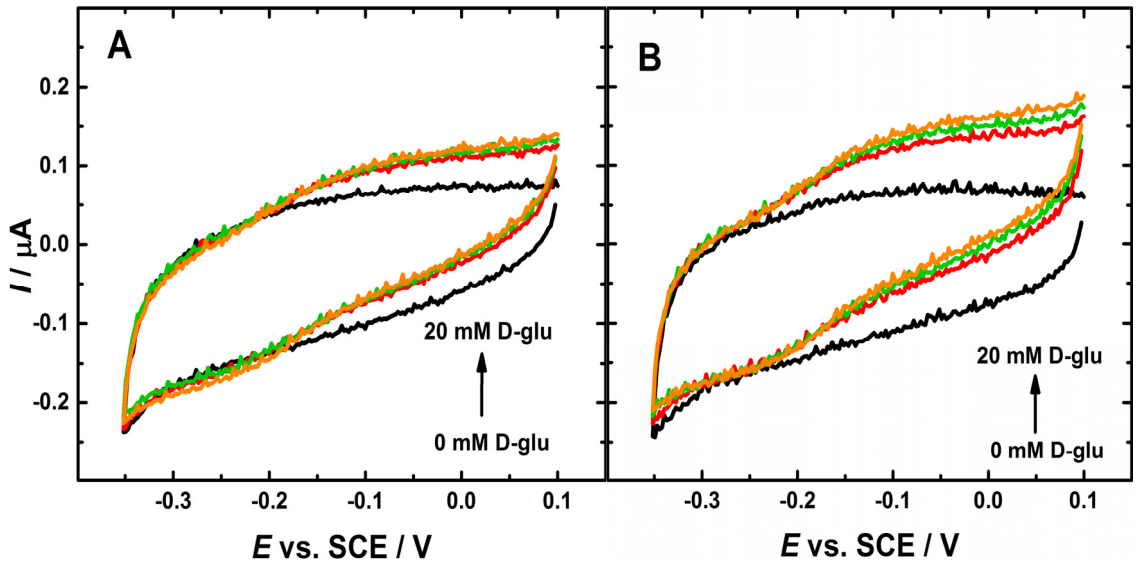

Figure 4.37. *Cyclic voltammograms of (A) D813 and (B) E522 CDH-modified GC/MWCNT electrode in deoxygenated 50 mM PBS (pH 7.4) at 1 mV/s. Black lines: background current without glucose; colored lines: after the addition of 5, 10, 20 mM D-glucose.*

Studies by Ludwig *et al.*[297, 325, 327] indicated that the presence of $CaCl_2$ leads to an increase in the catalytic current generated by *Mt*CDH. In their work, Ludwig *et al.* have concluded that this increase is due to the adoption of a closed conformation for *Mt*CDH in the presence of divalent cations, which exert a bridging effect between the two enzymatic domains by neutralising electrostatic repulsion and, thereby, increasing the internal electron transfer (IET) rate. The authors have also confirmed that the effect of $CaCl_2$ is more significant at neutral pH, which is actually not the optimal pH for *Mt*CDH. Indeed, at slightly alkaline conditions the CYT_{CDH} and DH_{CDH} no longer interact with each other because of the electrostatic repulsion of the negatively charged amino acids located in the interfacial region between the haem and flavin domains. At more acidic conditions the electrostatic repulsion between the two domains is already less pronounced.[328] In the present study, the effect of $CaCl_2$ on the DET and MET catalytic currents was also investigated to gain more understand the mechanisms of the DET and MET reactions. With this aim, T701 CDH-modified GC/MWCNT electrodes were tested for DET and MET at neutral and acidic pH with increasing concentrations of calcium chloride in the presence of glucose in solution. Figure 4.38 shows the catalytic current as a percentage for increasing concentrations of $CaCl_2$, at pH 5.5 and 7.4, in the presence and absence of mediator in solution. It is clear that when the mediator is present in solution (triangles) there is no effect upon addition of $CaCl_2$ at either pH. Indeed, this behaviour is expected if the mediator used in the

experiments (ferrocenecarboxylic acid) only interacts with the FAD domain, responsible for the sugar oxidation (Scheme 4.6). Therefore, the haem domain may be excluded from the MET catalytic process as the IET is not occurring, because the presence of the divalent cations does not affect the catalytic current in these conditions. On the other hand, in the absence of the mediator (circles), a significant increase in the catalytic current was obtained by increasing the concentration of calcium chloride in the solution, indicating that the calcium cations have a significant effect in the DET catalytic process. As expected, the effect is greater at neutral pH (green circles), where the current increased by ca. 500 % upon the addition of 30 mM $CaCl_2$, whereas, it is less pronounced at acidic pH (pink circles) where the presence of 30 mM $CaCl_2$ increased the current by ca. 350 %. This further proves that DET pathway is consistent with that shown in Scheme 4.6, with electrons passing from the FAD domain to the haem and from the haem to the electrode surface. Indeed, divalent cations exert a bridging effect between the two domains increasing the IET rate and, consequently, the overall DET rate.

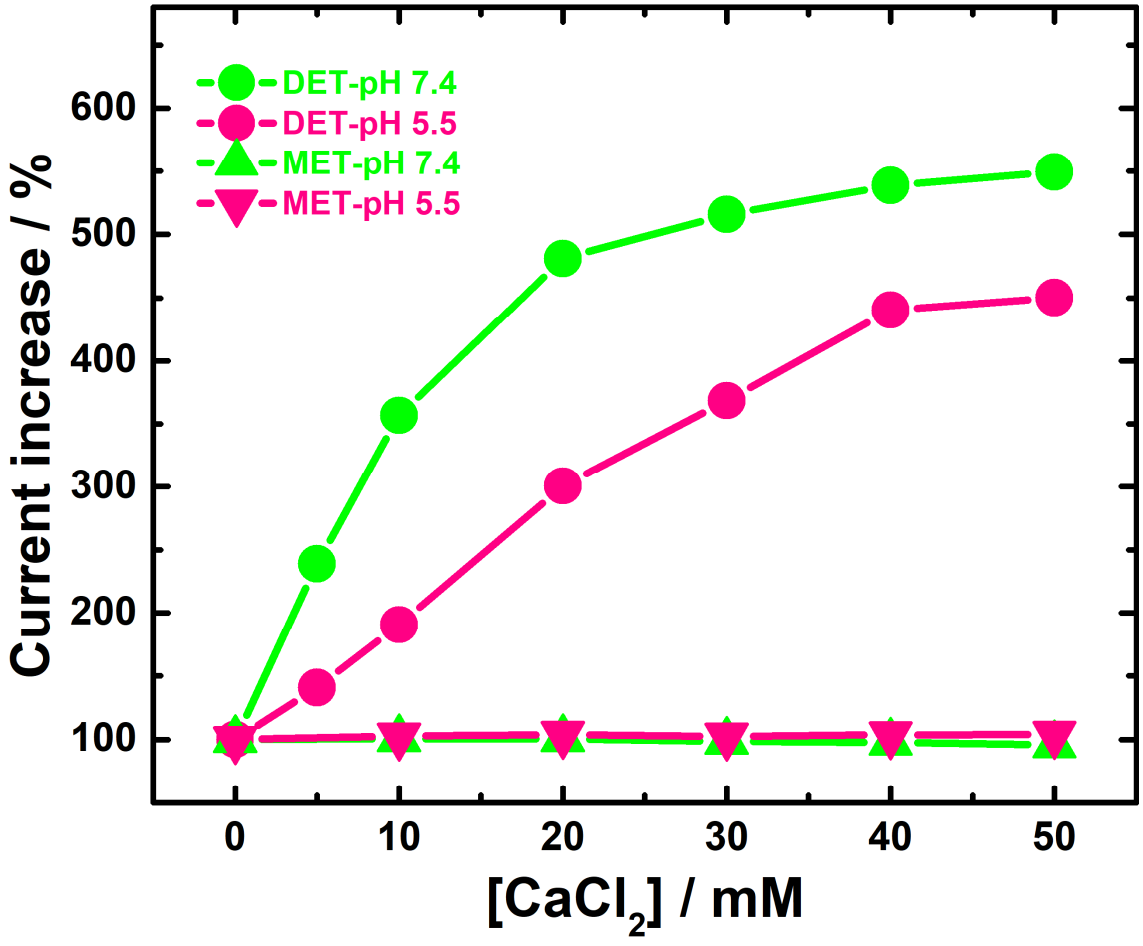

Figure 4.38. *Percentages of current increase for DET (circles) and MET (triangles) measured at pH 7.4 (green) and pH 5.5 (pink) vs. $CaCl_2$ concentration for GC/MWCNT electrodes covalently modified with T701-CDH. Data were recorded by CV in deoxygenated 50 mM acetate buffer pH 5.5 (pink) and 50 mM Tris buffer pH 7.4 (green), containing 70 mM glucose, in the absence (circles) and presence (triangles) of 0.2 mM ferrocene.*

4.9.5 Effect of solution pH

The effect of solution pH was also investigated. Figure 4.39 shows the cyclic voltammograms of a CDH-modified GC/MWCNT electrode recorded on the same day first in pH 7.4, then in pH 5.5 and finally in pH 7.4 again. The experimental results indicate that the catalytic activity of the electrode measured at pH 7.4 decreased by only 8 % between the first and the last set of experiment, suggesting an excellent stability of the electrode towards changes of pH. Furthermore, we note that the catalytic current decreased when the electrode was in the more acidic buffer (pH 5.5). Indeed, it has been reported that the optimal pH for *Mt*CDH is around 5.5 because in acidic conditions the IET and, consequently, the DET catalytic currents are improved.[325, 329] However, the presence of 30 mM $CaCl_2$ in the solution already improves the IET, bringing it to the maximum performance. Hence, in this case, the changes of pH do not affect the mechanism of IET and consequently the DET catalytic currents. Therefore, the decrease in the DET current at the acidic pH is most probably due to lower enzyme affinity; neutral pH is the optimal condition for the flavin domain or for the glucose oxidation by the FAD group.[325] This conclusion was supported by a higher enzyme catalytic efficiency k_{cat} / K_m obtained for the same variant at pH 7.4 of about 0.125 mM s^{-1} as compared to 0.04 mM^{-1} s^{-1} obtained (by my collaborator, M. Meneghello) at pH 5.5, *vide infra*.

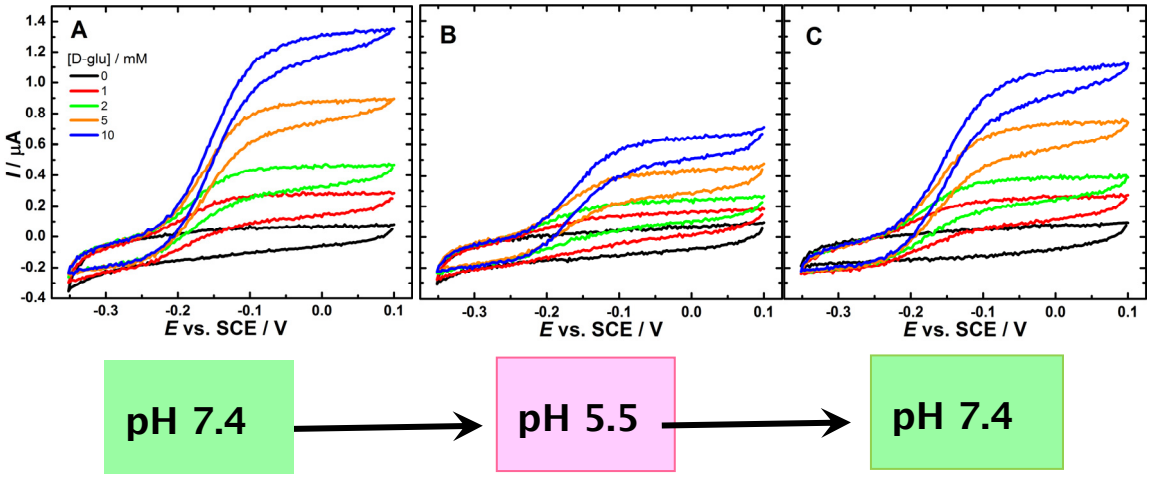

Figure 4.39. *Cyclic voltammograms for a CDH-modified GC/MWCNT electrode (variant T701) in deoxygenated 50 mM Tris buffer (pH 7.4) (A and C) and 50 mM acetate buffer (pH 5.5) (B), both containing 30 mM $CaCl_2$ and increasing concentrations of glucose. The electrode potential was swept at 1 mV/s from -0.35 to 0.1 V vs. SCE. The measurements were carried out sequentially first in pH 7.4, then in pH 5.5 and finally in pH 7.4 buffer again.*

4.10 Understanding the DET and the MET mechanisms

The results obtained from the analysis and the experiments performed in this Chapter were gathered together in order to have a better understanding of the mechanisms of the direct and

the mediated electron transfer between the *Mt*CDH and the electrode surface. Such mechanisms can be outlined as in Scheme 4.6.

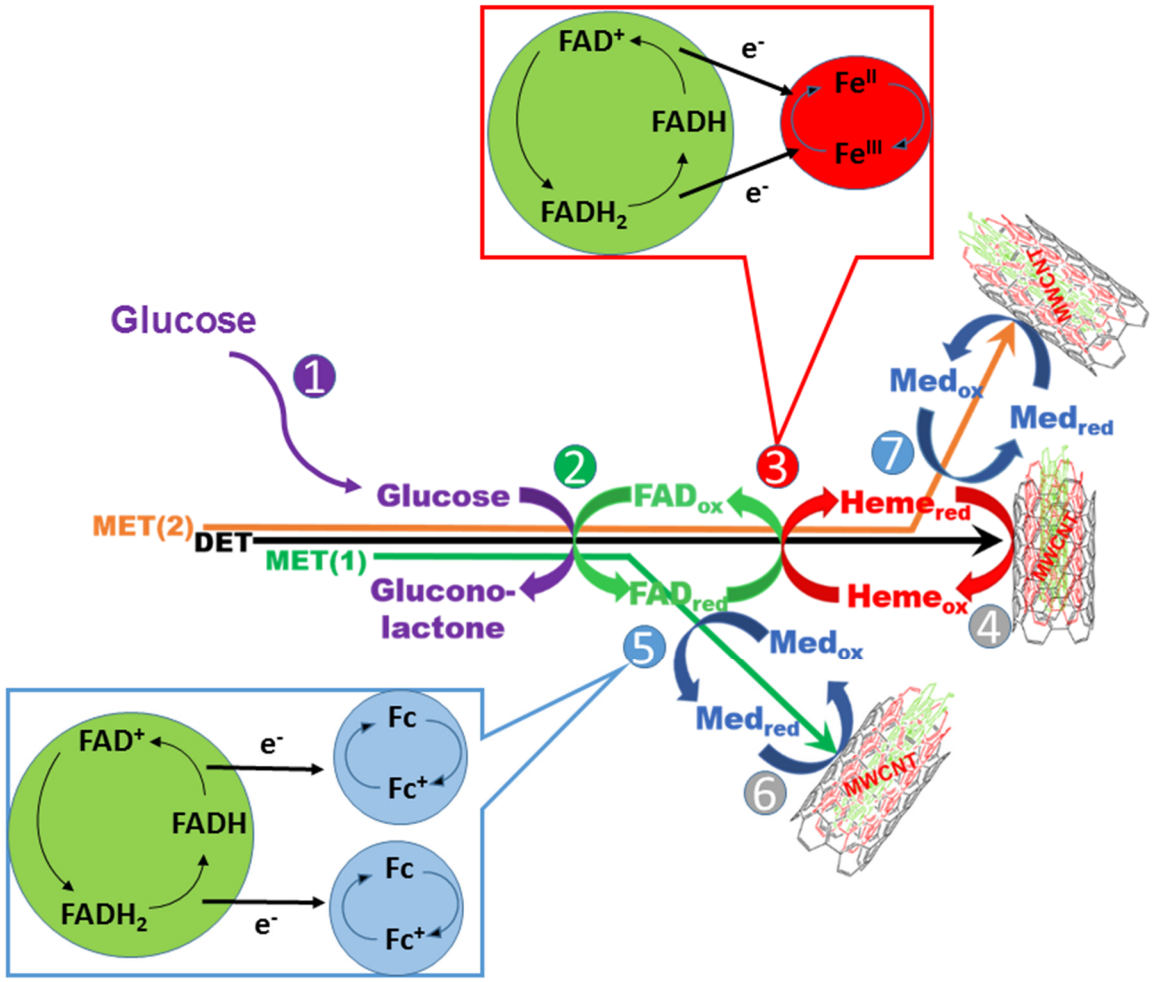

Scheme 4.6. *Proposed mechanisms for the direct and the mediated electron transfer. Med = ferrocene monocarboxylic. The numbers indicate the steps in the mechanisms.*

The experiments with calcium chloride (Section 4.9.4) confirm that the presence of $CaCl_2$ in the solution strongly increased the catalytic current in DET, but not in MET experiments. Since the divalent cations such as Ca^{2+} exert a bridging effect between the two domains, therefore affecting IET. We can assume that in the DET, glucose diffuses to the enzyme on the electrode surface (Scheme 4.6-step 1), and is then oxidised to gluconolactone by FAD^+ (FAD_{ox}) which in turn is reduced to $FADH_2$ (FAD_{red}) (Scheme 4.6-step 2). The $FADH_2$ is then turned back to FAD by Fe^{3+} in two one electron steps ($Heme_{ox}$) which is in turn reduced to Fe^{2+} ($Heme_{red}$) (Scheme 4.6-step 3) and, the Fe^{2+} is re-oxidised electrochemically at the MWCNT to Fe^{3+} (Scheme 4.6-step 4). In other words, the FAD group is reduced by glucose and oxidised back by the haem, which act as a bound mediator between the electrode and the DH_{CDH} domain; $FADH_2$ is first oxidised to the FADH radical by donating one electron to the haem, then FADH is oxidised to FAD^+ by transferring another electron to the haem. On the other hand, in MET the calcium

chloride has no effect, indicating that the mediator interacts directly with the DH_{CDH}, out competing the haem in the catalytic process. As shown in Scheme 4.6 MET (1): Glucose diffuses to where the enzyme is on the electrode surface (Scheme 4.6-step 1), and is then oxidised to gluconolactone by FAD^+ which is reduced to $FADH_2$ (Scheme 4.6-step 2), $FADH_2$ is then oxidised to FAD via two one electron steps by Fc^+ which is reduced to Fc (Scheme 4.6-step 5), then Fc is oxidised back to Fc^+ electrochemically on the MWCNT (Scheme 4.6-step 6).

4.10.1 Michaelis-Menten constants for the CDH variants

The kinetic description of an enzyme mechanism is fundamental to understanding how it functions. Nearly a century ago, Michaelis and Menten[330] suggested a straightforward model which describe the kinetic characteristics of many enzymes. According to that model, an enzyme (E) combines with a substrate (S) to form an enzyme-substrate (ES) complex with a rate constant k_1. The ES complex has two possible fates. It can proceed on to form a product (P), with a rate constant k_2 or to dissociate back into E and S, with a rate constant k_{-1},[331] as shown in the reaction below

$$E + S \underset{k_{-1}}{\overset{k_1}{\rightleftharpoons}} ES \underset{k_{-2}}{\overset{k_2}{\rightleftharpoons}} E + P$$

The simplest explanation of steady-state enzyme kinetics is based on the Michaelis and Menten model.[1] Enzyme kinetics are often investigated at the onset of the catalytic reaction. Therefore, the back reaction can be neglected, and the k_2 rate constant may be re-named k_{cat} (also termed turnover number), the catalytic rate constant for conversion of the ES complex into E and P. Thus, the Michaelis-Menten equation presumes the study of the initial velocity of the reaction (V_0) which can be defined as the rate of increase in [P] with time when [P] is low; that is, at times close to zero. V_0 is given by the Michaelis-Menten equation:

$$V_0 = V_{max} \frac{[S]}{[S] + [K_m]} \qquad (Eq. 4.6)$$

Where V_{max} is the maximum velocity of the reaction when the enzyme is totally saturated with substrate, $V_{max} = k_{cat}[E_o]$, where E_o is the total enzyme concentration, [S] is the substrate concentration and K_m, the Michaelis-Menten constant, is the substrate concentration at which the reaction rate is half maximal.[311, 332] K_m may be estimated from a plot of reaction rate vs substrate concentration, via the substrate concentration at which the rate is half of the V_{max} value. K_m is related to the rate constants by $K_m = (k_{-1} + k_2)/ k_1$. The K_m value is fundamental as it indicates the strength of binding between the enzyme and substrate. The catalytic efficiency of an enzyme is best defined by the ratio k_{cat} / K_m.[331-332]

GC/MWCNT electrodes modified with the CDH variant (E522) were tested for DET by cyclic voltammetry in a pH 7.4 buffer. As we have already shown in Section 4.7.1, increasing the

concentration of D-glucose in solution leads to an increase in the limiting current at the anodic potential of the voltammogram (Figure 4.40A). The limiting current taken at 0.0 V *vs.* SCE can then be plotted versus the glucose concentration (Figure 4.40C), showing a typical Michaelis-Menten behaviour with the plot being linear for small substrate concentrations (between 0-10 mM glucose) and reaching saturation at *ca.* 50-70 mM glucose. Initially, these experimental data can be fitted with the electrochemical form of the Michaelis-Menten equation,[1, 16] in which the dependent variable is represented by the limiting current:

$$i_{\mathrm{L}} = \frac{i_{\max} \cdot [\mathrm{S}]}{[\mathrm{S}] + K_{\mathrm{m}}^{\mathrm{app}}} \qquad (Eq.\ 4.7)$$

where [S] is the substrate concentration, $K_{\mathrm{m}}^{\mathrm{app}}$ is the apparent Michaelis-Menten constant and $i_{\max}$ is the apparent maximum current that can be reached upon saturation and can be written as $i = 2FA\Gamma k_2$, where F is the Faraday constant, $A\Gamma$ the total amount of electroactive enzyme and k_2 the first-order rate constant for "glucose oxidation".[333] Assuming the total amount of electroactive CDH to be ≈ 5.0 pmol for the GC/MWCNT electrode modified with E522 CDH, *vide supra*, k_2 was calculated (glucose as a substrate) to be about 1.3 s^{-1}.

The Michaelis-Menten constant, K_{m}, represents the affinity between the enzyme and the substrate. Therefore, it would be different using different substrates. For the GC/MWCNT electrode modified with E522 CDH, $K_{\mathrm{m}}^{\mathrm{app}}$ was found to be about 12 mM with glucose (Figure 4.40C). On the other hand, the value of $i_{\max}$ is almost 1.27 μA. It has been reported that the k_{cat} value of the *Mt*CDH in solution (glucose as a substrate) is about 14 s^{-1}.[284] Therefore, the $i_{\max}$ value obtained in Figure 4.40C is not limited by the enzyme-substrate kinetics and hence, it might be limited by IET rate. This is also supported by the fact that the limiting current ($i_{\max}$) achieved with another substrate (cellobiose) was about 1.37 μA (Figure 4.40D) but with a different $K_{\mathrm{m}}^{\mathrm{app}}$ value of around 0.8 mM.

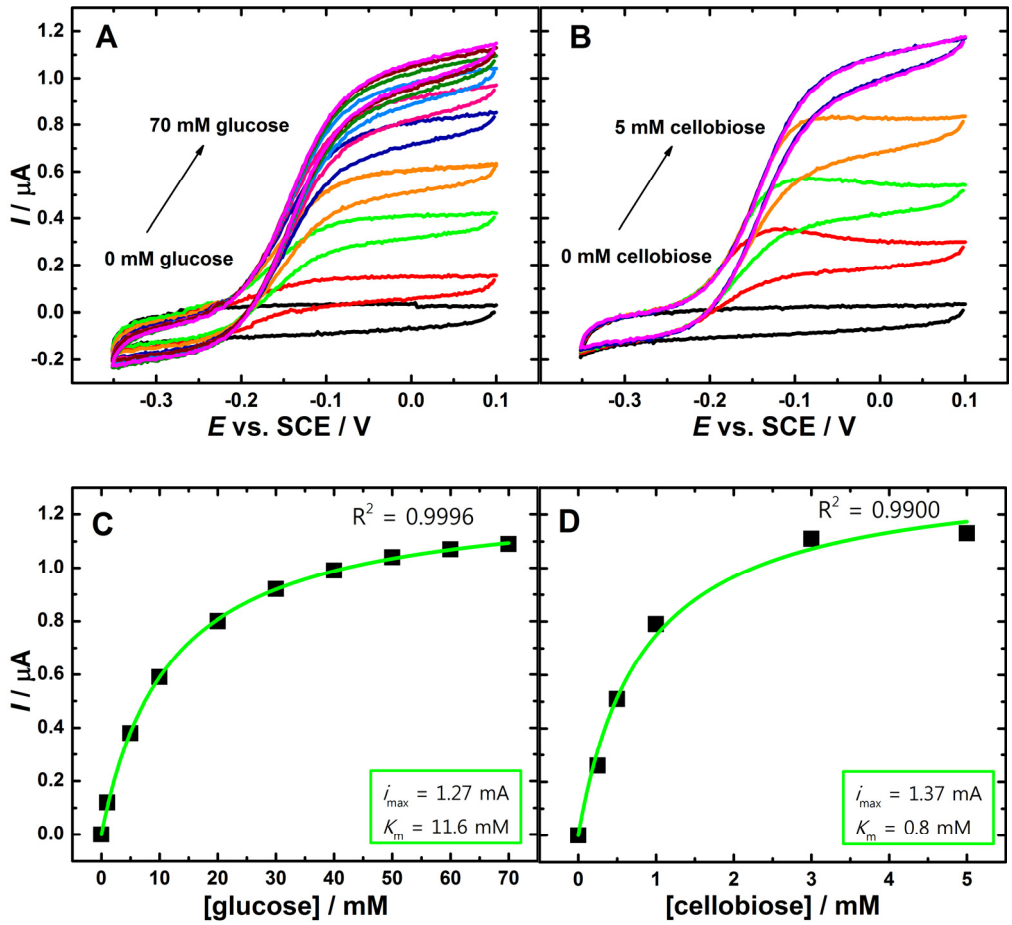

Figure 4.40. *Top: Cyclic voltammograms for a CDH-modified GC/MWCNT electrode (E522-CDH) in deoxygenated 50 mM Tris buffer (pH 7.4), containing 30 mM $CaCl_2$ and increasing concentrations of (A) glucose and (B) cellobiose. The electrode potential was swept at 1 mV/s from -0.35 to 0.1 V vs. SCE. Bottom: Plots of the current measured at 0.1 V in the voltammograms on the top (subtracted for the background current) versus sugar concentration: (C) glucose and (D) cellobiose. Data were fitted with the Michaelis-Menten equation (Eq. 4.7, green lines) and the parameters obtained by the fitting are reported in the insets.*

To study the kinetic parameters of the direct and the mediated electron transfers for the CDH variants, the limiting currents obtained in Figure 4.27 and Figure 4.31 were replotted versus the glucose concentrations and the data were fitted to the Michaelis-Menten equation (*Eq.* 4.7). Figure 4.41 shows the plots attributable to the Michaelis-Menten behaviour (DET mode) for the CDH variants: (A) D813C, (B) E522C, (C) T701C and (D) E674C. These plots are not identical for the different CDH variants, exhibiting different values of i_{max}, whereas K_m^{app} is almost the same, with values between 11 and 13 mM (Table 4.3). Figure 4.41 and Table 4.3-DET, show that the variant T701 generates the highest value of i_{max}, the variant D813 the lowest and the other two variants have intermediate values. Indeed, the accurate comparison between them should consider the fact that i_{max} does not only depend on the turnover number (k_{cat}), but also on the enzyme surface coverage on each electrode surface; $i_{max}^{app} = k_{cat}^{app}$ [*enz*] = $2FA\Gamma k_2$.[333] However, the amounts of the enzyme immobilised onto each electrode were

previously calculated (Section 4.9.3.5) to be 5.5±0.2 pmol, indicating that the different magnitudes of the currents obtained for each variant (Figure 4.41) are not the result of different coverage of enzyme on the surface of the electrode. Consequently, the different catalytic currents are most probably due to covalent binding of CDH at the maleimide-modified electrodes that occurred in more appropriate orientation (see Figure 4.26), the results presented so far suggest that the different catalytic currents observed for each variant in Figure 4.27 were due to differences in the IET rate for the different variants. Figure 4.42 shows the plots attributable to the Michaelis-Menten behaviour (MET mode) for the CDH variants: (A) D813C, (B) E522C, (C) T701C and (D) E674C. In contrast to the ones of DET mode (Figure 4.41), such plots are almost identical for the different CDH variants, exhibiting ca. the same values of i_{max}. Table 4.3-MET shows that the values of K_m^{app} for the MET are very similar to the ones for DET, with values between 10 and 14 mM. On the other hand, i_{max} is much higher, with values around 8-9 μA, when the mediator is employed.

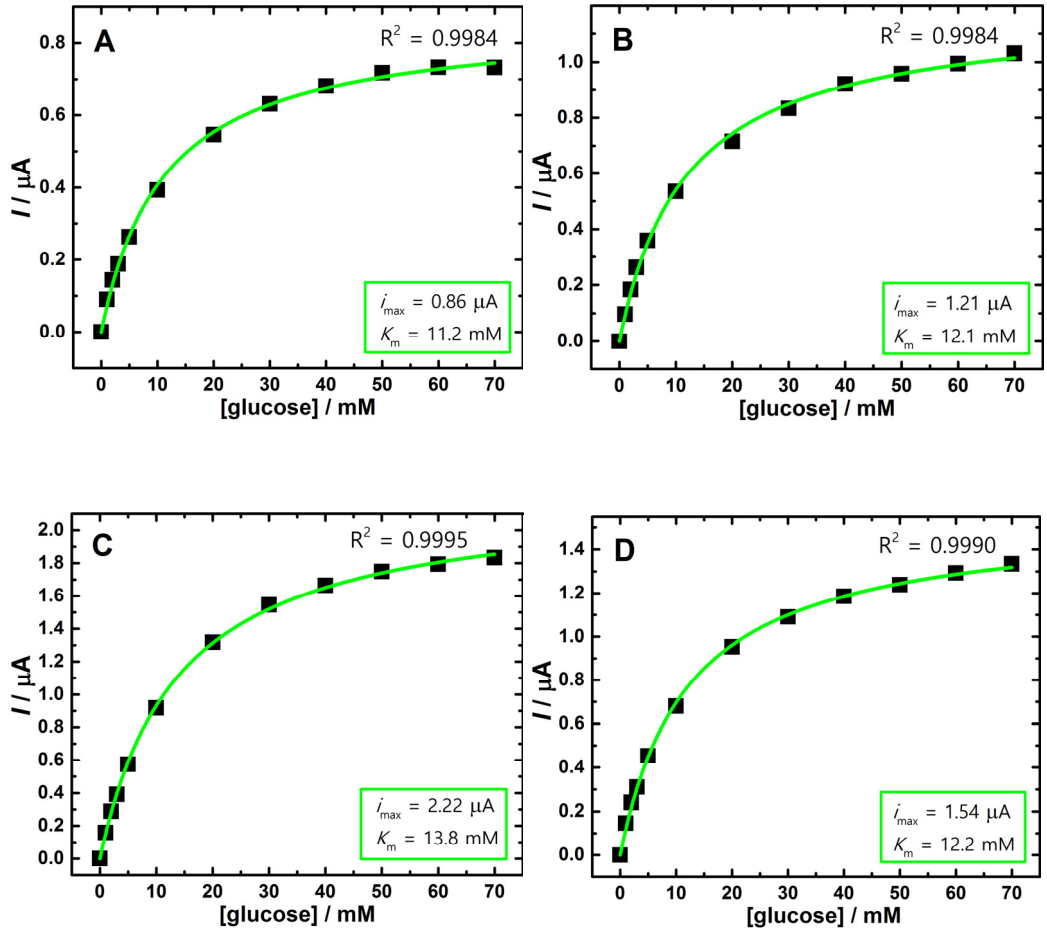

Figure 4.41. *Plots of the currents of the CDH-modified GC/MWCNT electrodes for various variants: (A) D813C, (B) E522C, (C) T701C and (E) E674C measured at 0.0 V in the voltammograms (subtracted for the background current) versus glucose concentration. Data were fitted with the Michaelis-Menten equation (Eq.4.7, green lines) and the parameters obtained by the fitting are reported in the insets. CVs were recorded in deoxygenated 50 mM Tris buffer (pH 7.4), containing 30 mM $CaCl_2$ by scanning the potential at 1 mV/s vs. SCE.*

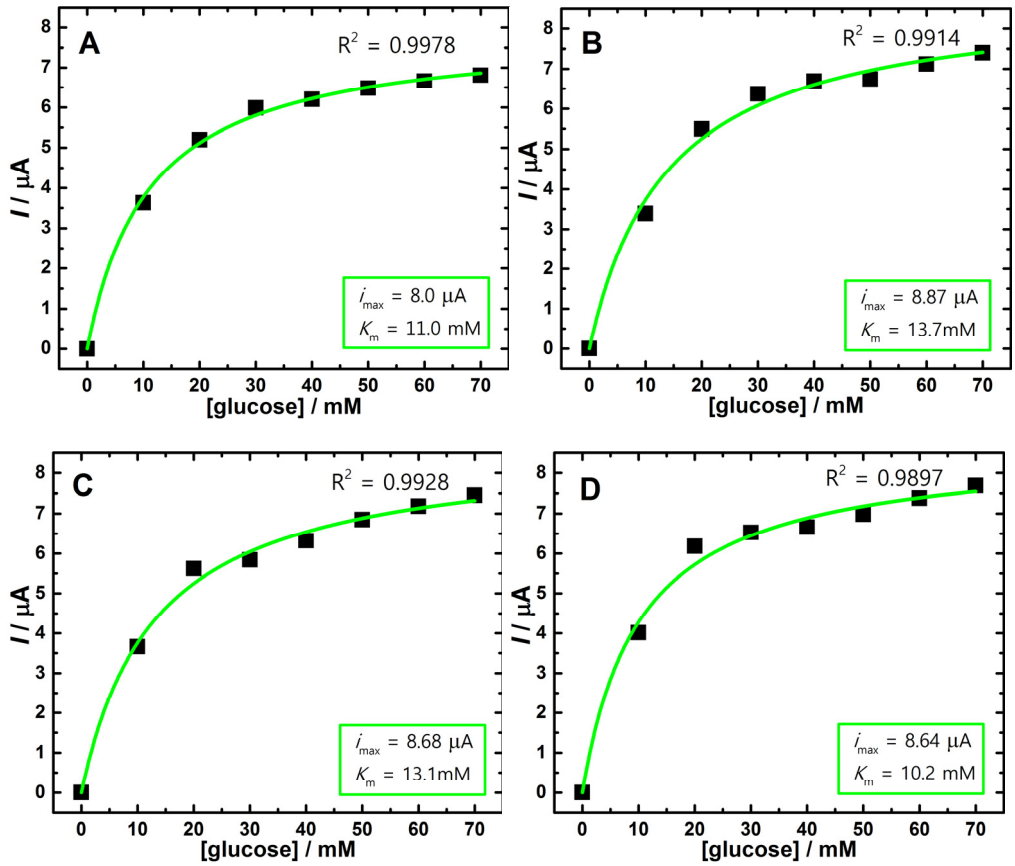

Figure 4.42. *Plots of the currents of the CDH-modified GC/MWCNT electrodes for various variants: (A) D813C, (B) E522C, (C) T701C and (E) E674C measured at 0.3 V in the voltammograms (subtracted for the background current) versus glucose concentration. Data were fitted with the Michaelis-Menten equation (Eq. 4.7, green lines) and the parameters obtained by the fitting are reported in the insets. CVs were recorded in deoxygenated 50 mM Tris buffer (pH 7.4), containing 30 mM $CaCl_2$ and 0.2 mM ferrocene monocarboxylic by scanning the potential at 2 mV/s vs. SCE.*

Table 4.3. *Values of apparent i_{max}, K_m and k_{cat} for the different CDH variants for DET and MET. The values were calculated by fitting the experimental data in Figure 4.41 and 4.42 with the Michaelis-Menten equation (Eq. 4.7).*

	DET				MET	
CDH variant	**i_{max}^{app} (µA)**	**K_m^{app} (mM)**	**k_{cat}^{app} (s^{-1})**	**k_{cat}^{app}/ K_m^{app} (M^{-1} s^{-1})**	**i_{max}^{app} (µA)**	**K_m^{app} (mM)**
D813	0.86±0.01	11.2±0.5	0.8±0.01	72±2	8.0±0.1	11.0±1.3
E522	1.21±0.01	12.1±0.5	1.1±0.01	91±2	8.87±0.3	13.7±1.8
T701	2.22±0.01	13.8±0.3	2±0.01	153±5	8.68±0.3	13.1±1.6
E674	1.54±0.01	12.2±0.4	1.45±0.01	120±4	8.64±0.3	10.2±1.5

4.11 Conclusion

In this Chapter, a novel procedure for the covalent immobilization of redox proteins and enzymes at carbon electrodes was described. The results presented so far have conclusively demonstrated a flexible and structured approach to the oriented immobilization of redox proteins and enzymes at electrode surfaces. The method uses site-directed mutagenesis to introduce cysteine residues at a particular sites on the protein surface followed by the reaction between the free thiol group and maleimide groups formed on the electrode surface to attach the mutated enzymes. The carbon-based electrodes (GC/MWCNT, BDD and GC) were first covalently modified with maleimide groups using a method combining electrochemical and solid phase synthesis approaches. The electrografiting has been used to form mixed monolayers at carbon electrode surfaces where the majority component is a passivating group, in the present case *N*-(2-aminoethyl) acetamide, and the minority component is a mono-Boc protected diamine, in this case *N*-Boc-1,6-hexanediamine. Meanwhile, solid state synthesis methodology was used for the subsequent removal of the Boc protecting group and coupling to the resulting free amine at the surface; this allows a spacer to be added, in the present case 6-aminohexanoic acid, followed by the reactive group, maleimide. In this way, the modular construction of the surface modifying layer allows a controlled partial coverage of the reactive group on the surface, compatible with the surface of the protein around the attachment point and suitable for accommodating large biomolecules such as enzymes. Such construction enables a controlled length and chemistry of the linking chain, and orientation of the protein through choice of the mutation site. Maleimide was chosen because it easily reacts, at room temperature and neutral pH, with the free cysteine residue introduced at the surface of the genetically engineered protein. The method can be easily applied to a variety of enzymes and proteins bearing a cysteine at the surface. Using the *Mt*CDH variant E522C (as a model for the cysteine-modified genetically engineered protein) we have shown that this approach leads to an extraordinary stable attachment of the enzyme to the electrode surface and that the immobilised enzyme is active for the electrochemical oxidation of D-glucose without added redox mediators.

Five *Mt*CDH variants, genetically engineered to bear a free cysteine in different positions at the surface of the flavin domain, were covalently immobilised onto GC/MWCNT electrodes. The CDH variants have been effectively attached to the GC/MWCNT electrodes through covalent binding, and different orientations for the CDH variants have been successfully discriminated. The covalent immobilisation through the thioether bond has been shown to be a powerful strategy for discriminating between CDH variants, in contrast to physical absorption, which gives the same catalytic current for the different variants. Cyclic voltammetry experiments with the *Mt*CDH-modified electrodes were carried out in buffered solutions at pH 7.4

(physiological pH), with increasing concentrations of glucose, showing direct electron transfer (DET) between the enzyme and the electrode surface and allowing discrimination between the different *Mt*CDH variants. The results obtained indicated that DET for the CDH variants under investigation always occurs via the haem group, one of the two CDH redox sites, located in two distinct domains of the enzyme. Calibration curves for glucose were recorded and the data were fitted to the Michaelis-Menten equation, allowing the determination of apparent kinetic parameters for the different *Mt*CDH variants. Moreover, tests in the presence and absence of calcium chloride were carried out to reach a better understanding of the DET and MET mechanisms of this enzyme. The results have suggested that the different catalytic currents observed for each variant were due to the differences in the IET rate. In order to further understand the kinetics of the CDH at the electrode surface, a kinetic analysis for both DET and MET results are performed and this is discussed in the next Chapter.

Chapter 5 Modelling *Mt*CDH-modified electrode responses

5.1 Overview

A kinetic model of an enzyme electrode may be used to identify the key experimental factors such as the rates of mass transport, rates of reactions and the loading of the enzyme component. These factors determine the response of the sensor which then provide a link between these key experimental factors; the concentration of the substrate and the biosensor response. A model gives a mathematical explanation of the substantial processes occurring within the system. Once we obtain a suitable kinetic model for a given amperometric enzyme electrode, we can employ this model to guide a number of improvements. Improving a kinetic model is an effective experimental method. Also, it gives understanding into the mechanisms and processes involved in the operation of the electrode. This is particularly true when we attempt the analysis applying approximate analytical approaches. This can yield a rich reward in terms of the new facts and insights that can be achieved.[1, 334] This chapter aims to provide a kinetic analysis for the DET and the MET results obtained in Chapter 4, based on the steady-state kinetics.

5.2 Steady-State kinetics model for the *Mt*CDH electrode reactions

To understand the kinetics of the *Mt*CDH at the electrode surface, further analysis for the results obtained (in Chapter 4) in the DET and the MET experiments can be done by looking closer at the current of each step in Scheme 4.6. In the following lines we will term FAD^+ as F_1, FADH as F_2 and $FADH_2$ as F_3. Furthermore, the two oxidation states of the ferrocene (mediator) will be termed Fc and Fc^+. On the other hand, the two oxidation states of haem will be termed as Fe^{II} and Fe^{III}. The reaction steps with the relative kinetic constants are shown in Table 5.1.

It is clear that several different kinetic processes are involved in the overall operation of the *Mt*CDH modified GC/MWCNT. These will include the reactions i) between the enzyme and its substrate, ii) the IET, iii) between the enzyme and the electrode, iv) between the enzyme and a redox mediator, and v) between the redox mediator and electrode. In addition, the various mass transport processes which bring the substrate to the electrode and take products away will also play a role. In this Section we describe the mathematical model that is necessary to understanding kinetic analyses of our *Mt*CDH modified GC/MWCNT electrode. Nevertheless, it

should be highlighted that the recorded DET current reflects the participation of three steps in the ET pathway, namely, CAT, IET, and DET. On the other hand, the registered MET current displays the involvement of two steps in ET pathway, viz, CAT and MET,[335] see Scheme 4.6.

Another assumption in the Michaelis-Menten treatment is that the concentration of the enzyme–substrate (ES) complex can be given using the steady-state hypothesis, meaning that the concentration of ES complex does not change with time. Indeed, this is not correct instantaneously after the substrate and enzyme are mixed together, namely, when the concentration of the ES complex is building up and will only be correct as long as the concentration of substrate is not considerably consumed by the progression of the reaction.[1] Therefore, we will assume that there is no mass-transport limitation for the substrate (glucose) so that the concentration of glucose at the electrode surface is the same as in the bulk.[16]

Table 5.1. *Reaction steps for the DET and MET oxidation of a sugar via MtCDH, with the relative kinetics constants.*

Step	Reaction	Kinetic constants
Substrate-enzyme reaction	$S + F_1 \rightleftharpoons \{SF_1\}$	$k_f, k_b, K_m = \frac{k_b + k_{cat}}{k_f}$
	$\{SF_1\} \longrightarrow P + F_3$	k_{cat}
Re-oxidation of FAD by haem	$F_3 + Fe^{III} \longrightarrow F_2 + Fe^{II}$ $F_2 + Fe^{III} \longrightarrow F_1 + Fe^{II}$	$k_{int(1)}$ $k_{int(2)}$
Re-oxidation of FAD by mediator	$F_3 + Fc^+ \longrightarrow F_2 + Fc$ $F_2 + Fc^+ \longrightarrow F_1 + Fc$	$k_{med(1)}$ $k_{med(2)}$
Re-oxidation of FAD by mediator (Michaelis–Menten type kinetics)	$F_3 + Fc^+ \rightleftharpoons \{F_3Fc^+\}$ $\{F_3Fc^+\} \longrightarrow F_2 + Fc$ and $F_2 + Fc^+ \rightleftharpoons \{F_2Fc^+\}$ $\{F_2Fc^+\} \longrightarrow F_1 + Fc$	$K_{mFc(1)}$ $k_{Fc(1)}$ $K_{mFc(2)}$ $k_{Fc(2)}$
Electrode reaction	$Fe^{II} \longrightarrow Fe^{III} + e^-$	Fast step, see Section 4.9.3.5
	$Fc \longrightarrow Fc^+ + e^-$	Fast step, see Section 4.9.3.4

According to the Michaelis-Menten model, in the first step of the CDH kinetics FAD^+ (F_1) combines with the substrate to form (SF_1). The SF_1 complex can proceed on to a product (P) and $FADH_2$ (F_3), the relative kinetic constants are shown in Table 5.1. As mentioned in Chapter

4, the Michaelis-Menten constant is related to the rate constants by $K_m = (k_{-1} + k_2)/ k_1$. In the following text we will call k_{-1} as k_b, and k_1 as k_f. Assuming that this step (breakdown of SF1 complex) is the rate limiting step of the whole reaction, the reaction rate (v) can be given by:

$$v = [SF_1]k_{cat} \qquad (Eq. 5.1)$$

As a flavocytochrome, *Mt*CDH exhibits a unique structure; it contains an electron-transfer cytochrome domain (CYT) that is connected to a carbohydrate-oxidizing dehydrogenase domain (DH). Electrons gained from sugar oxidation are transferred from the DH to the CYT by internal electron transfer (IET).[297] Scheme 4.6 shows the mechanisms for the direct and the mediated electron transfer of the CDH. It assumes that the released F_3 from the enzyme-substrate complex may be oxidised back via transferring two electrons to the haem group (Scheme 4.6-step 3) or to the ferrocene (Scheme 4.6-step 5) in two one electron steps. Under these circumstances, F_3 would be oxidised to a semiquinone intermediate F_2 which in turn is oxidised to F_1 with the relative kinetic constants shown in table 5.1. Thus, there will be two rate constants for the re-oxidation of F_1 (FAD) via the haem group, namely, $k_{int(1)}$ and $k_{int(2)}$ and two rate constants for the re-oxidation of F_1 via the ferrocene, $k_{med(1)}$ and $k_{med(2)}$

The results obtained in Figure 4.24B and Figure 4.36B, D and F, from the plots of log $[(i_L - i)/i]$ versus E, for an n-electron electrochemical process are linear with n ~ 1. Figure 4.24 and 4.36 show a significant linear relationship indicating a fast DET mechanism. Therefore, step 4 in Scheme 4.6 is not the rate limiting step. Step 6 in Scheme 4.6 is well known as a Nernstian reversible step. Thus, it is not the rate limiting step. Moreover, step 5 and 6 are [Fc] independent because the Fc concentration used was 0.2 mM which is sufficient to produce reversible MET (see Section 4.9.3.4). Therefore, the last steps in Table 5.1 are described as fast reversible electrochemical reactions.

5.3 Construction of a potential-dependent Michaelis-Menten model

To construct a potential-dependent Michaelis-Menten model for the *Mt*CDH modified GC/MWCNT electrode we can assume that the total concentration of immobilised enzyme (in mol cm^{-2}) is given by:

$$[enz] = [SF_1] + [F_1] + [F_2] + [F_3] \qquad (Eq. 5.2)$$

and the total concentration of mediator is:

$$[M] = [Fc] + [Fc^+] \qquad (Eq. 5.3)$$

Assuming that the electron transfer kinetics of the haem and the mediator are fast (reversible), the Nernst equation can be applied for the two cases, *vide supra*:

$$E = E'_{\mathrm{Fe}} + \frac{RT}{F} ln\left(\frac{[\mathrm{Fe^{III}}]}{[\mathrm{Fe^{II}}]}\right) \qquad (haem) \qquad (Eq.5.4)$$

$$E = E'_{\mathrm{Fc}} + \frac{RT}{F} ln\left(\frac{[\mathrm{Fc^{+}}]}{[\mathrm{Fc}]}\right) \qquad (mediator) \qquad (Eq.5.5)$$

Hence, the concentration of Fc^+ , which depends on the applied potential and is also accountable for the re-oxidation of FAD, may be given by rearranging *Eq.* 5.5 and introducing the expression given by *Eq.* 5.3:

$$\frac{[\mathrm{Fc^{+}}]}{[\mathrm{Fc}]} = exp\left\{\frac{F}{RT}(E - E'_{\mathrm{Fc}})\right\} \quad \Longrightarrow$$

$$[\mathrm{Fc^{+}}] = \frac{[\mathrm{M}] \cdot \exp(\vartheta_{\mathrm{Fc}})}{\exp(\vartheta_{\mathrm{Fc}}) + 1} \qquad \text{with } \vartheta_{\mathrm{Fc}} = \left\{\frac{F}{RT}(E - E'_{\mathrm{Fc}})\right\} \qquad (Eq.5.6)$$

On the other hand, the situation for the haem depends on whether we assume that the haem of a CDH molecule can oxidise the FAD of a different CDH molecule or not. Initially, we will assume that this is not the case in order to simplify the derivation. Hence, the haem of a particular enzyme molecule could be in the reduced (Fe^{II}) or oxidised (Fe^{III}) state. The probability for the haem to be in reduced state is Φ_{FeII}, and the probability for it to be in the oxidised state is Φ_{FeIII}, in this case:

$$\phi_{\mathrm{FeII}} + \phi_{\mathrm{FeIII}} = 1 \qquad (Eq.5.7)$$

Thus, the probability of the haem being in the oxidised form (Φ_{FeIII}), which depends on the applied potential and is also accountable for the re-oxidation of FAD, may be given by rearranging *Eq.* 5.4, and introducing the expression given by *Eq.* 5.7:

$$\phi_{\mathrm{FeIII}} = \frac{\exp(\vartheta_{\mathrm{Fe}})}{\exp(\vartheta_{\mathrm{Fe}}) + 1} \qquad \text{with } \vartheta_{\mathrm{Fe}} = \left\{\frac{F}{RT}(E - E'_{\mathrm{Fe}})\right\} \qquad (Eq.5.8)$$

Now, we are ready to write the kinetic expressions for all the different states of the enzyme as follows using the kinetic constants shown in Table 5.1.

$$\frac{d[\mathrm{F_1}]}{dt} = -k_{\mathrm{f}}[\mathrm{S}][\mathrm{F_1}] + k_{\mathrm{b}}[\mathrm{SF_1}] + k_{\mathrm{int(2)}}[\mathrm{F_2}]\phi_{\mathrm{FeIII}} + k_{\mathrm{med(2)}}[\mathrm{F_2}][\mathrm{Fc^{+}}] \qquad (Eq.5.9)$$

$$\frac{d[\mathrm{F_2}]}{dt} = k_{\mathrm{int(1)}}[\mathrm{F_3}]\phi_{\mathrm{FeIII}} - k_{\mathrm{int(2)}}[\mathrm{F_2}]\phi_{\mathrm{FeIII}} + k_{\mathrm{med(1)}}[\mathrm{F_3}][\mathrm{Fc^{+}}] - k_{\mathrm{med(2)}}[\mathrm{F_2}][\mathrm{Fc^{+}}] \qquad (Eq.5.10)$$

$$\frac{d[\mathrm{F_3}]}{dt} = -k_{\mathrm{cat}}[\mathrm{SF_1}] - k_{\mathrm{int(1)}}[\mathrm{F_3}]\phi_{\mathrm{FeIII}} - k_{\mathrm{med(1)}}[\mathrm{F_3}][\mathrm{Fc^+}] \qquad (Eq.\,5.11)$$

$$\frac{d[\mathrm{SF_1}]}{dt} = k_{\mathrm{f}}[\mathrm{S}][\mathrm{F_1}] - k_{\mathrm{b}}[\mathrm{SF_1}] - k_{\mathrm{cat}}[\mathrm{SF_1}] \qquad (Eq.\,5.12)$$

At this point, it is helpful to explain about the electrochemical reaction at the electrode surface (electrode-electrolyte interface). Such electrochemical reaction converts the flux of substrate J_S into a flux of electrons (current) that flows through the external circuit, in this case the current is given by[1]

$$i = nFA\,J_S = -\,nFA\,D_{\mathrm{S}}\left(\frac{dS}{dx}\right)_{x=0} \qquad (Eq.\,5.13)$$

Where n (number of electrons) is negative for oxidation and positive for reduction so that, by agreement (according to IUPAC) oxidation currents are positive and reduction currents negative, F is the Faraday constant, A is the electrode area, D_S is the diffusion coefficient of the substrate.[1] It has been assumed (see Scheme 4.6) that for each molecule of glucose oxidised by the immobilised CDH two electrons are donated to the electrode. Therefore, the number of the electrons (n) is equivalent to 2. The enzyme and enzyme-substrate complex are both immobilised at the electrode surface and the breakdown of such complex produces the products and the two electrons. Therefore, the flux of substrate J_S in *Eq.*5.13 can be equated to the rate of the reaction in *Eq.* 5.1 so that the current is given by:

$$i = 2nFA[\mathrm{SF_1}]k_{\mathrm{cat}} \qquad (Eq.\,5.14)$$

We can now apply the steady state approximation, assuming that [Fc^+], [S] and Φ_{FeIII} are constant considering the assumptions we have previously made about mass transport and reversibility of the redox reactions. Furthermore, applying the steady-state approximation as described in the Michaelis-Menten model assumes that the concentration of SF_1, F_1, F_2 and F_3 does not change with the reaction course.

We can now write the concentration of the substrate-enzyme complex, [SF_1], as follows using *Eq.* 5.12:

$$[SF_1] = \frac{k_{\mathrm{f}}[\mathrm{S}][\mathrm{F_1}]}{k_{\mathrm{b}} + k_{\mathrm{cat}}} \qquad (Eq.\,5.15)$$

The concentration of $FADH_2$, F_3, using *Eq.* 5.11:

$$[\mathrm{F_3}] = \frac{k_{cat}[\mathrm{SF_1}]}{k_{\mathrm{int(1)}}\phi_{\mathrm{FeIII}} + k_{\mathrm{med(1)}}[\mathrm{Fc^+}]} \qquad (Eq.\,5.16)$$

The concentration of FADH, F_2, using *Eq.* 5.10 and *Eq.* 5.16 in substitution of F_3:

$$[F_2] = \frac{[F_3]\left(k_{int(1)}\phi_{FeIII} + k_{med(1)}[Fc^+]\right)}{k_{int(2)}\phi_{FeIII} + k_{med(2)}[Fc^+]}$$

$$= \frac{k_{cat}[SF_1]\left(k_{int(1)}\phi_{FeIII} + k_{med(1)}[Fc^+]\right)}{\left(k_{int(1)}\phi_{FeIII} + k_{med(1)}[Fc^+]\right)\left(k_{int(2)}\phi_{FeIII} + k_{med(2)}[Fc^+]\right)}$$

$$= \frac{k_{cat}[SF_1]}{k_{int(2)}\phi_{FeIII} + k_{med(2)}[Fc^+]} \qquad (Eq.5.17)$$

The concentration of FAD$^+$, F_1, using *Eq.* 5.9 and *Eq.* 5.17 in substitution of F_2:

$$[F_1] = \frac{[F_2]\left(k_{int(2)}\phi_{FeIII} + k_{med(2)}[Fc^+]\right) + k_b[SF_1]}{k_f[S]}$$

$$= \frac{k_{cat}[SF_1] + k_b[SF_1]}{k_f[S]} \qquad (Eq.5.18)$$

Substituting *Eq.* 5.15, 5.16, 5.17 and 5.18 in *Eq.* 5.2, the total amount of immobilised enzyme will be:

$$[enz] = [SF_1]\left\{1 + \frac{k_{cat} + k_b}{k_f[S]} + \frac{k_{cat}}{k_{int(2)}\phi_{FeIII} + k_{med(2)}[Fc^+]} + \frac{k_{cat}}{k_{int(1)}\phi_{FeIII} + k_{med(1)}[Fc^+]}\right\} \qquad (Eq.5.19)$$

By rearranging *Eq.* 5.19, the concentration of the substrate-enzyme complex is given by *Eq.* 5.19b:

$$[SF_1] = \frac{[enz]}{\left\{1 + \frac{k_{cat} + k_b}{k_f[S]} + \frac{k_{cat}}{k_{int(2)}\phi_{FeIII} + k_{med(2)}[Fc^+]} + \frac{k_{cat}}{k_{int(1)}\phi_{FeIII} + k_{med(1)}[Fc^+]}\right\}}$$

Then, substituting $[SF_1]$ (*Eq.* 5.19b) in *Eq.* 5.14, the current will be given by *Eq.* 5.20:

$$i = \frac{2nFAk_{cat}[enz]}{\left\{1 + \frac{k_{cat} + k_b}{k_f[S]} + \frac{k_{cat}}{k_{int(2)}\phi_{FeIII} + k_{med(2)}[Fc^+]} + \frac{k_{cat}}{k_{int(1)}\phi_{FeIII} + k_{med(1)}[Fc^+]}\right\}}$$

knowing that $K_m = (k_b + k_{cat})/k_f$ (see the kinetics constants in Table 5.1), therefore *Eq.* 5.20 can be re-written as:

$$i = \frac{2nFAk_{cat}[enz]}{\left\{1 + \frac{K_m}{[S]} + \frac{k_{cat}}{k_{int(2)}\phi_{FeIII} + k_{med(2)}[Fc^+]} + \frac{k_{cat}}{k_{int(1)}\phi_{FeIII} + k_{med(1)}[Fc^+]}\right\}}$$

Looking closer at the latter equation for the current, we can emphasise that the first term at the denominator ($1 + K_m/[S]$) is due to the enzyme-substrate kinetics, whereas the other two terms with k_{cat} are due to the internal electron transfer (IET) or the flavin/mediator kinetics.

These two terms can be written as $k_{cat}/k_x(x)$, with $k_x(x)$ representing the re-oxidation kinetics of FAD, either due to the haem or to the mediator, and being equal to:

$$k_x(x) = \frac{\left(k_{int(2)}\phi_{FeIII} + k_{med(2)}[Fc^+]\right)\left(k_{int(1)}\phi_{FeIII} + k_{med(1)}[Fc^+]\right)}{\left(k_{int(1)} + k_{int(2)}\right)\phi_{FeIII} + \left(k_{med(1)} + k_{med(2)}\right)[Fc^+]} \qquad (Eq.5.21)$$

$k_x(x)$ can be simplified depending on whether the IET or the MET is the dominant process, providing thus:

$$k_x^{int}(x) = \frac{k_{int(1)}\, k_{int(2)}}{k_{int(1)} + k_{int(2)}}\phi_{FeIII} \qquad \text{(IET dominant)} \qquad (Eq.5.21a)$$

$$k_x^{med}(x) = \frac{k_{med(1)}\, k_{med(2)}}{k_{med(1)} + k_{med(2)}}[Fc^+] \qquad \text{(MET dominant)} \qquad (Eq.5.21b)$$

In this study, we will adopt an idea that the rates of the two semi-oxidation reactions are the same, for both the haem and mediator cases:

$$k_{int(1)} = k_{int(2)} \quad \text{and} \quad k_{med(1)} = k_{med(2)}$$

So that $k_x(x)$ can be simplified as:

$$k_x^{int}(x) = \frac{k_{int}}{2}\,\phi_{FeIII} \qquad \text{(IET dominant)} \qquad (Eq.5.21c)$$

and

$$k_x^{med}(x) = \frac{k_{med}}{2}\,[Fc^+] \qquad \text{(MET dominant)} \qquad (Eq\ 5.21d)$$

Hence, the equation for the current, *Eq.* 5.20, can now be re-written as follow:

$$i = \frac{2nFAk_{cat}[enz]}{\left\{1 + \frac{K_m}{[S]} + \frac{k_{cat}}{k_x(x)}\right\}} = \frac{2nFAk_{cat}[enz][S]}{[S]\left(1 + \frac{k_{cat}}{k_x(x)}\right) + K_m} \qquad (Eq.5.22)$$

$$\text{or} \quad i = \frac{i_{max}^{app}[S]}{[S] + K_m^{app}} \qquad (Eq.5.22a$$

$$K_m^{app} = \frac{K_m}{1 + \frac{k_{cat}}{k_x(x)}} \qquad (Eq.5.22b)$$

$$k_{cat}^{app} = \frac{k_{cat}}{1 + \frac{k_{cat}}{k_x(x)}} \qquad (Eq.5.22c)$$

$$i_{\max}^{\text{app}} = 2FAk_{cat}^{app}[\text{enz}] \qquad (Eq.5.22\text{d})$$

The apparent kinetic parameters of the direct and the mediated electron transfers for the CDH variants were previously obtained in Section 4.10.1 using the same equation obtained in *Eq.* 5.22a.

5.4 Simulation of the DET and MET catalytic voltammograms

In this section we compare the experimental voltammetric results obtained in the DET and MET modes with simulation results. The software MS Excel 2010 was used for simulation, *Eq.*5.22 was employed in a spreadsheet. This equation shows the current dependency on the applied potential by the expression k_x(x). Indeed this expression was extracted from *Eq.*5.21 and it corresponds to k_{int} and k_{med}, the activity of the haem in the oxidised form (Φ_{FeIII}) as well as the concentration of the ferrocenium (Fc^+). The concentration of Fc^+ and (Φ_{FeIII}) depends on the applied potential (see *Eq.* 5.6 and *Eq.* 5.8). Thus, such parameters deliver the potential dependency of the current.

The concentrations of the substrate and the mediator are known for the particular experiment. The other parameters which were employed to assemble *Eq.*5.22 in the spreadsheet are: i) Faraday constant (F) = 96485 C mol^{-1}, ii) surface area of the electrode (A) = 14 cm^2 (see Section 4.9.1), iii) gas constant (R) = 8.314 J mol^{-1} K^{-1}, iv) temperature (T) = 293 K, v) redox potential of the haem (E_{Fe}) = - 0.14 V vs. SCE (see Section 4.9.3.5), and vi) redox potential of the ferrocene (E_{Fc}) = 0.275 V vs. SCE (see Section 4.9.3.4). Fortunately, we were able to confirm that the quantity of CDH molecules capable of undergoing DET immobilised on each electrode was almost the same with a value of $n^{enz} \approx 5.5$ pmol, see Section 4.9.3.5. Therefore, another constant parameter in *Eq.* 5.22 would be [enz].

Thus, the parameters that are yet to be defined in *Eq.*5.22 are K_m, k_{cat}, k_{med} and k_{int}. The Michaelis-Menten constants (K_m and k_{cat}) are a characteristic feature of each enzyme[336] and they should not vary for the different CDH variants. However, k_{int} might vary across the family of CDH variants due to different orientations on the surface of electrodes, the latter assumption will be investigated later. Moreover, we would assume k_{med} to be the same for the different variants because the reaction between the mediator and FAD should not be affected by different enzyme orientations. As the $k_{med\,(1)}$ and $k_{med\,(2)}$ were assumed to be identical, they are defined as k_{med}, the same assumption was also made for $k_{int\,(1)}$ and $k_{int\,(2)}$.

More than 70 experimental voltammograms were compared to the simulated curves by iteratively adjusting the following kinetic parameters: K_m, k_{cat}, k_{int} and k_{med}. The value of K_m reported in the literature for *Mt*CDH in solution (glucose as a substrate) of 250 mM, was

initially employed.[284] Since there are four parameters to be adjusted, sometimes good agreement can be obtained with several possibilities. achieved.[1, 334] Therefore, we tried to constrain the kinetic constants; firstly within an interval centered in the estimated values and second, by varying the initial values close to the real values for better estimation.[334] We have previously shown that the electron transfer kinetics of the mediator are fast and reversible, see Section 4.9.3.4. The analysis confirmed that a very small concentration of ferrocenium ion, ≈ 0.4 μM, is sufficient to react with the enzyme and, consequently, generate the observed catalytic current; by increasing the ferrocene concentration in solution, a less positive potential value is required to have the minimum sufficient concentration of ferrocenium ions to support the MET reaction. The conclusion was that the rate for the reaction between the DH domain (FAD group) and Fc^+ has to be very fast. Therefore, we decided to apply a value for k_{med} = 1 x 10^6 L mol^{-1} s^{-1}. This value was adjusted later to be 4 x 10^6 L mol^{-1} s^{-1} to perfectly match with the experimental voltammogram, see Figure 5.1A and B. Hence the latter value for k_{med} was adopted in the following simulations. An experimental voltammograms recorded at newly prepared CDH-modified GC/MWCNT electrode (E674-CDH) was simulated, using a K_m value of 250 mM. The k_{cat} and k_{int} were adjusted to match with the experimental data, whereas a constant value of n^{enz} = 5 pmol were always employed. The better simulation that fit the experimental data was obtained by applying values for k_{cat} = 36 s^{-1}, k_{int} = 3.3 s^{-1} and k_{med} = 4 x 10^6 L mol^{-1} s^{-1}. Figure 5.1B shows that the simulated voltammogram (red line) matches reasonably with both DET-CV (black line) and MET-CV (green line).

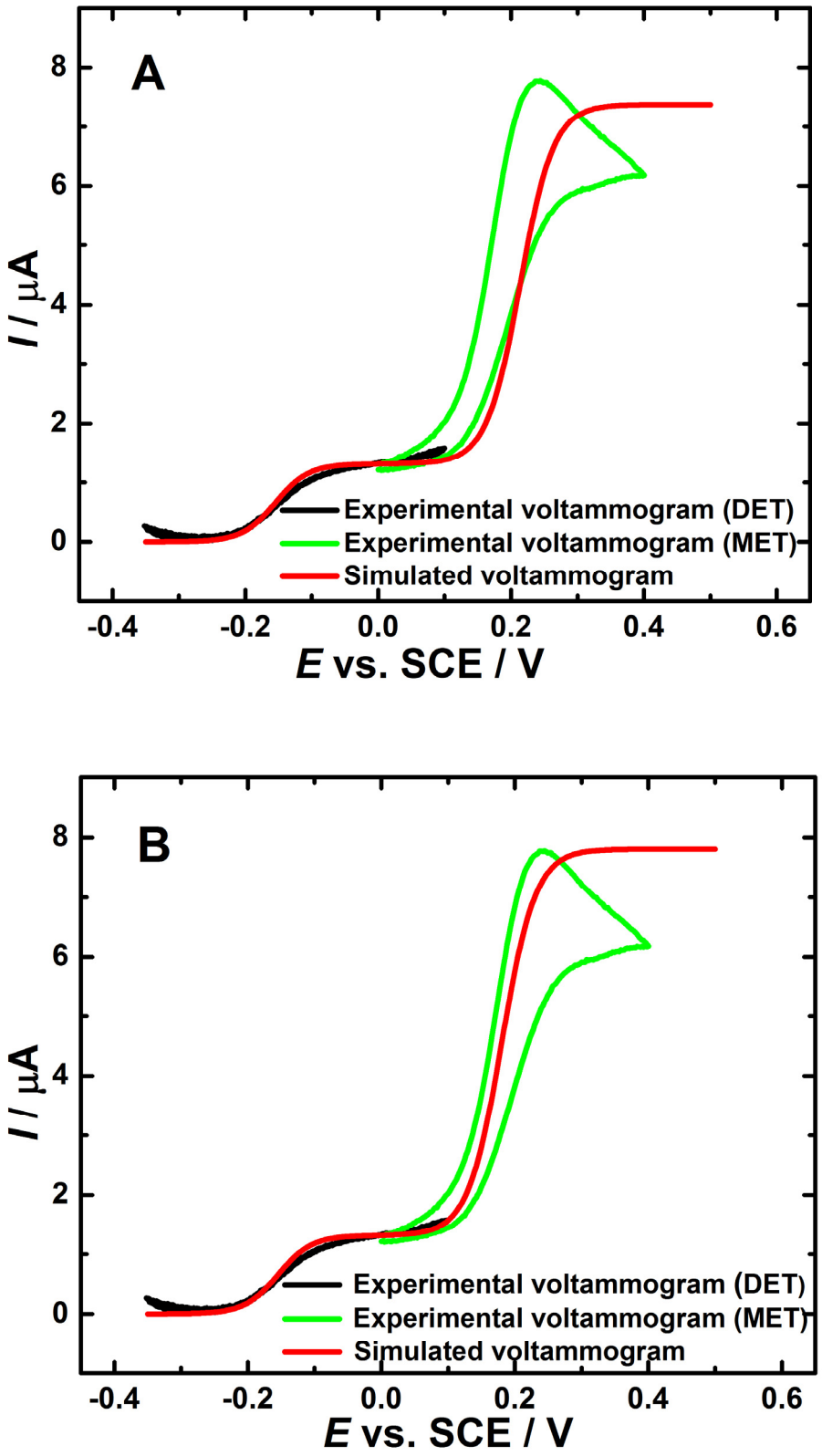

Figure 5.1. *Experimental voltammogram after background subtraction for a newly prepared CDH-modified GC/MWCNT electrode (E674-CDH). CVs were recorded in deoxygenated 50 mM Tris buffer (pH 7.4), containing 30 mM $CaCl_2$ and 70 mM glucose in the presence (green lines) and in the absence (black lines) of 0.2 mM ferrocene monocarboxylic, sweeping the potential at 2 mV/s (green lines) and 1 mV/s (black lines). The red lines are simulated voltammograms using Eq. 5.22, employing the parameters: K_m = 250 mM, k_{cat} = 36 s^{-1}, k_{int} = 3.3 s^{-1} and n^{enz} = 5 pmol, a value of k_{med} = 1 x 10^6 L mol^{-1} s^{-1} was used in (A) and = 4 x 10^6 L mol^{-1} s^{-1} was used in (B). The other constant parameters were employed as mentioned before.*

In Section 4.10.1, the apparent values of K_m and k_{cat} for the different CDH variants (for DET and MET) were rendered via fitting the experimental data of the glucose experiments, see Table 4.3. This was done using the electrochemical form of the Michaelis-Menten equation (*Eq.* 4.7) which is widely reported in the literature.[1, 16] The acquired apparent values were in a big disagreement with the real K_m and k_{cat} that have been reported for the same enzyme (in the solution), *Mt*CDH,[284] making it necessary to make an attempt to obtain the real K_m and k_{cat} values for our immobilised *Mt*CDH, via employing *Eq.* 5.22. Looking closer at *Eq.* 5.22b, it is clear that K_m^{app} depends on the values of K_m, k_{cat} and $k_x(x)$. The latter parameter depends on the k_{med} and k_{int} and does not depend on the real K_m and k_{cat} due to the fact that Michaelis-Menten constants are a characteristic feature of each enzyme[336] and they should not vary for the different CDH variants. Furthermore, $k_x(x)$ depends on the $[Fc^+]$ and $[Fe^{III}]$ which are electrochemically determined by the applied potential; where, the IET (and consequently DET) is the dominant process between -0.25 and 0.05 V, whereas MET is the dominant process between 0.1 and 0.3 V. The k_{med} value was shown to be in the order of 10^6 L mol^{-1} s^{-1}, however k_{int} is expected to be reasonably small. Accordingly, the $k_x(x)$ in the DET potential range should be relatively small because it depends on k_{int}. However, the $k_x(x)$ in the MET potential range is expected to be higher as it depends on k_{med}. Therefore, according to *Eq.* 5.22, for a given glucose concentration, the MET currents have to be much bigger than the DET currents.

According to *Eq.*5.22d, k_{cat}^{app} depends on i_{max}^{app} and on the amount of immobilised enzyme. An estimation of the amount of immobilised CDH was done before, and it was shown that the amount of CDH molecules capable of undergoing DET immobilised on each electrode was almost the same with the value of ≈ 5.5 pmol, see Section 4.9.3.5. However, the estimation of k_{cat}^{app} for MET experiments was not possible due to the absence of the FAD redox peaks in the non-catalytic voltammogram. Therefore, a precise estimation of k_{cat}^{app} for MET is unfeasible. The results obtained in Table 4.3 show that i_{max}^{app} values acquired for MET are much bigger than the ones obtained for DET. This can be explained by taking in to consideration that i_{max}^{app} (according to *Eq.* 5.22d) depends on the k_{cat}^{app}. On the other hand, k_{cat}^{app} depends on the k_{cat} and $k_x(x)$ as defined in *Eq.* 5.22c. k_{cat} is a characteristic feature of each enzyme. Therefore, k_{cat}^{app} is directly proportional to $k_x(x)$, which has a higher value in the potential range where MET is the dominant process compared to a smaller value when DET is dominant.

5.4.1 Simulations of DET and MET currents for E674-CDH

To verify that the values of K_m, k_{cat}, k_{int} and k_{med} that were used in Figure 5.1 could be applied to the catalytic voltammograms recorded at a different concentration of the substrate (glucose), the experimental voltammograms for E674-CDH for DET and MET experiments (Figure 4.27 and Figure 4.31) were simulated. This was done by employing the same values of

the parameters as in Figure 5.1 and varying the glucose concentration. The values of DET-current (recorded at 0.0 V *vs.* SCE) and MET-current (recorded at 0.3 V *vs.* SCE) in the simulated voltammograms were plotted with the experimental results, see Figure 5.2.

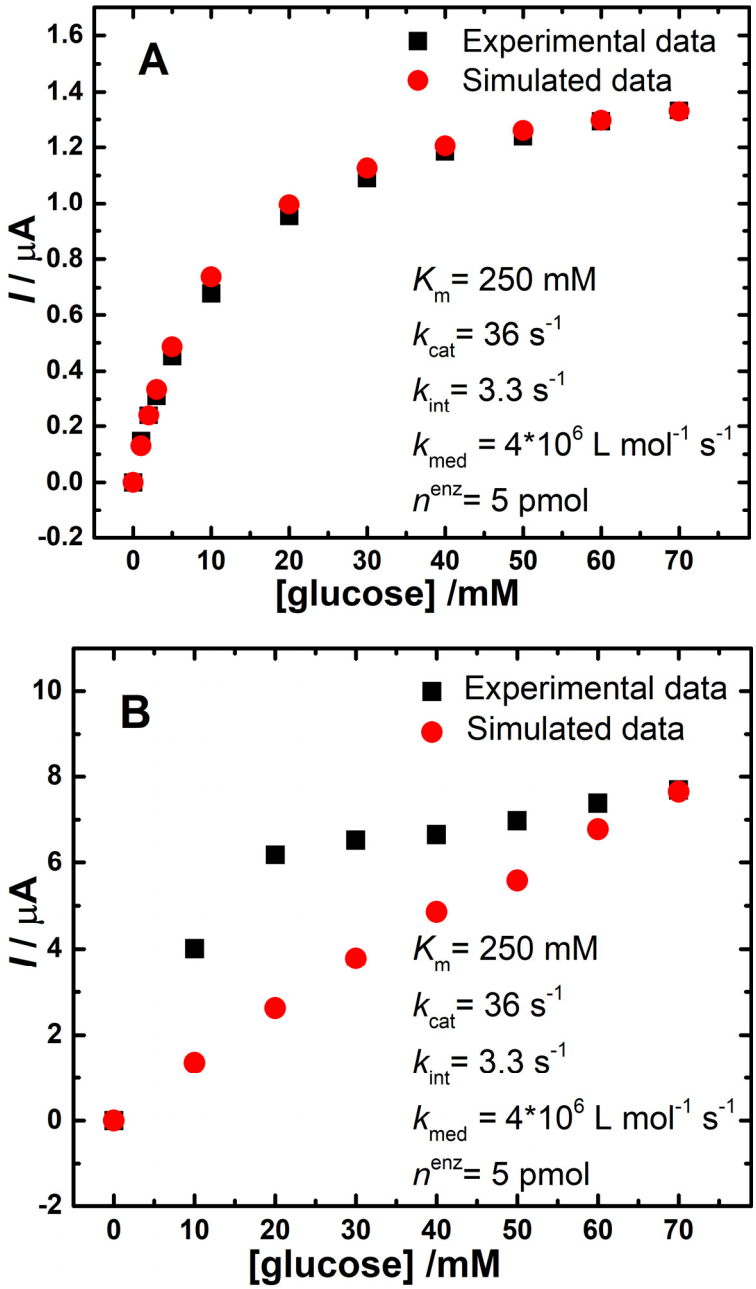

Figure 5.2. *Black squares; relative background subtracted currents for the CV experiments that recorded at the CDH-modified GC/MWCNT electrode (E674-CDH) in deoxygenated 50 mM Tris buffer (pH 7.4), containing 30 mM $CaCl_2$ and 0 to 70 mM glucose in the absence (A) and in the presence (B) of 0.2 mM ferrocene monocarboxylic). The red circles are simulated data using Eq. 5.22, at different substrate concentrations, the parameters employed in the simulation are reported in the legends. The other constant parameters were employed as mentioned before.*

In the case of the DET mode (Figure 5.2A), the simulated data reasonably match with the experimental data over the whole range of the glucose concentrations (1 to 70 mM). One of the

ways to evaluate the simulation data is by fitting them with the potential dependent Michaelis-Menten equation *Eq.* 5.22a. An extracted value for K_m^{app} = 11 mM were obtained for the simulated data in Figure 5.2A. This value is in a good agreement with the value of 12 mM that was obtained for the experimental result, see Table 4.3, showing that the real K_m value of 250 mM that was used in our simulation is fairly reasonable.

The same values of the parameters that were used for the DET mode (Figure 5.2A) were also employed for the MET mode, in this case, the simulated data do not match with the experimental results, see Figure 5.2B. At this point it should be highlighted that the MET experiments were regularly performed the next day after conducting the ones for DET. According to our previous investigation in Section 4.7.2.3 we concluded that the quantity of the enzyme on the electrode surface was decreased (about 50%) by desorption of physically adsorbed CDH, which diffuses away from the electrode surface within a few days, see Figure 4.10. Therefore, the amount of the enzyme in the case of the MET experiment has decreased from the total amount (≈ 5 pmol) that was recorded on the first day when the DET experiment has completed. However, the other possibility is that the simulation parameters used in Figure 5.2 were not precise. Indeed, there is another value for K_m, 157 mM, which has been reported in the literature[337] for *Mt*CDH in solution. Therefore, a new set of simulated data was performed using a K_m value of 157 mM, the k_{cat} and k_{int} were adjusted to match with the experimental data, whereas a constant value of n^{enz} = 5 pmol was always employed. The values of DET-current (recorded at 0.0 V *vs.* SCE) and MET-current (recorded at 0.3 V *vs.* SCE) in the simulated voltammograms were plotted with the experimental results, see Figure 5.3.

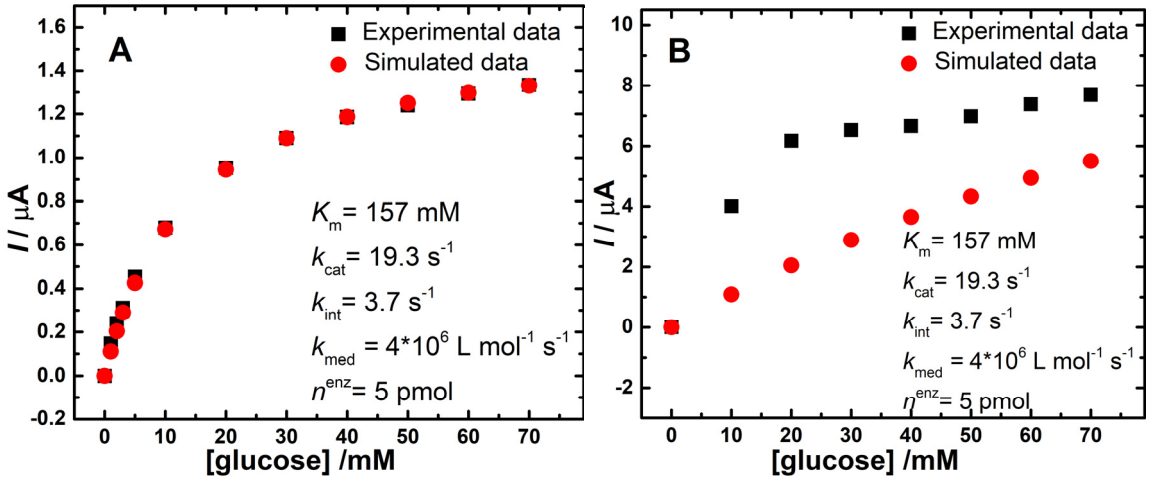

Figure 5.3. *Black squares; relative background subtracted currents for the CV experiments that recorded at the CDH-modified GC/MWCNT electrode (E674-CDH) in deoxygenated 50 mM Tris buffer (pH 7.4), containing 30 mM $CaCl_2$ and different glucose concentrations (0-70 mM) in the absence (A) and in the presence (B) of 0.2 mM ferrocene monocarboxylic). The red circles are simulated data using Eq. 5.22, at different substrate concentrations, the parameters employed in the simulation are reported in the legends. The other constant parameters were employed as mentioned before.*

Interestingly, this time again, the simulated data match well with the DET experimental data (Figure 5.3A). Unfortunately, as before (Figure 5.2B) the MET experimental data are still in disagreement with the simulated ones, see Figure 5.3B. Although the MET experiments were always performed one day after the DET ones, it is clear that the value of the n^{enz} = 5 pmol that was employed in the simulation is not correct for the MET case and a bigger value should be tried. This means that the number of the enzyme molecules that are properly oriented, to produce DET, on the surface of the electrode, is less than the total number of the enzyme molecules that can undergo MET. Note that the mediator used in this study was ferrocenecarboxylic acid, which is directly exchanging electrons with FAD in the DH domain. Thus, the other possibility is that all the immobilised enzyme molecules are in perfect orientation but some of them are not able to produce DET due to the cytochrome domain being detached from the enzyme and consequently they are not able to produce DET, however they are still able to catalyse the substrate oxidation and generate MET currents. Therefore, it can be concluded that there are two different types, "populations", of immobilised *Mt*CDH. The first population is able to undergo DET and MET, "DET enzyme", however the second population is only able to undergo MET, "MET enzyme".

At this point, it is helpful to design a new spreadsheet for simulation. This was done because the one that we used so far was designed for one population of the immobilised enzyme that can undergo both DET and MET. Therefore, the new spreadsheet has to include "DET enzyme" current, "MET enzyme" current and the total current. To this aim, the term $k_x(x)$ in *Eq.* 5.22 was defined according to *Eq.* 5.21 in order to simulate the "DET enzyme" current. On the other hand, *Eq.* 5.21b was used to define $k_x(x)$ in *Eq.* 5.22 to simulate "MET enzyme" current. Thus, the total current can be given by

$$i = \frac{2nFAk_{cat}[enz^{DET+MET}][S]}{[S]\left(1+\frac{k_{cat}}{k_x^{DET+MET}(x)}\right)+K_m} + \frac{2nFAk_{cat}[enz^{MET}][S]}{[S]\left(1+\frac{k_{cat}}{k_x^{MET}(x)}\right)+K_m} \qquad (Eq.\,5.23)$$

where $[enz^{DET+MET}]$ is the concentration of "DET enzyme", $[enz^{MET}]$ is the concentration of "MET enzyme", $k_x^{DET+MET}(x)$ contains both k_{int} and k_{med} and $k_x^{MET}(x)$ contains k_{med}, *vide supra*. *Eq.* 5.23 can now be used to simulate the experimental voltammograms for both DET and MET simultaneously. Therefore, the experimental voltammograms that were recorded at the E674-CDH-modified GC/MWCNT electrode for both DET and MET were simulated using the same parameters that were used in Figure 5.3. However, a value of n^{enz} for the "DET enzyme" ($n_{DET}{}^{enz}$) = 5 pmol, and a value of n^{enz} for the MET enzyme ($n_{MET}{}^{enz}$) = 2 pmol were employed. Figure 5.4A shows that the simulated voltammogram (red line) perfectly matches with DET-CV (black lines), however it is slightly shifted to a more negative potential compared to the experimental MET-CV (green line). The value of k_{med} was adjusted before to be 4 x 10^6 L mol^{-1}

s^{-1} in order to perfectly match with the experimental MET-voltammogram (Figure 5.1B). However, this value was selected for an n_{DET}^{enz} = 5 pmol, in the current simulation the total amount of the CDH that can undergo MET (n_{DET}^{enz} + n_{MET}^{enz}) = 7 pmol. Thus, the value of k_{med} was re-adjusted to be 3 x 10^6 L mol^{-1} s^{-1} to perfectly match with the experimental voltammogram, see Figure 5.4B.

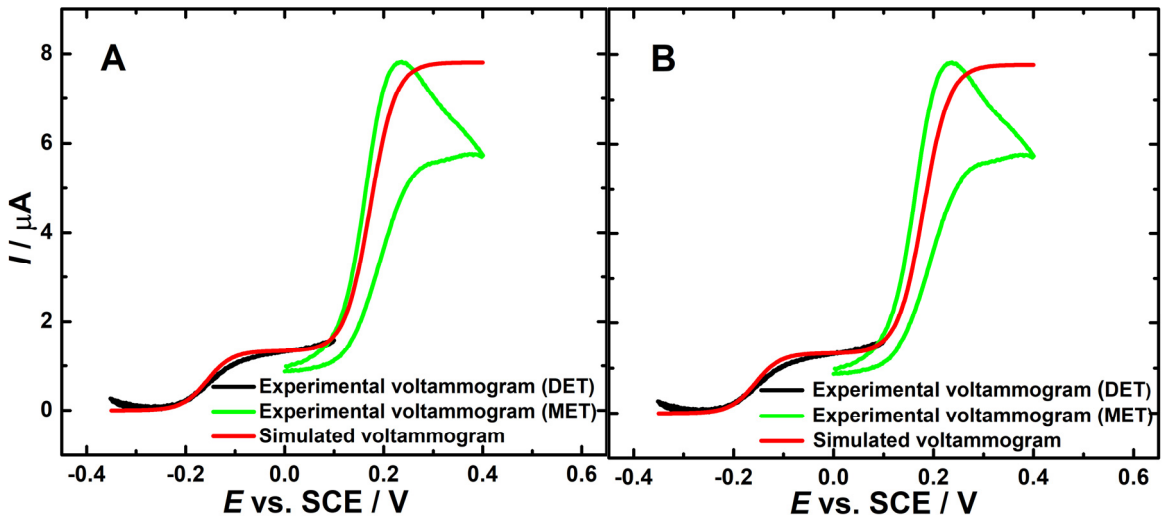

Figure 5.4. *Experimental voltammogram after background subtraction for the CDH- modified GC/MWCNT electrode (E674-CDH). CVs were recorded in deoxygenated 50 mM Tris buffer (pH 7.4), containing 30 mM $CaCl_2$ and 70 mM glucose in the presence (green lines) and in the absence (black lines) of 0.2 mM ferrocene monocarboxylic, sweeping the potential at 2 mV/s (green lines) and 1 mV/s (black lines). The red lines are simulated voltammograms using Eq. 5.23, employing the parameters: K_m = 157 mM, k_{cat} = 19.3 s^{-1}, k_{int} = 3.7 s^{-1} and n_{DET}^{enz} = 5 pmol, n_{MET}^{enz} = 2 pmol, a value of k_{med} =4 x 10^6 L mol^{-1} $s^{-1}$was used in (A) and = 3 x 10^6 L mol^{-1} $s^{-1}$was used in (B). The other constant parameters were employed as mentioned before.*

Eq. 5.23 was also used to simulate the DET and MET data obtained for the CDH-modified GC/MWCNT electrode (E674-CDH) at different glucose concentrations. To this aim, the same values for K_m, k_{cat}, k_{int} and k_{med} that were used in Figure 5.4 were employed. This was done by employing values of n_{DET}^{enz} = 5 pmol to simulate the DET currents, and n_{MET}^{enz} = 2 pmol to simulate the MET currents. The values of DET-current (recorded at 0.0 V *vs.* SCE) and MET-current (recorded at 0.3 V *vs.* SCE) in the simulated voltammograms were plotted with the experimental results. Figure 5.5A shows that the simulated data reasonably match with the DET-experimental results, however they do not match with the MET-experimental data (Figure 5.5B), being less than the experimental ones.

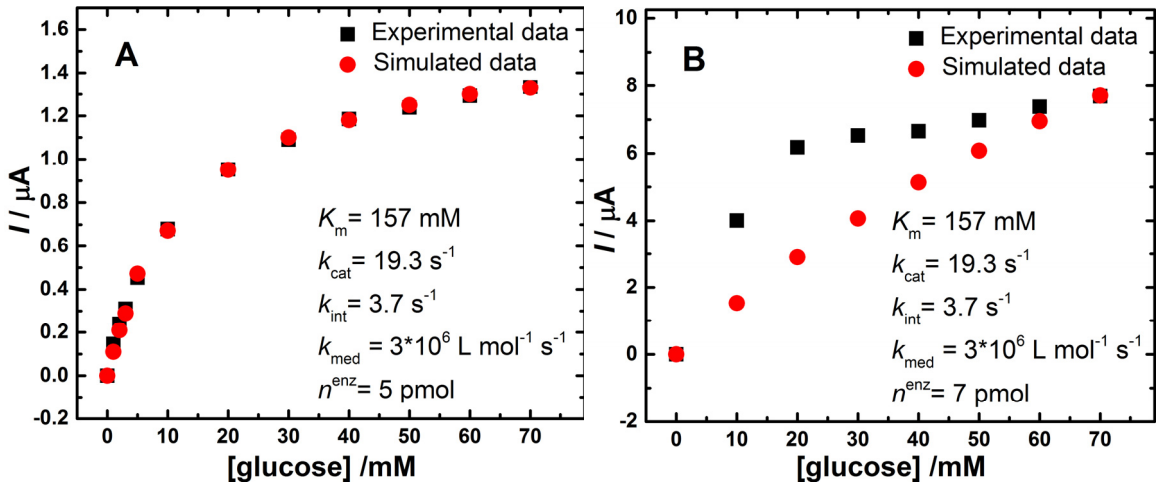

Figure 5.5. *Black squares; relative background subtracted currents for the CV experiments that recorded at the CDH-modified GC/MWCNT electrode (E674-CDH) in deoxygenated 50 mM Tris buffer (pH 7.4), containing 30 mM $CaCl_2$ and different glucose concentrations (0-70 mM) in the absence (A) and in the presence (B) of 0.2 mM ferrocene monocarboxylic. The red circles are simulated data using Eq. 5.23, at different substrate concentrations, the parameters employed in the simulation are reported in the legends. $n^{enz} = n_{DET}{}^{enz}$ in (A), and $n^{enz} = n_{DET}{}^{enz} + n_{MET}{}^{enz}$ in (B). The other constant parameters were employed as mentioned before.*

At this point, a new idea has arisen by analysing *Eq.* 5.22b, ($K_m^{app} = K_m / (1 + k_{cat}/k_x(x))$). As mentioned before, the real Michaelis-Menten constants (K_m and k_{cat}) are a characteristic feature of each enzyme[336] and they should not vary. Therefore, the value of K_m^{app} depends on $k_x(x)$, the latter term was defined by *Eq.* 5.21 and it depends on k_{med}. The k_{med} value was shown to be in the order of 3 to 4 x 10^6 L mol^{-1} s^{-1}. Accordingly, the $k_x(x)$ in the MET potential range is expected to be large because it depends on k_{med}. Thus, the value of the denominator in *Eq.* 5.22b should be close to 1 and consequently, the K_m^{app} value will approach to K_m. To test this assumption, the simulated data that was obtained in Figure 5.5B was fitted by using *Eq.* 5.22b, an extracted value for K_m^{app} = 148 mM was acquired. Interestingly, this value is in a good agreement with the K_m value of 157 mM that was used in the simulation, suggesting that a K_m value that is close to the K_m^{aap} for the MET experimental results, see Table 4.3, should be tried. Therefore, a new set of simulated data was generated using a K_m value of 13 mM, the k_{cat} and k_{int} were adjusted to match with the experimental data, and a value of n_{DET}^{enz} = 5 to simulate the DET currents and an n_{MET}^{enz} = 2 pmol to simulate the MET currents were employed. The values of DET-current (recorded at 0.0 V *vs.* SCE) and MET-current (recorded at 0.3 V *vs.* SCE) in the simulated voltammograms were plotted with the experimental results. Figure 5.6B shows that the simulated data reasonably match with MET- experimental data, however they do not match well with the DET-experimental data (Figure 5.6A), being larger than the experimental ones, showing that the assumption we made is not correct.

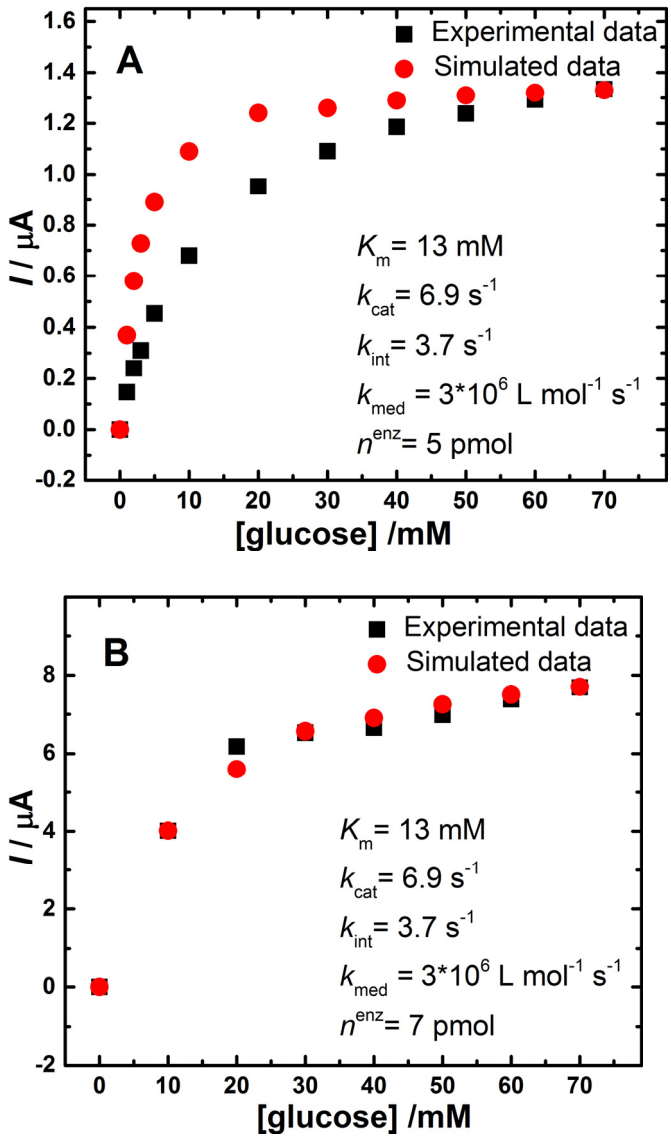

Figure 5.6. *Black squares; relative background subtracted currents for the CV experiments that recorded at the CDH-modified GC/MWCNT electrode (E674-CDH) in deoxygenated 50 mM Tris buffer (pH 7.4), containing 30 mM $CaCl_2$ and different glucose concentrations (0-70 mM) in the absence (A) and in the presence (B) of 0.2 mM ferrocene monocarboxylic. The red circles are simulated data using Eq. 5.23, at different substrate concentrations, the parameters employed in the simulation are reported in the legends. $n^{enz} = n_{DET}{}^{enz}$ in (A), and $n^{enz} = n_{DET}{}^{enz} + n_{MET}{}^{enz}$ in (B). The other constant parameters were employed as mentioned before.*

Before giving up the last assumption (that the K_m value should be close to $K_m{}^{aap}$ for the MET experimental data), another attempt was performed. Indeed, this assumption is true only if k_{med} has a large value (of the order of 10^6). Furthermore, the value of K_m = 13 mM that we have used in the last simulation is far away from the K_m values of 250 or 157 mM that have been reported in the literature[284, 337] for the same enzyme (*Mt*CDH) in solution. However, the next simulation was performed by using a larger K_m value (25 mM) and the other parameters were adjusted in order to match with the experimental data, a value of $n_{DET}{}^{enz}$ = 5 to simulate the DET

currents and n_{MET}^{enz} = 7 pmol to simulate the MET currents were employed, see Figure 5.7A and B. This time the simulated data match well with both DET and MET-experimental ones.

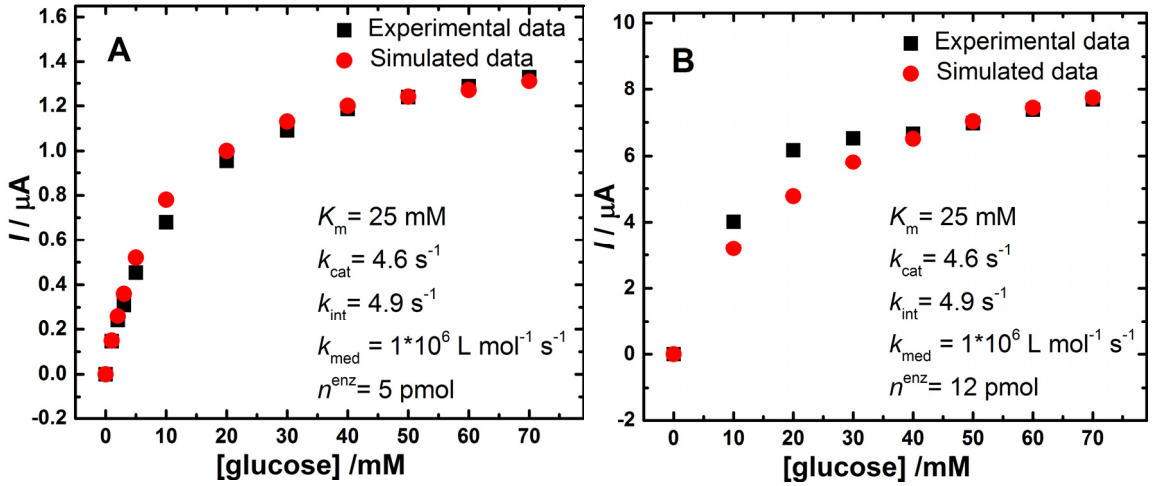

Figure 5.7. *Black squares; relative background subtracted currents for the CV experiments that grecorded at the CDH-modified GC/MWCNT electrode (E674-CDH) in deoxygenated 50 mM Tris buffer (pH 7.4), containing 30 mM $CaCl_2$ and different glucose concentrations (0-70 mM) in the absence (A) and in the presence (B) of 0.2 mM ferrocene monocarboxylic, sweeping the potential at 2 mV/s (green lines) and 1 mV/s (black lines). The red circles are simulated data using Eq. 5.23, at different substrate concentrations, the parameters employed in the simulation are reported in the legends.* $n^{enz} = n_{DET}{}^{enz}$ *in (A), and* $n^{enz} = n_{DET}{}^{enz} + n_{MET}{}^{enz}$ *in (B). The other constant parameters were employed as mentioned before.*

Independent of the precise/imprecise details of the simulation data shown in Figure 5.7, it is clear that in this model the enzyme kinetics are slow ($k_{cat} < k_{int}$), however this is inconsistent with higher catalytic currents observed with MET compared to DET, also it is inconsistent with the Ca^{2+} effect on the internal electron transfer (IET). Indeed, k_{int} describes the rate of IET process, and it has been widely reported that the addition of Ca^{2+} increases the DET current. The same effect was also observed in the current study, see Section 4.9.4. In their work, Ludwig *et al.*[297, 325, 327] have concluded that this increase is due to the adoption of a closed conformation for *Mt*CDH in the presence of divalent cations, which exert a bridging effect between the two enzymatic domains by neutralising electrostatic repulsion and, thereby, increase the internal electron transfer (IET) rate. As there is no evidence that the Ca^{2+} effects the enzyme kinetics (k_{cat}), the enzyme-substrate reaction should not be the rate determining step.

If we look closer at the MET data (Figure 5.7B), what do we assume is the factor that causes the current to reach a plateau? Is it that it is now limited by the rate of reaction of the glucose with the flavin? If this is the case then K_m has to be around 25 mM to fit. Hence we started to wonder whether the problem was with the rate of the ferrocene reaction. However, the problem there is that the current does not increase when we add more ferrocenecarboxylic acid. It does to begin with but then it becomes constant, see Figure 5.8. Thus for low ferrocene concentration

the current is dependent on ferrocene concentration. When it becomes independent of ferrocene concentration, either, the glucose reaction becomes limiting which we are seeing here (Figure 5.7), or we have Michaelis–Menten type kinetics for the ferrocene reaction[338] which is another model, and therefore it is limiting here. Indeed, the Ca^{2+} effect can come in if this MET-current is limited by the ferrocene rate because we give it another route, and the current can go up, when we switch on the DET. It is this last model that we consider in the next Section.

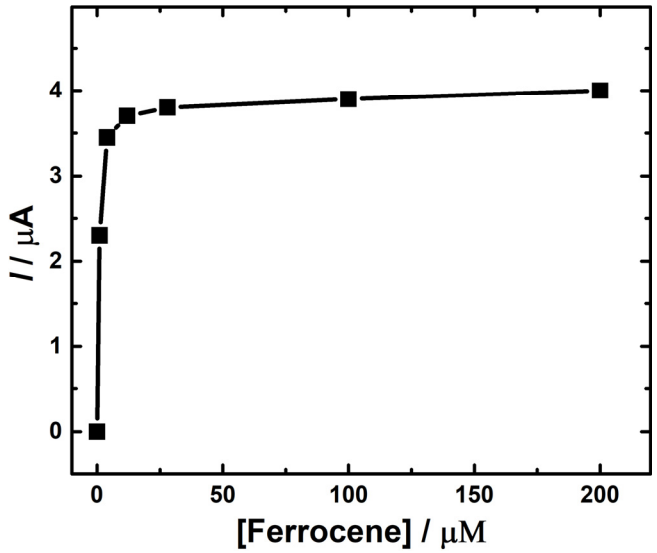

Figure 5.8. *Plot of the experimental data for the current vs. concentration of ferrocene. The original CVs are shown in Figure 4.32A which were recorded At CDH-modified GC/MWCNT electrode (variant E674) in deoxygenated 50 mM tris buffer (pH 7.4), containing 30 mM $CaCl_2$, 10 mM glucose and increasing concentrations of ferrocenecarboxylic acid. The electrode potential was swept at 2 mV/s from 0.0 to 0.4 V vs. SCE.*

So far, the potential-dependent Michaelis-Menten model (*Eq.* 5.22) was able to simulate the experimental results obtained with the CDH-modified GC/MWCNT electrode (E674-CDH) for the DET experiments. However, this model is not able to simulate the experimental results for the MET. The first set of the simulated data was performed using a reasonable K_m value of 250 mM. In this case, the simulated data were perfectly match with the DET experimental data. The second set of the simulated data was performed using another reasonable value for K_m, 157 mM, which also has been reported in the literature. This time again, the simulated data match well with the DET experimental data however, the MET experimental data are still in disagreement with the simulated ones. In the third set of the simulated data, the presence of two different "populations", of the immobilised *Mt*CDH, "DET enzyme" and "MET enzyme" was introduced. The last set of the simulated data was performed based on the assumption that the K_m value should be close to K_m^{aap} for the MET experimental data. This time the simulated data match well with both DET and MET-experimental ones. However, the enzyme kinetics was

slow ($k_{cat} < k_{int}$), which is inconsistent with higher catalytic currents observed with MET compared to DET and also with the results of the Ca^{2+} effect on the IET rate. Thus, a Michalis-Menten type kinetics for the ferrocenecarboxylic acid reaction which is another model is now introduced.

5.4.2 Michaelis–Menten kinetics for ferrocenecarboxylic acid: A new model

In this model, we assume that there is a complex formed between the ferrocenecarboxylic acid and the flavin in the same way that a complex is formed between glucose and flavin and then the electron transfer occurs in that complex, so if we have high concentrations of ferrocenium the rate becomes independent of the concertation of the ferrocenium because it is now determined by the reaction in that complex just as in the Michaelis–Menten kinetics of glucose. This provides a mechanism for the current plateauing for the MET case, but not because of glucose kinetics. Indeed, the plateauing in DET case is because of the IET. However, in the MET case if we just assume a first order reaction between the Fc and the enzyme then we should attribute the current plateauing to the glucose kinetics. A similar behaviour occurs with a wide range of electron acceptors which were reported to be reduced by the flavin domain of CDH. Ludwig *et al.*[338] have reported K_m value of 5.2 µM for the ferrocene-CDH interactions, showing a pure Michaelis-Menten behaviour. Another study by Zamocky *et al.*[287] has also reported a K_m values in the order of few µM for the interaction of the flavin domain of CDH with different electron acceptors.

To introduce the Michaelis-Menten-like interaction between CDH and ferrocene we will substitute k_{med} in *Eq.* 5.21 with the following expression:

$$k_{med} = \frac{{k_{cat}}^{med}}{{K_m}^{med} + [Fc^+]} \qquad (Eq. 5.24)$$

This new model was tested to simulate the DET and MET data obtained for the CDH-modified GC/MWCNT electrode (E674-CDH) at different glucose concentrations. This time a reasonable values of K_m of 200 mM and k_{cat} of 25 s^{-1} were employed, these values are very close to the ones that have been reported in the literature[284, 337] for the same enzyme (*Mt*CDH) in solution. The other parameters k_{int}, K_{Fc} and k_{Fc} were adjusted to perfectly match with the experimental data. However, this was done by employing values of n^{enz} ($n_{DET}{}^{enz}$) = 5.3 to simulate the DET currents, and n^{enz} ($n_{DET}{}^{enz} + n_{MET}{}^{enz}$) = 25 pmol to simulate the MET currents. The values of DET-current (recorded at 0.0 V *vs.* SCE) and MET-current (recorded at 0.3 V *vs.* SCE) in the simulated voltammograms were both plotted with the experimental results. Figure 5.9 shows that the simulated data reasonably match with both DET-experimental results (Figure 5.9A) and MET-experimental data (Figure 5.9B).

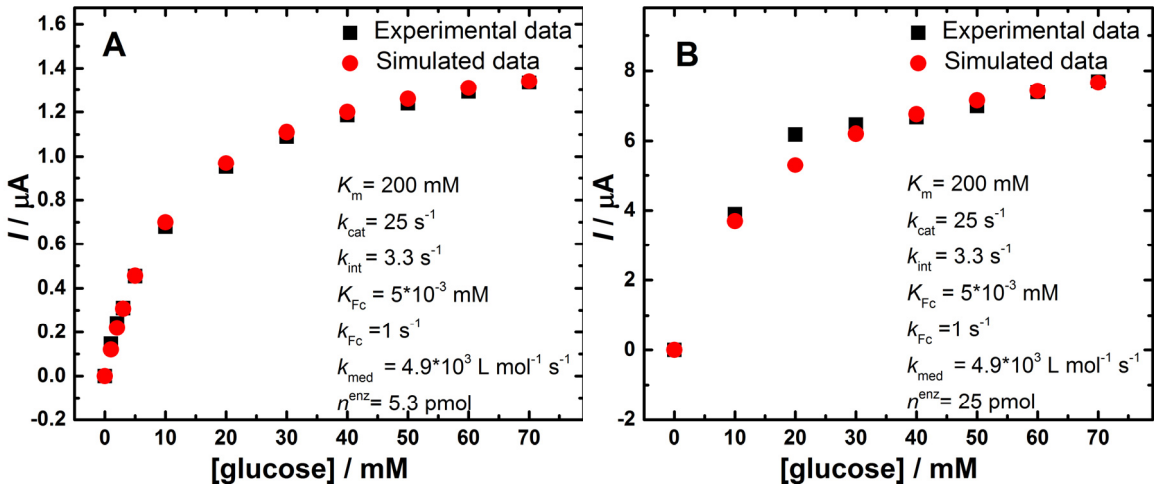

Figure 5.9. *Black squares; relative background subtracted currents for the CV experiments that recorded at the CDH-modified GC/MWCNT electrode (E674-CDH) in deoxygenated 50 mM Tris buffer (pH 7.4), containing 30 mM $CaCl_2$ and different glucose concentrations (0-70 mM) in the absence (A) and in the presence (B) of 0.2 mM ferrocene monocarboxylic. The red circles are simulated data using Eq. 5.22, at different substrate concentrations, the parameters employed in the simulation are reported in the legends.* $n^{enz} = n_{DET}{}^{enz}$ *in (A), and* $n^{enz} = n_{DET}{}^{enz} + n_{MET}{}^{enz}$ *in (B). The other constant parameters were employed as mentioned before.*

It can be assumed that the Michaelis-Menten constants (K_m and k_{cat}) are the same, for the different CDH variants. In principle, they describe the reaction between FAD and the substrate, and consequently, they should not be altered via the enzyme orientation on the electrode surface. In the next Section, we will attempt to simulate the experimental data obtained for the four different CDH variants in the DET and MET experiments.

5.4.3 Simulations of DET and MET currents for different CDH variants

The *Mt*CDH variants were engineered to bear a free cysteine residue in different positions at the surface of the flavin domain of the enzyme. In this way, we would expect the different CDH variants to be immobilised with different orientation on the electrode surface (Figure 4.26). Thus, the different variants would have different electron transfer distances, namely, the distance between the haem group and the electrode surface. However, the experimental results obtained in Section 4.9.3.5 showed that this step is always fast and independent of the enzyme orientation. Hence, one might expect that the different catalytic currents observed for each variant in Figure 4.27 were due to difference in the IET rate for the different variants. To confirm this assumption, we need to show that the simulation parameters that have been determined in the last simulation (Figure 5.9) are also applicable for the other *Mt*CDH variants results, however the k_{int} value should be varied and have different values depending on the variant under investigation. Therefore, the results recorded for the different variants for both

DET and MET modes were simulated by using the same kinetic parameters that have been used in Figure 5.9, see Figure 5.10.

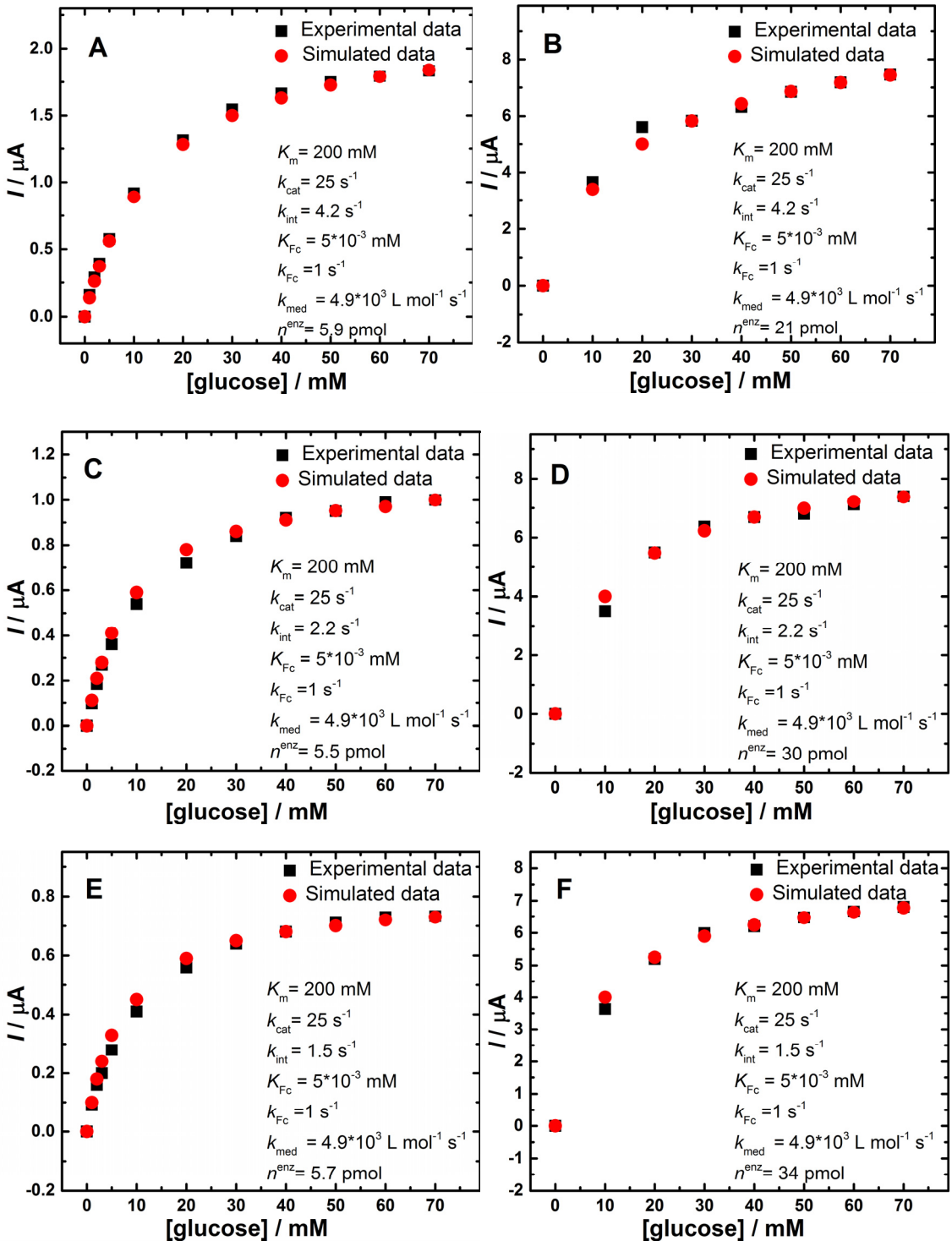

Figure 5.10. *Black squares: Relative background subtracted currents for the CV experiments that recorded at the CDH-modified GC/MWCNT electrode, (A, B) T701, (C, D) E522 and (E, F) D813, in deoxygenated 50 mM Tris buffer (pH 7.4), containing 30 mM $CaCl_2$ and different glucose concentrations (0-70 mM) in the absence (A, C, E) and in the presence (B, D, F) of 0.2 mM ferrocene monocarboxylic The red circles are simulated data using Eq. 5.22, at different substrate concentrations, the parameters used in the simulation are reported in the legends. $n^{enz} = n_{DET}{}^{enz}$ in (A, C, E), and $n^{enz} = n_{DET}{}^{enz} + n_{MET}{}^{enz}$ in (B, D, F). The other constant parameters were employed as mentioned before.*

Figure 5.10 shows that the simulated data reasonably match with both DET-experimental results (Figure 5.10A, C and E) and MET-experimental data (Figure 5.10B, D and F). Fortunately, the employed amount of the enzyme capable of DET was almost the same for the three variants, which are basically the same as the one used in Figure 5.9A for the E674 variant. Interestingly, the values of k_{int} that was used to match the simulated data with the experimental ones exhibit a similar trend as the obtained experimental DET currents (see Table 5.2), showing that the different enzyme orientations can alter the IET rate. It is not clear how the k_{int} would be affected by varying the orientation of the enzyme on the electrode surface. However, it can be argued that the great flexibility of the linker that connects the CDH domains allows the haem domain to freely move around the immobilisation point to obtain its appropriate position on the electrode surface. This movement mechanism might be affected by different enzyme orientation, and consequently the IET distance would be different for the different CDH variants.

Table 5.2. *Values of apparent i_{max}, and k_{cat} for the different CDH variants for DET. The values were calculated by fitting the experimental data in Figure 4.41 with Michaelis-Menten equation (Eq. 4.7). The k_{int} values were obtained from the simulation data in Figures 5.9 and 5.10.*

	DET		
CDH variant	**i_{max}^{app} (µA) obtained from Table 4.3**	**k_{cat}^{app} (s^{-1}) obtained from Table 4.3**	**k_{int} (s^{-1})**
D813	0.86±0.01	0.8±0.01	1.5
E522	1.21±0.01	1.1±0.01	2.2
E674	1.54±0.01	1.45±0.01	3.3
T701	2.22±0.01	2±0.01	4.2

Looking closer at Table 5.2, it is clear that the estimated values of k_{cat}^{app} are always half of the k_{int} values employed in the simulation. As the IET step was shown to be the rate determined step in our proposed mechanism/model (Scheme 4.6), the estimated k_{cat}^{app} values are indeed the apparent k_{int}. Knowing that the $FADH_2$ is re-oxidised to FAD by Fe^{3+} in two one electron steps. Therefore, the k_{int} value describes the rate constant for one step. $k_{int\,(1)}$ and $k_{int\,(2)}$ were assumed to be identical, hence, the apparent k_{int} can be given by

$$k_{int}{}^{app} = \frac{k_{int}}{2} \qquad Eq.\,4.25$$

Thus, the values of k_{int} that was used to match the simulated data with the experimental ones exhibits a similar trend to the estimated values of k_{cat}^{app}.

5.1 Conclusion

The kinetic analysis had been performed on the results obtained in Chapter 4 based on the steady state assumption. A potential-dependent Michaelis-Menten model for the CDH modified GC/MWCNT has been constructed and a master equation employed to simulate the DET and MET experimental results. More than 70 experimental cyclic voltammograms were compared to the simulation results by iteratively adjusting the kinetic parameters for the substrate-enzyme reaction, K_m and k_{cat}, as well as the rate constant of the re-oxidation reaction of FAD by haem (k_{int}) and the rate constant of the enzyme-mediator reaction (k_{med}). Several mechanisms have been tested to explain the DET and MET for the *Mt*CDH. The IET was deemed to be the rate determining step for our proposed mechanism. This is confirmed by the simulated data and our experimental results. On balance, the simulated data point strongly towards the presence of two populations of immobilised enzymes, MET and DET enzymes. Another important consideration is that the K_m values employed for the different CDH variants, close to 250 or 157 mM that have been reported in the literature[284, 337], indicate a good affinity between the immobilised enzyme and the substrate. Furthermore, the K_m values are the same for all the different CDH variants, indicating that: i) the site-directed mutagenesis to introduce cysteines at a specific surface site for immobilisation does not influence the enzyme affinity to the substrate, and ii) the active site of the CDH variants is not block by the immobilisation.Thus, our conclusion is that the combination of simulation and experimental work is a powerful strategy to extract the kinetic data.

With these promising results, a wide range of engineered enzymes could now be electro-kinetically investigated using our novel strategy; a detailed study of the enzyme kinetics of the immobilised bilirubin oxidase (BOD) mutants of interest are discussed in Chapter 6.

Chapter 6 Amperometric bilirubin oxidase electrode

6.1 Overview

The principle of a fuel cell dates back to 1839, from individual searches by Grove[339] and Schoenbein.[340] The fuel cell is a system for producing electrical energy directly from a chemical reaction by utilising noble metal catalysts. The electrical energy is continued as long as the reactants are supplied to the cell.[341] Fuel cells were a neglected field of research until the "space age" (for example in the Apollo and Gemini projects) when there became a need for reliable, lightweight power in challenging situations.[342] An enzymatic biofuel cell (EBC) is a fuel cell which can transform chemical energy into electrical energy via biochemical pathways[343] using redox enzymes as catalysts, and natural (organic) compounds, such as glucose and ethanol as the fuels. It consist of two electrodes: anode which is responsible for oxidation of a provided fuel, and cathode that usually contains an oxidoreductase that employs molecular oxygen as an electron acceptor and catalyses reduction to water in pH condition of interest.[344-345] Figure 6.1 shows a general diagram of a typical EBC consisting of a cathode and an anode.

Enzymes that frequently employed in anodes include glucose oxidase (GOx), glucose dehydrogenase (GDH), cellobiose dehydrogenase (CDH) and alcohol dehydrogenase (ADH).[346-347] For the biological cathodes, the enzymes are usually multi-copper oxidases such as bilirubin oxidases (BOD) and laccases.[346] EBCs have numerous advantages over traditional fuel cells, essentially the low cost of their components because the chemical reactions are driven by bio-fuels and biological catalysts. The employment of the enzymes in such application offers added advantages, for example the overpotential is often close to zero, low operational temperature, and operate in physiological conditions.[341] Furthermore, membranes are not needed in EBC design because of the high specificity and selectively of enzymes.[348] Another significant environmental advantage of BFCs is that they can be disposable and completely biodegradable devices. Finally, devices that use enzymes can be biocompatible, so that they could serve as implantable medical devices.[349-350] Nevertheless, the realisation of these desirable features is often hampered by low current density per catalyst (enzyme) volume, poor stability and restricted temperature range.[68, 341] Furthermore, efficient direct electron transfer (DET) to redox enzymes, which are close to the electrode surface is usually very slow, making necessary the use of redox mediators.[276, 351-352] However, the mediator not only adds an extra step to the electron transfer chain but also lowering the catalytic rate and decreasing the voltage in an

EBC. As in EBCs both oxidation and reduction are executed by enzymes, the major challenge is to prepare electrode surfaces allowing optimal immobilization of these biocatalysts.

In Chapter 4, we have shown that the covalent attachment of cysteine-modified genetically engineered cellobiose dehydrogenase (CDH) at maleimide modified electrodes leads to an extraordinarily stable attachment of the enzyme to the electrode surface. Moreover, the immobilised CDH was active for the electrochemical oxidation of D-glucose without added redox mediators. With these promising results, other genetically engineered enzyme such as bilirubin oxidase (BOD) could now be investigated.

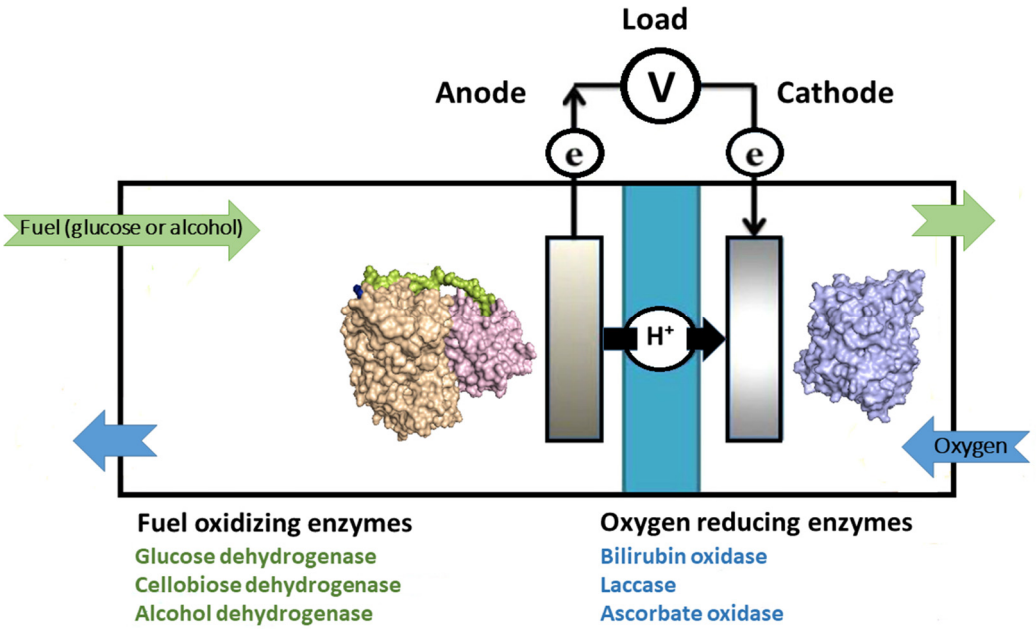

Figure 6.1. *General diagram of a typical EBC consisting of a cathode and an anode. The anode often layered by immobilized suitable enzyme for conversion of biofuels of choice. The cathode usually contains an oxidoreductase that employs molecular oxygen as the ultimate electron acceptor and catalyses reduction to water in pH condition of choice.*

6.2 Aim of the work

The validity of the flexible, selective immobilisation method based on the covalent attachment of cysteine-modified genetically engineered enzymes at maleimide modified electrodes, is further examined. Three BOD variants have been used in this study, which were modified to bear a free cysteine residue in different positions at the surface of the enzyme, allowing fast and selective attachment to maleimide-modified GC/MWCNT electrodes. It is likely that the majority of researchers involved in research on enzyme-based fuel cells are electrochemists. Nevertheless, despite the fact that it is crucial "to get the electrochemical principles right", the complexity of the redox enzymes should not be underestimated, and it is important that their features be fully comprehended and considered.[272] In contrary to laccases, BODs are considered to be Cl^- resistant. Nevertheless, there has not been a detailed study undertaken to

understand the related effect of Cl^- and pH on the redox state of immobilized BODs. In this Chapter, the catalytic mechanism of O_2 reduction by the *Magnaporthe oryzae* BOD covalently immobilized on multiwall carbon nanotube (MWCNT) electrodes, in the presence of NaCl and at different pH, has been electrochemically investigated.

6.3 Bilirubin oxidase (BOD)

Bilirubin oxidase (BOD) (EC 1.3.3.5) was discovered in 1981 by Tanaka and Murao,[353] first used for the detection of bilirubin[354] and then for the reduction of molecular oxygen.[355] It belongs to the multicopper oxidase (MCOs) family, a large group of enzymes, including laccase, CueO, Fet3p, and BOD.[356] The MCOs family is one of a few enzyme classes capable of reducing O_2 to water.[357] To date, seven BODs have been isolated,[345] among which are BOD from *Magnaporthae oryzae* (*Mo*BOD),[357] BOD from *Myrothecium verrucaria* (*Mv*BOD), BOD from *Trachyderma tsunodae* (*Tt*BOD),[358]and BOD from *Bacillus pumilus* (*Bp*BOD).[359] The two recently identified enzymes, *Mo*BOD and *Bp*BOD show a high activity at pH 7, good thermal stability and a low sensitivity toward NaCl. Indeed, there have been a numerous studies (of EBCs) that rely on BODs for one main reason; in contrary to laccases, BODs exhibit a high stability and activity in the presence of Cl^-at physiological pH.[360] However, only two crystal structures of BODs are available so far, for *Mo*BOD[356] and *Mv*BOD.[345, 361] Figure 6.2 shows the Pymol generated image of the structure of BOD, a 64-kDa protein, from *Magnaporthe oryzae* (*Mo*BOD) and shows the active centers.

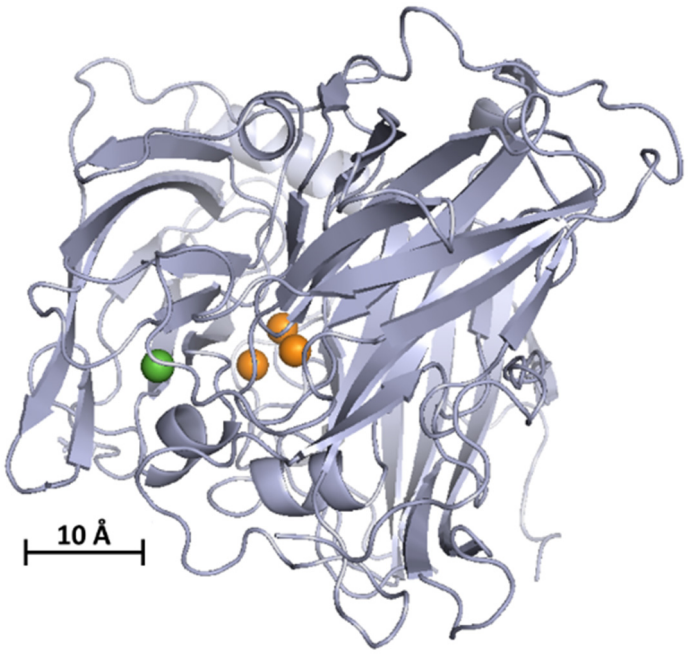

Figure 6.2. *Cartoon representation of the secondary structure of bilirubin oxidase from Magnaporthe oryzae. The Type 2 and Type 3 (TNC) coppers are represented by orange spheres, the Type 1 Cu is represented by the green sphere. The image was obtained with PyMol software, PyMol visualisations are based on the crystal structure of MoBOB, PDB code 2L9Y.*[362]

BODs contain four coppers classified depending on their optical and electron paramagnetic resonance properties. Their exact electronic pathway has yet to be confirmed, however it is assumed that the type one copper center (T1) receives electrons from an electron donating substrate and relays them to the O_2 reduction site through ~13 Å of Cys-His residues. The O_2 reduction site is a trinuclear cluster (TNC), composed of one type two copper ion (T2) and a pair of type three copper ions (T3).[362-363] BOD has been examined as a promising nominee for development of EBC because in nature it oxidizes bilirubin with simultaneous reduction of O_2.[362] Figure 6.3 shows the BOD active site with arrows marking electron flow from the T1 to the TNC.[364-365] These enzymes have been intensively investigated by electrochemist, particularly for their ability to execute oxygen reduction at positive potentials in physiological fluids. This is the reason why BODs and other types of MCOs, such as laccases, have been widely employed at cathodes of EBCs.[362]

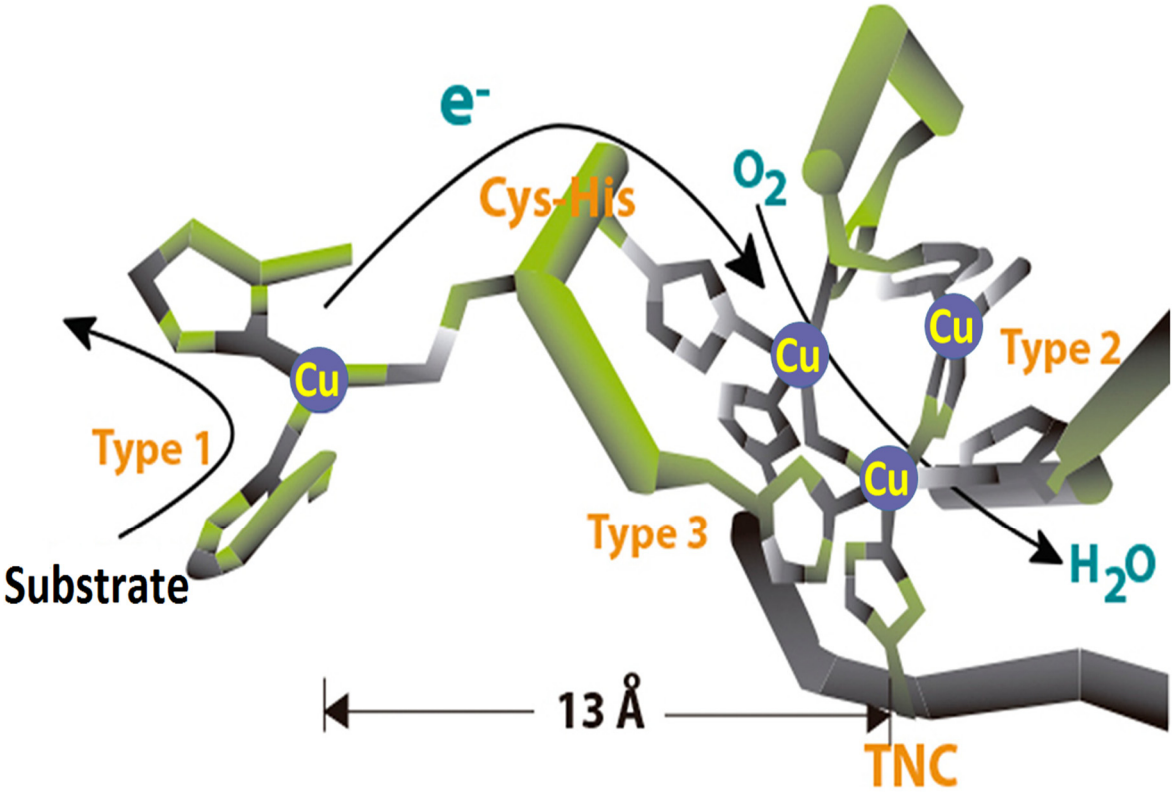

Figure 6.3. *Structure of the BOD active site with arrows marking flow of substrate, electron (e^-) from the T1 to the TNC, and O_2. Adapted from reference 365.*

6.4 Engineered *Mo*BOD

Three genetically engineered *Mo*BOD variants, S362C, A164C and N375C have been used in this study. They were modified to bear a free single cysteine residue in different positions on the enzyme surface (Figure 6.4) allowing site-specific attachment to the maleimide-modified

electrodes. The three variants were kindly provided by Dr Nicolas Mano from the Centre de Recherche Paul Pascal, Pessac, France.

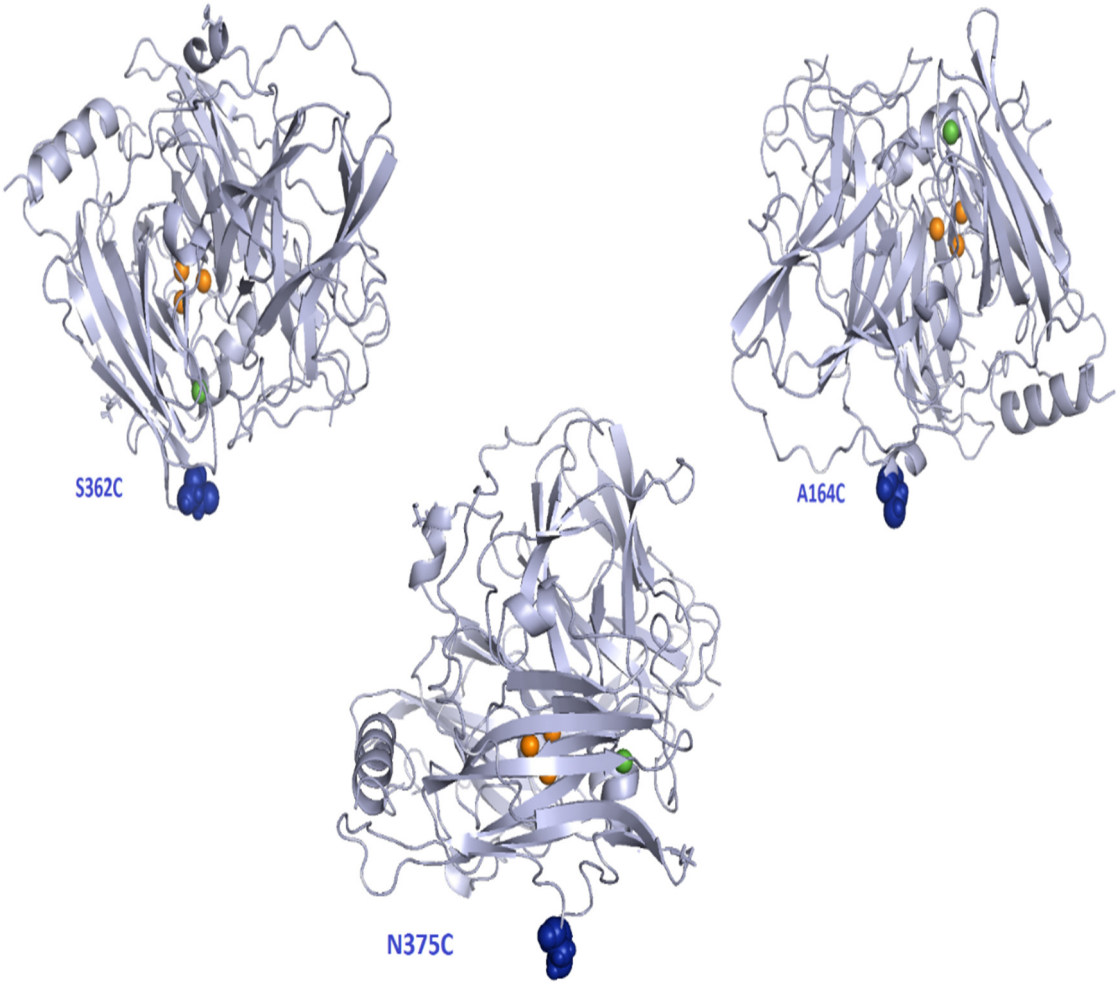

Figure 6.4. *Cartoon representation of the secondary structure of the three MoBOD variants. The free cysteine residues on the surface of the enzyme are highlighted in blue. (PyMol visualisations are based on the crystal structure of MoBOD, PDB code 2L9Y).*[362]

6.5 Method for the immobilization of BOD variants on GC/MWCNT electrodes

The modification of electrodes has been reported as an effective method to improve the interfacial electron transfer to BODs. These methods include covalent modification by diazonium coupling[366] or oxidation of amines,[367] physical adsorption[368] and utilization of functionalized carbon nanotubes (CNTs).[369] However, in many case they do not allow control over the orientation of the enzyme at the electrode surface. To address this problem of orientation several selective immobilization methods able to proceed under mild physiological conditions have received increasing attention.[22,78]

In this study, Multiwall carbon nanotube modified glassy carbon electrodes (GC/MWCNT) were selected as a template for carbon-based electrodes owing to their high surface area combined with comparatively low capacitance. These were modified with maleimide groups following a modular approach combining electrochemical surface attachment and solid phase synthesis methodology. The method for the covalent, site-specific immobilization of cysteine-modified proteins on GC/MWCNT electrodes has been fully described in Chapter 4 (see Scheme 4.3). The "linker" (*N*-Boc-1,6-hexanediamine) and the "passivating group" (*N*-(2-aminoethyl) acetamide) were electrochemically grafted to the GC/MWCNT electrodes from an acetonitrile solution containing 10 % of the "linker" and 90 % of the "passivating group", holding the potential at +2 V *vs.* SCE for 3 min. Afterwards, removal of the Boc-protecting group on the linker results in a mixed monolayer that should contain 10 % coverage of a free primary amine. Therefore, a "spacer" was introduced between the linker and the "reactive group" to lengthen the tether, making it more flexible and accessible for the enzyme. We decided to work with a six carbon-long spacer, by coupling *N*-Boc-6-aminohexanoic acid onto the amino-modified surface in order to have, at the end of the modification, a tether approximately 3 nm long. After de-protection of the Boc group on the spacer, *N*-maleoyl-β-alanine was coupled to the amino-modified surface resulting in a maleimide-modified electrode. The key aspect of our procedure is its modular approach that allows the single elements of the modification to be varied independently. Coupling of the BOD variant (instead of CDH variant) was carried out by drop casting 3 μL of BOD solution (at pH 7.0) on the electrode and leaving it at 4 °C overnight, allowing the most efficient use of small quantities of purified enzyme.

6.6 Direct electron transfer at BOD-modified electrodes

One of the main challenges of employing an enzyme as an electro-catalyst is to obtain an effective electronic connection between the enzyme and the electrode, this can be attributed to the significant size of the protein molecule and the anisotropy (state of having different sizes or characteristics along different axes) of its electronic properties.[345] A poor electrical connection will result in kinetic losses. In the DET mechanism, electrons transfer directly between an enzyme and an electrode. This mechanism relies on the ability of the BOD to accept electrons from an electron donor such as the electrode.

GC/MWCNT electrodes modified with the BOD-S362 variant (see Figure 6.4 for the structure) were tested for direct electron transfer (DET) by cyclic voltammetry in 200 to 100 mM phosphate-citrate (McIlvaine) buffer solution, pH 7.4 at 10 mV/s at different oxygen concentrations. The catalytic wave for DET is positioned at a potential that is principally determined by the properties of the enzyme molecule.[345] Figure 6.5 (black line) shows that the current onset starts at around 0.46 V *vs.* SCE and reaches a plateau at about 0.3 V *vs.* SCE. This

current is dependent on the concentration of O_2 in solution because it decreases with the increasing length of time that the solution is sparged with Ar, and ultimately disappears when all the oxygen is eliminate from solution. The position of the electro-catalytic wave agrees with that reported in the literature for adsorbed BOD at carbon nanofibers (CNFs),[364] gold disk / gold nanoparticles[370] and carbon nanotube (CNT)[26] electrodes. Thus, the catalytic current is assigned to the DET-type bioelectrocatalytic reduction of molecular oxygen by the immobilised BOD.

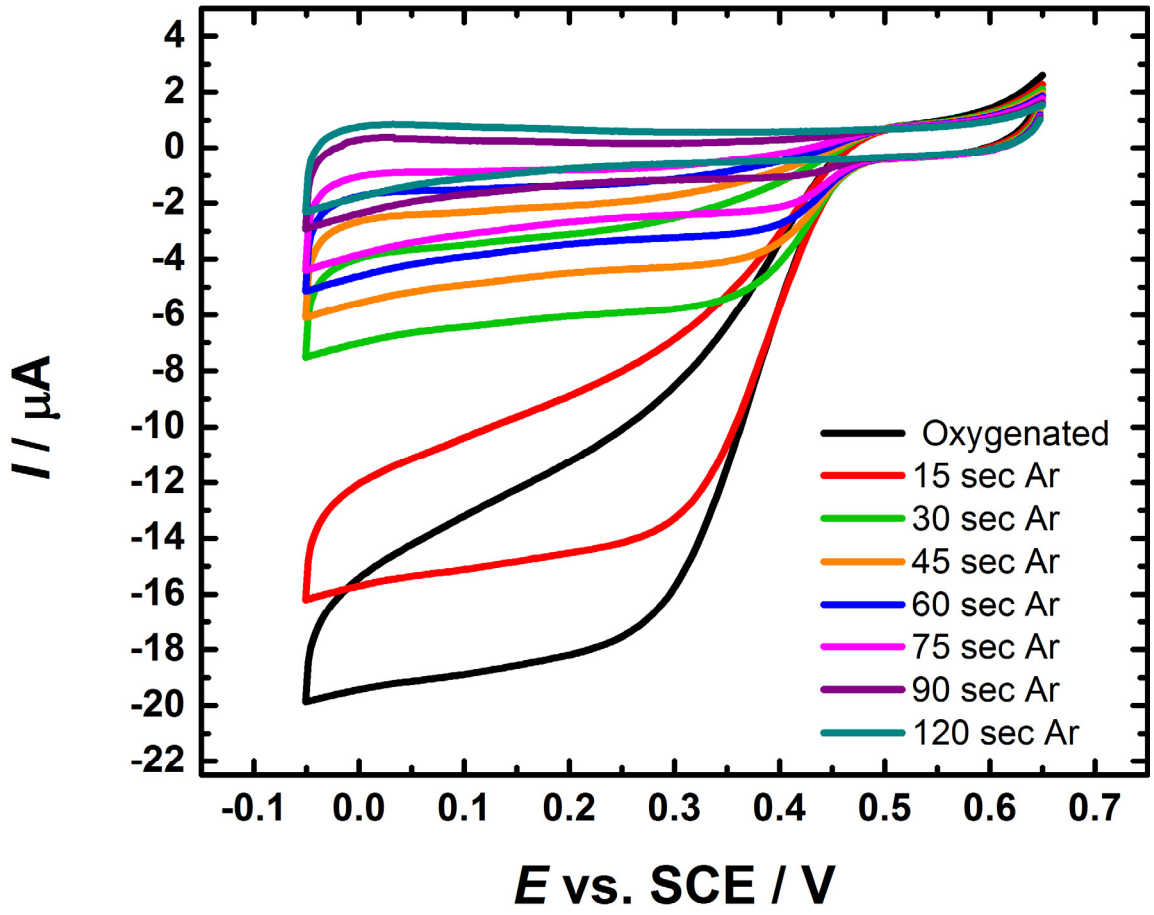

Figure 6.5. *Typical cyclic voltammograms showing the response of GC/MWCNT/BOD electrode in different oxygen concentration to ORR in 200 to 100 mM phosphate-citrate (McIlvaine) buffer solution, pH 7.0. CVs were scanned from -0.05 V to 0.65 V at a scan rate of 10 mV s^{-1}. The GC/MWCNT electrode was prepared by drop casting of 5 µL of 1 mg mL^{-1} MWCNT dispersion onto the cleaned surface of GC. The S362-BOD was immobilized on the GC/MWCNT electrode using covalent attachment.*

6.6.1 Covalent immobilization vs. physical adsorption

To verify that BOD was immobilized at the electrode surface through covalent bonding to the surface cysteine, we carried out a comparison using two different *Mo*BOD (cysteine-modified *Mo*BOD and a WT-*Mo*BOD). To this end, three different electrodes were prepared in which the covalent immobilisation method, as re-described in Section 6.5, and the physical adsorption

method were employed. The covalent immobilisation of *Mo*BOD variant S362C was performed on a maleimide-modified GC/MWCNT electrode. Meanwhile, the physical adsorption was done on two different electrodes; i) WT-*Mo*BOD was adsorbed onto a maleimide-modified GC/MWCNT electrode, and ii) *Mo*BOD variant S362C was adsorbed onto a bare unmodified GC/MWCNT electrode. The physical adsorption was made simply by drop casting 3 µL of the WT-*Mo*BOD or the *Mo*BOD variant S362C onto the aforementioned electrodes.

All GC/MWCNT electrodes modified with the BOD were examined for DET by cyclic voltammetry in 200 to 100 mM phosphate-citrate (McIlvaine) buffer solution, pH 7.4 at 10 mV/s (Figure 6.6). CVs were first carried out in argon–saturated solution (black lines). The background current capacitance is very similar for the electrodes used in Figure 6.6A and B (compare the black lines). However, the electrode in Figure 6.6C exhibits a bigger background current capacitance. This does not indicate that the quantity of MWCNTs is greater at the surface of the electrode (in Figure6.6C) but rather than that the maleimide-modification affects the electrode capacitance (in Figure 6.6A and B).

All GC/MWCNT/BOD electrodes were then investigated in oxygen-saturated buffer solution. Direct electron transfer was observed for both modification methods, all electrodes exhibit bioelectrocatalytic activity towards oxygen reduction, starting at onset potentials of around 0.46 V vs. SCE (Figure 6.6 green lines). For the covalently immobilized BOD at GC/MWCNT electrode (Figure 6.6A), a sigmoidal wave typical of the catalytic reduction of O_2 is observed as cyclic voltammetry proceeds, reaching a plateau at about 0.3 V vs. SCE. However, the catalytic currents for physically adsorbed BOD (Figure 6.6B and C) were lower than those for covalently immobilized BOD. Also, the reduction current for the electrode in Figure 6.6C is less than the current in Figure 6.6B by a factor of about 60 %. This might be attributed to a smaller quantity of enzyme molecules immobilised onto the electrode surface, *vide infra.*

The shape of the electrocatalytic waves is different depending on the corresponding immobilization technique (Figure 6.6). The main difference is the slope of the current at more negative overpotential, particularly, for WT-*Mo*BOD adsorbed onto the maleimide-modified GC/MWCNT (Figure 6.6B) and MoBOD variant S362C adsorbed onto the bare unmodified GC/MWCNT electrodes (Figure 6.6C). It has been reported that when a redox protein undergoes catalytic DET with an electrode, the voltammograms often exhibit a "residual slope" over a wide range of electrode potential, even though it is basically expected that it should reach a plateau. Indeed, this behavior is obtained with several multi-centered redox enzymes.[16, 371-373] However, less complex enzymes such as cytochrome *c* peroxidase[374] also show this behavior. Thus, it is not likely that this performance results from an electric field effect on the rate of intramolecular ET.[375] It has been proposed that disorder among the immobilised enzyme molecules participating in DET results in a sped of spread electron

transfer rates reflected by the trailing edge in the catalytic cyclic voltammogram.[375] Kinetic models that obtain information from voltammograms provide useful and detailed information. Indeed, several models have been developed by Tsujimura *et al.*,[376] Armstrong *et al.*,[375] and Hexter *et al.* to explain that "residual slope". On one hand, Tsujimura *et al.*,[376] assumed that all the electrochemically active enzyme molecules have an identical orientation. Thus, heterogeneous ET can be defined by a unique average rate constant, k_0. On the other hand, Armstrong[375] and others[377-378] have proposed a different kinetic model to describe this mechanism. Their model explains reversible bioelectrocatalytic reaction in which electrons enter or exit the redox protein in sequential single-electron steps; it is believed that enzymes adopt an arrangement of slightly different orientations. Consequently, the distance between the redox center and the electrode surface is equally scattered between a minimal distance (d_{min}), and a distance (d_{min} + d_0). The product βd_0 (*Eq.* 6.1) reveals the distribution of orientations and determines the shape of the wave at increasing over-potential.[345] The slope of i vs E is given by

$$\frac{di}{dE} = \frac{i_{\lim}}{\beta d_0}\frac{F}{2RT} \qquad (Eq.6.1)$$

Where β is the decay constant in the Marcus theory (see Chapter 1, Section 1.1), R is the universal gas constant, T is the absolute temperature and F is the Faraday constant. Hence, the green voltammograms in Figure 6.6B and C are consistent with numerous orientations of BOD at the surface of the electrode, which is responsible for changing ET rates.

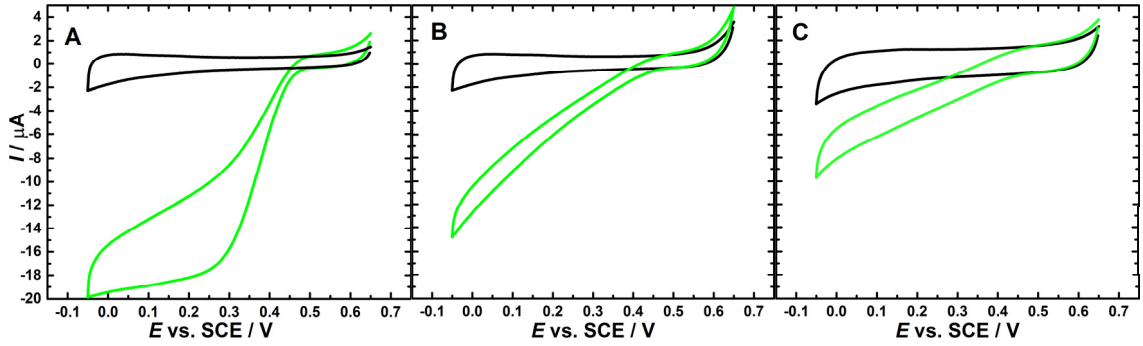

Figure 6.6. *Cyclic voltammograms recorded at maleimide-modified electrodes (A, B), bare unmodified GC/MWCNT electrode (C) with BOD variant S362 (A, C) and WT-MoBOD (B). CVs were carried out in oxygen–saturated (green lines) and deoxygenated (black lines) 200 to 100 mM (McIlvaine) phosphate-citrate buffer solution, pH 7.0, sweeping the potential at 10 mV / s from -0.05 to 0.65 V vs. SCE.*

Thus, the results in Figure 6.6A are consistent with covalent binding of the cysteine-modified *Mo*BOD at the maleimide-modified electrodes. The higher catalytic currents and the sigmoidal

wave typical of the catalytic reduction of O_2 obtained with the covalently modified electrode (Figure 6.6A) can be explained by the fact that the covalently immobilized enzyme is held in a more suitable orientation for DET as compared to the randomly orientated physically adsorbed BOD (Figure 6.6B and C).

Indeed, to assess the productivity of the adopted approach toward enzymes orientation, it is conceivable to assess the increase in DET, which however reflects also a greater quantity of enzyme molecules immobilised onto the electrode. Therefore, the comparison DET/MET, which is a reciprocal function of the quantity of perfectly oriented enzymes, is more precise.[345]

Thus, to exclude the possibility that the different catalytic currents in Figure 6.6 might be obtained from different enzyme loading on electrodes surfaces, 2, 2'-azino-bis (3-ethylbenzothiazoline-6-sulphonic acid) (ABTS), was introduced as a mediator.[25] The mediator in the solution should react with all of the enzyme molecules on the surface of the electrode.[36] Therefore, the mediated electron transfer (MET) experiment can be employed as an approach to relate the currents observed in Figure 6.6 to the real amounts of the BOD on each electrode. To this end, the same three electrodes were re-tested by monitoring the catalytic current caused by MET in the presence of ABTS as a mediator (Figure 6.7).

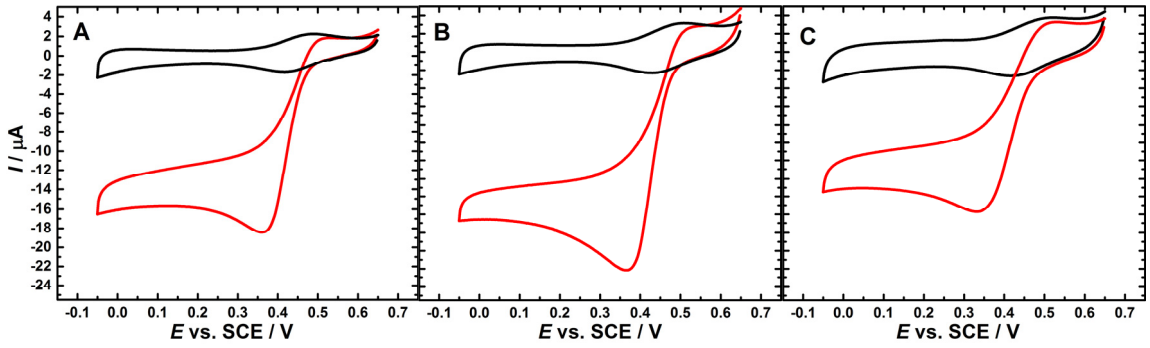

Figure 6.7. *Cyclic voltammograms recorded at maleimide-modified electrodes (A, B), bare unmodified GC/MWCNT electrode (C) with BOD variant S362 (A, C) and WT-MoBOD (B). CVs were carried out in oxygen–saturated (red lines) and deoxygenated (black lines) 200 to 100 mM phosphate-citrate (McIlvaine) buffer solution in presence of 0.3 mM ABTS, pH 7.0, sweeping the potential at 10 mV / s from -0.05 to 0.65 V vs. SCE.*

From the sigmoidal wave typically obtained for the catalytic reduction of O_2 in Figure 6.6A (*Mo*BOD variant S362C was immobilised at the maleimide-modified GC/MWCNT electrode via the thioether bond), the addition of ABTS has a negligible effect on the reduction wave shape as well as the catalytic current (Figure 6.7A). This experiment indicates that all immobilized BOD are favorably orientated towards the enzyme active site (most probably the T1 copper site). On the other hand, the addition of ABTS for the electrodes used in Figure 6.6B (WT-*Mo*BOD on maleimide-modified GC/MWCNT electrode) and in Figure 6.6C (*Mo*BOD

variant S362C on bare unmodified GC/MWCNT) generates an increase of the bioelectrocatalytic oxygen reduction current (Figure 6.7B and C), which verifies that not all immobilized BOD are favorably oriented on the electrode surfaces. Moreover, the lower MET current value for the electrode used in Figure 6.7C compared with that used in Figure 6.7B is consistent with the current for the same electrode in Figure 6.6C being less than the current observed for the other electrode in Figure 6.6B. Thus, the more catalytic current obtained in Figure 6.6B compared to the one in Figure 6.6C was due to higher BOD surface coverage.

6.6.2 The influence of the cysteine position

DET between BOD and an electrochemical interface may be achieved via suitable modifications of the electrode surface.[364, 367] Efficient DET requires a good connection between the electrode and enzyme with the correct orientation and favourable distance as suggested by Marcus theory.[364]

As we have already shown in Section 6.5, the free surface cysteine reacts with maleimide groups previously introduced at the electrode surface. In this way, we would expect the different BOD variants (see Figure 6.4 for the structures) to be immobilised with different orientations on the electrode, depending on the position of their free cysteine residues. Figure 6.8 shows the presumed orientations for the three *Mo*BOD variants on maleimide-modified electrodes. The different variants should have different electron transfer distances (distance between the T1 copper cluster and the electrode surface) and, consequently, different direct electron transfer rates.

To test this prediction, maleimide-modified GC/MWCNT electrodes were used to immobilise the three different BOD variants. DET and MET of the BOD-modified GC/MWCNT electrodes (for each variant) are tested by cyclic voltammetry in oxygen-saturated 200 to100 mM phosphate-citrate (McIlvaine) buffer solution, pH 7.4 at 10 mV / s before and after and the addition of 0.3 mM ABTS (Figure 6.9). Direct electron transfer was observed for the three variants (Figure 6.9, green lines), all electrodes exhibit bioelectrocatalytic activity towards oxygen reduction, starting at onset potentials of around 0.46 V vs. SCE. For the GC/MWCNT electrode modified with S364C variant (Figure 6.9A, green line), a sigmoidal wave typical of the catalytic reduction of O_2 is observed as cyclic voltammetry proceeds, reaching a plateau at about 0.3 V vs. SCE. However, the currents did not reach a plateau for any of the other variants (Figure 6.9, B and C, green lines), meaning that the interfacial electron transfer was a quite slow process.[345, 379] It should be noticed that CVs were reproduced on at least two different electrodes for each variant. Thus, the shape of the CVs during catalysis is different depending on the variant. This can be attributed to the different orientation of the BOD variants on the

electrode surface, because each variant has a free cysteine group in a different position on the surface of the enzyme (see Figure 6.8).

The same electrodes were re-tested for MET. All electrodes exhibit mediated bioelectrocatalytic activity towards oxygen reduction, starting at onset potentials of 0.5 V vs. SCE (Figure 6.9, red lines). The mediator in the solution was employed to relate the ORR current observed in the DET mode for each variant to the real amount of that variant on the electrode surfaces. Experiments were carried out in the presence of ABTS as a mediator. From the results, it is clear that the amounts of the S362C-BOD and A164C-BOD on each electrode is almost the same. Thus it can be concluded that the fast direct electron transfer achieved for the S362C-BOD is due to a more favourable orientation of this variant on the surface of the electrode rather than due to higher enzyme surface coverage.

The N375-BOD variant was re-tested again but to no avail. The results were compared to the other variants and there were very small reduction currents before and after the addition of 0.3 mM ABTS (Figure 6.9C). This was reported to our collaborator (the enzyme supplier) and a new batch of N375C was prepared. However, the new N375C batch had a similar low activity, like the old batch, when compared to the other variants. Therefore, the bad performance obtained in Figure 6.9C can be accounted for by the low enzyme activity due to the mutation. Indeed, such behaviour (Figure 6.9C) can be taken as evidence that the different shape of the CVs during catalysis obtained for variant A164C (Figure 6.9B) compared to variant S362C (Figure 6.9A) was not due to less enzyme activity rather than a better orientation of the S362C variant which allows the mononuclear T1 copper cluster to be brought closer to the electrode surface with the favourable distance as suggested by Marcus theory.

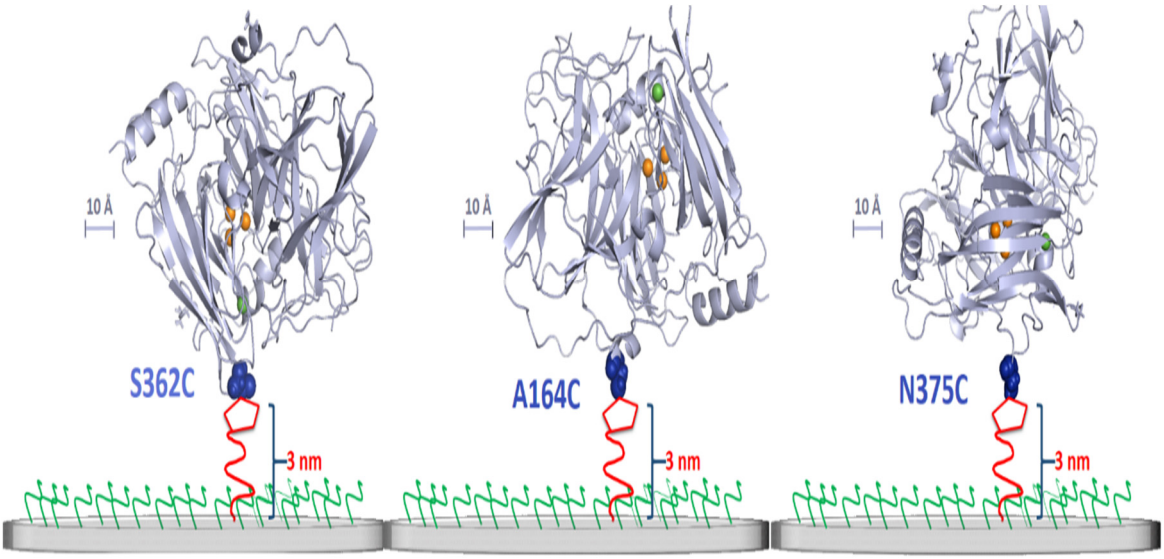

Figure 6.8. *The presumed orientations for the five MtCDH variants on to maleimide-modified electrodes. The variants images were obtained with PyMol software, PyMol visualisations are based on the crystal structure of MoBOB, PDB code 2L9Y.*[362]

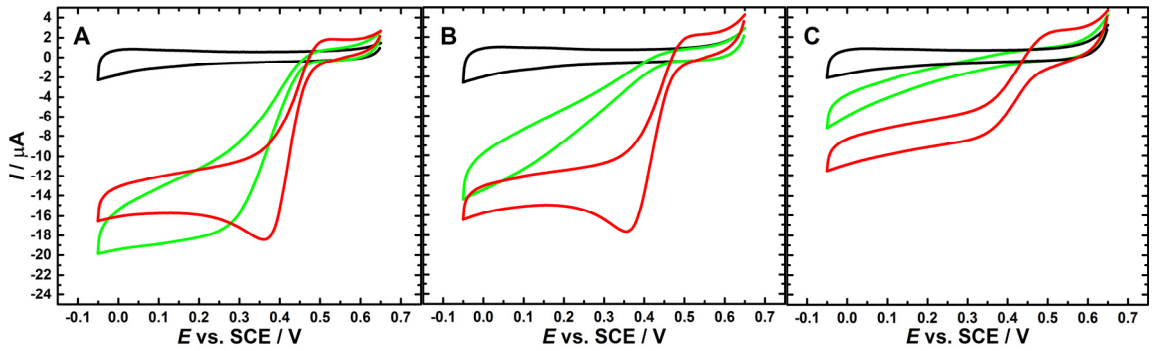

Figure 6.9. *Typical cyclic voltammograms showing the response of GC/MWCNT electrodes for various variants: (A) S362, (B) A164 and (C) N375 to ORR in oxygen-saturated (red lines) and deoxygenated (black lines) 200 to 100 mM phosphate-citrate (McIlvaine) buffer solution, pH 7.0, and after the addition of 0.3 mM ABTS (red lines). CVs were scanned from -0.05 V to 0.65 V at a scan rate of 10 mV s^{-1}. The GC/MWCNT electrodes were prepared by drop casting of 5 µL of 1 mg mL^{-1} MWCNT dispersion onto the cleaned surface of GC. The BOD variants were immobilised at the electrode surfaces via the thioether bond.*

6.6.3 Stability of the BOD-modified electrodes

The stability over time of the bioelectrocatalytic activities of the BOD-modified GC/MWCNT electrodes (S362-BOD) to bioelectrocatalytic reduction of dioxygen was also studied. To this aim, a comparison between the stability of the BOD immobilised through maleimide and a physically adsorbed WT-BOD on maleimide-modified GC/MWCNT electrode was performed. The storage stability of the GC/MWCNT electrodes modified with BOD was investigated by keeping the electrodes in a deoxygenated wet condition in the refrigerator (4 °C) for six days. Figure 6.10 shows that the enzyme immobilised through the thioether bond (black line) is much more stable than the control for the WT-BOD on maleimide-modified GC/MWCNT electrode (red line), where the catalytic response decays much more rapidly. The GC/MWCNT electrode covalently modified with S362C-BOD variant electrodes can still retain about 95% of the initial response after 3 days storage as shown in Figure 6.10. On the other hand, the GC/MWCNT electrode physically modified with WT-*Mo*BOD retains ca. 40% of its initial activity.

By analogy with our previous study with CDH (see Chapter 4, Section 4.7.2.2.), it is clear that CDH was much more stable (for about two months) at the surface of the maleimide modified GC/MWCNT. However, this would support a conclusion that the dramatic decay on the BOD activity after 3 days is because of the enzyme denaturation, probably due to loss of copper from the enzyme-active site. Indeed, this conclusion can be supported by the finding of numerous studies which suggested that the decrease in cathodic current over the time cannot be related

to BOD loss but most probably to enzyme denaturation or structural rearrangement on different electrode surfaces.[380-382]

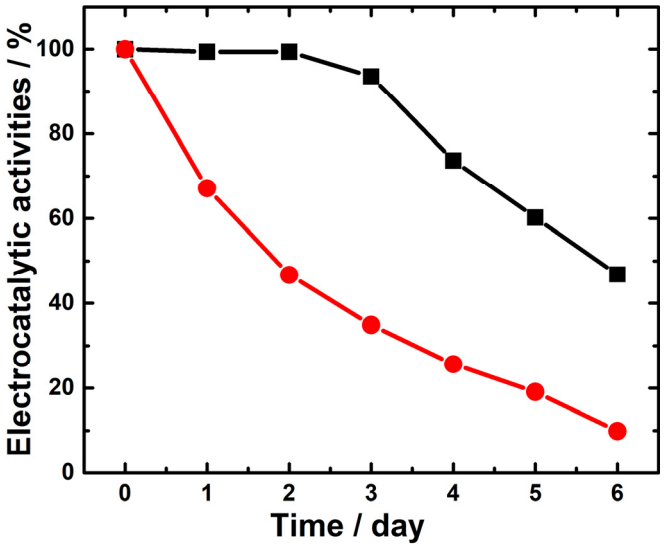

Figure 6.10. *The maximum electro-catalytic activities of the maleimide modified GC/MWCNT electrodes covalently modified with S362C-BOD variant (black line) and physically modified with WT-BOD (red line) over a period of time. CVs were recorded oxygen-saturated 200 to 100 mM phosphate-citrate (McIlvaine) buffer solution, pH 7.0, sweeping the potential at 10 mV / s from -0.05 to 0.65 V vs. SCE.*

6.7 Effect of solution pH

It is widely believed that the cathodic current onset starting at around 0.46 V *vs.* SCE at pH 7 (see Figure 6.5) corresponds to the BOD-T1 site.[383-386] Indeed, it has been difficult to obtain electrochemical evidence of BOD electroactive at lower potentials. However, some authors tried to assign peaks observed at 300–500 mV vs. Ag/AgCl to the BOD-T3 site[20, 383, 387] and peaks in the potential window of 100–300 mV vs. Ag/AgCl to the BOD-T2 site.[384, 387]

In this study, the cyclic voltammetry measurements of BOD at maleimide-modified GC/MWCNT electrodes was carried out (*vs.* SMSE, *vide infra*) within the pH range of 4.0 to 7.6 (Figure 6.11A). An almost constant current of about 16 μA was observed over the pH range of 4.0–7.0. The onset potential for reduction of O_2 was pH dependent and shifted negatively with increasing pH (Figure 6.11B). With decreasing pH from 7.6 to 6 (using a universal buffer system, 200 to 100 mM phosphate-citrate (McIlvaine) buffer) the onset potential for reduction of the BOD-T1 site shifted positively with a slope -dE/dpH of about 57 mV. According to the Nernst equation -dE/dpH = 0.0592 x (m/n), with m being the number of proton transferred and n being the number of electrons transferred, such a value (57 mV/pH) is in an excellent agreement with a value of 59 mV/pH expected for a redox process involving transfer of an equal number of electrons and protons.[388] However, when the pH decreased further (from 6.0

to 4.0) a slope -d*E*/dpH of 28 mV was obtained, implying that two electron transfer is accompanied with one proton transfer at this pH window. Thus, in the pH range of 4.0 to 7.6, there is one value of pH at which the slope of *E* vs. pH for the BOD-T1 site changes, namely, at a pH close to 6.0.

Filip and Tkac[389] recently reported, in a detailed study, a decrease of the redox potential for the T1 site with pH with a slope of 66 mV/pH in two different buffer systems (acetate and HEPES) for pH between 5.0 and 7.5. Another study by Weigel *et al.*[390] observed a slope of 54.5 mV/pH in the pH range of 4.0 to 8.0 using a citrate-phosphate buffer for dependence of a formal redox potential of the BOD-T1 site on pH. However, Shleev *et al.*[391] stated in a detailed study a decrease of a redox potential for the BOD-T1 site with pH with a slope of 23 mV/pH in a universal buffer (phosphoric, boric and acetic acids) at pH between 4.2 and 7.0. The reason for the disagreement between the latter report by Shleev *et al.* and the others is unknown. Nevertheless, it can be attributed to a different enzyme immobilization method and/or different buffer used for the cyclic voltammetry measurements.[389] Indeed, it has often been suggested that the choice of buffer components can have a significant impact on interfacial electrochemistry of various enzymes.[392-394]

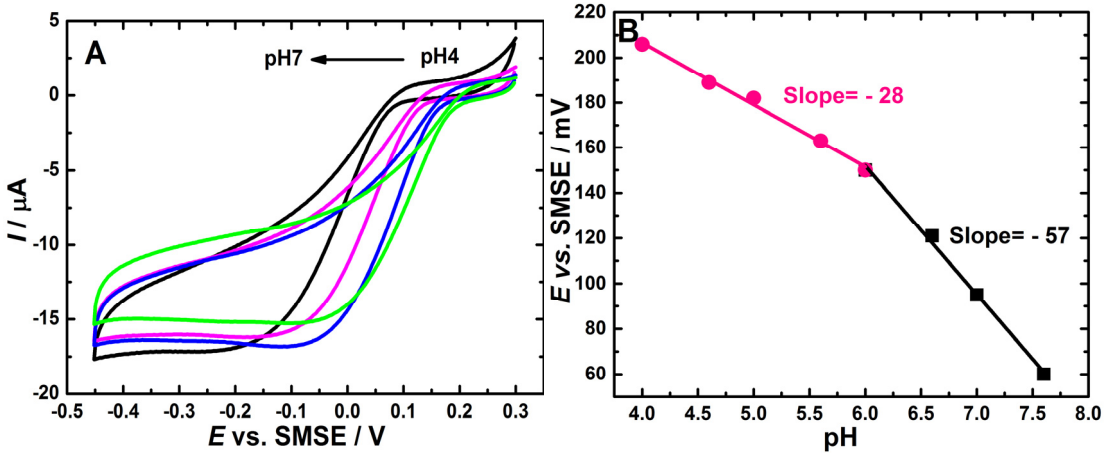

Figure 6.11. *(A) Cyclic voltammograms of BOD at maleimide-modified GC/MWCNT electrode in various oxygenated solutions (pH 4.0, 5.0, 6.0, and 7) at 10 mV s^{-1}. Measurements were performed in universal buffer system (200 to 100 mM phosphate-citrate (McIlvaine) buffer) vs. SMSE. (B) The onset potential of reduction of O_2 plotted vs. pH.*

To the best of our knowledge, in a very small number of examples the effect of the amino acids involved in a proton-coupled electron transfer has been examined during the intensive electrochemical studies of BODs. Indeed, the behavior obtained in Figure 6.11B is consistent with previous studies of the potential/pH dependence of other copper enzymes, such as azurin[389,395] or CueO.[396]

On one hand, a recent study by Cosnier *et al.*[25] has suggested that a pK_{ox} of 6.0 (K_{ox} is the proton dissociation constant for the oxidized form of BOD-T1 copper) is related to the acid/base couple of an amino acid, such as histidine (His) in the vicinity of the BOD-T1 copper center (see Scheme 6.1), which effects structural rearrangement of copper upon the redox process. On the other hand, there is agreement that two acidic amino acids, namely, glutamic acid Glu and aspartic acid Asp,[389] which are highly conserved amongst all MCOs,[397-400] are crucial for the enzymatic activity with participation in proton transfer during catalysis.[389] In the current study, Glu/464 and Asp/107 are present in the *Mo*BOD in a close proximity to the trinuclear cluster (TNC), see Scheme 6.1. The *Mo*BOD structure was rendered with PyMol software, the PyMol visualisations are based on the crystal structure of *Mo*BOB (PDB code 2L9Y).[362] In their work Filip and Tkac[389] suggested that the Asp identified in the exit channel of the *Mv*BOD-TNC is involved in the reductive separation of the oxygen-oxygen bond at acidic pH, in supporting protonation of the hydroxyl groups bound to the BOD-T2 copper ion or in governing protonation of a Glu residue and in the activation of proton of the BOD-T2 bound water at high pH. However, Glu located in the O_2 entrance channel of the *Mv*BOD-TNC was shown to be involved in a proton transfer to the peroxide during the reductive separation of the oxygen-oxygen bond at around pH 7.[397, 401] Hence, the break point observed at pH 6 (Figure 6.11B) can be attributed to the activity of the Asp/107 residue. A question that arises from this conclusion is: Why do amino acids identified in the BOD-TNC influence the BOD-T1 electrochemistry? However, a study conducted by the modulation of redox potential of the BOD-T1 site by different states (various oxygen functionalities) of the BOD-TNC have shown that BOD-T1 site is firmly interconnected in terms of electrochemical disruption by the BOD-TNC.[389,402]

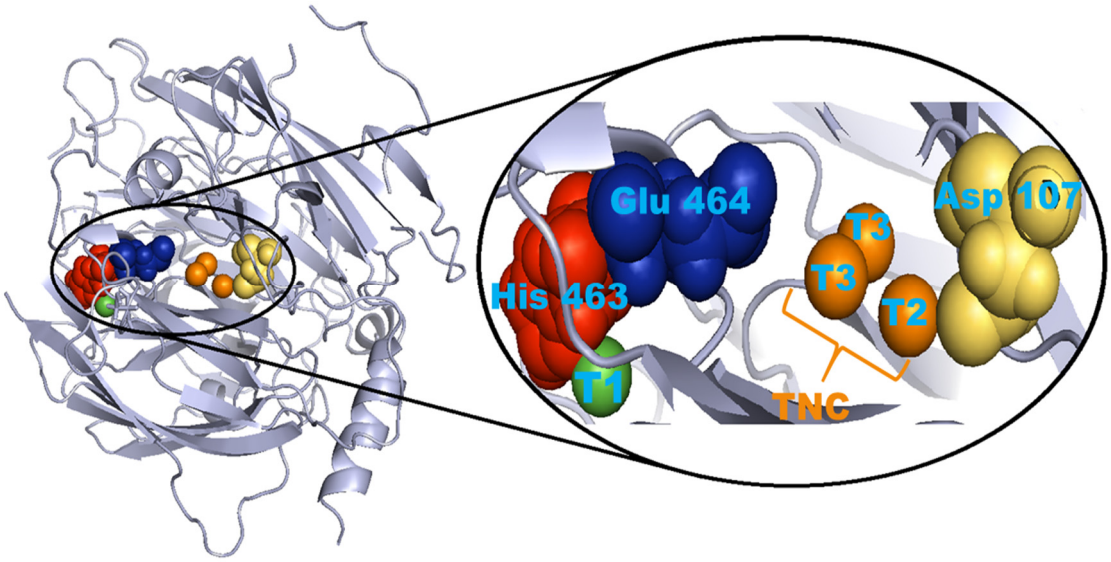

Scheme 6.1. *A schematic representation of BOD with the Cu active sites and positions of Asp 107, Glu 464 and His 463 amino acids in the enzyme shown. The BOD structure was rendered with PyMol software, PyMol visualisations are based on the crystal structure of MoBOB, PDB code 2L9Y.*[362]

It is worth mentioning that this study was initially carried out using a SCE as the reference electrode. However, unusual behavior was observed, namely at pH 4 (see Figure 6.12A), apart from a peculiar CV shape, by proceeding from pH 5 to pH 4, no onset potential shift in the reduction of O_2 was witnessed. This behaviour could be attributed to chloride ion contamination from the SCE. To verify this conclusion, a control experiment was performed using a saturated mercurous sulfate electrode (SMSE) instead of SCE, the potential was then converted with respect to that of a SCE by adding 0.395 V[306] (see black line in Figure 6.12B). A normal sigmoidal wave typical of the catalytic reduction of O_2 is observed as cyclic voltammetry proceeds. After that the SMSE was replaced by an SCE and the the cyclic voltammetry measurements were repeated immediately, after 5 and 10 minutes (see coloured lines in Figure 6.12B). On one hand, in the forward scan, the onset for O_2 reduction shifts down and is observed at less positive potential. On the other hand, the reverse scan is less affected, confirming that the chloride contamination from the SCE causes an inactivation process of BOD for O_2 reduction. Detailed discussion will be provided in the next Section.

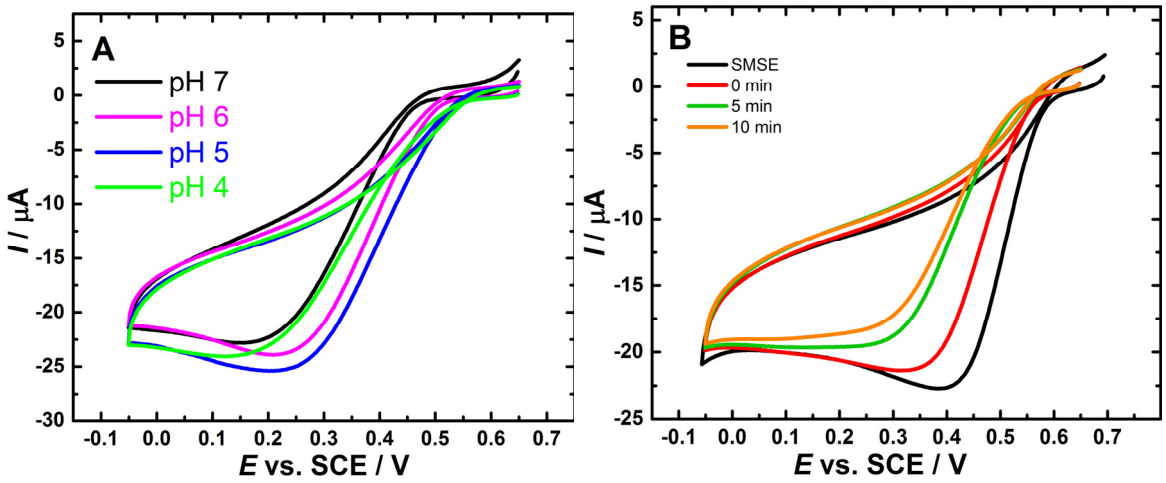

Figure 6.12. *(A) Cyclic voltammograms (first scan) of BOD at a maleimide-modified GC/MWCNT electrode in various oxygenated solutions (pH 4.0, 5.0, 6.0, and 7) at 10 mV s^{-1}. Measurements were performed in universal buffer system (200 to 100 mM phosphate-citrate (McIlvaine) buffer) vs. SCE. (B) Cyclic voltammograms of BOD at a maleimide-modified GC/MWCNT electrode in oxygenated (pH 4.0) 200 to 100 mM phosphate-citrate (McIlvaine) buffer solution at 10 mV s^{-1}. Measurements were performed vs. SMSE then converted with respect to that of a SCE by adding 0.395 V (black line), then SMSE was replaced by SCE and the the cyclic voltammetry measurements were repeated immediately, after 5 and 10 minutes (coloured lines).*

6.8 The influences of pH and chloride on the redox state of BOD

In recent years, numerous BOD investigations[345, 356, 364, 403] have been conducted to explore the precise nature of the electron transfer, as outlined in Scheme 6.2. Basically, after the substrate oxidation at the T1 site, electrons are transferred to the TNC where the reduction of O_2 occurs

via two, two-electron steps. The first step produces the peroxide intermediate (PI). In the second two-electron step, the O-O bond is cleaved with a fast rate constant leading to the formation of the native intermediate (NI).[404] Where, in the absence of substrate, NI gradually decays to the resting oxidized (RO) form and only reenters the catalytic cycle upon reduction with a substrate. Whereas, in the presence of substrate, NI is reduced to the fully reduced form of the enzyme and is ready for another catalytic cycle.[364] Another resting state, called the alternative resting form (AR), was identified in some BODs. These two resting forms were shown to exist in *Mo*BODs and *Mv*BOD.[356] For AR, It was demonstrated that only one of the three TNC Cu site is oxidized. Meanwhile in RO, all three TNC Cu site are oxidized.[403]

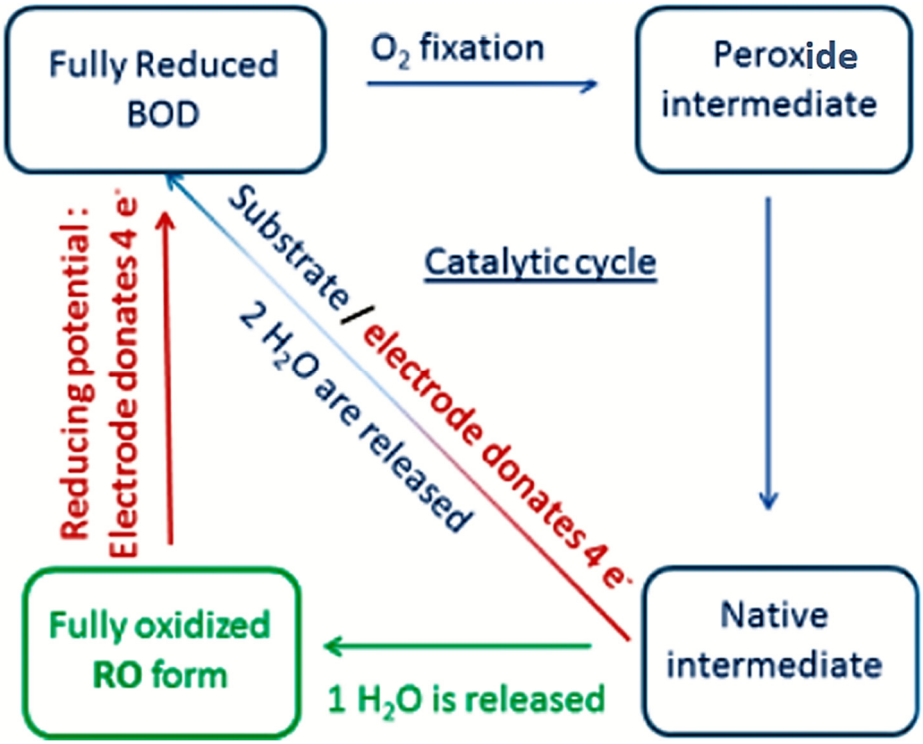

Scheme 6.2. *A mechanism for the O_2 reduction by BODs based on the study by Solomon* et al.[404] *The catalytic cycle is colored blue; the non-catalytically related forms are colored green, and electrode-driven redox changes are colored red. Adapted from reference 364.*

Since a different resting structure have been detected in multicopper oxidases (MCOs) and might be even mixed, hence, there has been some sort of disagreement as to which is the pertinent form for initiation for catalysis.[397] However, a spectroscopic characterization, supported by crystallographic data has been suggested that *Mo*BOD (our model enzyme) has two distinct inter-convertible resting forms: the RO form, produced upon re-oxidation of fully reduced enzyme, and the AR form, detected in the as-isolated enzyme and upon Cl^- addition to RO,[356] Scheme 6.3 shows the AR formation and reactivation for BOD from *Bacillus pumilus* in the presence of chloride ions based on the work of Lojou *et al.*[364]

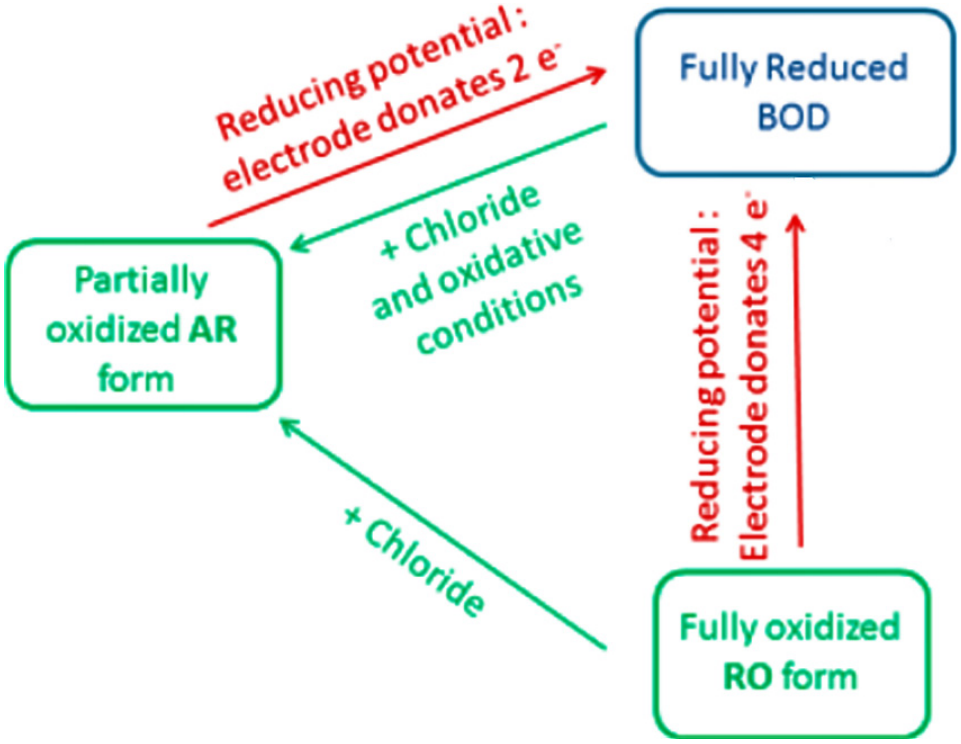

Scheme 6.3. *AR formation and reactivation in the presence of chloride ions based on the work of Lojou et al.*[364] *The non-catalytically related forms are colored green, and electrode- driven redox changes are colored red. Adapted from reference 364.*

Herein, we electrochemically define both the RO and the AR forms of *Mo*BOD and show that they can interconvert. Figure 6.13 shows the response of a GC/MWCNT/BOD electrode to ORR in oxygenated 200 to100 mM phosphate-citrate buffer solution, pH 7.0, first scan (black line) and second scan (red line). Essentially, the voltammograms of the first and second scans are not the same, with onset of catalytic current monitored at ~+425 mV (*vs.* SCE) on the first scan, shifting to ~+470 mV on the second scan. This behavior is similar to the that observed in Laccase from *Podospora anserine* (PaL)[403] where the lower onset potential in the first scan was ascribed to reduction of the one-electron oxidized Cu of the AR-form TNC after which electrocatalytic turnover was launched with electron transfer via the T1 Cu, consistent with the higher initiation potential detected on the following scan. Where the RO form (Figure 6.13, red line) is catalytically active under experimental conditions, whereas the AR form (Figure 6.13, black line), needs a low potential to be fully reduced for O_2 reactivity. This can be attributed to the fact that the AR form has a partially reduced TNC that is not efficient for ORR. Therefore, the AR form can be activated for O_2 catalysis at adequately low electrode potentials, consistent with the observation of Kjaergaard *et al.*[356] of a lower potential TNC Cu, whereas the RO form is activated at the higher potential of the T1 Cu.

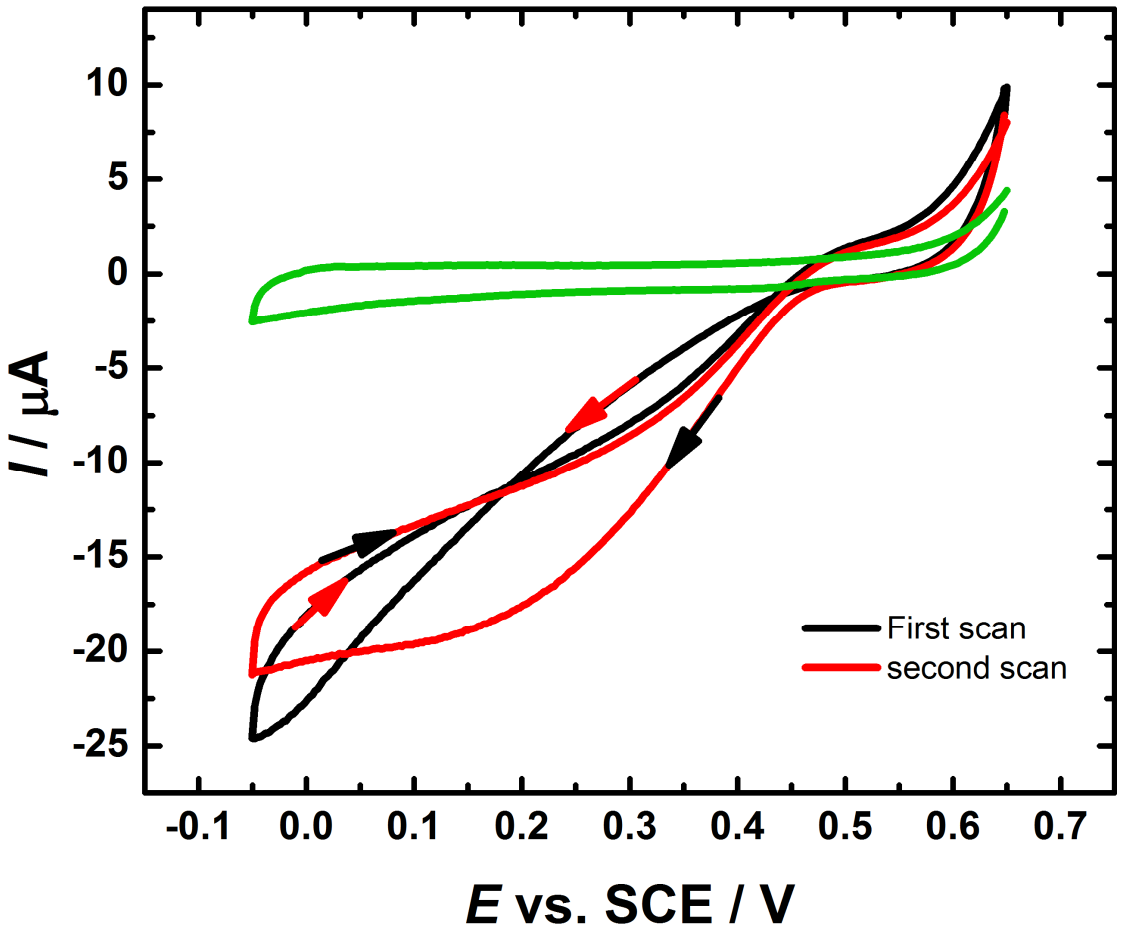

Figure 6.13. *Typical cyclic voltammograms showing the response of a GC/MWCNT/BOD electrode to ORR in deoxygenated (green line) and oxygenated 200 to100 mM phosphate-citrate (McIlvaine) buffer solution, pH 7.0, first scan (black line), second scan (red line)at 10 mV* s^{-1}*. The S362- BOD was immobilized on the GC/MWCNT electrode using covalent attachment.*

The effects of pH and chloride ions on the BOD activity are of great importance, particularly if BOD-based bio-cathodes are projected for BFCs operating in physiological conditions.[360] In this section, GC/MWCNT electrodes covalently modified with *Mo*BOD were further electrochemically studied in 200 to 100 mM phosphate-citrate (McIlvaine) buffer solution with varying NaCl concentrations at different pH. Indeed, apart from a very recent contribution,[364] there has not been a detailed study undertaken to understand the related effect of Cl^- and pH on the redox state of immobilized BODs. Pertinent information can be acquired from the catalytic voltammograms of the immobilized enzyme, particularly because this technique can define the redox potential of a redox species. For instance, it allowed investigation of the mechanism of O_2 reduction by BOD on electrodes.[341, 405] To this aim, the covalent immobilisation of *Mo*BOD variant S362C was performed, as re-described in Section 6.5, on a maleimide-modified GC/MWCNT electrode. The influence of chloride on BOD activity as a function of pH was investigated by using cyclic voltammetry. Figure 6.14 shows the response of GC/MWCNT/BOD electrode to ORR in oxygenated 200 to 100 mM phosphate-citrate

(McIlvaine) buffer solution (A) pH 4 (B) pH 6 and (C) pH 7 (black lines) and after the addition of different concentrations of Cl^- (coloured lines).

At pH 4, before the addition of NaCl, the onset for O_2 reduction is observed at 0.6 V vs. SCE (Figure 6.14A, black line). A sigmoidal wave typical of the catalytic reduction of O_2 is observed as cyclic voltammetry proceeds. After addition of 1.5, 5, and 10 mM NaCl to the electrolyte, a progressive decrease in the catalytic current occurs. Furthermore, on the forward scan, the onset for O_2 reduction shifts down by 50, 100, and 120 mV respectively. The reverse scan is less influenced by NaCl, suggesting that O_2 reduction is more efficient after the enzyme has been exposed to reducing potentials. This unusual CV shape reveals an inactivation/reactivation of BOD for O_2 reduction. Similar behavior has been obtained with the thermostable BOD from *Bacillus pumilus* adsorbed on a graphite electrode modified with CNFs as reported previously.[364] Also, our results are in good agreement with the literature data reported by Dagys *et al.*[406] for the influence of F^- on O_2 reduction by a high-potential laccase (LCA). In their work Dagys *et al.*[406] demonstrated that, F^-, a well-known LAC inhibitor, reduced both bioelectrocatalytic current and onset potentials of O_2 reduction, and these effects were more pronounced at low pH. Reportedly, BODs were considered to be Cl^- resistant, as opposed to laccases.[345, 360, 363-364] However, taking into account that both Cl^- and OH^- bind to the T2/T3 Cu cluster and obstruct the IET from the T1 site to the Cu cluster without affecting the ability of TNC to bind O_2,[407] It can be concluded that the inhibition by chloride is due to the formation of the alternative resting form of the enzyme.

The peculiar CV shape in the presence of chloride (Figure 6.14A) with a reactivation process at low potential (Figure 6.13), may be attributed to the coexistence of the two resting forms of the enzyme, i.e., fully oxidized RO and partially oxidized AR, as previously suggested for *Mo*BOD.[356] However, the orientation of the T2/T3 cluster towards the electrode surface is not favorable for DET. Nonetheless, a very recent modulation study[408] have been focused on the "curvature effect" of mesoporous structures on the long range electron transfer kinetics of the BOD active-site. This study assumed a spherical enzyme with a radius of *r*, an active site situated at a certain distance from the center of the enzyme, and a spherical pore with a radius of R_p in which the enzyme is immobilized. The authors have concluded that when R_p becomes close to *r*, the mesoporous electrodes are able to provide platforms suitable for DET-type bioelectrocatalysis of enzymes. Such "curvature effects" of mesoporous electrodes become particularly important for rather large sized enzymes such as BOD. To test this hypothesis, additional work needs to be performed. However, the study was stopped at this point due to very low enzyme availability and time limitation.

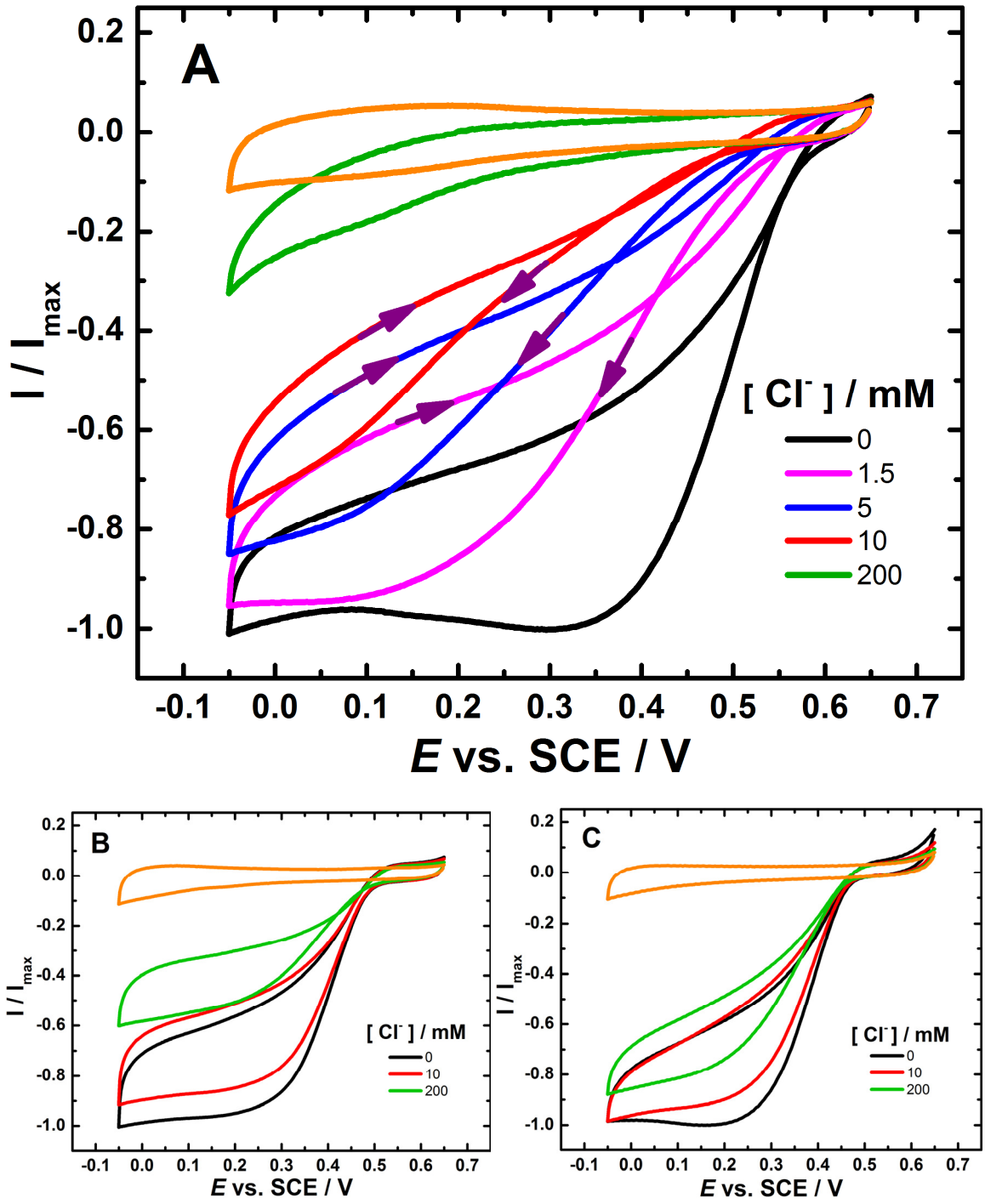

Figure 6.14. *CVs showing the response of GC/MWCNT/BOD electrode to ORR in oxygenated 200 to 100 mM phosphate-citrate (McIlvaine) buffer solution (A) pH 4 (B) pH 6 and (C) pH 7 (black lines) and after the addition of different Cl^- concentration (coloured lines). CVs were scanned from -0.05 V to -0.65 V at a scan rate of 10 mV s^{-1}. The GC/MWCNT electrode was prepared by drop casting of 5 µL of 1 mg mL^{-1} MWCNT dispersion onto the cleaned surface of GC. The S362C-BOD was immobilized on the GC / CNT electrode using covalent attachment.*

Nevertheless, by comparison with previous work by Solomon and co-workers[356, 403] it can be concluded that the *Mo*BOD is in the RO form and is switched to the AR form upon addition of Cl^-, see Scheme 6.3. At pH 6 and 7 (Figure 6.14B and C), however, on the time scale of the

experiments the *Mo*BOD remains in its oxidized resting state even after addition of Cl^-. Similar results were recently reported for *Bacillus pumilus* BOD by Lojou *et al.*[364] as a first evidence that the inter-conversion between the two resting forms generated by addition of NaCl is pH-dependent.

6.9 Conclusion

In this Chapter, the flexible and structured approach that was used in Chapter 4, for the oriented immobilization of genetically engineered redox proteins and enzymes at electrode surfaces (maleimide/thiol coupling reaction) has been further examined. The maleimide group was chosen because it undergoes spontaneous reaction with free thiols in aqueous solution at neutral pH and room temperature, allowing efficient use of small quantities of the cysteine-modified genetically engineered enzyme.

Using three variants of *Magnaporthe oryzae* bilirubin oxidase (*Mo*BOD) we have shown that this approach can be applied to different enzymes, leads to stable attachment of the enzyme to the electrode surface, and that the immobilised BOD enzyme is active for the DET-type bioelectrocatalytic reduction of di-oxygen on the electrode, without added redox mediators. Comparison of the three different *MoBOD* variants shows that the position of the mutation on the enzyme surface affects the measured catalytic currents.

The effect of Cl^- on *Mo*BOD is of outmost importance for the use of this enzyme in the field of biofuel cells and biosensors, specifically under physiological conditions. This Chapter highlights for the first time the effect of Cl^- on the direct oxygen reduction by *Mo*BOD as a function of pH. The results have confirmed that the power of hydrogen has an effect on Cl^- inhibition, and offers understanding into the decrease in performance observed upon long-term operation under physiological conditions. In this study, we have focused on the coexistence of the two resting forms of the enzyme, i.e., fully oxidized RO form and partially oxidized AR form. The AR form, which was identified in as-isolated enzyme, can be stimulated for O_2 catalysis only at adequately low electrode potentials. However, if an electrode with immobilized activated enzyme (i.e., RO form) is placed in pH 4 NaCl buffer the CV exhibits a return to the low activation potential.

Indeed, RO/AR reciprocal conversion is not particular or unique to *Mo*BOD. It is a common feature of BODs as well as other MCOs containing four coppers. For instance, a group have reported the same effect with laccase from *Bacillus subtilis*.[364] Also, the same behavior has been observed with BODs from *Bacillus pumilus* as well as from *Myrothecium verrucaria*.[365] We have shown that for the immobilized *Mo*BOD the RO/AR changeover only happens in the presence

of Cl^-. The results obtained in this Chapter are consistent with a model in which both BOD-T1 and TNC are in direct electronic contact with the surface of the GC/MWCNT electrode.

Chapter 7 Conclusion

This Chapter presents an answer to the question that has arisen from this work: What evidence is required to demonstrate DET? The following discussion has been put together by taking into account what experimental results would be crucial to demonstrate DET for any redox enzyme.

First, it is fundamental to recognize that, some redox enzymes have exposed redox centres as a result of the nature of their biological function, and/or they have identified redox pathways that allow them to exchange electrons with other large biological redox species such as cytochrome *c* or biopolymers such as lignin.[255] In these cases, direct electron transfer to electrode surfaces should be feasible, provided that the surface is correctly modified; examples of such enzymes include horseradish peroxidase (HRP), laccase, bilirubin oxidase (BOD), and cellobiose dehydrogenase (CDH). In this work, the latter two enzymes have been investigated using a flexible and structured approach to the oriented immobilisation of redox enzymes at electrode surfaces. This has been achieved based on the use of site directed mutagenesis to introduce cysteine residues at specific locations on the enzyme surface and using the reaction between the free thiol and a maleimide group on the electrode surface. On the other hand, some redox enzymes, such as glucose oxidase (GOx), have one region, namely, the vicinity of the prosthetic group, where the ET reaction between the substrate and redox active sites of the redox enzyme happens. Since there is no natural requirement for long range ET pathways to the surface of the protein, DET is very difficult to achieve. In Chapter 3, we have demonstrated that the results presented in the literature, in the vast majority of cases, in support of DET to GOx at carbon nanotube electrodes, are unconvincing, arguable or debatable. This study has shown that the surface redox peaks that are observed in these cases are due to free, adsorbed flavin and not, as claimed, due to DET to flavin within the enzyme.

Second, as supplied, commercial enzymes are not pure and usually contain added substances to maintain them in a stable chemical and/or physical condition. Therefore, it is essential to purify the commercial enzymes since these impurities can have a substantial effect on their electrochemistry. In Chapter 3, we have demonstrated that in contrast to the situation for as supplied GOx from Sigma, the redox peaks produced by purified GOx from BBI are negligible. Thus, it can be concluded that the surface redox peaks observed in these cases are not associated with DET of GOx but instead arise from free flavin and/or catalase, present as impurities that can be adsorbed, and concentrated, on high surface nanomaterials, and thus dominate the electrochemical response.

Third, it is recommended to execute control experiments to confirm that the enzyme selectivity is maintained. In the cases of GOx and CDH this is readily achieved using L-glucose. One

evidence that the catalytic current is due to the oxidation of the glucose by the immobilised enzyme is delivered by the control experiment using L-glucose. We have shown that the increase in current was not seen on addition of L-Glucose, which is not oxidised by CDH or GOx, and therefore can be used to check for any non-enzyme specific effects, such as direct, non-enzyme catalysed oxidation of the glucose, that might occur. The L-glucose control experiment is highly recommended in the case of high surface area electrode materials since even very inefficient direct oxidation could lead to a noticeable signal for high (>10 mM) glucose concentrations. Another strategy here is to employ an inhibitor for the enzyme to show that upon addition of the inhibitor the electrocatalytic response is decreased as expected.

Fourth, it is fundamental to look for the "signature" for the electrocatalytic response upon addition of the substrate and to look at the magnitudes of these catalytic currents and their substrate concentration dependence. In the case of CDH, we have demonstrated that the current starts to increase at *ca.* -0.2 V *vs*. SCE, and this position of the onset of the catalytic current agrees with that reported in the literature for immobilised *Mt*CDH at different electrodes and corresponds to DET from the haem to the electrode. However, In the case of GOx the oxidation of glucose should be seen at potentials starting from the redox potential of the bound flavin accompanied by the disappearance of the corresponding flavin reduction peak, which did not occur.

Finally, it is significant to perform experiments using different substrates with different enzyme reaction kinetics. This is a powerful strategy to test whether the enzymatic activity and selectivity are totally maintained or whether the structure of the enzyme has undergone considerable disruption. For GOx this can be achieved by measuring the response to other substrates such as 2-deoxy-D-glucose and D-mannose.[194, 409]

These same general criteria can be equally well applied to studies of other redox enzymes.

The results presented in Chapter 3 have conclusively demonstrated that the surface redox peaks observed on the MWCNT electrodes with adsorbed GOx are not due to DET to the active site of the enzyme but, rather, are due to the adsorption of some impurity, probably free flavin and/or catalase, onto the electrode surface. Thus, the evidence presented in the literature for the vast majority of cases in support of DET to GOx at electrodes constructed for various nanomaterials, particularly CNTs of various forms, is unconvincing, arguable or debatable. As a consequence of the clear drawbacks with GOx, there has been a continuous investigation for alternative carbohydrate-oxidation enzymes. CDH was selected as the model redox enzyme system in Chapter 4. Therefore, with the cysteine-modified genetically engineered *Mt*CDH, we have shown that our immobilisation approach (based on the covalent attachment of cysteine-modified genetically engineered enzymes at maleimide modified electrodes) leads to

a very stable attachment of the enzyme to the electrode surface and the fact that the immobilised enzyme is electrochemically active without added redox mediators. To broaden the validity of the same immobilisation method, BOD, a promising redox enzyme in the field of biofuel cells was chosen (in Chapter 6) as another model enzyme. We have shown that this method can be applied to different enzymes, leads to stable immobilisation of the enzyme to the electrode surface, and that the immobilised BOD enzyme is electrochemically active without added redox mediators.

7.1 Future work

A wide range of engineered enzymes can now be electro-kinetically investigated using such a novel strategy. However, the stability of the enzyme on the surface will still need improvement for applications such as biosensors and biofuel cells. Indeed, it is not clear why the BOD was not very stable, like CDH, on the maleimide modified GC/MWCNT electrodes. However, the length of the "spacer" should be optimised, and a better enzyme-compatible "passivating group" should be investigated. Also, the use of a polymer film on top of the enzyme can be attempted. The method of attachment could also be investigated in more detail; the electrochemical oxidation of amines does not lead to coupling on all types of electrode material, for example it does not work on gold, one of the common metals used for electrodes. Hence, an alternative method involving reduction of diazonium salts could be investigated.

Bibliography

1. Bartlett, P. N., *Bioelectrochemistry : Fundamentals, Experimental Techniques and Applications*. John Wiley & Sons Ltd, The Atrium, Southern Gate, Chichester: West Sussex, England, 2008.
2. Freire, R. S.; Pessoa, C. A.; Mello, L. D.; Kubota, L. T., *J. Braz. Chem. Soc.* **2003,** *14* (2), 230-243.
3. Marcus, R. A., *J. Electroanal. Chem.* **1997,** *438* (1-2), 251-259.
4. Marcus, R. A., *Rev. Mod. Phys.* **1993,** *65* (3), 599-610.
5. Torres, L. M.; Gil, A. F.; Galicia, L.; Gonzalez, I., *J. Chem. Educ.* **1996,** *73* (8), 808-810.
6. Marcus, R. A., *Angew. Chem. Int. Ed.* **1993,** *32* (8), 1111-1121.
7. Marcus, R. A.; Sutin, N., *Biochim. Biophys. Acta* **1985,** *811* (3), 265-322.
8. Eckermann, A. L.; Feld, D. J.; Shaw, J. A.; Meade, T. J., *Coord. Chem. Rev.* **2010,** *254* (15-16), 1769-1802.
9. Gray, H. B.; Winkler, J. R., *Q. Rev. Biophys.* **2003,** *36* (3), 341-372.
10. Langen, R.; Chang, I. J.; Germanas, J. P.; Richards, J. H.; Winkler, J. R.; Gray, H. B., *Science* **1995,** *268* (5218), 1733-1735.
11. Gray, H. B.; Winkler, J. R., *Proc. Natl. Acad. Sci. U. S. A.* **2005,** *102* (10), 3534-3539.
12. Kuhlbrandt, W., *BMC Biol.* **2015,** *13* (1), 89-100.
13. Murphy, C. J.; Arkin, M. R.; Jenkins, Y.; Ghatlia, N. D.; Bossmann, S. H.; Turro, N. J.; Barton, J. K., *Science* **1993,** *262* (5136), 1025-1029.
14. Finkelstein, J., *Nature* **2009,** *460* (7257), 813-813.
15. Yue, H. J.; Waldeck, D. H., *Curr. Opin. Solid State Mater. Sci.* **2005,** *9* (1-2), 28-36.
16. Leger, C.; Heffron, K.; Pershad, H. R.; Maklashina, E.; Luna-Chavez, C.; Cecchini, G.; Ackrell, B. A. C.; Armstrong, F. A., *Biochemistry* **2001,** *40* (37), 11234-11245.
17. Jeuken, L. J. C., *Biochim. Biophys. Acta, Bioenergetics* **2003,** *1604* (2), 67-76.
18. Bullen, R. A.; Arnot, T. C.; Lakeman, J. B.; Walsh, F. C., *Biosens. Bioelectron.* **2006,** *21* (11), 2015-2045.
19. Cinquin, P.; Gondran, C.; Giroud, F.; Mazabrard, S.; Pellissier, A.; Boucher, F.; Alcaraz, J. P.; Gorgy, K.; Lenouvel, F.; Mathe, S.; Porcu, P.; Cosnier, S., *PLoS One* **2010,** *5* (5), e10476.
20. Shleev, S.; Tkac, J.; Christenson, A.; Ruzgas, T.; Yaropolov, A. I.; Whittaker, J. W.; Gorton, L., *Biosens. Bioelectron.* **2005,** *20* (12), 2517-2554.
21. Demin, S.; Hall, E. A. H., *Bioelectrochemistry* **2009,** *76* (1-2), 19-27.
22. Al-Lolage, F. A.; Meneghello, M.; Ma, S.; Ludwig, R.; Bartlett, P. N., *ChemElectroChem* **2017**, 1528-1534.
23. Cao, X.; Sun, Y.; Ye, Y.; Li, Y.; Ge, X., *Anal. Methods* **2014,** *6* (5), 1448-1454.

24. Wright, E. J.; Sosna, M.; Bloodworth, S.; Kilburn, J. D.; Bartlett, P. N., *Chem. Eur. J.* **2014,** *20* (19), 5550-5554.

25. Lalaoui, N.; Le Goff, A.; Holzinger, M.; Cosnier, S., *Chem. Eur. J.* **2015,** *21* (47), 16868-73.

26. Lalaoui, N.; Holzinger, M.; Le Goff, A.; Cosnier, S., *Chem. Eur. J.* **2016,** *22* (30), 10494-10500.

27. Bartlett, P. N.; Al-Lolage, F. A., *J. Electroanal. Chem.* **2017**, in press

28. Ghindilis, A. L.; Atanasov, P.; Wilkins, E., *Electroanalysis* **1997,** *9* (9), 661-674.

29. Grieshaber, D.; MacKenzie, R.; Voros, J.; Reimhult, E., *Sensors* **2008,** *8* (3), 1400-1458.

30. Blanford, C. F., *Chem. Commun.* **2013,** *49* (95), 11130-11132.

31. Yeh, P.; Kuwana, T., *Chem. Lett.* **1977,** (10), 1145-1148.

32. Noll, T.; Noll, G., *Chem. Soc. Rev.* **2011,** *40* (7), 3564-3576.

33. Li, S.-J.; Chen, T.-W.; Xia, N.; Hou, Y.-L.; Du, J.-J.; Liu, L., *J. Solid State Electrochem.* **2013,** *17* (9), 2487-2494.

34. Heller, A., *Acc. Chem. Res.* **1990,** *23* (5), 128-134.

35. Alvarezicaza, M.; Kalisz, H. M.; Hecht, H. J.; Aumann, K. D.; Schomburg, D.; Schmid, R. D., *Biosens. Bioelectron.* **1995,** *10* (8), 735-742.

36. Frew, J. E.; Hill, H. A. O., *Eur. J. Biochem.* **1988,** *172* (2), 261-269.

37. Milton, R. D.; Minteer, S. D., *J. Royal Soc. Interface* **2017,** *14* (131).

38. Zhao, J. G.; Henkens, R. W.; Stonehuerner, J.; Odaly, J. P.; Crumbliss, A. L., *J. Electroanal. Chem.* **1992,** *327* (1-2), 109-119.

39. Willner, I.; Katz, E., *Angew. Chem. Int. Ed.* **2000,** *39* (7), 1180-1218.

40. Harper, J. C.; Polsky, R.; Wheeler, D. R.; Brozik, S. M., *Langmuir* **2008,** *24* (5), 2206-2211.

41. Bartlett, P. N.; Pratt, K. F. E., *J. Electroanal. Chem.* **1995,** *397* (1-2), 53-60.

42. Baranton, S.; Belanger, D., *J. Phys. Chem. B* **2005,** *109* (51), 24401-24410.

43. Sarma, A. K.; Vatsyayan, P.; Goswami, P.; Minteer, S. D., *Biosens. Bioelectron.* **2009,** *24* (8), 2313-2322.

44. Christakopoulos, P.; Topakas, E., *Comput. Struct. Biotechnol. J.* **2012,** *2* (3), e201209001.

45. Purich, D. L., Chapter 1 - An Introduction to Enzyme Science. In *Enzyme Kinetics: Catalysis & Control*, Elsevier: Boston, 2010; pp 1-51.

46. Purich, D. L., Chapter 2 - Active Sites and their Chemical Properties. In *Enzyme Kinetics: Catalysis & Control*, Elsevier: Boston, 2010; pp 53-169.

47. Lonsdale, R.; Harvey, J. N.; Mulholland, A. J., *Chem. Soc. Rev.* **2012,** *41* (8), 3025-3038.

48. Donertas, H. M.; Cuesta, S. M.; Rahman, S. A.; Thornton, J. M., *PLoS One* **2016,** *11* (2), e0147952.

49. Murray, R. W.; Ewing, A. G.; Durst, R. A., *Anal. Chem.* **1987,** *59* (5), 379A–390A.

50. Watkins, B. F.; Behling, J. R.; Kariv, E.; Miller, L. L., *J. Am. Chem. Soc.* **1975,** *97* (12), 3549-3550.

51. Lane, R. F.; Hubbard, A. T., *J. Phys. Chem. A* **1973,** *77* (11), 1401-1410.

52. Moses, P. R.; Wier, L.; Murray, R. W., *Anal. Chem.* **1975,** *47* (12), 1882-1886.

53. Murray, R. W., *Acc. Chem. Res.* **1980,** *13* (5), 135-141.

54. Lupu, S.; Lete, C.; Marin, M.; Totir, N.; Balaure, P. C., *Electrochim. Acta* **2009,** *54* (7), 1932-1938.

55. Wang, S. Q.; Dong, H. F.; Liu, G. D.; Wen, Y. Q.; Wang, S. T.; Zhang, X. J., *Nanoscale* **2012,** *4* (12), 3786-3790.

56. Fan, J. Q.; Shi, H. J.; Xiao, H. S.; Zhao, G. H., *ACS Appl. Mater. Interfaces* **2016,** *8* (42), 28306-28315.

57. Niedziolka-Jonsson, J.; Barka, F.; Castel, X.; Pisarek, M.; Bezzi, N.; Boukherroub, R.; Szunerits, S., *Langmuir* **2010,** *26* (6), 4266-4273.

58. Georgakilas, V.; Otyepka, M.; Bourlinos, A. B.; Chandra, V.; Kim, N.; Kemp, K. C.; Hobza, P.; Zboril, R.; Kim, K. S., *Chem. Rev.* **2012,** *112* (11), 6156-6214.

59. Mulazimoglu, A. D.; Yilmaz, E.; Mulazimoglu, I. E., *Sensors* **2012,** *12* (4), 3916-3928.

60. Tanne, J.; Kracher, D.; Dietzel, B.; Schulz, B.; Ludwig, R.; Lisdat, F.; Scheller, F. W.; Bier, F. F., *Biosensors* **2014,** *4* (4), 370-86.

61. Niedzialkowski, P.; Bogdanowicz, R.; Zieba, P.; Wysocka, J.; Ryl, J.; Sobaszek, M.; Ossowski, T., *Electroanalysis* **2016,** *28* (1), 211-221.

62. Miller, H. E. Z. a. F. J., *Anal. Chem.* **1965,** *37* ((2)), 200–203.

63. Macpherson, J. V., *PCCP* **2015,** *17* (5), 2935-2949.

64. Lu, W.; Hartman, R.; Qu, L. T.; Dai, L. M., *J. Phys. Chem. Lett.* **2011,** *2* (6), 655-660.

65. Katchalski-Katzir, E., *Trends Biotechnol.* **1993,** *11*, 471-478.

66. Beatriz, M. B. F., Batista-Viera, Immobilization of Enzymes. In *Methods in Biotechnology: Immobilization of Enzymes and Cells*, Springer: Totowa, NJ, 2006.

67. Hanefeld, U.; Gardossi, L.; Magner, E., *Chem. Soc. Rev.* **2009,** *38* (2), 453-468.

68. Homaei, A. A.; Sariri, R.; Vianello, F.; Stevanato, R., *J. Chem. Biol.* **2013,** *6* (4), 185-205.

69. Mohamad, N. R.; Marzuki, N. H. C.; Buang, N. A.; Huyop, F.; Wahab, R. A., *Biotechnol. Biotechnol. Equip.* **2015,** *29* (2), 205-220.

70. Ma, L.; Wang, X. T.; You, D. L.; Tang, S.; Huang, Z. L.; Cheng, Y. H., *Appl. Biochem. Biotechnol.* **1996,** *56*, 223-233.

71. Yon, R. J., *Biochem. J.* **1974,** *137*, 127-130.

72. Solomon, B., Hollaander, Z., Koppel, R., and Katchalski-Kazir, E., Use of monoclonal antibodies for the preparation of highly active immobilized enzymes. In *Methods Enzymol.*, Academic Press: London, 1987; Vol. 135, pp 160–170.

73. Cabral, J. M. S.; Novais, J. M.; Kennedy, J. F., *Appl. Microbiol. Biotechnol.* **1986,** *23*, 157-162.

74. Foulds, N. C.; Lowe, C. R., *J. Chem. Soc. Faraday Trans. 1* **1986,** *82*, 1259-1264.

75. Cosnier, S., *Biosens. Bioelectron.* **1999,** *14*, 443–456.

76. Scouten, W. H., [2] A survey of enzyme coupling techniques. In *Methods Enzymol.*, Academic Press: 1987; Vol. 135, pp 30-65.

77. Torres, M. D. G.; Foresti, M. L.; Ferreira, M. L., *Amb Express* **2013,** *3* (1), 25.

78. Liu, W.; Wang, L.; Jiang, R., *Top. Catal.* **2012,** *55* (16-18), 1146-1156.

79. Kalia, J.; Raines, R. T., *ChemBioChem* **2006,** *7* (9), 1375-1383.

80. Moses, J. E.; Moorhouse, A. D., *Chem. Soc. Rev.* **2007,** *36* (8), 1249-1262.

81. Kalia, J.; Abbott, N. L.; Raines, R. T., *Bioconjugate Chem.* **2007,** *18*, 1064-1069.

82. Tam, A.; Raines, R. T., *Methods Enzymol.* **2009,** *462*, 25-44.

83. Kohn, M.; Breinbauer, R., *Angew. Chem. Int. Ed.* **2004,** *43* (24), 3106-3116.

84. Paborsky, L. R.; Dunn, K. E.; Gibbs, C. S.; Dougherty, J. P., *Anal. Biochem.* **1996,** *234* (50), 60-65.

85. Oshige, M.; Yumoto, K.; Miyata, H.; Takahashi, S.; Nakada, M.; Ito, K.; Tamegai, M.; Kawaura, H.; Katsura, S., *OJPChem.* **2013,** *3* (1), 6-10.

86. Hardy, J. A., Chapter 17 A Link Means a Lot: Disulfide Tethering in Structure-Based Drug Design. In *Computational and Structural Approaches to Drug Discovery: Ligand-Protein Interactions*, The Royal Society of Chemistry: 2008; pp 319-348.

87. Thevenot, D. R.; Toth, K.; Durst, R. A.; Wilson, G. S., *Biosens. Bioelectron.* **2001,** *16* (1-2), 121-131.

88. Reach, G.; Wilson, G. S., *Anal. Chem.* **1992,** *64* (6), A381-A386.

89. Wang, J., *Electroanalysis* **2001,** *13* (12), 983-988.

90. Wang, J., *Chem. Rev.* **2008,** *108* (2), 814-825.

91. Heller, A., *Curr. Opin. Biotechnol.* **1996,** *7* (1), 50-54.

92. Albery, W. J.; Bartlett, P. N.; Cass, A. E.; Craston, D. H.; Haggett, B. G. D., *J. Chem. Soc., Faraday Trans, I* **1986,** *82*, 1033-1050.

93. Clark, L. C., Jr.; Lyons, C., *Ann. N. Y. Acad. Sci.* **1962,** *102*, 29-45.

94. Liu, J.; Wang, J., *Food Technol. Biotechnol.* **2001,** *39* (1), 55-58.

95. Chaubey, A.; Malhotra, B. D., *Biosens. Bioelectron.* **2002,** *17* (6-7), 441-456.

96. Schuhmann, W.; Zimmermann, H.; Habermuller, K. V.; Laurinavicius, V., *Faraday Discuss.* **2000,** *116*, 245-255.

97. Mao, F.; Mano, N.; Heller, A., *J. Am. Chem. Soc.* **2003,** *125* (16), 4951-4957.

98. Zhang, W. J.; Li, G. X., *Anal. Sci.* **2004,** *20* (4), 603-609.

99. Yoo, E.-H.; Lee, S.-Y., *Sensors* **2010,** *10* (5), 4558-4576.

100. Khan, G. F.; Ohwa, M.; Wernet, W., *Anal. Chem.* **1996,** *68* (17), 2939-2945.

101. Čenas, N. K.; Kulys, J. J., *Bioelectrochem. Bioenerg.* **1981,** *8* (1), 103-113.

102. Palmisano, F.; Zambonin, P. G.; Centonze, D.; Quinto, M., *Anal. Chem.* **2002,** *74* (23), 5913-5918.

103. Retama, J. R.; Cabarcos, E. L.; Mecerreyes, D.; Lopez-Ruiz, B., *Biosens. Bioelectron.* **2004,** *20* (6), 1111-1117.

104. Aizawa, M.; Yabuki, S.; Shinohara, H.; Ikariyama, Y., *Ann. N.Y. Acad. Sci.* **1990,** *613*, 827-831.

105. Koopal, C. G. J.; Deruiter, B.; Nolte, R. J. M., *J. Chem. Soc., Chem. Commun.* **1991,** (23), 1691-1692.

106. Wu, J.; Qu, Y., *Anal. Bioanal. Chem.* **2006,** *385* (7), 1330-5.

107. Gorton, L.; Lindgren, A.; Larsson, T.; Munteanu, F. D.; Ruzgas, T.; Gazaryan, I., *Anal. Chim. Acta* **1999,** *400*, 91-108.

108. Wu, Y.; Hu, S., *Microchim. Acta* **2007,** *159* (1-2), 1-17.

109. Armstrong, F. A., *Curr. Opin. Chem. Biol.* **2005,** *9* (2), 110-117.

110. Borgmann, S.; Schulte, A.; Neugebauer, A.; Schuhmann, W., Amperometric Biosensors. In *Electrochemical Science and Engineering: Bioelectrochemistry*, Richard C. Alkire, D. M. K., Jacek Lipkowski, Ed. Wiley-VCH Verlag GmbH & Co. KGaA. : Weinheim, Germany, 2012; Vol. 13.

111. Deng, C.; Chen, J.; Chen, X.; Mao, C.; Nie, L.; Yao, S., *Biosens. Bioelectron.* **2008,** *23* (8), 1272-1277.

112. Cao, H.; Zhu, Y.; Tang, L.; Yang, X.; Li, C., *Electroanalysis* **2008,** *20* (20), 2223-2228.

113. Gao, R.; Zheng, J., *Electrochem. Commun.* **2009,** *11* (3), 608-611.

114. Deng, S.; Jian, G.; Lei, J.; Hu, Z.; Ju, H., *Biosens. Bioelectron.* **2009,** *25* (2), 373-377.

115. Horng, Y.-Y.; Hsu, Y.-K.; Ganguly, A.; Chen, C.-C.; Chen, L.-C.; Chen, K.-H., *Electrochem. Commun.* **2009,** *11* (4), 850-853.

116. Fu, C.; Yang, W.; Chen, X.; Evans, D. G., *Electrochem. Commun.* **2009,** *11* (5), 997-1000.

117. Wang, K.; Liu, Q.; Guan, Q.-M.; Wu, J.; Li, H.-N.; Yan, J.-J., *Biosens. Bioelectron.* **2011,** *26* (5), 2252-2257.

118. Li, J.; Zhao, F.; Wang, G.; Gui, Z.; Xiao, F.; Zeng, B., *Electroanalysis* **2009,** *21* (2), 150-156.

119. Shan, C.; Yang, H.; Han, D.; Zhang, Q.; Ivaska, A.; Niu, L., *Biosens. Bioelectron.* **2010,** *25* (5), 1070-1074.

120. Wu, X.; Zhao, F.; Varcoe, J. R.; Thumser, A. E.; Avignone-Rossa, C.; Slade, R. C. T., *Bioelectrochemistry* **2009,** *77* (1), 64-68.

121. Liu, Q.; Lu, X.; Li, J.; Yao, X.; Li, J., *Biosens. Bioelectron.* **2007,** *22* (12), 3203-3209.

122. Agui, L.; Yanez-Sedeno, P.; Pingarron, J. M., *Anal. Chim. Acta* **2008,** *622* (1-2), 11-47.

123. Chen, C.; Xie, Q.; Yang, D.; Xiao, H.; Fu, Y.; Tan, Y.; Yao, S., *Rsc Advances* **2013,** *3* (14), 4473-4491.

124. Das, P.; Das, M.; Chinnadayyala, S. R.; Singha, I. M.; Goswami, P., *Biosens. Bioelectron.* **2016,** *79*, 386-397.

125. Harper, A.; Anderson, M. R., *Sensors* **2010,** *10* (9), 8248-8274.

126. Luong, J. H. T.; Glennon, J. D.; Gedanken, A.; Vashist, S. K., *Microchim. Acta* **2017,** *184*, 369-388.

127. L. Jiang; McNeil, C. J.; Cooper, J. M., *Chem. Commun.* **1995**, 1293-1295.

128. Demin, S.; Hall, E. A. H., *Bioelectrochemistry* **2009,** *76*, 19-27.

129. Liu, J. Q.; Chou, A.; Rahmat, W.; Paddon-Row, M. N.; Gooding, J. J., *Electroanalysis* **2005,** *17* (1), 38-46.

130. Iijima, S., *Nature* **1991,** *354* (6348), 56-58.

131. Richard C. Alkire, P. N. B., and Jacek Lipkowski, *Advances in Electrochemical Science and Engineering: Electrochemistry of Carbon Electrodes*. Wiley-VCH Verlag GmbH & Co. KGaA, Boschstr. 12, 69469 Weinheim, Germany, 2015; Vol. 16.

132. Lehman, J. H.; Terrones, M.; Mansfield, E.; Hurst, K. E.; Meunier, V., *Carbon* **2011,** *49* (8), 2581-2602.

133. Ajayan, P. M., *Chem. Rev.* **1999,** *99* (7), 1787-1799.

134. Kaushik, B. K.; Majumder, M. K., Carbon Nanotube: Properties and Applications. In *Carbon Nanotube Based VLSI Interconnects: Analysis and Design*, Springer India: New Delhi, 2015; pp 17-37.

135. Masheter, A. T.; Xiao, L.; Wildgoose, G. G.; Crossley, A.; John, H. J. C.; Compton, R. G., *J. Mater. Chem.* **2007,** *17* (33), 3515-3524.

136. Thorogood, C. A.; Wildgoose, G. G.; Jones, J. H.; Compton, R. G., *New J. Chem.* **2007,** *31* (6), 958-965.

137. Che, G. L.; Lakshmi, B. B.; Fisher, E. R.; Martin, C. R., *Nature* **1998,** *393* (6683), 346-349.

138. Agui, L.; Yanez-Sedeno, P.; Pingarron, J. M., *Anal. Chim. Acta* **2008,** *622* (1-2), 11-47.

139. Britto, P. J.; Santhanam, K. S. V.; Rubio, A.; Alonso, J. A.; Ajayan, P. M., *Adv. Mater.* **1999,** *11* (2), 154-157.

140. Musameh, M.; Wang, J.; Merkoci, A.; Lin, Y. H., *Electrochem. Commun.* **2002,** *4* (10), 743-746.

141. Wang, J.; Musameh, M., *Anal. Chem.* **2003,** *75* (9), 2075-2079.

142. Donaldson, K.; Aitken, R.; Tran, L.; Stone, V.; Duffin, R.; Forrest, G.; Alexander, A., *Toxicol. Sci.* **2006,** *92* (1), 5-22.

143. Bartlett, P. N., Conducting organic salt electrodes. In *Biosensors : A Practical Approach*, CASS, A. E. G., Ed. Oxford University Press: Oxford, 1990.

144. Vogt, S.; Schneider, M.; Schafer-Eberwein, H.; Noll, G., *Anal Chem* **2014,** *86* (15), 7530-7535.

145. Clark, L. C.; Lyons, C., *Ann. N. Y. Acad. Sci.* **1962,** *102*, 29-45.

146. Turner, A. P. F.; Karube, I.; Wilson, G. S., *Biosensors. Fundamentals and Applications*. OUP: Oxford, 1987.

147. Guilbault, G. G.; Lubrano, G. J., *Anal. Chim. Acta* **1973,** *64* (3), 439-455.

148. Cass, A. E. G.; Davis, G.; Francis, G. D.; Hill, H. A. O.; Aston, W. J.; Higgins, I. J.; Plotkin, E. V.; Scott, L. D. L.; Turner, A. P. F., *Anal. Chem.* **1984,** *56*, 667-671.

149. Guiseppi-Elie, A.; Lei, C. H.; Baughman, R. H., *Nanotechnology* **2002,** *13* (5), 559-564.

150. Cai, C. X.; Chen, J.; Lu, T. H., *Sci China B* **2004,** *47* (2), 113-119.

151. Cai, C. X.; Chen, J., *Anal. Biochem.* **2004,** *332* (1), 75-83.

152. Yin, Y. J.; Lu, Y. F.; Wu, P.; Cai, C. X., *Sensors* **2005,** *5* (4-5), 220-234.

153. Liu, Y.; Wu, S.; Ju, H. X.; Xu, L., *Electroanalysis* **2007,** *19* (9), 986-992.

154. Rivas, G. A.; Rubianes, M. D.; Rodriguez, M. C.; Ferreyra, N. E.; Luque, G. L.; Pedano, M. L.; Miscoria, S. A.; Parrado, C., *Talanta* **2007,** *74* (3), 291-307.

155. Tachikawa, H.; Jingdong, Z.; Manliang, F., *Biosens. Bioelectron.* **2007,** *22* (12), 3036-41.

156. Ivnitski, D.; Artyushkova, K.; Rincon, R. A.; Atanassov, P.; Luckarift, H. R.; Johnson, G. R., *Small* **2008,** *4* (3), 357-364.

157. Jia, F.; Shan, C.; Li, F.; Niu, L., *Biosens. Bioelectron.* **2008,** *24* (4), 945-950.

158. Zhou, Y.; Yang, H.; Chen, H.-Y., *Talanta* **2008,** *76* (2), 419-423.

159. Ahammad, A. J. S.; Lee, J.-J.; Rahman, M. A., *Sensors* **2009,** *9* (4), 2289-2319.

160. Jeykumari, D. R. S.; Narayanan, S. S., *Carbon* **2009,** *47* (4), 957-966.

161. Li, F.; Song, J.; Li, F.; Wang, X.; Zhang, Q.; Han, D.; Ivaska, A.; Niu, L., *Biosens. Bioelectron.* **2009,** *25* (4), 883-888.

162. Deng, C.; Chen, J.; Nie, Z.; Si, S., *Biosens. Bioelectron.* **2010,** *26* (1), 213-219.

163. Harper, A.; Anderson, M. R., *Sensors* **2010,** *10* (9), 8248-8274.

164. Lee, K.-P.; Komathi, S.; Nam, N. J.; Gopalan, A. I., *Microchem. J.* **2010,** *95* (1), 74-79.

165. Ryu, J.; Kim, H.; Lee, S.; Hahn, H. T.; Lashmore, D., *J. Nanosci. Nanotechnol.* **2010,** *10* (2), 941-947.

166. Won, K., *Mol. Cryst. Liq. Cryst.* **2010,** *528*, 195-195.

167. Ahmadalinezhad, A.; Wu, G.; Chen, A., *Biosens. Bioelectron.* **2011,** *30* (1), 287-293.

168. Janegitz, B. C.; Pauliukaite, R.; Ghica, M. E.; Brett, C. M. A.; Fatibello-Filho, O., *Sens. Actuator B-Chem* **2011,** *158* (1), 411-417.

169. Nejadnik, M. R.; Deepak, F. L.; Garcia, C. D., *Electroanalysis* **2011,** *23* (6), 1462-1469.

170. Gutierrez, F.; Rubianes, M. D.; Rivas, G. A., *Sens. Actuator B-Chem* **2012,** *161* (1), 191-197.

171. Jose, M. V.; Marx, S.; Murata, H.; Koepsel, R. R.; Russell, A. J., *Carbon* **2012,** *50* (11), 4010-4020.

172. Wang, Y.; Yao, Y., *Microchim. Acta* **2012,** *176* (3-4), 271-277.

173. Zhu, Z.; Garcia-Gancedo, L.; Flewitt, A. J.; Xie, H.; Moussy, F.; Milne, W. I., *Sensors* **2012,** *12* (5), 5996-6022.

174. Goran, J. M.; Mantilla, S. M.; Stevenson, K. J., *Anal. Chem.* **2013,** *85* (3), 1571-1581.

175. Hui-Fang, C.; Kuan, Z.; Yong-Fang, Z.; Yu-Long, S.; Jia, W.; Wei-De, Z.; Luong, J. H. T., *Biosens. Bioelectron.* **2013,** *46*, 113-18.

176. Kamyabi, M. A.; Hajari, N.; Turner, A. P. F.; Tiwari, A., *Talanta* **2013,** *116*, 801-808.

177. Li, J.; Yang, Z.; Tang, Y.; Zhang, Y.; Hu, X., *Biosens. Bioelectron.* **2013,** *41*, 698-703.

178. Li, M.; Feng, B.; Ding, Y.; Fei, J., *NNL* **2013,** *5* (6), 712-718.

179. Moumene, M.; Rochefort, D.; Mohamedi, M., *Int. J. Electrochem. Sci.* **2013,** *8* (2), 2009-2022.

180. Vesali-Naseh, M.; Mortazavi, Y.; Khodadadi, A. A.; Parsaeian, P.; Moosavi-Movahedi, A. A., *Sens. Actuator B-Chem* **2013,** *188*, 488-495.

181. Won, K.; Kim, Y.-H.; An, S.; Lee, H. J.; Park, S.; Choi, Y.-K.; Kim, J. H.; Hwang, H.-I.; Kim, H. J.; Kim, H.; Lee, S. H., *Appl. Biochem. Biotechnol.* **2013,** *171* (5), 1194-1202.

182. Wu, Y.-L.; Li, Q.-W.; Zhang, X.-L.; Chen, X.; Wang, X.-M., *Chin. Chem. Lett.* **2013,** *24* (12), 1087-1090.

183. Palanisamy, S.; Cheemalapati, S.; Chen, S.-M., *Mater Sci Eng C Mater Biol Appl* **2014,** *34*, 207-213.

184. Wooten, M.; Karra, S.; Zhang, M.; Gorski, W., *Anal. Chem.* **2014,** *86* (1), 752-757.

185. Yu, Y.; Chen, Z.; He, S.; Zhang, B.; Li, X.; Yao, M., *Biosens. Bioelectron.* **2014,** *52*, 147-152.

186. Degani, Y.; Heller, A., *J. Phys. Chem.* **1987,** *91* (6), 1285-1289.

187. Hecht, H. J.; Schomburg, D.; Kalisz, H.; Schmid, R. D., *Biosens. Bioelectron.* **1993,** *8* (3-4), 197-203.

188. Borgmann, S.; Schulte, A.; Neugebauer, A.; Schuhmann, W., Amperometric Biosensors. In *Electrochemical Science and Engineering: Bioelectrochemistry*, Wiley-VCH Verlag GmbH & Co. KGaA. : Weinheim, 2011; Vol. 13.

189. Wilson, R.; Turner, A. P. F., *Biosens. Bioelectron.* **1992,** *7* (3), 165-185.

190. Hecht, H. J.; Schomburg, D.; Kalisz, H.; Schmid, R. D., *Biosens. Bioelectron.* **1993,** *8*, 197-203.

191. Bankar, S. B.; Bule, M. V.; Singhal, R. S.; Ananthanarayan, L., *Biotechnol. Adv.* **2009,** *27* (4), 489-501.

192. Ferri, S.; Kojima, K.; Sode, K., *J. Diabetes Sci. Technol.* **2011,** *5* (5), 1068-76.

193. Hecht, H. J.; Kalisz, H.; Hendle, J.; Schmid, R. D.; Schomburg, D., *J. Mol. Biol.* **1993,** *229*, 153-172.

194. Raba, J.; Mottola, H. A., *Crit. Rev. Anal. Chem.* **1995,** *25*, 1-42.

195. Pazur, J. H.; Kleppe, K.; Balls, E. M., *Arch. Biochem. Biophys.* **1963,** *103*, 515-518.

196. Swoboda, B. E. P.; Massey, V., *J. Biol. Chem.* **1965,** *240*, 2209-2215.

197. Kalisz, H. M.; Hecht, H.-J.; Schomburg, D.; Schmid, R. D., *Biochim. Biophys. Acta* **1991,** *1080*, 138-142.

198. Gray, H. B.; Winkler, J. R., *Quart. Rev. Biophys.* **2003,** *36*, 341-372.

199. Moser, C. C.; Keske, J. M.; Warncke, K.; Farid, R. S.; Dutton, P. L., *Nature* **1992,** *355*, 796-802.

200. Marcus, R. A.; Sutin, N., *Biochim. Biophys. Acta* **1985,** *811*, 265-322.

201. M., K. A.; Ulstrup, J., *Electron Transfer in Chemistry and Biology. An Introduction to the Theory*. John Wiley & Sons Ltd.: Chichester, 1999.

202. Peigney, A.; Laurent, C.; Flahaut, E.; Bacsa, R. R.; Rousset, A., *Carbon* **2001,** *39* (4), 507-514.

203. Holt, R. E.; Cotton, T. M., *J. Amer. Chem. Soc.* **1987,** *109* (6), 1841-1845.

204. Frew, J. E.; Hill, H. A. O., *Eur. J. Biochem.* **1988,** *172* (2), 261-269.

205. Szot, K.; Joensson-Niedziolka, M.; Rozniecka, E.; Marken, F.; Opallo, M., *Electrochim. Acta* **2013,** *89*, 132-138.

206. Laviron, E., *J. Electroanal. Chem.* **1979,** *101* (1), 19-28.

207. Campos, R.; Ferapontova, E. E., *Electrochim. Acta* **2014,** *126*, 151-157.

208. Bard, A. J.; Faulkner, L. R., *Electrochemical Methods: Fundamental and Applications*. 2nd Edition edn ed.; John Wiley & Sons, Inc.,: United States, 2001.

209. Correa, C. C.; Santhiago, M.; Barboza Formiga, A. L.; Kubota, L. T., *Electrochim. Acta* **2013,** *90*, 309-316.

210. Roullier, L.; Laviron, E., *J. Electroanal. Chem.* **1983,** *157*, 193-203.

211. Honeychurch, M. J.; Rechnitz, G. A., *Electroanalysis* **1998,** *10* (5), 285-293.

212. Honeychurch, M. J.; Rechnitz, G. A., *Electroanalysis* **1998,** *10* (7), 453-457.

213. Luo, Z.; Yuwen, L.; Han, Y.; Tian, J.; Zhu, X.; Weng, L.; Wang, L., *Biosens. Bioelectron.* **2012,** *36* (1), 179-185.

214. Ianniello, R. M.; Lindsay, T. J.; Yacynych, A. M., *Anal. Chem.* **1982,** *54* (7), 1098-1101.

215. Jiang, L.; McNeil, C. J.; Cooper, J. M., *J. Chem. Soc., Chem. Commun.* **1995,** (12), 1293-1295.

216. Scheller, F.; Strnad, G.; Neumann, B.; Kuhn, M.; Ostrowski, W., *Bioelectrochem. Bioenerg.* **1979,** *6* (2), 117-122.

217. O. Blumenfeld, J. L., G.E. Perlmann, *J. Biol. Chem* **1960** *235* 379-82.

218. He, X. M.; Carter, D. C., *Nature* **1992,** *358*, 209-215.

219. Swoboda, B. E. P., *Biochim. Biophys. Acta* **1969,** *175*, 365-379.

220. Pontikos, N. M.; McCreery, R. L., *J. Electroanal. Chem.* **1992,** *324* (1-2), 229-242.

221. Liu, L.-M.; Wen, J.; Liu, L.; He, D.; Kuang, R.-y.; Shi, T., *Anal. Biochem.* **2014,** *445*, 24-29.

222. Karuppiah, C.; Palanisamy, S.; Chen, S.-M.; Veeramani, V.; Periakaruppan, P., *Sensors Actuators B: Chem.* **2014,** *196*, 450-456.

223. Bai, Y.-F.; Xu, T.-B.; Luong, J. H. T.; Cui, H.-F., *Anal. Chem.* **2014,** *86* (10), 4910-8.

224. Zhao, H.; Yu, S. H.; Yoo, P. J.; Park, J. H.; Lee, J. Y., *Mol. Cryst. Liq. Cryst.* **2013,** *580* (1), 22-28.

225. Razmi, H.; Mohammad-Rezaei, R., *Biosens. Bioelectron.* **2013,** *41*, 498-504.

226. Peng, H.-P.; Liang, R.-P.; Zhang, L.; Qiu, J.-D., *Biosens. Bioelectron.* **2013,** *42*, 293-299.

227. Nasri, Z.; Shams, E., *Electrochim. Acta* **2013,** *112*, 640-647.

228. Jianing, H.; Jiewu, C.; Guangqing, X.; Adeloju, S. B.; Yucheng, W., *Mater Lett* **2013,** *108*, 88-91.

229. Liu, L.; Cheng, Y.; Sun, F.; Yang, J.; Wu, Y., *J. Solid State Electrochem.* **2012,** *16* (3), 1003-1009.

230. Lee, S.; Ringstrand, B. S.; Stone, D. A.; Firestone, M. A., *ACS Appl. Mater. Interfaces* **2012,** *4* (5), 2311-2317.

231. Jiang, Y.; Zhang, Q.; Li, F.; Niu, L., *Sens. Actuator B-Chem* **2012,** *161* (1), 728-733.

232. Cai, C.-J.; Xu, M.-W.; Bao, S.-J.; Lei, C.; Jia, D.-Z., *Rsc Advances* **2012,** *2* (21), 8172-8178.

233. Zhang, Q.; Wu, S.; Zhang, L.; Lu, J.; Verproot, F.; Liu, Y.; Xing, Z.; Li, J.; Song, X.-M., *Biosens. Bioelectron.* **2011,** *26* (5), 2632-2637.

234. Wang, Z.; Liu, S.; Wu, P.; Cai, C., *Anal. Chem.* **2009,** *81* (4), 1638-1645.

235. Wang, K.; Yang, H.; Zhu, L.; Ma, Z.; Xing, S.; Lv, Q.; Liao, J.; Liu, C.; Xing, W., *Electrochim. Acta* **2009,** *54* (20), 4626-4630.

236. Shan, C.; Yang, H.; Song, J.; Han, D.; Ivaska, A.; Niu, L., *Anal. Chem.* **2009,** *81* (6), 2378-2382.

237. Kang, X.; Wang, J.; Wu, H.; Aksay, I. A.; Liu, J.; Lin, Y., *Biosens. Bioelectron.* **2009,** *25* (4), 901-905.

238. Park, J. Y.; Kim, Y. H.; Seong, A.; Yoo, Y. J., *Biotechnol. Bioprocess Eng.* **2008,** *13* (4), 431-435.

239. Wang, G.; Thai, N. M.; Yau, S. T., *Biosens. Bioelectron.* **2007,** *22* (9-10), 2158-64.

240. Salimi, A.; Sharifi, E.; Noorbakhsh, A.; Soltanian, S., *Biosens. Bioelectron.* **2007,** *22* (12), 3146-3153.

241. Nadzhafova, O.; Etienne, M.; Walcarius, A., *Electrochem. Commun.* **2007,** *9* (5), 1189-1195.

242. Liu, H.; Hu, N., *Electroanalysis* **2007,** *19* (7-8), 884-892.

243. Liu, G.; Paddon-Row, M. N.; Gooding, J. J., *Electrochem. Commun.* **2007,** *9* (9), 2218-2223.

244. Vidal, J. C.; Garcia, E.; Castillo, J. R., *Biosens. Bioelectron.* **1998,** *13* (3-4), 371-382.

245. Xu, Q.; Gu, S.-X.; Jin, L.; Zhou, Y.-e.; Yang, Z.; Wang, W.; Hu, X., *Sens. Actuator B-Chem* **2014,** *190*, 562-569.

246. Elahi, M. Y.; Khodadadi, A. A.; Mortazavi, Y., *J. Electrochem. Soc.* **2014,** *161* (5), B81-B87.

247. Liang, B.; Fang, L.; Yang, G.; Hu, Y.; Guo, X.; Ye, X., *Biosens. Bioelectron.* **2013,** *43*, 131-136.

248. Schonbaum, G. R.; Chance, B., Catalase. In *The Enzymes*, Boyer, P. D., Ed. Academic Press: New York, 1976; Vol. 13, pp 363-408.

249. Murthy, M. R.; Reid , T. J.; Sicignano, A.; Tanaka, N.; Rossmann, M. G., *J. Mol. Biol.* **1981,** *152*, 465-499.

250. Fita, I.; Silva, A. M.; Murthy, M. R. N.; Rossmann, M. G., *Acta Crystallogr. Sect. B: Struct. Sci.* **1986,** *42*, 497-575.

251. Prakash, P. A.; Yogeswaran, U.; Chen, S.-M., *Sensors* **2009,** *9*, 1821-1844.

252. Jiang, H.-J.; Yang, H.; Akins, D. L., *J. Electroanal. Chem.* **2008,** *623*, 181-186.

253. Vilian, A. T. E.; Chen, S.-M.; Lou, B.-S., *Biosens. Bioelectron.* **2014,** *61*, 639-647.

254. Zhang, Z.; Chouchane, S.; Magliozzo, R. S.; Rusling, J. F., *Anal. Chem.* **2002,** *74*, 163-170.

255. Bartlett, P. N., Bioenergetics and biological electron transport. In *Bioelectrochemistry: Fundamentals, Experimental Techniqies and Applications*, Bartlett, P. N., Ed. John Wiley & Sons: Chichester, 2008; pp 1-38.

256. Swartz, D. B.; Wilson, G. S., *Anal. Biochem.* **1971,** *40* (2), 392-400.

257. Lowe, H. J.; Clark, W. M., *J. Biol. Chem.* **1956,** *221*, 983-992.

258. Wei, H.; Omonovic, S., *Chem. Biodiversity* **2008,** *5*, 1622-1638.

259. Yang, Z.; Cao, Y.; Li, J.; Jian, Z.; Zhang, Y.; Hu, X., *Anal. Chim. Acta* **2015,** *871* (Supplement C), 35-42.

260. Eskandari, K.; Zarei, H.; Ghourchian, H.; Amoozadeh, S.-M., *J. Anal. Chem.* **2015,** *70*, 1254-1260.

261. Li, J.; Lu, M.; Tan, Z.; Xu, Y.; Zhang, Y.; Hu, X.; Yang, Z., *Microchim Acta* **2016,** *183*, 1705-1712.

262. Kruusenberg, I.; Alexeyeva, N.; Tammeveski, K., *Carbon* **2009,** *47* (3), 651-658.

263. Byers, J. C.; Güell, A. G.; Unwin, P. R., *J. Am. Chem. Soc.* **2014,** *136*, 11252−11255.

264. Goran, J. M.; Phan, E. N. H.; Favela, C. A.; Stevenson, K. J., *Anal. Chem.* **2015,** *87*, 5989−5996.

265. Wang, L.; Pumera, M., *Chem. Commun.* **2014,** *50* (84), 12662-12664.

266. Mello, P. A.; Rodrigues, L. F.; Nunes, M. A. G.; Mattos, J. C. P.; Mueller, E. I.; Dressler, V. L.; Flores, E. M. M., *J. Braz. Chem. Soc.* **2011,** *22* (6), 1040-U62.

267. Wenrong, Y.; Ratinac, K. R.; Ringer, S. P.; Thordarson, P.; Gooding, J. J.; Braet, F., *Angew. Chem. Int. Ed.* **2010,** *49* (12), 2114-38.

268. Wang, Y.; Shan, H.; Hauge, R. H.; Pasquali, M.; Smalley, R. E., *J. Phys. Chem. B* **2007,** *111* (6), 1249-1252.

269. McCreery, R. L.; McDermott, M. T., *Anal. Chem.* **2012,** *84* (5), 2602-2605.

270. McCreery, R. L., *Chem. Rev.* **2008,** *108* (7), 2646-2687.

271. Wilson, G. S., *Biosens. Bioelectron.* **2016,** *82*, vii-viii.

272. Cracknell, J. A.; Vincent, K. A.; Armstrong, F. A., *Chem. Rev.* **2008,** *108*, 2439–2461.

273. Tasca, F.; Harreither, W.; Ludwig, R.; Gooding, J. J.; Gorton, L., *Anal Chem* **2011,** *83* (8), 3042-9.

274. Palmore, G. T. R.; Kim, H. H., *J.Electroanal. Chem.* **1999,** *464*, 110–117.

275. Cass, A. E. G.; Davis, G.; Francis, G. D.; Hill, H. A. O.; Aston, W. J.; Higgins, I. J.; Plotkin, E. V.; Scott, L. D. L.; Turner, A. P. F., *Anal. Chem.* **1984,** *56* (4), 667-671.

276. Kavanagh, P.; Leech, D., *Phys. Chem. Chem. Phys.* **2013,** *15* (14), 4859-4869.

277. Guzik, U.; Hupert-Kocurek, K.; Wojcieszyńska, D., *Molecules* **2014,** *19*, 8995-9018.

278. Rodrigues, R. C.; Ortiz, C.; Berenguer-Murcia, Á.; Torres, R.; Fernández-Lafuente, R., *Chem. Soc. Rev.* **2013,** *42*, 6290-6307.

279. Osman, M. H.; Shah, A. A.; Walsh, F. C., *Biosens. Bioelectron.* **2011,** *26* (7), 3087-3102.

280. Lowe, A. B., *Polym. Chem.* **2010,** *1* (1), 17-36.

281. Loo, T. W.; Clarke, D. M., *J. Biol. Chem.* **2001,** *276* (34), 31800-5.

282. Henriksson, G.; Johansson, G.; Pettersson, G., *J. Biotechnol.* **2000,** *78*, 93-113.

283. Tasca, F.; Zafar, M. N.; Harreither, W.; Noell, G.; Ludwig, R.; Gorton, L., *Analyst* **2011,** *136* (10), 2033-2036.

284. Ludwig, R.; Harreither, W.; Tasca, F.; Gorton, L., *ChemPhysChem* **2010,** *11* (13), 2674-97.

285. Zafar, M. N.; Safina, G.; Ludwig, R.; Gorton, L., *Anal. Biochem.* **2012,** *425* (1), 36-42.

286. Ludwig, R.; Ortiz, R.; Schulz, C.; Harreither, W.; Sygmund, C.; Gorton, L., *Anal. Bioanal. Chem.* **2013,** *405* (11), 3637-3658.

287. Zamocky, M.; Ludwig, R.; Peterbauer, C.; Hallberg, B. M.; Divne, C.; Nicholls, P.; Haltrich, D., *Curr. Protein Peptide Sci.* **2006,** *7* (3), 255-280.

288. Tan, T. C.; Kracher, D.; Gandini, R.; Sygmund, C.; Kittl, R.; Haltrich, D.; Hallberg, B. M.; Ludwig, R.; Divne, C., *Nat Commun* **2015,** *6*, 7542-7553.

289. Hallberg, B. M.; Henriksson, G.; Pettersson, G.; Divne, C., *J. Mol. Biol.* **2002,** *315* (3), 421-434.

290. Hallberg, B. M.; Henriksson, G.; Pettersson, G.; Vasella, A.; Divne, C., *J. Biol. Chem.* **2003,** *278* (9), 7160-6.

291. Henriksson, G.; G., J.; Pettersson, G., *J. Biotechnol.* **2000,** *78*, 93-113.

292. Ludwig, R.; Harreither, W.; Tasca, F.; Gorton, L., *Chem. Phys. Chem.* **2010,** *11* (13), 2674-2697.

293. Wilson, M. T.; Hogg, N.; Jones, G. D., *Biochem. J* **1990,** *270* (1), 265-267.

294. Igarashi, K.; Momohara, I.; Nishino, T.; Samejima, M., *Biochem. J* **2002,** *365*, 521-526.

295. Cox, M. C.; Rogers, M. S.; Cheesman, M.; Jones, G. D.; Thomson, A. J.; Wilson, M. T.; Moore, G. R., *FEBS Lett.* **1992,** *307* (2), 233-236.

296. Harris JM, R. C., Lopez GP., *J. Diabetes Sci. Technol.* **2013,** *4*, 1030-8.

297. Kracher, D.; Zahma, K.; Schulz, C.; Sygmund, C.; Gorton, L.; Ludwig, R., *FEBS J.* **2015,** *282* (16), 3136-3148.

298. Tasca, F.; Gorton, L.; Harreither, W.; Haltrich, D.; Ludwig, R.; Noll, G., *J. Phys. Chem. C* **2008,** *112* (26), 9956-9961.

299. Kielb, P.; Sezer, M.; Katz, S.; Lopez, F.; Schulz, C.; Gorton, L.; Ludwig, R.; Wollenberger, U.; Zbger, I.; Weidinger, I. M., *ChemPhysChem* **2015,** *16*, 1960-1968.

300. Ludwig, R.; Harreither, W.; Tasca, F.; Gorton, L., *ChemPhysChem* **2010,** *11*, 2674-2697.

301. Sasajima, K. I.; Sinskey, A. J., *Biochim. Biophys. Acta* **1979,** *571* (1), 120-126.

302. Pricelius, S.; Ludwig, R.; Lant, N.; Haltrich, D.; Guebitz, G. M., *Appl. Microbiol. Biotechnol.* **2009,** *85* (1), 75-83.

303. Lowe, A. B., *Polym. Chem.* **2010,** *1* (1), 17-36.

304. Gregory, J. D., *J. Am. Chem. Soc* **1955,** *77 (14)*, 3922–3923.

305. Grimsley, G. R.; Scholtz, J. M.; Pace, C. N., *Protein Sci.* **2009,** *18* (1), 247-251.

306. Pletcher, D., *A first Course in Electrode Processes*. RSC Publishing: Cambridge, UK, 2009.

307. Brownson, D. A. C., Banks, Craig E, Interpreting Electrochemistry. In *The Handbook of Graphene Electrochemistry*, Springer-Verlag London Ltd. : London, 2014.

308. Guo, L. H.; Hill, H. A. O., *Adv. Inorg. Chem.* **1991,** *36*, 341-375.

309. Schulz, C.; Kittl, R.; Ludwig, R.; Gorton, L., *ACS Catal.* **2016,** *6* (2), 555-563.

310. Mayhew, S. G., *Eur. J. Biochem.* **1999,** *265* (2), 698-702.

311. Scholz, A. J. B. G. I. F., *Electrochemical Dictionary*. Springer-Verlag Berlin Heidelberg: Berlin, 2008.

312. Limoges, B.; Saveant, J. M., *J. Electroanal. Chem.* **2004,** *562* (1), 43-52.

313. Kielb, P.; Sezer, M.; Katz, S.; Lopez, F.; Schulz, C.; Gorton, L.; Ludwig, R.; Wollenberger, U.; Zebger, I.; Weidinger, I. M., *ChemPhysChem* **2015,** *16* (9), 1960-1968.

314. Lindgren, A.; Larsson, T.; Ruzgas, T.; Gorton, L., *J. Electroanal. Chem.* **2000,** *494* (2), 105-113.

315. Uhlig, H., *Industrial Enzymes and their Applications.* . 1st ed.; John Wiley and Sons: New York, 1998.

316. Amri, E. M., F, *Am J Biochem Biotechnol* **2012,** *8* (2), 99-104.

317. Cameron, M. D.; Aust, S. D., *Biochemistry* **2000,** *39* (44), 13595-13601.

318. Baminger, U.; Subramaniam, S. S.; Renganathan, V.; Haltrich, D., *Appl. Environ. Microbiol.* **2001,** *67* (4), 1766-1774.

319. Cohen, J. D.; Bao, W.; Renganathan, V.; Sai Subramaniam, S.; Loehr, T. M., *Arch. Biochem. Biophys.* **1997,** *341*, 321-328.

320. Igarashi, K.; Verhagen, M.; Samejima, M.; Schulein, M.; Eriksson, K. E. L.; Nishino, T., *J. Biol. Chem.* **1999,** *274* (6), 3338-3344.

321. Lange, M. A.; Chambers, J. Q., *Anal. Chim. Acta* **1985,** *175* (SEP), 89-97.

322. Jonsson, G.; Gorton, L.; Pettersson, L., *Electroanalysis* **1989,** *1* (1), 49-55.

323. Forrow, N. J.; Sanghera, G. S.; Walters, S. J., *J. Chem. Soc., Dalton Trans.* **2002,** (16), 3187-3194.

324. Stoica, L.; Lindgren-Sjolander, A.; Ruzgas, T.; Gorton, L., *Anal. Chem.* **2004,** *76*, 4690-4696.

325. Schulz, C.; Ludwig, R.; Gorton, L., *Anal. Chem.* **2014,** *86* (9), 4256-4263.

326. Coman, V.; Harreither, W.; Ludwig, R.; Haltrich, D.; Gorton, L., *Chem. Anal. (Warsaw)* **2007,** *52* (6), 945-960.

327. Schulz, C.; Ludwig, R.; Micheelsen, P. O.; Silow, M.; Toscano, M. D.; Gorton, L., *Electrochem. Commun.* **2012,** *17*, 71-74.

328. Kracher, D.; Zahma, K.; Schulz, C.; Sygmund, C.; Gorton, L.; Ludwig, R., *FEBS J.* **2015,** *282*, 3136-3148.

329. Harreither, W.; Coman, V.; Ludwig, R.; Haltrich, D.; Gorton, L., *Electroanalysis* **2007,** *19* (2-3), 172-180.

330. Michaelis, L.; Menten, M. L.; Johnson, K. A.; Goody, R. S., *Biochemistry* **2011,** *50* (39), 8264-9.

331. Berg JM, T. J., Stryer L., The Michaelis-Menten Model Accounts for the Kinetic Properties of Many Enzymes. In *Biochemistry*, 5th ed.; W H Freeman: New York, 2002.

332. Muller, P., *Pure Appl. Chem.* **1994,** *66* (5), 1077-1184.

333. Leger, C.; Bertrand, P., *Chem. Rev.* **2008,** *108* (7), 2379-2438.

334. Flexer, V.; Ielmini, M. V.; Calvo, E. J.; Bartlett, P. N., *Bioelectrochemistry* **2008,** *74* (1), 201-209.

335. Stoica, L.; Ruzgas, T.; Ludwig, R.; Haltrich, D.; Gorton, L., *Langmuir* **2006,** *22* (25), 10801-10806.

336. Craig, N. L.; Green, R.; Cohen-Fix, O.; Greider, C.; Storz, G., *Molecular Biology: Principles of Genome Function*. Oxford University Press: 2014.

337. Zamocky, M.; Schumann, C.; Sygmund, C.; O'Callaghan, J.; Dobson, A. D.; Ludwig, R.; Haltrich, D.; Peterbauer, C. K., *Protein Expr. Purif.* **2008,** *59* (2), 258-65.

338. Sygmund, C.; Kracher, D.; Scheiblbrandner, S.; Zahma, K.; Felice, A. K. G.; Harreither, W.; Kittl, R.; Ludwig, R., *Appl. Environ. Microbiol.* **2012,** *78* (17), 6161-6171.

339. Grove, W., *Phil. Mag. J. Sci* **1839,** *14*, 127-130.

340. Schœnbein, C. F., *Philos. Mag.* **1839,** *14* (85), 43-45.

341. Cracknell, J. A.; Vincent, K. A.; Armstrong, F. A., *Chem. Rev.* **2008,** *108* (7), 2439-2461.

342. Cameron, D., *Chem. Tech.* **1979,** *9* (10), 633-637.

343. Osman, M. H.; Shah, A. A.; Walsh, F. C., *Biosens. Bioelectron.* **2011,** *26* (7), 3087-3102.

344. Filip, J.; Andicsova-Eckstein, A.; Vikartovska, A.; Tkac, J., *Biosens. Bioelectron.* **2017,** *89*, 384-389.

345. Mano, N.; de Poulpiquet, A., *Chem. Rev.* **2017**, in press

346. Cadet, M.; Gounel, S.; Stines-Chaumeil, C.; Brilland, X.; Rouhana, J.; Louerat, F.; Mano, N., *Biosens. Bioelectron.* **2016,** *83*, 60-7.

347. Moore, C. M.; Minteer, S. D.; Martin, R. S., *LChip* **2005,** *5* (2), 218-225.

348. Kim, H. H.; Mano, N.; Zhang, X. C.; Heller, A., *J. Electrochem. Soc.* **2003,** *150* (2), A209-A213.

349. Bullen, R. A.; Arnot, T. C.; Lakeman, J. B.; Walsh, F. C., *Biosens. Bioelectron.* **2006,** *21* (11), 2015-2045.

350. Cinquin, P.; Gondran; Giroud, F.; Mazabrard, S.; Pellissier, A.; Boucher, F.; Alcaraz, J. P.; Gorgy, K.; Cosnier, F. S., *PLoS ONE* **2010,** *5* (5), e10476.

351. Palmore, G. T. R.; Kim, H. H., *J. Electroanal. Chem.* **1999,** *464*, 110–117.

352. Cass, A. E. G.; Davis, G.; Francis, G. D.; Hill, H. A. O.; Aston, W. J.; Higgins, I. J.; Plotkin, E. V.; Scott, L. D. L.; Turner, A. P. F., *Anal. Chem.* **1984,** *56* (4), 667-671.

353. Murao, S.; Tanaka, N., *Agric. Biol. Chem.* **1981,** *45* (10), 2383-2384.

354. Goldfinch, M. E.; Maguire, G. A., *Ann. Clin. Biochem.* **1988,** *25*, 73-77.

355. Tsujimura, S.; Tatsumi, B.; Ogawa, J.; Shimizu, S.; Kano, K.; Ikeda, T., *J. Electroanal. Chem.* **2001,** *496* (1-2), 69-75.

356. Kjaergaard, C. H.; Durand, F.; Tasca, F.; Qayyum, M. F.; Kauffmann, B.; Gounel, S.; Suraniti, E.; Hodgson, K. O.; Hedman, B.; Mano, N.; Solomon, E. I., *J. Am. Chem. Soc.* **2012,** *134* (12), 5548-51.

357. Durand, F.; Gounel, S.; Kjaergaard, C. H.; Solomon, E. I.; Mano, N., *Appl. Microbiol. Biotechnol.* **2012,** *96* (6), 1489-1498.

358. Mano, N.; Kim, H.-H.; Heller, A., *J. Phys. Chem. B* **2002,** *106* (34), 8842-8848.

359. Durand, F.; Kjaergaard, C. H.; Suraniti, E.; Gounel, S.; Hadt, R. G.; Solomon, E. I.; Mano, N., *Biosens. Bioelectron.* **2012,** *35* (1), 140-146.

360. Jacquot, C. H.; Lamicq, G.; Salvador, D.; Gounel, S.; Stines-Chaumeil, C.; Mano, N., *FEBS J.* **2014,** *281*, 240-241.

361. Mizutani, K.; Toyoda, M.; Sagara, K.; Takahashi, N.; Sato, A.; Kamitaka, Y.; Tsujimura, S.; Nakanishi, Y.; Sugiura, T.; Yamaguchi, S.; Kano, K.; Mikami, B., *Acta Crystallogr. Sect. F Struct. Biol. Cryst. Commun.* **2010,** *66*, 765-770.

362. Mano, N.; Edembe, L., *Biosens. Bioelectron.* **2013,** *50*, 478-85.

363. Mano, N., *Appl. Microbiol. Biotechnol.* **2012,** *96* (2), 301-307.

364. de Poulpiquet, A.; Kjaergaard, C. H.; Rouhana, J.; Mazurenko, I.; Infossi, P.; Gounel, S.; Gadiou, R.; Giudici-Orticoni, M. T.; Solomon, E. I.; Mano, N.; Lojou, E., *ACS Catalysis* **2017,** *7* (6), 3916-3923.

365. Tasca, F.; Farias, D.; Castro, C.; Acuna-Rougier, C.; Antiochia, R., *PLoS One* **2015,** *10* (7), e0132181.

366. dos Santos, L.; Climent, V.; Blanford, C. F.; Armstrong, F. A., *PCCP* **2010,** *12* (42), 13962-13974.

367. Xia, H.-q.; Kitazumi, Y.; Shirai, O.; Kano, K., *J. Electroanal. Chem.* **2016,** *763*, 104-109.

368. Cracknell, J. A.; McNamara, T. P.; Lowe, E. D.; Blanford, C. F., *DTr* **2011,** *40* (25), 6668-6675.

369. Jonsson-Niedziolka, M.; Kaminska, A.; Opallo, M., *Electrochim. Acta* **2010,** *55* (28), 8744-8750.

370. Pita, M.; Gutierrez-Sanchez, C.; Toscano, M. D.; Shleev, S.; De Lacey, A. L., *Bioelectrochemistry* **2013,** *94*, 69-74.

371. Jones, A. K.; Sillery, E.; Albracht, S. P. J.; Armstrong, F. A., *Chem. Commun.* **2002,** (8), 866-867.

372. Butt, J. N.; Thornton, J.; Richardson, D. J.; Dobbin, P. S., *Biophys. J.* **2000,** *78* (2), 1001-1009.

373. Hirst, J.; Sucheta, A.; Ackrell, B. A. C.; Armstrong, F. A., *J. Am. Chem. Soc.* **1996,** *118* (21), 5031-5038.

374. Bateman, L.; Leger, C.; Goodin, D. B.; Armstrong, F. A., *J. Am. Chem. Soc.* **2001,** *123* (38), 9260-9263.

375. Leger, C.; Jones, A. K.; Albracht, S. P. J.; Armstrong, F. A., *J. Phys. Chem. B* **2002,** *106* (50), 13058-13063.

376. Tsujimura, S.; Nakagawa, T.; Kano, K.; Ikeda, T., *Electrochemistry* **2004,** *72* (6), 437-439.

377. Hexter, S. V.; Grey, F.; Happe, T.; Climent, V.; Armstrong, F. A., *Proc. Natl. Acad. Sci. U. S. A.* **2012,** *109* (29), 11516-11521.

378. Hexter, S. V.; Esterle, T. F.; Armstrong, F. A., *PCCP* **2014,** *16* (24), 11822-11833.

379. Zheng, W.; Zhao, H. Y.; Zhou, H. M.; Xu, X. X.; Ding, M. H.; Zheng, Y. F., *J. Solid State Electrochem.* **2009,** *14* (2), 249.

380. Gutierrez-Sanchez, C.; Ciaccafava, A.; Blanchard, P. Y.; Monsalve, K.; Giudici-Orticoni, M. T.; Lecomte, S.; Lojou, E., *ACS Catalysis* **2016,** *6* (8), 5482-5492.

381. Kamitaka, Y.; Tsujimura, S.; Ikeda, T.; Kano, K., *Electrochemistry* **2006,** *74* (8), 642-644.

382. Singh, K.; McArdle, T.; Sullivan, P. R.; Blanford, C. F., *Energy Environ. Sci.* **2013,** *6* (8), 2460-2464.

383. Ramirez, P.; Mano, N.; Andreu, R.; Ruzgas, T.; Heller, A.; Gorton, L.; Shleev, S., *Biochim. Biophys. Acta, Bioenergetics* **2008,** *1777* (10), 1364-1369.

384. Christenson, A.; Shleev, S.; Mano, N.; Heller, A.; Gorton, L., *Biochim. Biophys. Acta, Bioenergetics* **2006,** *1757* (12), 1634-1641.

385. Ivnitski, D.; Artyushkova, K.; Atanassov, P., *Bioelectrochemistry* **2008,** *74* (1), 101-10.

386. Brocato, S.; Lau, C.; Atanassov, P., *Electrochim. Acta* **2012,** *61*, 44-49.

387. Ivnitski, D. M.; Khripin, C.; Luckarift, H. R.; Johnson, G. R.; Atanassov, P., *Electrochim. Acta* **2010,** *55* (24), 7385-7393.

388. Huynh, M. H. V.; Meyer, T. J., *Chem. Rev.* **2007,** *107* (11), 5004-5064.

389. Filip, J.; Tkac, J., *Bioelectrochemistry* **2014,** *96*, 14-20.

390. Weigel, M. C.; Tritscher, E.; Lisdat, F., *Electrochem. Commun.* **2007,** *9* (4), 689-693.

391. Shleev, S.; Andoralov, V.; Falk, M.; Reimann, C. T.; Ruzgas, T.; Srnec, M.; Ryde, U.; Rulisek, L., *Electroanalysis* **2012,** *24* (7), 1524-1540.

392. Frasconi, M.; Boer, H.; Koivula, A.; Mazzei, F., *Electrochim. Acta* **2010,** *56* (2), 817-827.

393. Lee, S. K.; George, S. D.; Antholine, W. E.; Hedman, B.; Hodgson, K. O.; Solomon, E. I., *J. Am. Chem. Soc.* **2002,** *124* (21), 6180-6193.

394. Tkac, J.; Svitel, J.; Vostiar, I.; Navratil, M.; Gemeiner, P., *Bioelectrochemistry* **2009,** *76* (1-2), 53-62.

395. Jeuken, L. J. C.; Wisson, L. J.; Armstrong, F. A., *Inorg. Chim. Acta* **2002,** *331*, 216-223.

396. Miura, Y.; Tsujimura, S.; Kurose, S.; Kamitaka, Y.; Kataoka, K.; Sakurai, T.; Kano, K., *Fuel Cells* **2009,** *9* (1), 70-78.

397. Bento, I.; Silva, C. S.; Chen, Z.; Martins, L. O.; Lindley, P. F.; Soares, C. M., *BMC Struct. Biol.* **2010,** *10* (1), 28-42.

398. Iwaki, M.; Kataoka, K.; Kajino, T.; Sugiyama, R.; Morishita, H.; Sakurai, T., *FEBS Lett.* **2010,** *584* (18), 4027-4031.

399. Silva, C. S.; Damas, J. M.; Chen, Z.; Brissos, V.; Martins, L. O.; Soares, C. M.; Lindley, P. F.; Bento, I., *Acta Crystallogr. D* **2012,** *68* (2), 186-193.

400. Quintanar, L.; Stoj, C.; Wang, T. P.; Kosman, D. J.; Solomon, E. I., *Biochemistry* **2005,** *44*, 6081-6091.

401. Brissos, V., Chen, Z., & Martins, L. O., *DTr* **2012,** *41* (20), 6247-6255.

402. Chen, Z.; Durao, P.; Silva, C. S.; Pereira, M. M.; Todorovic, S.; Hildebrandt, P.; Bento, I.; Lindley, P. F.; Martins, L. O., *Dalton Trans* **2010,** *39*, 2875-2882.

403. Kjaergaard, C. H.; Jones, S. M.; Gounel, S.; Mano, N.; Solomon, E. I., *J. Am. Chem. Soc.* **2015,** *137* (27), 8783-94.

404. Solomon, E. I.; Augustine, A. J.; Yoon, J., *Dalton Trans* **2008**, 3921-3932.

405. Cracknell, J. A.; Blanford, C. F., *Chem. Sci.* **2012,** *3* (5), 1567-1581.

406. Dagys, M.; Laurynenas, A.; Ratautas, D.; Kulys, J.; Vidziunaite, R.; Talaikis, M.; Niaura, G.; Marcinkeviciene, L.; Meskys, R.; Shleev, S., *Energy Environ. Sci.* **2017,** *10* (2), 498-502.

407. Hirose, J.; Inoue, K.; Sakuragi, H.; Kikkawa, M.; Minakami, M.; Morikawa, T.; Iwamoto, H.; Hiromi, K., *Inorg. Chim. Acta* **1998,** *273* (1), 204-212.

408. Sugimoto, Y.; Kitazumi, Y.; Shirai, O.; Kano, K., *Electrochemistry* **2017,** *85* (2), 82-87.

409. Bright, H. J.; Appleby, M., *J. Biol. Chem.* **1969,** *244*, 3625-31334.